Liquid Chromatography-Mass Spectrometry Strategies for *in vivo* Neurochemical Monitoring with Microdialysis

by

Jenny-Marie T. Wong

A dissertation submitted in partial fulfillment
of the requirements for the degree of
Doctor of Philosophy
(Chemistry)
in the University of Michigan
2016

Doctoral Committee:

Professor Robert T. Kennedy, Chair
Professor Kristina I. Håkansson
Professor Mark E. Meyerhoff
Professor Martin G. Myers Jr.

DEDICATION

To my friends and family who have always supported me.

ACKNOWLEDGEMENTS

I thank Professor Robert T. Kennedy for accepting me into his group, and challenging me to think deeper and to achieve more. His support and encouragement during my time at the University of Michigan means so much. I also extend my gratitude to my dissertation committee members, Professor Kristina Håkansson, Professor Mark Meyerhoff, and Professor Martin G. Myers Jr., whose insight, thoughtful questions, and advice has helped shape my research, given me a broader perspective, and deepened my understanding.

I extend special thanks to my previous mentors Professor Joseph A. Gardella, Dr. AnneMarie Block, Dr. Susan Leong, and Mrs. Anne Ruppert, who continue to mentor me, and encouraged me to pursue chemistry with research opportunities early in my academic career. Your support and encouragement has made this journey possible.

I also thank my colleagues Dr. Omar Mabrouk, Dr. Neil Hershey, Dr. Peng Song, Dr. Thomas Slaney, Dr. Jing Nie, Dr. Shuwen Sun, Dr. Ying Zhou, Dr. Kennon Deal, Dr. Shi Jin, Dr. Erik Guetschow, Doc Colladeen Dugan, Dr. Jim Grinias, Dr. Katy Nesbitt, Paige Malec, Non Ngernsutivorakul, Alec Valenta, Daniel Steyer, Claire Ouimet, Dr. Kirsten Porter-Stransky, Dr. Ream Al-Hassani, Dr. Jordan McCall, Dr. Christa Patterson-Polidori, Dr. Jeffery Pettibone, and Dr. Sarah Mikelman. I have learned so much from each of you, and have valued your patience, willingness to lend a hand, and friendship. A

special thanks to Dr. Omar Mabrouk and Dr. Neil Hershey for my initial training, Dr. Ying Zhou for guidance on neuropeptides, and Dr. Jim Grinias for teaching me fundamental chromatography and being a great friend in and out of lab.

To my friends I made here, who have supported me throughout graduate school: Julia Bourg, Qi Zhang, Betsy Brown, and Sarah Mikelman. You have been my support and my role models. You were there when the stress felt like too much, and always reminded me that I could do it. Without your friendship, graduate school would have been impossible, boring, and less fun.

To my family, especially my dad, Tai-Gue, and Tai-Gue Cheung. Without the unconditional love and support you have provided me throughout my life, I am certain I would not have made it to where I am today. You stood by me in the worst times, consoled me, and reminded me that life is both yin and yang. Even in my darkest times, I knew I was always loved. I could always count on you to make me laugh, smile, and remind me that there are silver linings in every situation.

And finally to Sam. You have always seen the best in me, believed in me, and made me a better person. You have been my rock, keeping me sane through this journey, my partner in adventure, my better half, and my on-call editor. Your love and support through these last few years mean more to me than words can say. I have loved the adventures we have shared, and look forward to the future adventures that lie ahead.

TABLE OF CONTENTS

LIST OF FIGURES

LIST OF TABLES

LIST OF APPENDICES

LIST OF ABBREVIATIONS

3MT	3-methoxytyrosine
5HIAA	5-hydroxyindole-3-acetic acid
6OHDA	6-hydroxydopamine
ACh	acetylcholine
aCSF	artificial cerebrospinal fluid
AIMs	abnormal involuntary movements
BBB	blood brain barrier
BzCl	benzoyl chloride
CAD	collision activated dissociation
CE-LIF	capillary electrophoresis-laser induced fluorescence
cFos	*Fos* gene
Ch	choline
ChR2	channelrhodopsin
CNO	clozapine-N-oxide
CSF	cerebrospinal fluid
D1R	dopamine receptor D1
D2R	dopamine receptor D2
DA	Dopamine
DBS	deep brain stimulation
dMRM	dynamic multiple reaction monitoring
DMSO	dimethyl sulfoxide
dNAcSh	dorsal nucleus accumbens shell
DOPAC	3,4-dihydroxyphenylacetic acid
DREADDs	designer receptors exclusively activated by designer drugs
Dyn	dynorphin

DYN	dynorphin A_{1-8}
DYN*	isotope dynorphin A_{1-8}
EC_{50}	half maximal effective concentration
ECD	electrochemical detection
ENK	enkephalins
ESI	electrospray ionization
FITC	fluorescein isothiocyanate
GABA	4-amino butyric acid
Glu	glutamate
Gpe	globus pallidus external segment
GPi	globus pallidus internus
HA	hemaglutinin
HCRT	hypocretin
HILIC	hydrophilic interaction liquid chromatography
HPLC	high performance liquid chromatography
HVA	homovanillic acid
i.p.	intraperitoneal
ICV	intracerebroventricular
IR	immunoreactivity
KOR	kappa opioid receptors
LC	liquid chromatography
LE	leu-enkephalin
LepRb	leptin receptor
LHA	lateral hypothalamic area
LIDs	L-DOPA induced dyskinesias
LOD	limit of detection
m/z	mass-to-charge ratio
MAO	monoamine oxidase
ME	met-enkephalin
MLDA	mesolimbic dopamine
MS	mass spectrometry
MS/MS	tandem mass spectrometry
MSN	medium spiny neurons

MWCO	molecular weight cut-off
NAc	nucleus accumbens
NAcSh	nucleus accumbens shell
NBD-F	7-fluoro-4-nitrobenzoxadiazole
NDA	naphthalene-2,3-dicarboxyaldehyde
NT	neurotensin
NTR1	neurotensin receptor 1
OPA	ortho-phthaladehyde
ORL1	opioid receptor like 1
OT	oxytocin
OT*	isotope labeled oxytocin
OTR	oxytocin receptor
PBS	phosphate buffered saline
PD	Parkinson's disease
PEI	polyethylenimine
RPLC	reverse phase liquid chromatography
RSD	relative standard deviation
SNr	substantia nigra pars reticulata
SPTPP	(5-*N*succinimidoxy-5-oxopentyl)triphenylphosphonium bromide
t-BuSH	tert-butyl thiol
VCO_2	carbon dioxide consumption
vNAcSh	ventral nucleus accumbens shell
VO_2	oxygen consumption
VTA	ventral tegmental area

ABSTRACT

Liquid chromatography mass spectrometry (LC-MS) is a powerful analytical tool for multi-analyte quantification. This method can be combined with microdialysis sampling to study small molecules and neuropeptides within discrete brain regions. This thesis focuses on the development of targeted LC-MS assays to analyze dialysate samples collected from awake animals to correlate neurochemical dynamics with behavior.

Previous LC-MS assays used benzoyl chloride derivatization to enable quantification of 17 neurotransmitters and metabolites in dialysate samples. In this work, derivatization conditions were modified to improve sensitivity up to 25-fold and reduce complexity of the procedure. The assay was also expanded to 70 compounds including amino acids, polyamines (e.g., putrescine, spermidine, spermine), compounds from catecholamine biosynthesis pathways (e.g., tyrosine and tryptophan metabolic pathways), and trace amines (e.g., tyramine, octopamine, synephrine). Besides measurements in dialysate, the method was able to analyze plasma and cerebrospinal fluid samples. This work improves the utility of benzoyl chloride, which labels multiple important functional groups, for widely targeted metabolomics methods.

Neuropeptides constitute the largest group of neurotransmitters in the central nervous system. Neuropeptide signaling is involved in many physiological functions but detection *in vivo* is challenging due to low picomolar concentrations. Targeted capillary

LC-MS methods were developed for neurotensin, oxytocin, dynorphin, and enkephalins. The assays utilize desalting and preconcentration on a single analytical column to achieve low picomolar limits of detection. Detection was improved by optimizing all facets of neuropeptide handling from sampling to detection with capillary LC-MS.

These techniques were applied to examine several aspects of neuronal function. Specific neuronal circuits were defined, confirmed, and targeted by combining these analytical tools with pharmacogenetic and optogenetic methods. Novel pathophysiological changes to opioid neuropeptide (dynorphin and enkephalins) dynamics were elucidated in a rat model of Parkinson's disease, and a potential neuropeptide-based treatment was established to reduce the abnormal dyskinetic movements associated with chronic dopamine replacement therapies in Parkinson's Disease. These new multiplexed approaches will advance our understanding of the complex processes underlying neuronal function at the molecular and circuit levels, as well as provides an improved set of experimental tools to better understand lingering questions in the field of neuroscience.

CHAPTER 1: INTRODUCTION

Submitted, in part, as a book chapter in Advances in Real-Time Neuroscience, Volume 2.
Editorial contributions from co-authors Dr. Samuel S. Pappas and Dr. Robert T. Kennedy.

The extracellular space of the brain contains chemicals involved in neurotransmitter signaling, metabolism, and communication with the periphery. Microdialysis sampling of this environment enables measurement of endogenous neurochemicals and exogenous (e.g., drugs) chemicals *in vivo*. Such measurements provide valuable insights into the neurochemical substrates in relation to behavior, diseases, and drug effects.

Microdialysis is a simple and robust technique to collect multiple extracellular analytes within discrete brain regions (Figure 1-1). Microdialysis probes utilize inlet and outlet capillaries ensheathed in a semipermeable membrane. When used in the brain, a perfusion media such as ringer solution or artificial cerebral spinal fluid, similar in ionic composition to the surrounding extracellular environment, is passed through the semipermeable probe membrane. This membrane excludes proteins and enzymes above a given molecular weight cut-off (MWCO). By filtering these large molecules from the collected perfusate, it decreases the complexity of the sample and decreases the rate of enzymatic degradation. Neurochemicals that are below the MWCO diffuse across the membrane from higher to lower concentration regions. Fractions are collected and

analyzed, preserving temporal information which can be correlated to behavior or stimuli. Extracellular neurochemicals in the collected dialysate can then be measured using a number of different analytical methods.

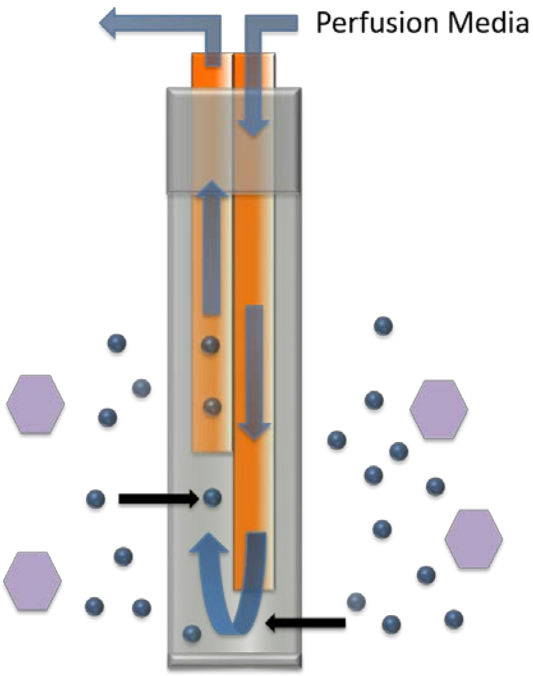

Figure 1-1 Microdialysis probes utilize inlet and outlet capillaries ensheathed by a semi-permeable membrane allowing for sampling of surrounding tissue. Compounds below the MWCO (blue spheres) of the membrane diffuse in and out of the probe based on concentration gradients. The semi-permeable membrane excludes large molecules (purple octagons) such as proteins and enzymes.

Depending on the method, multiple neurotransmitters and metabolites may be measured within each fraction to provide a comprehensive view of the neurochemical environment. Multi-analyte measurements are invaluable for understanding the interactions of neurotransmitter systems, discovering unexpected chemical changes or associations between neurotransmitters, and discerning how multiple neurotransmitters coordinate to drive behavior and other physiological functions. For example, glucose, lactate, pyruvate, glutamate, and the protein tau were monitored in patients with traumatic brain injury to examine potential biomarkers of injury severity[1]. This study

demonstrated that the protein tau could be used to assess damage severity, whereas other metabolic markers were less reliable.

Microdialysis sampling provides a relatively unbiased sample of the low molecular weight compounds present in brain extracellular space, but comprehensive analytical techniques for monitoring a wide range of neurotransmitters and their metabolites have been lacking. As a result, most attempts to broadly measure many neurochemicals have used multiple analytical techniques on collected fractions.

Liquid chromatography (LC) is the mostly widely used method for measuring neurochemicals in dialysate, but different detection modes are required depending on the analyte. LC with electrochemical detection (ECD) is commonly employed to detect electroactive compounds such as dopamine, norepinephrine, serotonin, and some metabolites[2, 3]. LC-ECD is also used to measure acetylcholine (ACh), which is not electroactive, but may be monitored indirectly *via* the formation of electrochemically detectable hydrogen peroxide from a reaction with acetylcholinesterase and choline oxidase[4, 5]. LC effluent may also be exposed to enzymes *via* post-column addition or immobilized enzyme reactors[6-8]. These assays typically utilize phosphate buffer at pH 8 as mobile phase, a compromise between column stability and optimized enzyme reaction conditions. Because of this mobile phase pH requirement, ACh and choline are measured in separate assays from other electroactive compounds.

LC with fluorescence detection is commonly used for detecting amino acid neurotransmitters in dialysate. Most amino acids do not naturally fluoresce, so pre-column derivatization is employed to add a fluorescent tag using commercially available kits or reagents such as OPA (ortho-phthaladehyde)[9, 10], NDA (naphthalene-2,3-

dicarboxyaldehyde)[11-13], or FITC (fluorescein isothiocyanate)[14-16]. Derivatization also allows LC-ECD for amino acids as well. For example, precolumn derivatization of amines with OPA and a thiol such as β-mercaptoethanol or tert-butyl thiol (t-BuSH) forms products that are both fluorescent[17] and easily oxidized, permitting the use of either fluorescent or ECD[18, 19]. LC-ECD with sample derivatization by OPA and t-BuSH detects neuroactive amino acids in the picomolar range[18, 20]. Capillary LC-ECD allows for preconcentration prior to detection, while optimized gradient and buffer conditions enable detection of multiple amino acids and catecholamines in dialysate and brain homogenate in a single run[21]. However, this method has not been often used to measure amines and amino acids simultaneously.

Capillary electrophoresis-laser induced fluorescence (CE-LIF) has also been used to measure multiple neurotransmitters in a single assay[22-24]. Derivatization with NDA[11-13], FITC[14, 15] or carboxyfluorescein succinimidyl ester[16, 25] has been used to measure neurotransmitters such as dopamine, norepinephrine, glutamate, and aspartate. In some cases, the high-speed of CE-LIF allows on-line measurements on the seconds time scale. However, in general it has been possible to optimize conditions for only a sub-set of neurotransmitters and metabolites. Thus, despite the power of separation techniques, the complexity of dialysate samples has made it difficult to measure large numbers of neurotransmitters and metabolites in a single assay. Instead, multiple assays are performed, requiring split samples and added time, or multiple animals. For example, previous dialysis monitoring of dynorphin B, dopamine, and 4-amino butyric acid (GABA) required a single sample to be split into three and analyzed with radioimmunoassay, ECD, and ECD with OPA and t-BuSh derivatization, respectively[26].

Another study employed several assays to monitor multiple analytes: glutamate, aspartate and GABA with precolumn derivatization and fluorimetric detection, the monoamines dopamine and serotonin and their metabolites 3,4-dihydroxyphenylacetic acid (DOPAC), homovanillic acid (HVA), and 5-hydroxyindole-3-acetic acid (5HIAA) with LC-ECD, and pyruvate and lactate with LC-ultra violet detection[27].

A single assay measuring multiple neurochemical classes and their metabolites would remove the technical limitations that arise from the use of multiple assays. LC-mass spectrometry (MS) is well suited for measuring many components in complex samples because of its high resolution, selectivity, and sensitivity. Indeed, several LC-MS methods have been developed to allow measurements of multiple neurotransmitters and metabolites from dialysate samples[28-34]. Although MS can potentially detect neurotransmitters directly without a dedicated separation step[35], LC separation helps to pre-concentrate and remove salt and other interferences present in the dialysate that result in ionization suppression and reduced efficiency of droplet formation, which limit the number of ions reaching the detector, during electrospray ionization (ESI)[36]. The added resolving power and specificity of MS allow selective detection even if the neurochemicals are not fully resolved by LC. In tandem MS (MS/MS), a specific mass-to-charge ratio is isolated and fragmented by the addition of energy through an energetic collision with an inert gas to form unique fragments, or product ions. In multiple reaction monitoring, a second stage of MS then detects the selected product ion(s) of analytes of interest based on a selected fragmentation pathway. MS/MS decreases noise levels, thereby improving signal-to-noise ratios, which improves the limit of detection (LOD).

The combined use of LC and MS/MS provides high selectivity by utilizing retention time, mass to charge ratio, and characteristic fragmentation patterns.

Detection of small molecules in dialysate

A key to using LC-MS is that the mobile phase conditions must be compatible with ESI, i.e., mobile phases that contain low concentrations of salts and are preferably volatile. The most common form of LC, reversed phase LC (RPLC), generally has mobile phases that are compatible with ESI. However, most classical neurotransmitters are polar and poorly retained by RPLC, where retention is by hydrophobic or lipophilic interactions. Ion-pairing agents such as long-chain sulfonic acids can be used to enhance retention of polar neurochemicals on RPLC columns, e.g., with ECD; however, these agents are generally considered to be harmful to mass spectrometers and therefore this is not a desirable approach for LC-MS assays. Detection on RPLC columns has been used to detect monoamines and amino acids ranging from 0.7-30 nM for dopamine, norepinephrine, serotonin, GABA, glutamate, and lysine[30, 37].

A second option for separation of the polar compounds is hydrophilic interaction liquid chromatography (HILIC). HILIC columns utilize a polar stationary phase, similar to normal-phase LC, with a mobile phase containing water and a high percent of organic solvent such as acetonitrile[38]. Retention of analytes is based on the partitioning between mobile phase and a water-enriched layer on the hydrophilic stationary phase[39-41]. This method is advantageous because it retains polar compounds using mobile phases that are compatible with ESI-MS. As a result, it has become popular for metabolomics assays of polar metabolites. Several studies have reported detection of multiple neurochemicals by HILIC-ESI-MS[33, 42-44]. However, the detection limits achieved by HILIC-ESI-MS for

many of the neurotransmitters is modest and less than satisfactory for many dialysis samples. For example, detection of proline, glutamate, aspartate, and glycine in a single assay reported detection limits of 3-8 μM for standards on HILIC[45]. Others have reported low to moderate detection limits of dopamine, serotonin, GABA, and glutamate ranging from 0.3-190 nM concentrations[33, 44] by HILIC-MS/MS.

A third method for LC-MS of neurotransmitters is to derivatize them for RPLC. Although LC-MS can be used to detect molecules without derivatization, several benefits arise from these labeling techniques. Labels enhance retention on reversed phase columns, enabling use of columns that are more efficient, stable, and widely available than HILIC. Also, poor retention on reversed phase columns results in spectral interference and ionization suppression from salt and early eluting polar compounds. Labels can also enhance the ionization of molecules by improving droplet formation in ESI, and therefore increase sensitivity. Furthermore, if the reagent can be obtained in a stable isotope-labeled form, it is possible to make internal standards for all of the derivatized analytes. The addition of an internal standard improves quantification by accounting for variability of ionization due to the sample and drift in the MS response.

Derivatization techniques with LC-MS for small molecules in dialysate

Several reagents are suitable for enhancing neurotransmitter analysis by RPLC-MS. Primary and secondary amine-containing analytes can be labeled with formaldehyde by a dimethylation reaction[46]. Diethylation can label primary amines[30] *via* reductive amination chemistry. These reagents require 10 and 25 min incubation times, respectively. Primary and secondary amines can also be derivatized at elevated

temperatures with 7-fluoro-4-nitrobenzoxadiazole (NBD-F) prior to LC-MS[47, 48]. Amine derivatization with (5-*N*-succinimidoxy-5-oxopentyl)triphenylphosphonium bromide (SPTPP) has also been reported. This reaction requires 10 min at elevated temperatures[49, 50]. N-α-Boc-L-tryptophan hydroxysuccinimide ester only labels primary amines but is completed in 5 min at neutral pH and room temperature[51]. Derivatization of carboxylic acids with custom synthesized *p*-dimethylaminophenacyl bromide is achieved with 60 min incubation requiring quenching with tripheylacetic acid, which is resolved with RPLC[52]. Propyl chloroformate derivatization reacts with both amines and carboxylic acid groups, but is tedious since it requires solvent evaporation prior to derivatization[37]. Dansyl chloride is a useful derivatization technique employed with LC-MS to label primary amines, secondary amines, and phenolic hydroxyls[53, 54]. Dansyl chloride derivatization is typically performed at high pH and elevated temperatures, which requires 20 min for the reaction, and produces light sensitive samples[31, 54].

In this work we explore benzoyl chloride (BzCl) based on previous studies by Song *et al.*[31]. BzCl reacts with primary and secondary amines, phenols, and ribose-hydroxyl groups (Figure 1-2), allowing it to be used for a wide range of neurochemicals[31]. This reactivity is similar to dansyl chloride, but contrasts with many other reagents that are limited to labeling amines. BzCl labeling has several other advantages relative to other derivatization techniques that make it attractive. BzCl is a liquid that can be easily added to a sample. The reaction is rapid at room temperature, with samples typically requiring < 1 min sample preparation prior to analysis. Unlike dansyl chloride, derivatized samples are not light sensitive and are stable at room temperature overnight (with stability for up to 6 months when frozen at -80 °C).

Benzoylated compounds fragment easily in the mass spectrometer, generating high yield of fragment ions, thereby allowing for sensitive detection. Furthermore, heavy isotope $^{13}C_6$-BzCl is commercially available at a relatively low cost, which allows for preparation of heavy isotope labeled internal standards for all labeled compounds of interest and improves quantitative analysis.

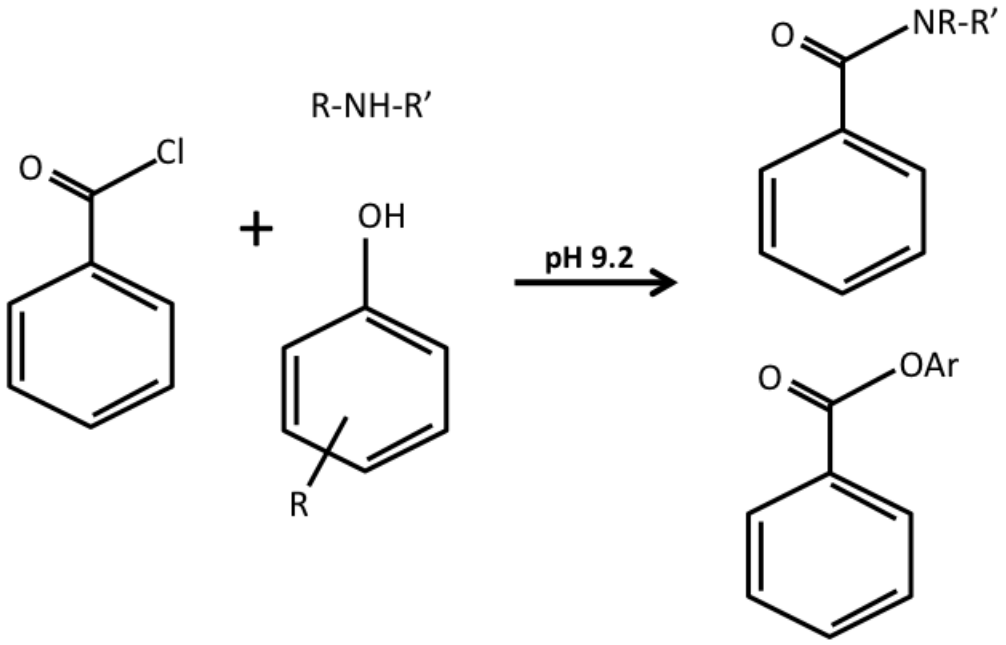

Figure 1-2 Reaction scheme of benzoyl chloride derivatization of primary and secondary amines, and phenols.

In the initial report of this method for LC-MS of neurochemicals, BzCl was used to label 16 analytes in microliter volumes of dialysate samples[31, 55]. This method detected the neurotransmitters ACh, adenosine, dopamine, norepinephrine, serotonin, histamine, glutamate, glycine, aspartate, GABA, serine, and taurine and the metabolites DOPAC, 3-methoxytyramine (3-MT), HVA, normetanephrine, and 5HIAA. ACh was not labeled, but was sufficiently ionized to yield sensitive detection in the same assay. Importantly, the assay not only labeled the amine neurotransmitters (catecholamines, indoleamines,

and amino acids) but adenosine and many metabolites as well. All of these compounds were separated in an 8 min gradient (Figure 1-3). Commercially available $^{13}C_6$-BzCl was used to generate isotope internal standards, which improved quantification and relative standard deviation for repeated sample injections. The LOD for monoamine neurotransmitters and metabolites ranged from 0.03 – 11 nM, amino acids from 2- 250 nM, 0.5 nM for ACh, 2 nM for histamine, and 25 nM for adenosine in 5 μL samples[31].

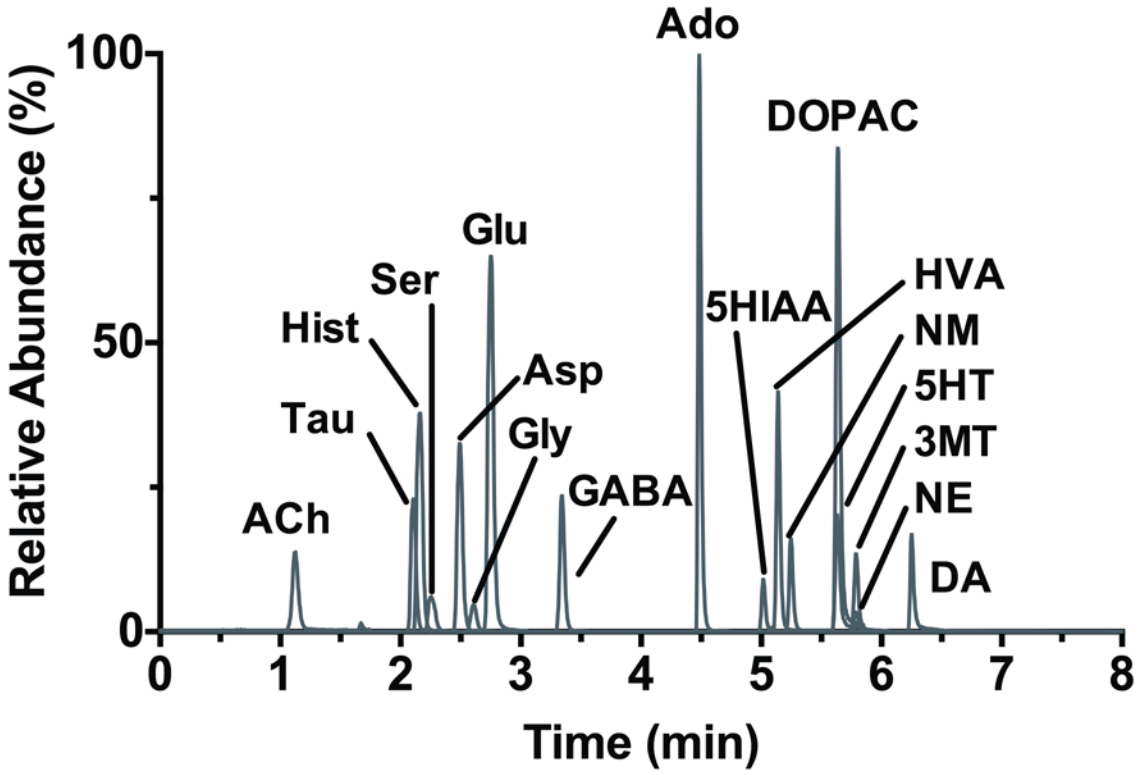

Figure 1-3 Reconstructed ion chromatogram for 17 analytes detected using benzoyl chloride derivatization.

To demonstrate that BzCl derivatization was viable for *in vivo* sampling, a dual probe microdialysis experiment of the mesolimbic pathway, i.e., the ventral tegmental area (VTA) and the nucleus accumbens (NAc), was conducted. Neurotransmitter changes were monitored locally in the VTA and distally in the NAc during a local VTA perfusion of the GABA receptor antagonist bicuculline (Figure 1-4)[31]. As expected, NAc dopamine

and metabolite DOPAC increased and GABA decreased as a result of bicuculline in the VTA; but bicuculline also resulted in unanticipated increases in serotonin, norepinephrine, glutamate, ACh, and histamine release. Locally in the VTA, bicuculline resulted in enhanced dendritic dopamine, DOPAC, serotonin, norepinephrine, ACh, adenosine, and glycine, showing the complexity of neuromodulation.

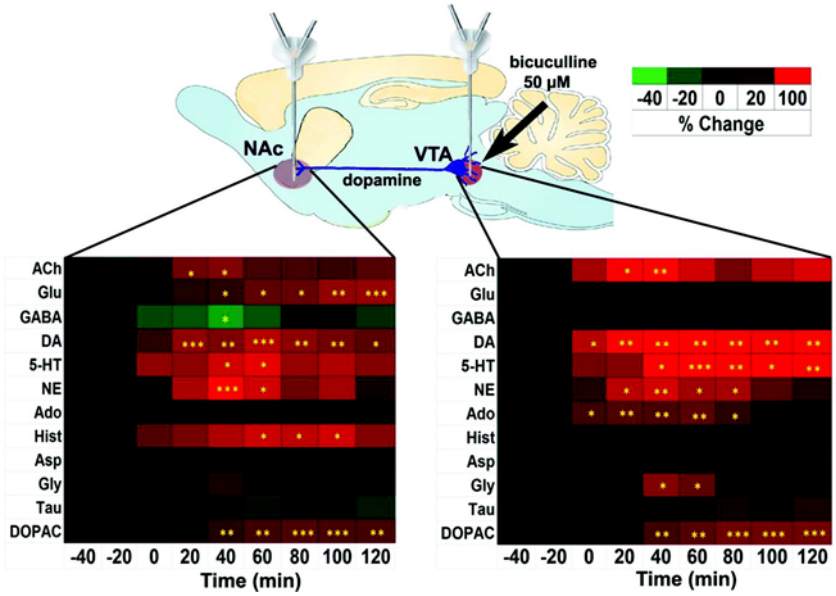

Figure 1-4 Dual probe microdialysis of the mesolimbic pathway (VTA and NAc). Neurotransmitters were monitored locally in the VTA and distally in the NAc during bicuculline (50 µM) perfusion in the VTA. The heat map shows color blocks correlating to changes in neurochemicals expressed as percent baseline. Times in the heat map are referenced to infusion of bicuculline. *$p < 0.05$, **$p < 0.01$, and ***$p < 0.001$ compared to basal level in respective brain region. Reprinted with permission from Song et al., 2012a. Copyright 2012 American Chemical Society.

While the report demonstrated a significant improvement over previous techniques with the simultaneous monitoring of 17 neurochemicals in a single fraction, this only covers a small proportion of potential neurochemical targets. One aim of this thesis is to further expand this method to monitor precursors and metabolites to study biosynthesis pathways (e.g., tyrosine and tryptophan metabolic pathways) in different sample matrixes beyond dialysate.

Detection of neuropeptides in dialysate

Neuropeptides are the largest class of neuromessengers in the central nervous system and act as neurotransmitters, neuromodulators, and hormones[56]. Monitoring neuropeptides by microdialysis is difficult because they are present at low picomolar extracellular concentrations. At these low levels, neuropeptides have traditionally been detected using immunoassays[57-60], which have low concentration LODs but require larger sample volumes and lack sequence specificity.

Capillary LC-MS (with column inner diameters of 25-100 μm) is an attractive alternative to immunoassays as it allows microliter samples to be preconcentrated into nanoliter volumes[15, 61-73]. The use of smaller bore columns also results in lower mobile phase consumption and better sensitivity due to increased ionization efficiency at low flow rates (nL/min) when coupled with ESI-MS/MS. This analytical method enables the detection of multiple analytes with sequence specificity and attomole LOD (corresponding to low picomolar concentration in microliter samples). Capillary LC-MS/MS has been used to detect endogenous neurotensin[61], leu-enkephalin (LE) and met-enkephalin (ME) surges during eating[74], dynorphin[67, 73], β-endorphin[67], angiotensin IV[66], oxytocin[68], and orexins A and B[75].

Neuropeptide processing

Neuropeptides are produced from precursor proteins, which are cleaved by various peptidases as well as convertases and undergo posttranslational modification to form bioactive peptides[76-78]. Protease-mediated prepropeptide processing into functional neuropeptides likely occurs during axonal transport of the propeptide in dense core

vesicles[79]. It is important to understand the degradation of bioactive fragments when using a targeted LC-MS assay, since these pathways may be compromised in disease states. Targeted approaches ignore other potential fragments derived from the same precursor protein, possibly missing important aspects of the neurobiology. While there are hundreds of neuropeptides that signal in the brain, the work in this thesis targets neurotensin, oxytocin, and the opioid peptides dynorphin, LE and ME.

Neurotensin is a tridecapeptide derived from a polypeptide encoded by the gene preproneurotensin/neuromedin N, which also encodes for neuromedin N[80] (Figure 1-5). Neurotensin neurons are found throughout the brain, and have been implicated in the control of feeding and regulation of the mesolimbic dopaminergic system[70, 80].

Oxytocin is a 9 amino acid polypeptide with wide ranging actions throughout the nervous system and periphery. Oxytocin is commonly studied for its role in maternity, affiliative behaviors and pair bonding[81]. The gene prepro-oxytocin/neurophysin 1 encodes for the propeptide precursor, which cleaves into oxytocin and neurophysin (Figure 1-5).

Opioid peptides are produced by the processing of four distinct genes: preproopiomelanocortin, preproenkephalin, preprodynorphin (also referred to as preproenkephalinB), and prepronociceptin/orphanin FQ[82, 83]. Proopiomelanocortin encodes for opioid peptide β-endorphin, and non-opioid peptides adrenocorticotropic hormone, α-melanocyte-stimulating hormone, and β-lipotropic pituitary hormone[82]. Pronociceptin/orphanin FQ encodes for a single copy of nociception, nocistatin, and orphanin FQ2[83, 84].

Both prodynorphin and proenkephalin are inactive precursors that require protease processing to produce biologically functional peptides[85, 86] (Figure 1-5). Prodynorphin products include neoendorphin, dynorphin A, dynorphin B, and bridge peptide domain sequences[86]. Proenkephalin contains four copies of ME, two extended copies of ME, and one copy of LE[87, 88]. While prodynorphin contains five LE sequences, prodynorphin products (i.e. dynorphin A and dynorphin B) rarely co-localize with LE due to the lack of cleavage of the dibasic Arg-Arg sequence[85, 86, 89]. Proenkephalin is the primary source of LE, even though it contains only one copy of the LE sequence, which is confirmed by LE immunoreactivity colocalized with ME[86].

The extent of pro-hormone processing depends on the available endoproteases in a given cell type and brain region. Disruption of peptide metabolism has been implicated in depression, anxiety, addiction, and diseases such as Parkinson's disease[90-93]. Traditional methods of peptide detection, such as immunoassays, often cannot discern between fragments due to lack of specificity, highlighting the advantage of untargeted LC-MS^n assays or targeted assays if the fragments can be predicted.

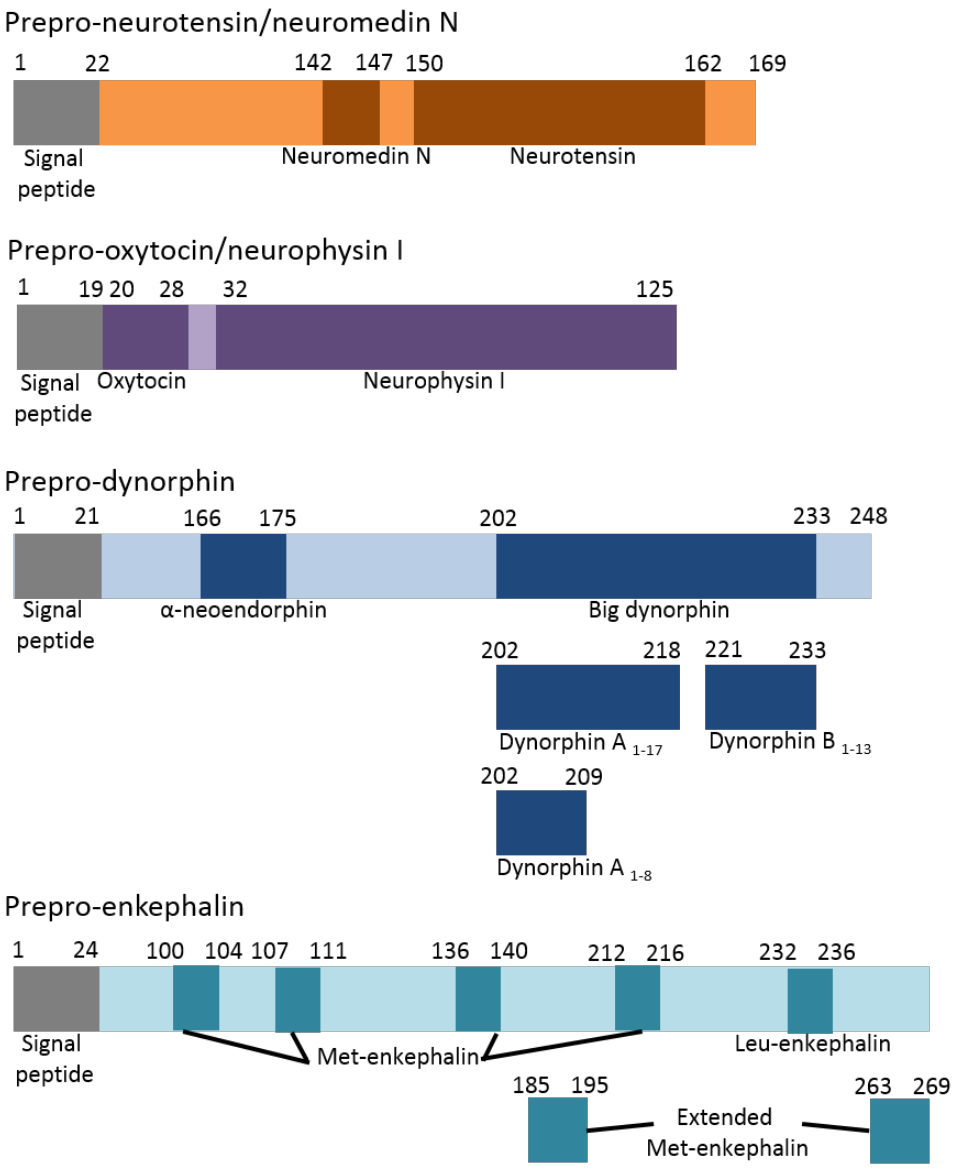

Figure 1-5 Graphical representation of precursor polypeptides with their respective peptide fragments. Fragments can be processed further to form smaller peptides. Not drawn to scale.

Capillary LC-MS of neuropeptides in dialysate

Several variations of capillary LC-MS have been employed to detect endogenous neuropeptides in dialysate. Table 1-1 lists various capillary LC-MS setups researchers have used to measure neuropeptides from dialysate or similar matrix. To achieve rapid preconcentration and desalting online prior to MS detection, a trap column with a wider

i.d. than the small bore analytical column can be used with high flow rates (μL/min), followed by back flushing the sample onto an analytical column and elution with lower flow rates (nL/min)[66, 69]. Dialysate samples can also be preconcentrated and desalted on a single analytical column to reduce dead volume[61, 63]. Ideally, samples would be quickly desalted and preconcentrated using higher flow rates. However, this can be challenging if a single column and pump are employed as the pump equilibration time would be ~20 min before using lower flow rates for elution. Conversely, if an LC pump desalted and preconcentrated a 5 μL sample at 100 nL/min, samples would take 50 min to load onto a column, which reduces sample throughput.

With our current capillary LC-MS setup, microliter samples are injected onto a single reverse phase capillary column for trapping and elution. We use 50 μm i.d. capillary columns packed in-house with C18 particle slurry suspended in acetone and water[70, 73]. The columns are connected by a Teflon union to a disposable emitter tip, allowing for column re-use if the tip is clogged. This setup typically allows for more than 80 injections per column. Analytes are stacked at the head of the packed bed and the sample is desalted and preconcentrated at high flow rates (μL/min) using a low elution strength solvent. A second LC pump is used to deliver an elution gradient, which allows for separation of multiple analytes at a slower flow rate (nL/min), and is more amenable to ESI. A six-port valve enables quick switching from high-to-low flow rates without waiting for pump equilibration.

Table 1-1 Instruments and column configurations used in capillary LC-MS to analyze neuropeptides.

Mass Spectrometer		LC Instruments	Trap Column	Analytical Column	Injection Volume	Peptide	Reference
Ion Trap	LTQ-XL (ThermoFisher)	Haskel high-pressure pump (Haskel Inc.) MicroPro (Eldex Laboratories)	n/a	25 μm i.d. × 4 cm, 5 μm C18 (Altima, Alltech)	5 μL	Dynorphin Enkephalins Endorphins	67
			n/a	25 μm i.d. × 10 cm, 5 μm C18 (Altima, Alltech)	5 μL	Enkephalins	94
			n/a	50 μm i.d. × 4 cm, 5 μm C18 (Altima, Alltech)	5 μL	Arg-Vasopressin Oxytocin	68
			n/a	50 μm i.d. × 3 cm, 5 um C18 (Altima, Alltech)	7.5 μL	Dynorphin Enkephalins	74
		ISCO 100D (Teledyne Isco) Agilent 1100 (Agilent)	n/a	75 μm i.d. × 4 cm, 5 μm C18 (Altima, Alltech)	8 μL	Dynorphin Enkephalins Endorphins Neurotensin Orexins	75
			n/a	50 μm i.d. × 3.5 cm, 5 μm C18 (Altima, Alltech)	5 μL	Neurotensin	70
		Ultimate 3000 (Dionex)	200 μm i.d. × 5 mm, monolith (PS-DVB, LC Packings)	100 μm i.d. × 5 cm, monolith (PepSwift, PS-DVB, LC Packings)	Not specified	Untargeted proteins and peptides	95

Mass Spectrometer		LC Instruments	Trap Column	Analytical Column	Injection Volume	Peptide	Reference
IonTrap	LCQ Deca XP Plus (Thermo Fisher)	ISCO 100D (Teledyne Isco) Waters 626 pump (Waters)	n/a	75 μm i.d. × 3.6 cm, 10 μm C18 (Altima, Alltech)	5 μL	DynorphinEnkephalins	[73]
		Haskel DSFH-151 (Haskel Inc.) ISCO 100D (Teledyne Isco)	n/a	25 μm i.d. × 2 cm, 5 μm C18 (Altima, Alltech)	1.8 μL	Enkephalins	[65]
		Haskel high-pressure pump (Haskel Inc.) MicroPro (Eldex Laboratories)	n/a	25 μm i.d. ×2 cm, 5 μm C18 (Altima, Alltech)	2.5 μL	Enkephalins	[96]
	HCTultra (Bruker Daltonics)	CapLC (Micromass)	n/a	300 μm i.d. × 15cm, 3 μm C18 (Acclaim PepMap100, Dionex)	1 μL	Angiotensin Bradykinins Neurotensin	[97]
Orbitrap	Orbitrap (ThermoFisher)	Ultimate 3000 (Dionex)	300 μm i.d. × 5 mm, 5 μm C18 (Pepmap™, LC Packings)	75 μm i.d. ×15 cm C18 (Gemini C18, Phenomenex)	Not specified	Untargeted proteins and peptides	[95]

Mass Spectrometer		LC Instruments	Trap Column	Analytical Column	Injection Volume	Peptide	Reference
Q-TOF	Q-TOF (Micromass-Waters)	nanoACQUITY UPLC (Waters)	n/a	75 μm i.d. ×10 cm, 3 μm C18 (Magic, Michrom)	Not specified	(Crab) Bradykinin Somatostatin Substance P	98
		Waters capillary LC system	300 μm i.d × 1 mm, 5 μm C18 (Pepmap™, LC Packings)	75 μm i.d. ×15 cm, 3 μm C18 (Microsil nano C18, Microtech Scientific)	1 - 3 μL	(Crab) Allatotatins Orcokinins Tachykinin	62
		JASCO	n/a	75 μm i.d. × 3 cm, 10 μm C18 (ODS-AQ 120A S-10, YMC Co.)	10 μL	Dynorphin	91
	Q-TOF Ultima (Waters)	Ultimate 3000 (Dionex)	300 μm i.d. × 5 mm, 5 μm C18 (Pepmap™, LC Packings)	75 μm i.d. ×15 cm C18 (LC Packings)	Not specified	Untargeted proteins and peptides	95
	Q-TOF hybrid Quadrupole (Micromass)	Ultimate (Dionex)	500 μm i.d. ×15 mm, strong cation exchange (Bio-SCX, LC Packings) C18 (μ-guard MGU-30, LC Packings)	100 μm i.d. × 10 cm, 3 μm C18 (Atlantis, Waters)	20 μL	(Caenorhabditis elegans) Untargeted, peptides	99

Mass Spectrometer		LC Instruments	Trap Column	Analytical Column	Injection Volume	Peptide	Reference
QQQ	Quattro Premier (Micromass-Waters)	nanoACQUITY UPLC (Waters)	180 μm i.d. × 20 mm, 5 μm C18 (Symmetry® C18, Waters)	100 μm i.d. ×10 cm, 1.7 μm C18 (ACQUITY UPLC® BEH 130, Waters)	5 μL	Neuromedin Neurotensin	[69]
		Ultimate™ quaternary (LC Packings, Dionex)	300 μm i.d. × 5 mm, 5 μm C18 (Pepmap™, LC Packings)	75 μm i.d. ×15 cm, 3 μm C18 (Pepmap™, LC Packings)	10 μL	Angiotensin Enkephalins Neurotensin	[66]
	Xevo TQ-S (Waters)	nanoACQUITY UPLC (Waters)	180 μm i.d. × 20 mm, 5 μm C18 (Symmetry® C18, Waters)	100 μm i.d. ×10 cm, 1.7 μm C18 (ACQUITY UPLC® BEH 130, Waters)	5 μL	Neuromedin Neurotensin	[69]
	Finnigan TSQ700 (Finnigan)	Not specified	n/a	50 μm i.d. ×2 cm, 10 μm C18 (YMC Co.)	10 μL	Enkephalin Neurotensin	[63]
		Not specified	n/a	50 μm i.d. × 10 cm, 10 μm C18 (YMC Co.)	10 μL	Neurotensin	[61]

Improving the repeatability of neuropeptide measurement in dialysate samples

Capillary LC-MS provides exquisite sensitivity, peptide sequence specificity, and potential for multiple peptide monitoring. However, low recovery from the probes and surfaces of the analytical system can prevent realization of neuropeptide detection. Several methods have been applied to improve relative recovery, including using probes with high MWCO membranes, push-pull microdialysis[100, 101], and affinity-enhanced microdialysis[98, 102-104]. Our recent studies using AN69 membrane demonstrate that membrane surface modification can dramatically alter recovery. AN69 is a copolymer of acrylonitrile and sodium methallylsulfonate, with an 80 kDa MWCO[105]. While the MWCO of AN69 is large, the copolymer composition of the membrane yields a negative charge due to embedded sulfonate groups, which may cause electrostatic interactions with peptides that have an overall positive charge (e.g., dynorphin A_{1-17}, mouse β-endorphin, and orexin B). Treatment of the dialysis membrane with polyethylenimine neutralized these negative charges and improved *in vitro* probe recovery 1.2 to 80 fold for a series of neuropeptides with a net positive charge[75].

Beyond recovery through the dialysis probe, sample loss due to adsorption during transport from the probe to the LC column can reduce detectability and reproducibility as well as increase carryover[75, 106]. Several studies show that addition of organic solvents such as ethanol[107], methanol[108], dimethylsulfonate[72], or acetonitrile[75, 106] to samples improves reproducibility and reduces carryover of peptides by reducing adsorption in LC lines during injection.

Polyethylenimine treatment of AN69 dialyzing membranes improves sample recovery and the addition of acetonitrile to samples and reduces sample loss due to

adsorption; these changes dramatically increased the detectability of some neuropeptides *in vivo*[75]. However, these techniques were only applied to a small number of neuropeptides in a preliminary study with potassium stimulation, and are yet to be fully tested with pharmacologic manipulations or behavioral applications.

Applications of LC-MS for dialysate analysis: Neurochemical monitoring during selective neuronal stimulation

While microdialysis is a powerful technique, it has been previously limited to examining the effects of drugs on neurotransmitter release, and to better understand processes underlying behavioral changes, such as feeding, pain, and drug self-administration[109]. However, advancements in molecular biology and transgenic techniques have provided novel ways to selectively activate or inhibit specific neuronal populations *in vivo* with external stimuli. The ability to modulate activity of neurons on command provides researchers with precise tools to parse out the underlying functions of neuronal circuits. Techniques for selective stimulation include optogenetics and designer receptors exclusively activated by designer drugs (DREADDs)[110, 111]. Work in this thesis combines both of these powerful selective stimulation techniques with microdialysis samples and analytical techniques to elucidate specific neuronal contributions to behavior and disease (see Chapters 3 and 4).

Optogenetics utilizes engineered ion channels and pumps (e.g., channel rhodopsin-2 and halorhodopsin) that are activated by light to selectively activate or silence neuronal activity *in vivo*[111]. Activation of channel rhodopsin-2 and halorhopsin *in vivo* is obtained *via* pulsed laser light through a fiber optic implanted near neurons

expressing these receptors. The temporal and spatial precision of optogenetic techniques allows for near instantaneous modulation of neuronal firing[112]. For example, optogenetics has been used to study the roles of specific neuronal populations in both normal physiological functions (e.g., basal ganglia-mediated control of motor output[113]), and disorders such as obsessive-compulsive disorder and drug seeking[114, 115].

Another technique for selective stimulation is DREADDs. DREADDs utilize modified G protein-coupled receptors (e.g., altered muscarinic receptors) that are activated by systemic administration of otherwise biologically inert compounds such as clozapine-N-oxide (CNO)[110, 116]. Selective expression of these receptors on neurons of interest allows for specific activation or inhibition of specific neuronal subsets. DREADDs works on longer time scales (minutes to hours) than optogenetics, in part due to the systemic route of CNO administration. However, activation and inhibition of neurons utilizing DREADDs technology is less invasive than optogenetics because receptor activation can be achieved through a systemic injection and without implantation of a fiber optic in the brain. DREADDs has been used to demonstrate that orexin and GABAergic neurons modulate sleep-wake cycles, and that D2-expressing striatal medium spiny neurons modulate cocaine self-administration in mice[117, 118].

These powerful techniques are often combined with behavioral, pharmacological, and *ex vivo* studies to further evaluate the physiological circuits and disease states under examination. However, while these studies allow selective stimulation, the actual neurotransmitter dynamics that result from such treatments typically have been inferred without direct measurements. Direct *in vivo* measurements of neurochemical dynamics with these selective stimulation techniques in awake, behaving animals have been

scarce[70, 119-122]. *In vivo* neurochemical monitoring is imperative to understand the relationship between neuronal activation and neurochemistry[123]. Selective modulation of discrete neuronal populations can potentially alter many different neurochemicals such as monoamines, amino acids, and neuropeptides. Local and distal measurements relative to the site of activation provide important information to help elucidate the role of neurochemical signaling in circuits. For example, extracellular glutamate and dopamine were measured in the NAc shell after optogenetic stimulation of glutamatergic terminals in the infralimbic cortex, showing a connection between these two regions[124].

In vivo neurochemical monitoring has been coupled with optogenetic stimulation to investigate catecholamines using carbon fiber electrodes with fast scan cyclic voltammetry[125], and microdialysis with LC-ECD[126, 127]. While these reports show neurochemical changes correlating with optical stimulation, the detection assays monitored single analytes, precluding the discovery of other related neurochemical alterations. Optogenetics coupled to MS has not yet been reported. The multi-analyte capabilities of LC-MS would provide a more comprehensive understanding of the multifaceted dynamic changes with optogenetic stimulations. Furthermore, the power of a comprehensive analysis of both neuropeptides and small molecules would establish the roles of different neural systems in behavior.

Dissertation overview

Improvements in monitoring small molecules and neuropeptides will yield new frontier and discoveries in neuroscience. As described in Chapter 2, derivatization conditions were modified to improve sensitivity and to expand a BzCl small molecule assay to detect other metabolites including amino acids, polyamines (e.g. putrescine, spermidine, spermine), compounds from catecholamine biosynthesis pathways (e.g. tyrosine and tryptophan metabolic pathways), and trace amines (e.g., tyramine, octopamine, synephrine). The assay was also used to analyze dialysate, plasma, and CSF samples. Thus, this method is easily employed for a wide range of samples and essentially can be used for any classical neurotransmitter or metabolite.

Chapters 3 and 4 focus on using complementary techniques to interrogate small molecule and neuropeptide dynamics with pharmacogenetic techniques to provide a more in-depth understanding of neurochemical interactions in multiple brain circuits. In Chapter 3, designer receptors exclusively activated by designer drugs were used in mice to investigate how a population of neurotensin neurons originating in the lateral hypothalamic area modulate the mesolimbic dopamine system (dopamine neurons in the ventral tegmental area that project to the nucleus accumbens). In Chapter 4, optogenetic techniques and analytical assays monitoring small molecules and opioid peptides were used to create a neurochemical profile within discrete sub-regions of the nucleus accumbens.

Chapters 5 and 6 describe the use of these small molecule and neuropeptide monitoring techniques, which were applied to elucidate pathophysiological changes in and a potential symptomatic treatment of a rat model of Parkinson's disease.

Advancements in spatial and temporal resolution combined with improvements in analytical methods will improve the sensitivity and selectivity for detecting multiple analytes in a single assay. Chapter 7 summarizes the findings in this thesis, and proposes potential future directions for the continuation of this work. These multiplexed approaches will advance our understanding of the complex processes underlying neuronal function at the molecular and circuit levels and will provide an improved set of experimental tools to enable better understanding of outstanding questions in neuroscience.

CHAPTER 2: BENZOYL CHLORIDE DERIVATIAZATION WITH LIQUID CHROMATOGRAPHY MASS SPECTROMETRY FOR TARGETED METABOLOMICS OF NEUROCHEMICALS IN BIOLOGICAL SAMPLES

Reproduced in part from Wong, Malec *et al*. Journal of Chromatography A 2016, 1446, 78 - 90.

Equal authorship was awarded to Wong and Malec. Specific contributions from Wong to this work included optimization of derivatization reagents, selection of compounds assayed, gradient optimization, and applications in rat dialysate and human cerebrospinal fluid.

Introduction

Metabolomics is a valuable approach for studying physiological mechanisms and identifying biomarkers. Both untargeted and targeted assays, also called metabolite profiling, are used in such studies. Targeted assays measuring a limited number of metabolites allow focus on important known compounds or pathways and offer better quantification, but they provide lower metabolome coverage compared to untargeted methods. Targeted assays that measure relatively large numbers of compounds (i.e., over 50) help mitigate the disadvantage of limited metabolome coverage. Gas chromatography-mass spectrometry (MS) and high performance liquid chromatography (HPLC)-MS are well-suited platforms for developing such widely targeted assays. Several methods for measuring over 100 known metabolites in a single assay using these techniques have been reported [129-134]. These widely targeted assays are powerful, but they rarely use more than a few internal standards, and for HPLC often make use of ion-pairing reagents[131, 134] or multiple LC pumps[132, 133] to account for the wide polarity range of the metabolites. Here we report a targeted method for 70 neurochemicals that uses

HPLC-MS/MS with benzoyl chloride (BzCl) as a derivatizing agent and avoids these limitations.

HPLC- tandem mass spectrometry (MS/MS) using a triple quadrupole mass spectrometer is well established as a sensitive, quantitative, and selective technique for metabolite profiling[135, 136]. Although compounds can be detected by MS/MS without labeling, the use of BzCl provides numerous advantages with only minor drawbacks. In particular, addition of a phenyl group to the polar analytes increases retention on reversed phase columns, which aids resolution and decreases ion suppression. Many compounds are detected with greater sensitivity after labeling, e.g. 1,000-fold increases in sensitivity have been reported for BzCl labeling[31]. The labeling step allows rapid creation of stable-isotope labeled internal standards by using ^{13}C-BzCl for labeling standards, thereby improving quantification for every analyte. BzCl is widely applicable because it derivatizes primary and secondary amines, phenols, thiols, and some alcohols (e.g., ribose hydroxyls and glucose). Indeed, it has previously been used with MS or ultraviolet absorption detection for monitoring neurochemicals in dialysate[31, 34], plasma[34], and human cerebrospinal fluid (CSF)[137]. It has also been used for other amine[138, 139] and alcohol[140, 141] containing compounds. These previous assays targeted a relatively narrow group of compounds.

Although we focus on BzCl, other reagents such as dansyl chloride may provide similar utility for metabolomics[51, 53, 54, 142]. We favor BzCl because it reacts faster (seconds at room temperature compared to 20 min at elevated temperature), has a wider pH range for reaction, is less prone to photodegradation, and is commercially available in ^{13}C-labeled form. Additionally benzoylated products are stable for a week at room

temperature[31], and standards and internal standards are stable for six months at -80°C (data not shown).

The 70 compound assay described here targets neurochemicals. Neurons specialize in storing and transmitting information using neurotransmitters and neuromodulators. Low molecular weight polar compounds represent an important class of neurotransmitters including acetylcholine, adenosine, catecholamines, indoleamines, amino acids, trace amines, and dipeptides. A variety of other compounds, such as energy metabolites, antioxidants, and polyamines that affect neuronal function or have been linked to neurological disease are also included in the assay (a complete list of the compounds included in the assay and their functions is in Table 2-1). This assay focuses on these compounds and their precursors and degradation products, as their measurement can provide insights into neuronal function to better understand the neurochemical changes in brain diseases. Although this is not a comprehensive assay for all neurochemicals, it demonstrates the wide applicability of BzCl derivatization. The method is an improvement over previous neurochemical assays which were limited to even smaller subsets of neurochemicals[28, 29, 32-34, 44, 45, 143], including our previously described 17 compound method based on similar technology[31].

This report demonstrates the utility of BzCl with HPLC-MS for targeted metabolomics on several sample types including tissue, serum, CSF, and microdialysate. Tissue samples are used to characterize concentrations at fixed time points and are best used for determining the overall production and metabolism of neurochemicals. We demonstrate the assay for *Drosophila melanogaster* tissue and hemolymph, an important neurochemical model system. Serum and CSF assays are useful for biomarker studies and

assessment of overall physiological state. Microdialysis samples the brain extracellular space and enables the measurement of released neurochemicals over time, making it valuable for correlating neurochemical dynamics to behavior, monitoring drug effects, and assessing the effect of disease states on neurochemical concentrations. However, the low samples volumes of microdialysate in our studies (typically 1 μL) make analysis challenging.

Although BzCl labeling with HPLC-MS/MS has been used for neurochemicals before, the current work increases the number of analyzed compounds by 4-fold, streamlines reagent addition, and improves labeling conditions to give better sensitivity and reproducibility for some compounds. Finally, the assay is shown to be useful for a wider range of sample types.

Table 2-1 Relevance of 70 compounds assayed and reported literature concentrations.

Abbreviation	Analyte	Relevance	Reference
DOMA	3,4-Dihydroxymandelic acid	Minor NE metabolite	144
DOPAC	3,4-Dihydroxyphenylacetic acid	DA metabolite	31
LDOPA	3,4-Dihydroxyphenylalanine	DA precursor	145
DOPEG	3,4-Dihydroxyphenylglycol	NE Metabolite	146
3HAA	3-Hydroxyanthranilic acid	Kyn metabolite	147
3HK	3-Hydroxykynurenine	Neurotoxic Kyn metabolite	148
MOPEG	3-Methoxy-4-hydroxyphenylglycol	NE Metabolite	149
3MT	3-Methoxytyramine	DA metabolite	31
GABA	4-Aminobutyric acid	Neurotransmitter	31
5HIAA	5-Hydroxyindoleacetic acid	5HT metabolite	31
5HTP	5-Hydroxytryptophan	Trp metabolite; 5HT precursor	150
5HTOL	5-Hydroxytryptophol	5HT metabolite; Marker of alcohol consumption	151
ACh	Acetylcholine	Neurotransmitter	31
Ado	Adenosine	Nucleoside; Neurotransmitter	31
Agm	Agmatine	Polyamine; Potential neurotransmitter	152
Ala	Alanine	Amino acid	153
Ans	Anserine	Dipeptide antioxidant	154
Arg	Arginine	Amino acid; Polyamine Precursor	155
Asn	Asparagine	Amino acid	156
Asp	Aspartate	Neuroactive amino acid	31
BAla	β-Alanine	Neuroactive isomer of Ala	157
Carn	Carnosine	Dipeptide antioxidant	154
Ch	Choline	Precursor to ACh	158
Cit	Citrulline	Intermediate in urea cycle	159

Abbreviation	Analyte	Relevance	Reference
CA	Cysteic acid	Cys metabolite; Tau precursor	160
Cys	Cysteine	Neuroactive amino acid	161
DA	Dopamine	Neurotransmitter	31
E	Epinephrine	Neurotransmitter; NE metabolite	162
ETA	Ethanolamine	Widely distributed amine	163
Glc	Glucose	Primary source of energy	164
Glu	Glutamate	Neuroactive amino acid	31
Gln	Glutamine	Neuroactive amino acid	153
GSH	Glutathione	Tripeptide antioxidant	161
Gly	Glycine	Neuroactive amino acid	31
Hist	Histamine	Neurotransmitter	31
His	Histidine	Amino acid; Hist Precursor	165
HCA	Homocysteic acid	Potential neurotransitter; Can induce seizures	166
HCY	Homocysteine	Met metabolite; Potential neurotransmitter	167
HSer	Homoserine	Nonproteinogenic amino acid	168
HVA	Homovanillic acid	DA metabolite	31
HTau	Hypotaurine	Potential antioxidant	169
KA	Kynurenic acid	Neuroprotective Kyn metabolite	170
Kyn	Kynurenine	Trp metabolite	148
Kyo	Kyotorphin	Dipeptide; Role in pain regulation	171
Leu	Leucine	Amino acid	172
Lys	Lysine	Amino acid	172
Met	Methionine	Amino acid	172
NAP	N-Acetylputrescine	Polyamine	173
NAS	N-Acetylserotonin	5HT metabolite; Melatonin precursor	174

Abbreviation	Analyte	Relevance	Reference
NE	Norepinephrine	Neurotransmitter; DA metabolite	31
NM	Normetanephrine	NE Metabolite	31
OA	Octopamine	Trace amine; TyrA metabolite	175
Orn	Ornithine	Intermediate in urea cycle	172
PhEt	Phenethylamine	Trace amine; Phe metabolite	176
Phe	Phenylalanine	Amino acid; Precursor to catecholamines	177
Pro	Proline	Amino acid	154
Put	Putrescine	Polyamine	172
Ser	Serine	Neuroactive amino acid	31
5HT	Serotonin	Neurotransmitter	31
Spd	Spermidine	Polyamine	178
Spm	Spermine	Polyamine	178
Syn	Synephrine	OA metabolite	179
Tau	Taurine	Neurotransmitter	31
Thr	Threonine	Amino acid	172
TrpA	Tryptamine	Trace amine; Trp metabolite	176
Trp	Tryptophan	5HT precursor; Kyn precursor	177
TyrA	Tyramine	Trace amine	176
Tyr	Tyrosine	Amino acid; Precursor to catecholamines	177
Val	Valine	Amino acid	172
VMA	Vanillylmandelic acid	NE Metabolite	180

Experimental

Chemicals and reagents

All chemicals were purchased from Sigma Aldrich (St. Louis, MO) unless otherwise noted. Water, methanol, and acetonitrile for mobile phases are Burdick & Jackson HPLC grade purchased from VWR (Radnor, PA). Stock solutions of 500 mM Glc; 10 mM DOMA, DOPAC (Acros Organics, Geel, Belgium), MOPEG, GABA, 5HIAA, 5HTP, Agm, Ala, Ans, Arg, Asn, Asp, βAla, Carn, Cit, CA, Cys, DA, E, ETA, Glu, Gln, GSH, Gly, Hist, His, HCA, HCY, HSer, HVA (Tocris, Bristol, UK), HTau, Kyo (MP Biomedicals, Santa Ana, CA), Leu, Lys, Met, NAP, NAS, NE, NM, OA, Orn (Acros Organics, Geel, Belgium), PhEt (MP Biomedicals, Santa Ana, CA), Pro, Put, Ser, 5HT, Spd, Spm, Syn, Tau, Thr, Val, and VMA; 5 mM ACh, 5HTOL (Cayman Chemical, Ann Arbor, MI), Ado, Kyn, LDOPA, Phe, and Trp; 2.5 mM 3HK; 2 mM Tyr; 1 mM DOPEG, 3HAA, 3MT, KA, and TyrA; 0.25 mM TrpA; and 20 mM isotopically labeled d4-ACh and d4-Ch (C/D/N isotopes, Pointe-Claire, Canada); were made in HPLC water and kept at -80 °C. A standard mixture was diluted from stocks with artificial cerebrospinal fluid (aCSF) consisting of 145 mM NaCl, 2.68 mM KCl, 1.4 mM $CaCl_2$, 1.0 mM $MgSO_4$, 1.55 mM Na_2HPO_4, and 0.45 mM NaH_2PO_4 adjusted pH to 7.4 with NaOH. Calibration curves were made using standards at 0.1, 0.5, 1, 5, 10, 25, 50 μM for Glc; 10, 50, 100, 500, 1000, 250, 5000 nM for 3HK, Asn, Asp, CA, GSH, Gly, HTau, Ser, and Tau; 1, 5, 10, 50, 100, 250, 500 nM for Ch, 3HAA, MOPEG, 5HIAA, 5HTP, 5HTOL, Ado, Agm, Ala, Ans, βAla, Carn, Cit, Cys, ETA, Glu, Gln, His, HCA, HCY, HSer, HVA, KA, Kyn, Met, NAP, Orn, Phe, Pro, Thr, Trp, Val, and VMA; 0.1, 0.5, 1, 5, 10, 25, 50 nM for ACh, DOMA, DOPAC, DOPEG, 3MT, GABA, Arg, DA, E, Hist,

Kyo, LDOPA, Leu, Lys, NAS, NE, NM, OA, PhEt, Put, 5HT, Spd, Spm, Syn, TrpA, TyrA, and Tyr. An internal standard stock was prepared with 5 mM Glc; 500 μM 3HK, Asn, Asp, CA, GSH, Gly, HTau, Ser, and Tau; 50 μM 3HAA, MOPEG, 5HIAA, 5HTP, 5HTOL, Ado, Agm, Ala, Ans, βAla, Carn, Cit, Cys, ETA, Glu, Gln, His, HCA, HCY, HSer, HVA, KA, Kyn, Met, NAP, Orn, Phe, Pro, Thr, Trp, Val, and VMA; 5 μM DOMA, DOPAC, DOPEG, 3MT, GABA, Arg, DA, E, Hist, Kyo, LDOPA, Leu, Lys, NAS, NE, NM, OA, PhEt, Put, 5HT, Spd, Spm, Syn, TrpA, TyrA, and Tyr; and derivatized with $^{13}C_6$-BzCl using a similar procedure as ^{12}C reagents.

Calibration standard and internal standard stocks were frozen at -80 °C in aliquots to prevent multiple freeze/thaw cycles. A single internal standard stock aliquot was thawed the day of use, diluted 100-fold in 20% (v/v) acetonitrile containing 1% (v/v) sulfuric acid, and spiked with deuterated acetylcholine and choline (C/D/N isotopes, Pointe-Claire, Canada) to a final concentration of 20 nM. A fresh benzoyl chloride solution was made daily.

Microdialysis in anesthetized rat

Adult male Sprague-Dawley rats (Harlan, Indianapolis, IN) weighing 250-275 g were used for microdialysis collection. Rats were housed with access to food and water *ad libitum* in a temperature and humidity controlled room with 12 h light/dark cycles. All animals were treated as approved by the University Committee on Use and Care of Animals at the University of Michigan, the National Institute of Health Guidelines for the Care and Use of Laboratory Animals. All precautions were taken to prevent animal

discomfort through the course of the experiments. In addition, all animal experiments were conducted within the guidelines of Animal Research Reporting *in vivo* Experiments.

A custom-made concentric microdialysis probe (4 mm dialyzing membrane), made using regenerated cellulose (Spectrum Laboratories, Inc., Rancho Dominguez, CA, USA) was implanted into the striatum. Rats were anesthetized with 1-4% isoflurane and placed into a stereotaxic frame (David Kopf, Tujunga, CA). A burr hole was placed above the striatum using the anterior-posterior +1.0 mm and lateral ±3.0 mm coordinates from bregma. The microdialysis probe was flushed with artificial CSF (aCSF) at a flow rate of 2 μL/min using a Fusion 400 syringe pump (Chemyx, Stafford, TX) as it was lowered 6.15 mm from top of skull. Once the probe was positioned, the probe was flushed at 2 μL/min for 30 min followed by 30 min at 1.0 μL/min prior to collection. Ten μL dialysate was derivatized using the modified method reported: 5 μL of 100 mM sodium carbonate, 5 μL BzCl (2% (v/v) in acetonitrile), and 5 μL internal standard mixture were added sequentially, with vortex mixing after each addition. At the completion of the experiment, animals were euthanized, brains were extracted and stored at 4 °C in 4% paraformaldehyde. Probe placement was confirmed with histology.

Human CSF

Pooled human CSF from healthy patients was obtained from the Batemen lab at Washington University School of Medicine, St. Louis, MO[181]. Samples were diluted 100-fold in water, and a 10 μL aliquot was derivatized using 5 μL of 100 mM sodium carbonate, 5 μL BzCl (2% (v/v) in acetonitrile), and 5 μL internal standard mixture before LC-MS analysis.

Human serum

Pooled human serum from the American Red Cross Detroit National Testing Lab was provided by the Michigan Regional Comprehensive Metabolomics Resource Core. To remove proteins, 20 µL of serum were diluted with 80 µL of ice-cold acetonitrile. The samples were vortexed briefly, then centrifuged for 10 min at 12,100 × g. 20 µL of the supernatant was derivatized by sequential addition of 10 µL of 100 mM sodium carbonate, 10 µL of BzCl (2% (v/v) in acetonitrile), and 10 µL of the internal standard mixture. Fifty µL of water were added to reduce the organic content of the samples. Calibration standards were prepared in aCSF, which is similar in composition to serum without proteins[182]. Five µL aliquots of the standards were diluted with 20 µL acetonitrile to match the sample composition, and then derivatized in the same manner as the serum supernatant.

Fly tissue homogenate

Homogenized *Drosophila* samples were provided by the Pletcher lab at the University of Michigan, Ann Arbor. Female flies were treated with 250 µM 5HTP for four days prior to harvesting. The flies were snap frozen in liquid nitrogen and vortexed to remove heads. The heads were homogenized in 4 µL of ice cold acetonitrile per head, and 20 µL ice-cold acetonitrile per body, using a pestle grinder. The homogenate was centrifuged at 18,000 × g for 5 min and the supernatant was removed and stored at -80 °C until derivatization. 20 µL of the supernatant was derivatized by sequential addition of 10 µL of 100 mM sodium carbonate, 10 µL of BzCl (2% (v/v) in acetonitrile), and 10 µL of the internal standard mixture. Finally, 50 µL of water were added to reduce the organic

content of the samples. Calibration standards were prepared in aCSF. Five µL aliquots of the standards were diluted with 20 µL acetonitrile to match the sample composition, and then derivatized in the same manner as the tissue homogenate supernatant.

Fly hemolymph

Hemolymph from *Drosophila* was provided by the Dus lab at the University of Michigan. Flies were reared in standard cornmeal-glucose medium at 25 °C in a 12:12 light/dark cycle. After eclosion groups of 100 $w1118^{CS}$ (*w1118* backcrossed to *CS* for 10 generations) males were placed in bottles and aged for 7-10 days until the time of hemolymph collection. Fresh food was provided every 2 days.

Hemolymph collection was performed as previously described, with modifications to the sated condition[183]. *w118CS* males in groups of 100 were moved into bottles containing agar and fasted for 24 h. For the starved condition, males were collected directly from the starvation bottles; for the sated condition, males were moved to bottles containing 5% sucrose agar and red food dye for 1 h, and then gathered for hemolymph collection. To generate a sufficient sample volume, multiple collections of hemolymph each from 100 males were pooled together. Hemolymph was stored at -80 °C until derivatization.

Twenty µL of hemolymph were diluted with 80 µL of ice-cold acetonitrile. The samples were vortexed, then centrifuged for 10 min at 12,100 × g. Twenty µL of the supernatant was derivatized by sequential addition of 10 µL of 100 mM sodium carbonate, 10 µL of BzCl (2% (v/v) in acetonitrile), and 10 µL of the internal standard mixture. Fifty µL of water were added. Calibration standards were prepared in aCSF.

Five µL aliquots of the standards were diluted with 20 µL acetonitrile to match the sample composition, and then derivatized in the same manner as the hemolymph supernatant.

Protein precipitation method validation

To validate the method and test recovery of the solvent precipitation, we spiked a mixture of isotopically labeled metabolites (500 nM $^{13}C_5$-glutamate, 50 nM d_6-GABA, 50 nM d_4-serotonin, and 50 nM $^{13}C_6$-dopamine) into 50 µL of pooled human serum. The spiked serum was diluted with 200 µL ice cold acetonitrile, followed by centrifugation for 10 minutes at 12,100 × g. 20 µL of supernatant was derivatized by sequential addition of 10 µL of 100 mM sodium carbonate, 10 µL of BzCl (2% (v/v) in acetonitrile), and 10 µL of the internal standard mixture. Three spiked serum samples were extracted and derivatized in parallel for triplicate analysis. Calibration standards were prepared in aCSF, and 5 µL aliquots of the standards were diluted with 20 µL acetonitrile to match the sample composition, and then derivatized in the same manner as the serum supernatant.

Small molecule neurochemical analysis using QQQ MS/MS

Derivatized samples were analyzed by LC-MS (as further described in the results section) using a Waters nanoAcquity UPLC (Milford, MA) coupled to an Agilent 6410 (Santa Clara, CA) triple quadrupole mass spectrometer operating in dynamic multiple reaction monitoring (dMRM) mode. Five µL were injected onto an Acquity HSS T3 C18 column (1 mm x 100 mm, 1.8 µm, 100 Å pore size) in partial loop injection mode.

Samples were analyzed in triplicate. Mobile phase A was 10 mM ammonium formate with 0.15% formic acid, and mobile phase B was acetonitrile. The flow rate was 100 µL/min and the elution gradient was as follows: initial, 0% B; 0.01 min, 15% B; 0.5 min, 17% B; 14 min, 55% B; 14.5 min, 70% B; 18 min, 100% B; 19 min, 100% B; 19.1 min, 0% B; and 20 min, 0% B. An additional 10 min of column equilibration at 0% B were required to achieve reproducible chromatography. The required pressure over the gradient was from 2,500 - 8,000 psi. The autosampler was kept at ambient temperature and the column was kept at 27 °C. Electrospray ionization was used in positive mode at 4 kV. The gas temperature was 350 °C, gas flow was 11 L/min, and the nebulizer was at 15 psi. Automated peak integration was performed using Agilent MassHunter Workstation Quantitative Analysis for QQQ, version B.05.00; all peaks were visually inspected to ensure proper integration.

Statistical analyses

All statistical analyses were performed in Prism 7 (GraphPad, La Jolla, CA). For statistical analysis unpaired Student's *t* test were applied. Differences were deemed significant if $p < 0.05$.

Results and Discussion

BzCl labeling has been previously reported for the analysis of small molecule neurotransmitters, polyamines and steroids with HPLC-MS or ultraviolet-absorption detection[31, 34, 184, 185]. Here we identify new reaction conditions that improve sensitivity for LC-MS/MS for many of the neurochemicals tested and demonstrate the wide applicability of BzCl derivatization for low molecular weight metabolites in a variety of complex sample matrices.

Effect of buffer and solvents on reaction conditions

The initial report of using BzCl with HPLC-MS/MS for neurochemicals utilized four reagent addition steps[31]: 1) sodium tetraborate buffer (100 mM) to the sample to achieve basic pH conditions required for BzCl labeling; 2) 2% (v/v) BzCl in acetonitrile; 3) internal standards diluted in dimethyl sulfoxide (DMSO) with 1% (v/v) formic acid, 4) d_4-ACh in water to provide an internal standard for this neurotransmitter that does not react with BzCl. Tetraborate buffer was originally selected because it forms a reversible complex with catechol groups[31, 186] to prevent oxidation under high pH conditions. Our present work first focused on modifying reaction conditions to improve sensitivity and reduce the number of steps. These initial studies used 17 neurochemicals as test analytes (Figure 2-1, Table 2-2).

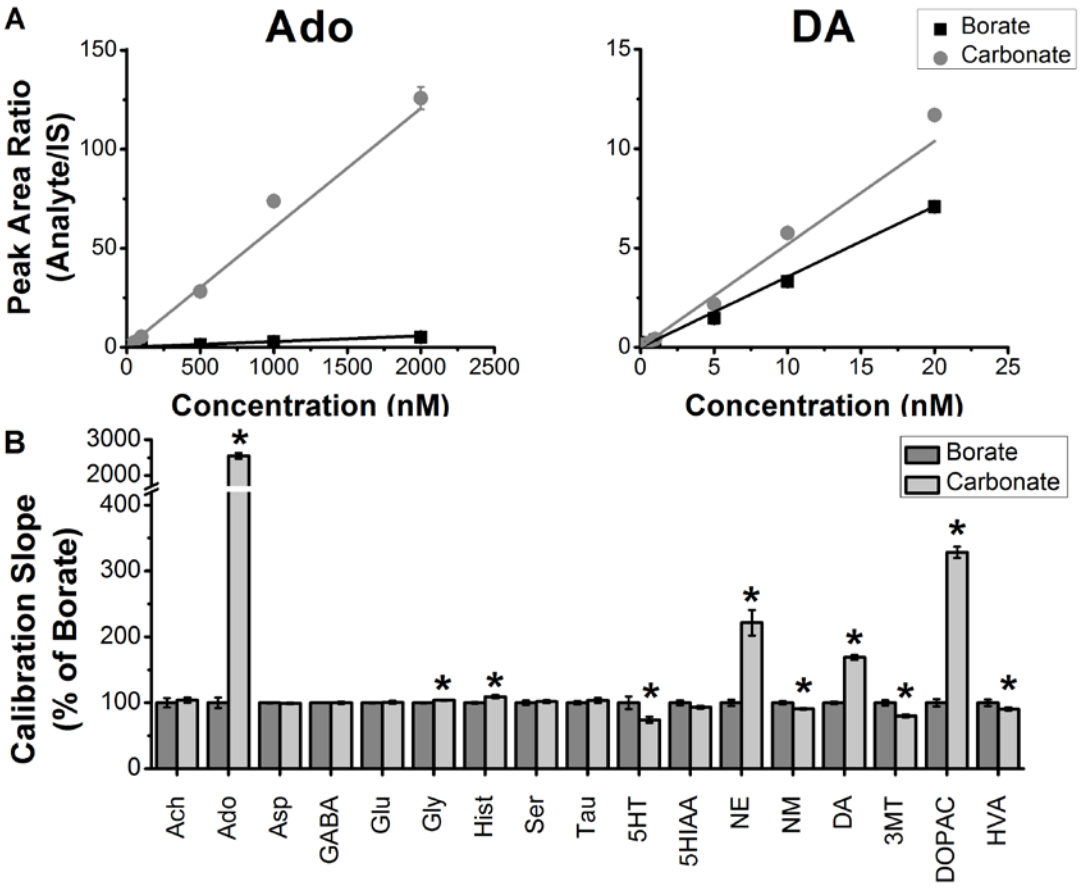

Figure 2-1 Normalized effect of sodium borate versus sodium carbonate buffer on calibration slope for select analytes. Standards made using sodium borate buffer and sodium carbonate buffer were analyzed with LC-MS in triplicate. A 6-point calibration curve for all analytes of interest was made to determine the average calibration slope for each analyte (n = 3 for each concentration tested). For the calibrations, the high concentrations were 20 nM for ACh, 5HT, NE, NM, DA and 3MT; 200 nM for Hist, GABA, 5HIAA, HVA, and DOPAC; and 2 μM for Tau, Ser, Asp, Ado, Gly, and Glu; followed by serial dilution. Analyte to internal standard ratios were plotted against known concentrations and a linear trend line was applied to determine slope (A). Sodium carbonate slopes were normalized to sodium borate slopes. Significant improvements to Ado, Gly, Hist, NE, DA, and DOPAC occurred when using 100 mM sodium carbonate as the buffer. Slopes were decreased for 5HT, NM, 3MT, and HVA. Unpaired two-tailed Students *t* test statistics were performed (B). Data expressed as percent borate ± SD. *$p < 0.05$, n = 3.

We found that sodium carbonate instead of borate buffer significantly improved sensitivity (i.e. slope of the calibration curve; Figure 2-1) for compounds containing a 1,2 diol group, such as dopamine, norepinephrine, and DOPAC (Figure 2-2A). Use of 100 mM carbonate buffer instead of 100 mM borate increased the slope of norepinephrine 221% ($t(4) = 19.6$, $p < 0.0001$), dopamine 170% ($t(4) = 27.7$, $p < 0.0001$),

and DOPAC 330% ($t(4) = 39.5$, $p < 0.0001$). The slope was increased 2550% for adenosine ($t(4) = 52.0$, $p < 0.0001$), which is also a diol. The slope increased slightly for two compounds without diols: glycine 103% ($t(4) = 5.6$, $p < 0.01$) and histamine 110% ($t(4) = 5.4$, $p < 0.01$). Although these compounds improved, the calibration slope was reduced 25% for serotonin ($t(4) = 4.2$, $p < 0.05$), 10% for normetanephrine ($t(4) = 5.3$, $p < 0.01$), 20% for 3MT ($t(4) = 7.7$, $p < 0.01$), and 10% for HVA ($t(4) = 2.9$, $p < 0.05$). These small decreases in slope are a reasonable trade-off for the large gains for the diols.

Improved catechol detection sensitivity may relate to how the buffers interact with 1,2 diol groups. Both borate and carbonate can be used as protecting groups for 1,2

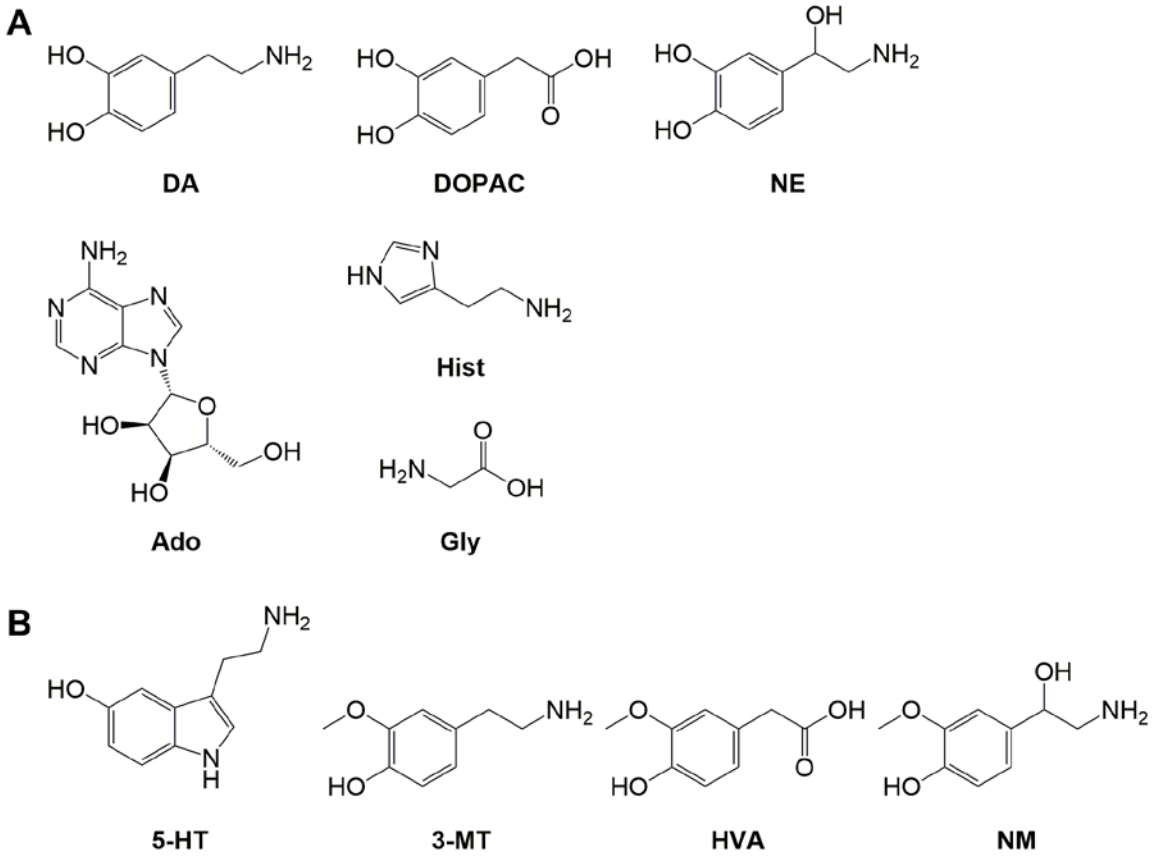

Figure 2-2 Chemical structures of neurochemicals enhanced by sodium carbonate buffer (A). Structures of neurochemical reduced with carbonate buffer (B).

diols[187]; however, cyclic borates are deprotected using dilute acid[187, 188], while cyclic carbonates hydrolyze in water[187, 189]. The protection of the carbonate group is more readily reversed than borate due to the high aqueous content of the sample, allowing for greater access of the diols for BzCl. The reason for the decreases in sensitivity of some compounds is unclear, but several of the compounds with decreased slopes have an ortho configuration of an alcohol and methoxy group (Figure 2-2B).

A potential problem with the BzCl assay is that organic solvent in the injected sample could cause poor peak shape for the most polar analytes, particularly acetylcholine (Figure 2-3). However, some organic solvent is needed to maintain solubility of the hydrophobic internal standards that are added to the sample. Replacing DMSO in the internal standard mixture with 20% (v/v) acetonitrile improved peak shape and signal intensity for acetylcholine, while retaining sufficient organic content to maintain solubility of hydrophobic compounds. The peak area for acetylcholine standards treated with internal standards in 20% (v/v) acetonitrile increased 5-fold relative to samples treated with internal standards in DMSO. This change in solvent reduces the final organic content of the samples, so band broadening is reduced for polar metabolites such as acetylcholine, as the sample composition is more closely matched in elution strength to the initial gradient conditions.

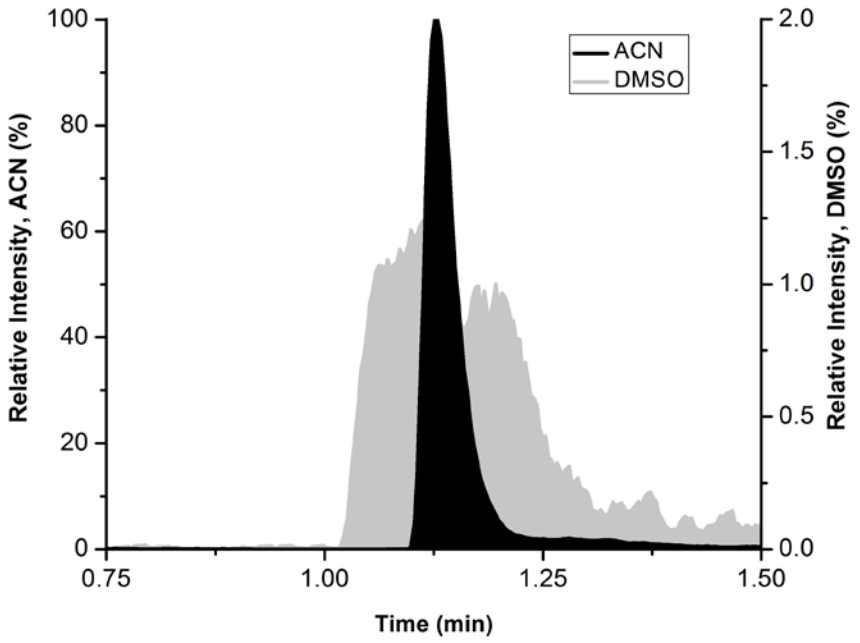

Figure 2-3 Replacement of DMSO with acetonitrile as solvent for internal standards improves the peak shape and area for early eluting metabolite ACh. Standards were derivatized with 2% BzCl (v/v in acetonitrile), 100 mM sodium carbonate, and an internal standard mixture diluted in either DMSO or 20% (v/v) acetonitrile. ACh ion chromatograms were extracted and normalized to the ACh peak in acetonitrile and overlaid.

Substituting 1% (v/v) sulfuric acid for 1% (v/v) formic acid in the internal standard mixture improved signals of late eluting compounds by 237% for normetanephrine, 165% for DOPAC, 481% for serotonin, 476% for norepinephrine, 440% for 3MT, and 468% for dopamine (Table 2-2). While the explanation for this increased signal is unclear, we hypothesize that it is due to the decreased formation of formate adducts late in the gradient. The production of undetectable formate adducts limits the production of detectable proton adducts. Formic acid is used in our mobile phase A, so early eluting compounds may still form formate adducts; whereas later eluting compounds have less likelihood of formate adducts due to the lack of formic acid in sample and mobile phase B.

Table 2-2 Improvements in sensitivity using sulfuric acid compared to formic acid additive to reagent mixture. Standards were derivatized with sodium carbonate (100 mM), BzCl (2% (v/v) in acetonitrile), and an internal mixture that contained 20% (v/v) acetonitrile with 1% (v/v) formic acid or sulfuric acid.

Analyte	Retention Time (min)	Concentration (nM)	Formic Acid Peak Area	Sulfuric Acid Peak Area	Increase with Sulfuric (%)
ACh	1.2	50	9409	8219	87
Tau	2.3	2000	17373	17723	102
Hist	2.3	200	78624	81494	104
Ser	2.6	5000	19108	20770	109
Asp	2.8	200	1118	1324	118
Gly	2.9	5000	4163	4695	113
Glu	3.1	2000	19442	23809	122
GABA	3.7	200	23076	30285	131
Ado	4.6	200	8894	12443	140
5HIAA	5.2	500	12758	16814	132
HVA	5.3	500	54869	69455	127
NM	5.5	20	13240	31391	237
DOPAC	5.9	500	158474	261578	165
5HT	5.9	20	2221	10703	482
NE	6.0	20	5974	28457	476
3MT	6.0	20	16229	71462	440
DA	6.4	20	21510	100588	468

To reduce the number of reagent addition steps and the dilution associated with derivatization, we added the d_4-acetylcholine internal standard to the ^{13}C-labeled internal standards and introduced all internal standards in one step. This modification had no effect on d_4-acetylcholine or the ^{13}C-labeled compounds.

Addition of new compounds

To illustrate the potential for more comprehensive measurement of neurochemical pathways with this assay, 53 compounds were added to the original 17 compound assay (Table 2-1). The selected 70 compounds include 19 proteinogenic amino acids and intermediates in the metabolism of phenylalanine, tyrosine, tryptophan, and arginine. Phenylalanine and tyrosine are precursors to the catecholamines and several trace amines, so many metabolites in this pathway were added. These include several norepinephrine metabolites (e.g., VMA and MOPEG), as well as tyrosine derivatives such as tyramine and octopamine. Trace amines (tyramine, octopamine, tryptamine, and phenethylamine) play prominent roles in many invertebrate species[190-194], and are present as metabolic by-products in the mammalian central nervous system, where they may neuromodulate biogenic amine signaling[176, 194]. Serotonin is derived from tryptophan, so several intermediates in tryptophan metabolism were included (Figure 2-4). These include 5HTP, the direct precursor to serotonin, as well as serotonin metabolite N-acetylserotonin, which is particularly relevant in flies[195, 196]. Monoamine oxidase (MAO) activity is limited in flies, so metabolites produced via MAO (e.g., 5HIAA) are not typically observed. Instead, monoamines are preferentially metabolized by N-acetylation, producing compounds such as N-acetylserotonin[195-197]. Tryptophan is also the precursor to kynurenine and its metabolites, which may have both neuroprotective and neurotoxic properties[198].

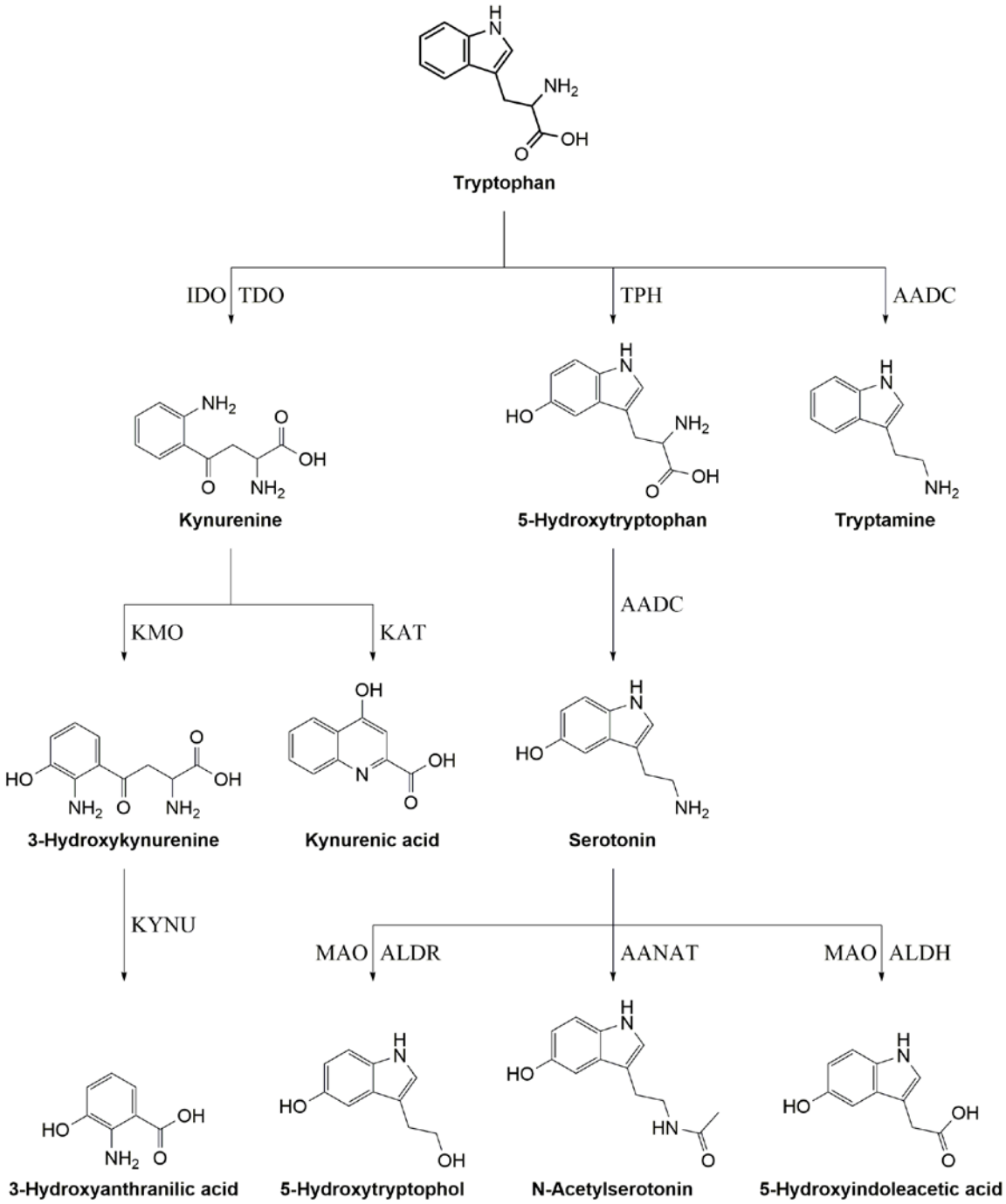

Figure 2-4 Tryptophan Metabolic Pathway. Abbreviations: aromatic amino acid decarboxylase (AADC), aralkylamine N-acetyltransferase (AANAT), aldehyde dehydrogenase (ALDH), aldehyde reductase (ALDR), indoleamine 2,3-dioxygenase (IDO), kynurenine aminotransferase (KAT), kynurenine 3-monooxygenase (KMO), kynureninase (KYNU), monoamine oxidase (MAO), tryptophan 2,3-dioxygenase (TDO), and tryptophan hydroxylase (TPH).

Several intermediates in arginine metabolism were also included in the method. Arginine is involved in the urea cycle and nitric oxide production. Ornithine, another member of the urea cycle, serves as a precursor for many polyamines, ubiquitous small molecules with a broad array of functions[199], whose dysfunction are associated with neurodegenerative disease[200, 201]. Thiol-containing dipeptide glutathione, and histidine-containing dipeptides, carnosine and metabolite anserine, have antioxidative effects in the brain[202-204], and decreased glutathione activity is associated with oxidative stress. Postmortem prefrontal-cortex tissue from human patients with psychiatric conditions such as bipolar, depression, and schizophrenia, show decreased levels of glutathione[204]. Carnosine may be neuroprotective by inhibiting the formation of β-amyloid polymerization and α-synuclein oligomerization[203], toxic species in Alzheimer's and Parkinson's diseases. Glucose indicates neuronal energy expenditure, and alterations of normal glucose metabolism can lead to synaptic dysfunction, including glucose hypometabolism in Alzheimer's disease and Parkinsonian patients with dementia[205-208].

All 70 analytes of interest and their internal standards are benzoylated, except acetylcholine and choline, and detected by MS/MS (Table 2-3 and Table 2-4). Analytes were labeled 1-4 times with BzCl depending on the functional groups. In all cases, only the fully labeled compounds were observed, indicating quantitative (i.e., complete labeling) reactions. As an example, dopamine is triply labeled; singly and doubly labeled dopamine were not detectable. Protonated benzoylation products (MW + 1) were observed for most compounds with ESI in positive mode. A protonated water loss was observed for octopamine, normetanephrine, and synephrine (MW – 18 + 1), and the ammonium adduct (MW + 18) was detected for VMA, MOPEG, 5HIAA, HVA. DOMA,

DOPEG, and DOPAC. A sodium adduct was observed for glucose (MW + 23). Other hexoses (e.g. fructose, mannose, and galactose) were resolved chromatographically or by MRM. For acetylcholine and choline, the unlabeled molecular ions were used for detection.

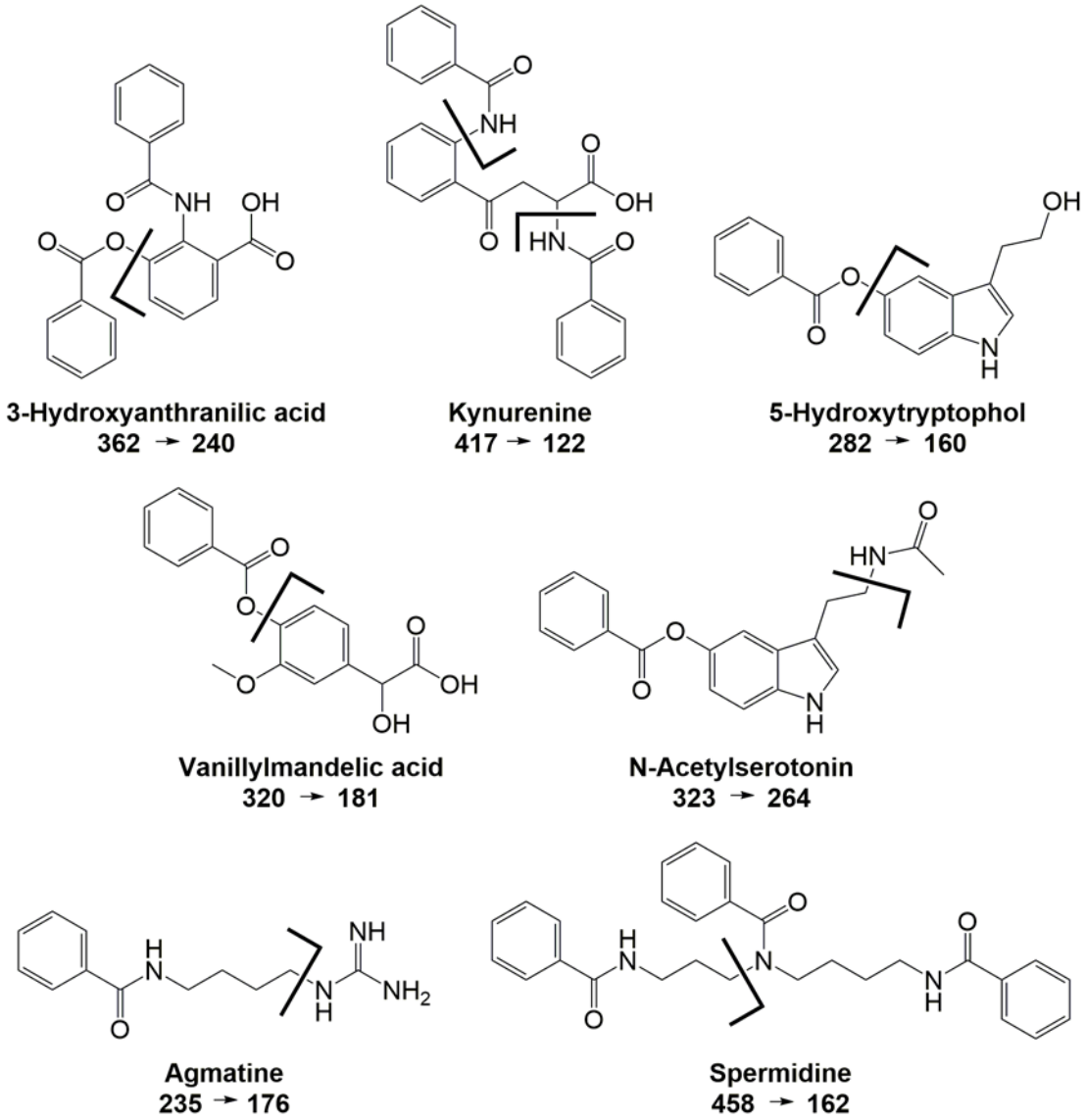

Figure 2-5 Fragmentation patterns for select benzoyl labeled compounds. Analytes were detected by MS/MS under collision activated dissociation (CAD) conditions. While the benzoyl fragment of 105 m/z was the most abundant product ion for most analytes detected, unique fragments were chosen for detection to increase the selectivity of the assay for these compounds.

Table 2-3 Labeling patterns and MRM conditions of 70 targeted metabolites

Analyte	Precursor (*m/z*)	Product (*m/z*)	Fragmentor (V)	Collision Energy (V)	Retention Time (min)	Labeling Pattern	MS Species
ACh	146	87	120	15	1.30	non	$[M]^+$
Ch	104	60	120	20	1.30	non	$[M]^+$
Bz-CA	274	105	120	10	2.31	mono	$[M + H]^+$
Bz-His	260	110	130	20	2.33	mono	$[M + H]^+$
Bz-Ans	345	105	130	30	2.40	mono	$[M + H]^+$
Bz-Carn	331	110	135	20	2.40	mono	$[M + H]^+$
Bz-HTau	214	105	120	20	2.48	mono	$[M + H]^+$
Bz-Tau	230	105	120	10	2.49	mono	$[M + H]^+$
Bz-Arg	279	105	135	30	2.58	mono	$[M + H]^+$
Bz-Hist	216	105	120	20	2.61	mono	$[M + H]^+$
Bz-Asn	237	105	120	20	2.62	mono	$[M + H]^+$
Bz-Ser	210	105	120	20	2.71	mono	$[M + H]^+$
Bz-Gln	251	105	120	20	2.72	mono	$[M + H]^+$
Bz-HSer	224	105	120	20	2.88	mono	$[M + H]^+$
Bz-Cit	280	105	120	20	2.91	mono	$[M + H]^+$
Bz-ETA	166	105	120	20	2.93	mono	$[M + H]^+$
Bz-Asp	238	105	120	10	2.98	mono	$[M + H]^+$
Bz-Agm	235	176	110	30	3.02	mono	$[M + H]^+$
Bz-Glc	307	185	130	20	3.10	mono	$[M + Na]^+$
Bz-Gly	180	105	120	10	3.10	mono	$[M + H]^+$
Bz-Glu	252	105	120	20	3.28	mono	$[M + H]^+$
Bz-BAla	194	105	120	20	3.53	mono	$[M + H]^+$
Bz-Ala	194	105	120	20	3.78	mono	$[M + H]^+$

Analyte	Precursor (*m/z*)	Product (*m/z*)	Fragmentor (V)	Collision Energy (V)	Retention Time (min)	Labeling Pattern	MS Species
Bz-NAP	235	176	135	20	3.85	mono	$[M + H]^+$
Bz-GABA	208	105	120	10	3.99	mono	$[M + H]^+$
Bz-Pro	220	105	120	20	4.60	mono	$[M + H]^+$
Bz-Ado	372	136	120	30	6.28	mono	$[M + H]^+$
Bz-Val	222	105	120	30	6.63	mono	$[M + H]^+$
Bz-Met	254	105	120	15	6.73	mono	$[M + H]^+$
Bz-Orn	341	174	120	15	7.50	bi	$[M + H]^+$
Bz-GSH	516	105	120	15	8.28	bi	$[M + H]^+$
Bz-Lys	355	188	120	20	8.35	bi	$[M + H]^+$
Bz-Put	297	105	120	30	8.79	bi	$[M + H]^+$
Bz-Leu	236	105	120	30	9.30	mono	$[M + H]^+$
Bz-Phe	270	120	120	10	9.67	mono	$[M + H]^+$
Bz-Thr	224	105	140	20	9.67	mono	$[M + H]^+$
Bz-VMA	320	181	120	10	9.77	mono	$[M + NH_4]^+$
Bz-Trp	309	159	120	10	9.96	mono	$[M + H]^+$
Bz-MOPEG	306	105	120	20	10.08	mono	$[M + NH_4]^+$
Bz-Kyo	546	175	110	30	11.35	bi	$[M + H]^+$
Bz-Cys	330	105	120	20	11.64	bi	$[M + H]^+$
Bz-KA	294	105	120	30	11.78	mono	$[M + H]^+$
Bz-Spd	458	162	120	30	12.00	tri	$[M + H]^+$
Bz-PhEt	226	105	120	15	12.23	mono	$[M + H]^+$
Bz-TrpA	265	144	130	30	12.38	mono	$[M + H]^+$
Bz-NAS	323	264	120	15	12.39	mono	$[M + H]^+$

Analyte	Precursor (*m/z*)	Product (*m/z*)	Fragmentor (V)	Collision Energy (V)	Retention Time (min)	Labeling Pattern	MS Species
Bz-5HIAA	313	146	120	15	12.60	mono	$[M + NH_4]^+$
Bz-5HTOL	282	160	130	20	12.73	mono	$[M + H]^+$
Bz-HCY	344	105	120	20	13.00	bi	$[M + H]^+$
Bz-3HAA	362	240	120	10	13.07	bi	$[M + H]^+$
Bz-HCA	288	105	120	10	13.13	mono	$[M + H]^+$
Bz-HVA	304	105	120	15	13.13	mono	$[M + NH_4]^+$
Bz-DOMA	410	105	130	20	13.35	bi	$[M + NH_4]^+$
Bz-Kyn	417	122	120	10	13.35	bi	$[M + H]^+$
Bz-Spm	619.6	497	135	25	13.52	quad	$[M + H]^+$
Bz-DOPEG	396	105	120	20	13.59	bi	$[M + NH_4]^+$
Bz-5HTP	429	279	120	15	13.82	bi	$[M + H]^+$
Bz-OA	344	105	140	20	13.84	bi	$[M - H_2O + H]^+$
Bz-NM	374	105	140	15	13.88	bi	$[M - H_2O + H]^+$
Bz-Tyr	390	105	120	30	14.12	bi	$[M + H]^+$
Bz-3HK	537	240	135	25	14.40	tri	$[M + H]^+$
Bz-Syn	358	105	140	20	14.43	bi	$[M - H_2O + H]^+$
Bz-5HT	385	264	140	20	15.46	bi	$[M + H]^+$
Bz-DOPAC	394	105	140	20	15.49	bi	$[M + NH_4]^+$
Bz-3MT	376	105	120	20	15.67	bi	$[M + H]^+$
Bz-LDOPA	510	105	120	25	15.67	tri	$[M + H]^+$
Bz-TyrA	346	105	135	25	15.73	bi	$[M + H]^+$
Bz-NE	482	105	140	30	15.77	tri	$[M + H]^+$
Bz-E	496	105	120	15	15.96	tri	$[M + H]^+$
Bz-DA	466	105	140	20	16.40	tri	$[M + H]^+$

Table 2-4 Transitions for $^{13}C_6$-BzCl labeled internal standard

Analyte	Precursor (m/z)	Product (m/z)	Fragmentor (V)	Collision Energy (V)	Retention Time (min)
d_4-Ach	150	91	120	15	1.30
d_4-Ch	108	60	120	20	1.30
$^{13}C_6$Bz-CA	280	111	120	10	2.31
$^{13}C_6$Bz-His	266	110	130	20	2.33
$^{13}C_6$Bz-Ans	351	111	130	30	2.40
$^{13}C_6$Bz-Carn	337	110	135	20	2.40
$^{13}C_6$Bz-HTau	220	111	120	20	2.48
$^{13}C_6$Bz-Tau	236	111	120	10	2.49
$^{13}C_6$Bz-Arg	285	111	135	30	2.58
$^{13}C_6$Bz-Hist	222	111	120	20	2.61
$^{13}C_6$Bz-Asn	243	111	120	20	2.62
$^{13}C_6$Bz-Ser	216	111	120	20	2.71
$^{13}C_6$Bz-Gln	257	111	120	20	2.72
$^{13}C_6$Bz-HSer	230	111	120	20	2.88
$^{13}C_6$Bz-Cit	286	111	120	20	2.91
$^{13}C_6$Bz-ETA	172	111	120	20	2.93
$^{13}C_6$Bz-Asp	244	111	120	10	2.98
$^{13}C_6$Bz-Agm	241	182	110	30	3.02
$^{13}C_6$Bz-Glc	313	185	130	20	3.10
$^{13}C_6$Bz-Gly	186	111	120	10	3.10
$^{13}C_6$Bz-Glu	258	111	120	20	3.28
$^{13}C_6$Bz-BAla	200	111	120	20	3.53
$^{13}C_6$Bz-Ala	200	111	120	20	3.78
$^{13}C_6$Bz-NAP	241	182	135	20	3.85
$^{13}C_6$Bz-GABA	214	111	120	10	3.99
$^{13}C_6$Bz-Pro	226	111	120	20	4.60
$^{13}C_6$Bz-Ado	378	136	120	30	6.28
$^{13}C_6$Bz-Val	228	111	120	30	6.63
$^{13}C_6$Bz-Met	260	111	120	15	6.73
$^{13}C_6$Bz-Orn	353	180	120	15	7.50
$^{13}C_6$Bz-GSH	528	111	120	15	8.28
$^{13}C_6$Bz-Lys	367	194	120	20	8.35
$^{13}C_6$Bz-Put	309	111	120	30	8.79
$^{13}C_6$Bz-Leu	242	111	120	30	9.30
$^{13}C_6$Bz-Phe	276	120	120	10	9.67
$^{13}C_6$Bz-Thr	230	111	140	20	9.67

Analyte	Precursor (m/z)	Product (m/z)	Fragmentor (V)	Collision Energy (V)	Retention Time (min)
$^{13}C_6$Bz-VMA	326	181	120	10	9.77
$^{13}C_6$Bz-Trp	315	159	120	10	9.96
$^{13}C_6$Bz-MOPEG	312	111	120	20	10.08
$^{13}C_6$Bz-Kyo	558	175	110	30	11.35
$^{13}C_6$Bz-Cys	342	111	120	20	11.64
$^{13}C_6$Bz-KA	300	111	120	30	11.78
$^{13}C_6$Bz-Spd	476	168	120	30	12.00
$^{13}C_6$Bz-PhEt	232	111	120	15	12.23
$^{13}C_6$Bz-TrpA	271	144	130	30	12.38
$^{13}C_6$Bz-NAS	329	270	120	15	12.39
$^{13}C_6$Bz-5HIAA	319	146	120	15	12.60
$^{13}C_6$Bz-5HTOL	288	160	130	20	12.73
$^{13}C_6$Bz-HCY	356	111	120	20	13.00
$^{13}C_6$Bz-3HAA	374	246	120	10	13.07
$^{13}C_6$Bz-HCA	294	111	120	10	13.13
$^{13}C_6$Bz-HVA	310	111	120	15	13.13
$^{13}C_6$Bz-DOMA	422	111	130	20	13.35
$^{13}C_6$Bz-Kyn	429	128	120	10	13.35
$^{13}C_6$Bz-Spm	643.6	515.6	135	25	13.52
$^{13}C_6$Bz-DOPEG	408	111	120	20	13.59
$^{13}C_6$Bz-5HTP	441	285	120	15	13.82
$^{13}C_6$Bz-OA	356	111	140	20	13.84
$^{13}C_6$Bz-NM	386	111	140	15	13.88
$^{13}C_6$Bz-Tyr	402	111	120	30	14.12
$^{13}C_6$Bz-3HK	555	246	135	25	14.40
$^{13}C_6$Bz-Syn	370	111	140	20	14.43
$^{13}C_6$Bz-5HT	397	270	140	20	15.46
$^{13}C_6$Bz-DOPAC	406	111	140	20	15.49
$^{13}C_6$Bz-3MT	388	111	120	20	15.67
$^{13}C_6$Bz-LDOPA	528	111	120	25	15.67
$^{13}C_6$Bz-TyrA	358	111	135	25	15.73
$^{13}C_6$Bz-NE	500	111	140	30	15.77
$^{13}C_6$Bz-E	514	111	120	15	15.96
$^{13}C_6$Bz-DA	484	111	140	20	16.40

Analytes were detected by MS/MS under collision activated dissociation (CAD) conditions. The fragmentation of each analyte was examined to determine the best product ion to use for quantification (Table 2-3 and Table 2-4). For benzoylated analytes, the benzoyl fragment of 105 *m/z* was usually the most abundant product ion, and used for dMRM. Unique fragments for acetylcholine, choline, histidine, carnosine, phenylalanine, kynurenine, adenosine, tryptamine, 5HIAA, tryptophan, 5HTOL, spermidine, ornithine, kyotorphin, agmatine, N-acetylputrescine, VMA, glucose, lysine, 3HAA, 3HK, N-acetylserotonin, serotonin, 5HTP, and spermine were identified. These correspond to immonium ions for histidine, phenylalanine, and tryptophan, *y* ions for kyotorphin and carnosine, and the adenine moiety for adenosine. Several fragmentation patterns are shown in Figure 2-5**.** When possible, unique fragments were chosen for quantification to increase the selectivity of the assay for these compounds, reducing the likelihood of interferences from unknowns with similar precursor masses. The unique fragments have comparable or increased sensitivity relative to the 105 fragments for those compounds.

After determining the MS/MS transitions, a gradient was developed to separate the analytes (Figure 2-6). The gradient was not designed to fully resolve all analytes but to spread the analytes out over the 20 min separation time and minimize the number of dMRMs at any given time. The gradient results show that even very polar compounds like dopamine can be well retained after benzoylation. Total analysis time for each sample is around 33 min including injection time, elution and column re-equilibration on the Waters nanoAcquity system. Higher throughput may be possible. In preliminary tests, the method was transferred to a higher flow rate HPLC with higher pressure limits

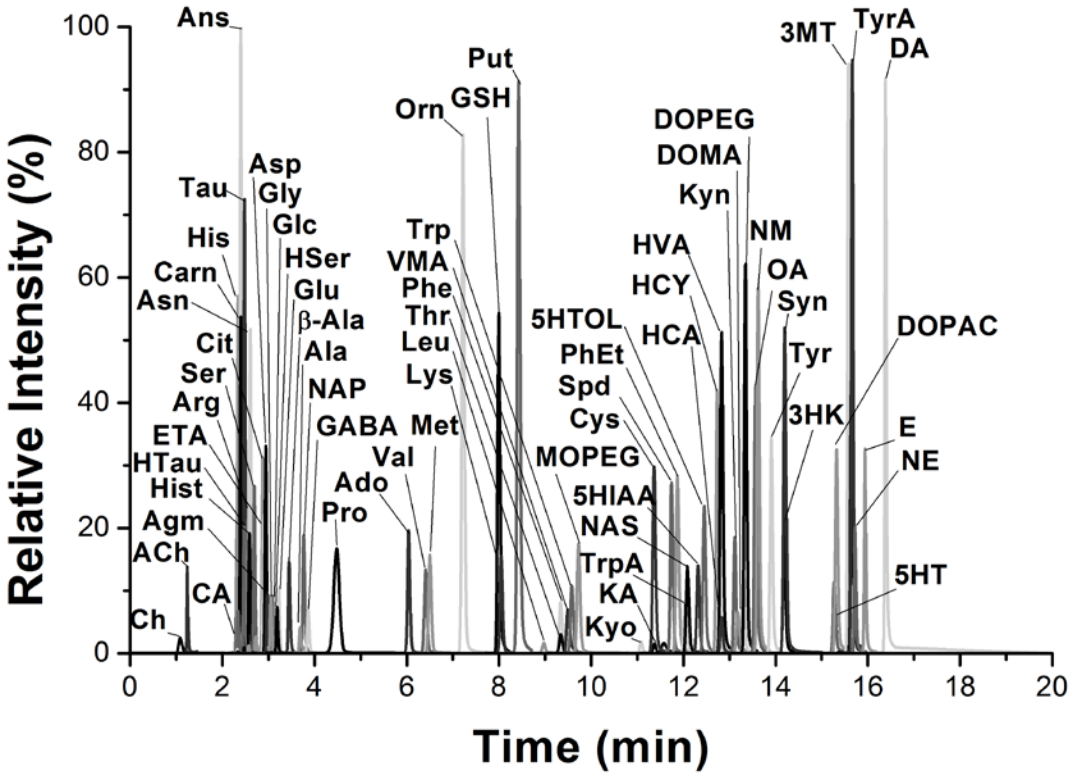

Figure 2-6 Reconstructed ion chromatogram of 70 compounds detected in 20 min. Extracted ion chromatograms for each compound at the highest concentration calibration standard run, were normalized to highest intensity and overlaid.

and the separation time was reduced to 12 min, with a total analysis time of around 14 min. Further reductions in the analysis time per sample can be achieved as LC pressure limits and MS scan rates continue to increase.

The method yields good detection limits, linearity, reproducibility and low carryover for all detected compounds (Table 2-5). All detection limits were better than 10 nM except for glutathione, alanine, citrulline, glycine, serine, and glucose[209]. While limits of detection (LOD) for these select compounds were higher than other reported compounds in the assay, these levels were below the observed concentrations in dialysate and CSF.

Table 2-5 Summary of limits of detection (LOD), carryover, relative standard deviation (n = 3), and R^2 value of a six-point calibration for aqueous standards.

Analyte	LoD (nM)	Carryover (%)	RSD (%)	Fit (R^2)	Analyte	LoD (nM)	Carryover (%)	RSD (%)	Fit (R^2)
ACh	1	1	0.7	0.9996	Thr	5	0.3	1	0.9995
Ch	3	0.2	1	0.9997	VMA	1	0.1	1	0.9999
CA	4	0.02	2	1.0000	Trp	1	0.1	0.9	0.9997
His	2	0.1	2	0.9996	MOPEG	0.7	0.08	0.6	0.9999
Ans	0.4	0.03	2	0.9999	Kyo	0.2	0.2	2	0.9998
Carn	0.8	0.04	2	0.9999	Cys	1	0.1	5	0.9971
HTau	7	0.05	4	0.9977	KA	1	0.1	0.9	0.9997
Tau	3	0.02	1	0.9998	Spd	0.09	0.1	0.5	0.9994
Arg	1	0.5	3	0.9576	PhEt	0.08	0.09	2	0.9989
Hist	0.09	0.04	3	0.9996	TrpA	0.1	0.09	3	0.9993
Asn	2	0.1	2	0.9999	NAS	0.09	0.06	0.8	0.9997
Ser	70	0.6	1	0.9976	5HIAA	0.7	0.08	0.8	0.9999
Gln	4	0.2	3	0.9998	5HTOL	0.9	0.07	1	0.9997
HSer	11	0.5	3	0.9994	HCY	0.9	0.08	1	0.9968
Cit	20	2	2	0.9965	3HAA	1	0.1	0.9	0.9996
ETA	6	0.4	2	0.9997	HCA	1	0.09	2	0.9998
Asp	8	0.05	1	0.9999	HVA	0.6	0.07	0.4	1.0000
Agm	1	0.03	4	0.9997	DOMA	0.3	0.2	3	0.9998
Glc	160	0.06	6	0.9997	Kyn	1	0.1	3	0.9994
Gly	30	0.09	7	0.9997	Spm	0.1	0.1	2	0.9984
Glu	0.3	0.2	1	1.0000	DOPEG	0.1	0.1	1	0.9992
BAla	5	0.09	1	1.0000	5HTP	2	0.2	3	0.9996
Ala	20	2	2	0.9994	OA	0.2	0.2	1	0.9983
NAP	0.5	0.05	1	0.9999	NM	0.08	0.09	2	0.9988
GABA	0.5	0.4	2	0.9997	Tyr	4	2	3	0.9950
Pro	5	0.5	0.4	0.9996	3HK	8	0.06	2	0.9941
Ado	1	0.1	0.2	0.9956	Syn	0.2	0.2	0.1	0.9982
Val	7	0.6	3	0.9998	5HT	0.4	0.4	1	0.9970
Met	0.7	0.09	1	0.9998	DOPAC	0.2	0.2	2	0.9999
Orn	7	0.4	0.2	0.9963	3MT	0.2	0.2	2	0.9987
GSH	10	0.1	2	0.9999	LDOPA	1	0.9	2	0.9999
Lys	4	2	0.7	0.9867	TyrA	0.2	0.3	1	0.9964
Put	0.1	0.1	1	0.9999	NE	0.3	0.2	2	0.9970
Leu	5	4	2	0.9894	E	0.3	0.2	1	0.9964
Phe	3	0.2	0.8	0.9999	DA	0.3	0.3	3	0.9965

Application of 70 compound assay in various matrices

To test the versatility of the assay, we analyzed several types of biological samples, including rat striatal dialysate, human CSF, human serum, and *Drosophila* tissue homogenate (Table 2-6, Table 2-7, Table 2-8). Fifty seven compounds were detected in dialysate samples, whereas 35 and 50 compounds were above the limits of detection in human CSF and serum samples, respectively. *Drosophila* heads and bodies were isolated and analyzed separately, with detection of 44 compounds in head and 42 compounds in bodies. 54 compounds were detected in hemolymph from *Drosophila.*

All commonly studied neurotransmitters (i.e., GABA, glutamate, and monoamines) were within expected ranges in rat striatal dialysate (Table 2-6). Several detectable compounds were not previously reported in rat dialysate or tissue homogenate studies, and include homoserine, a precursor to amino acids threonine and methionine; N-acetylputrescine, a metabolite of polyamine putrescine; and DOMA, a norepinephrine metabolite. Polyamines putrescine, spermidine, and spermine were also detected in the dialysate sample. The norepinephrine and normetanephrine metabolites MOPEG, DOPEG, and DOMA (but not epinephrine or VMA) were detected in rat dialysate, demonstrating the potential for analysis of metabolic pathways.

Analysis of human serum, derivatized after protein precipitation, revealed kyotorphin at 31 nM concentration. Kyotorphin is an endogenous analgesic dipeptide with potential neuroprotective properties. It has previously been found in rat brain tissue and human CSF samples[210, 211]. This is the first report of quantitative detection of kyotorphin in human serum. Kyotorphin is proposed to have indirect opioid-like actions by modulating enkephalin release[212]. Kyotorphin does not cross the blood brain barrier,

and is a candidate biomarker for neurodegenerative diseases such as Alzheimer's disease[210]. While previous studies detected kyotorphin in CSF samples obtained from lumbar puncture, less invasive blood sample collection would be beneficial for patients, with subsequent detection as reported here. Interestingly, kyotorphin was not detected in our analysis of pooled human CSF from healthy patients, which did not undergo a protein precipitation step prior to analysis.

Fly tissue homogenate contained detectable levels of tyramine and octopamine, which was expected as they are the fly analogs of epinephrine and norepinephrine, respectively. 5HTP pretreatment of the flies resulted in high levels of 5HTP in both bodies and heads. 5HTP metabolites serotonin and N-acetylserotonin were also elevated, though the effect was more pronounced in the bodies. Interestingly, 5HIAA was observed in both bodies and heads, despite the expected lack of MAO activity in flies, likely due to the excess of 5HTP[197].

Of the 54 compounds detected in fly hemolymph, 10 showed significant ($p < 0.05$) changes between starved and sated states (Figure 2-7). These compounds were Ch ($t(4) = 9.7$, $p < 0.0001$); Ser ($t(4) = 10.5$, $p < 0.0001$), Cit ($t(4) = 39.3$, $p < 0.0001$), Pro ($t(4) = 80.2$, $p < 0.0001$), Orn ($t(4) = 9.8$, $p < 0.0001$), OA ($t(4) = 17.9$, $p < 0.0001$), Tyr ($t(4) = 29.5$, $p < 0.0001$), DOPAC ($t(4) = 11.0$, $p < 0.0001$), TyrA ($t(4) = 13.1$, $p < 0.0001$), DA ($t(4) = 27.2$, $p < 0.0001$). Of particular note was a nearly 5-fold increase of octopamine in starved flies relative to sated flies. Increased octopamine activity has been reported in flies upon starvation, and has been linked to foraging-like behaviors as the flies presumably try to locate food[213, 214]. The roles of other implicated metabolites are currently undergoing further investigation.

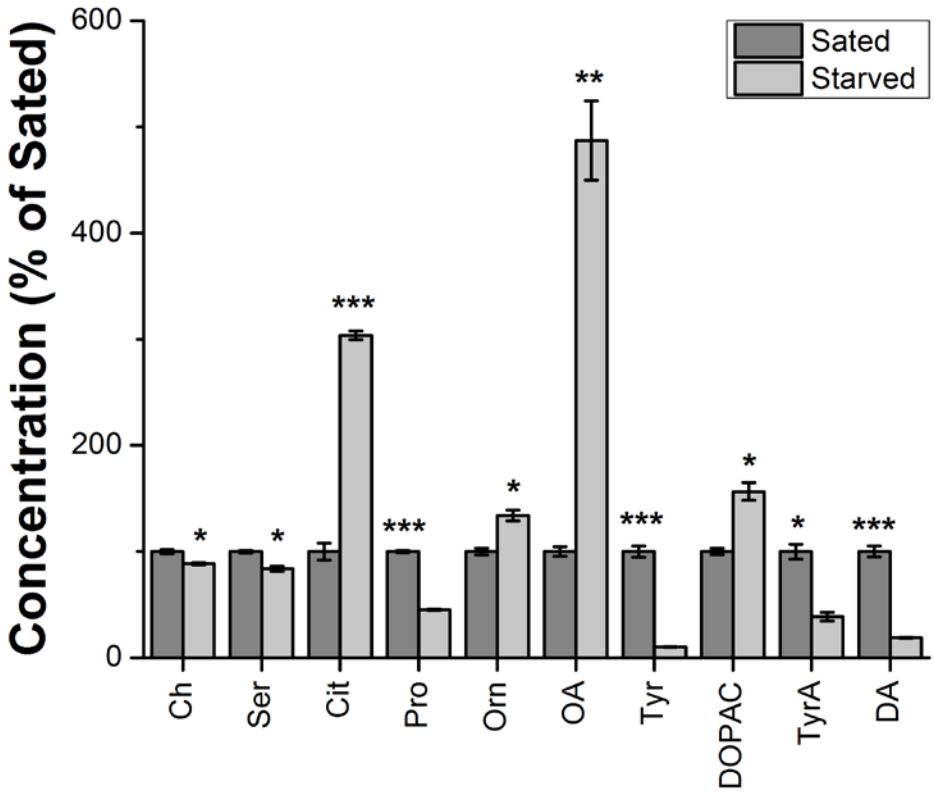

Figure 2-7 Metabolites showing significant differences between sated and starved states in fly hemolymph. Metabolite concentrations were normalized to total protein content, and then normalized to the sated sample. Each sample was run in triplicate. Unpaired two-tailed Students *t* tests were performed, and the Holm-Bonferroni correction was used. Data expressed as average ± SD. *$p < 0.05$; **$p < 0.01$; ***$p < 0.001$.

Protein removal prior to analysis of bodily fluids and tissue homogenate prevents column contamination and exposure of the HPLC-MS to high protein concentrations. Many extraction techniques are used in metabolomics[215-217]. These methods vary in effectiveness based on the sample type and target metabolites, and require optimization for each assay. Solvent precipitation with cold acetonitrile was selected for its simplicity and reproducibility. To evaluate the effect of protein precipitation on recovery and reproducibility we spiked known amounts of isotopically labeled glutamate, GABA, serotonin, and dopamine into serum prior to solvent precipitation. We then measured

concentrations of the isotopically labeled compounds after solvent precipitation and derivatization, and compared these measured concentrations to the known amount spiked into serum to determine the relative recovery (Figure 2-8). The recovery varied for each tested metabolite, but was reproducible (RSD < 8%). As such, we concluded that fair comparison could be made between samples analyzed using this method, though comparisons to other methods would require correction for recovery.

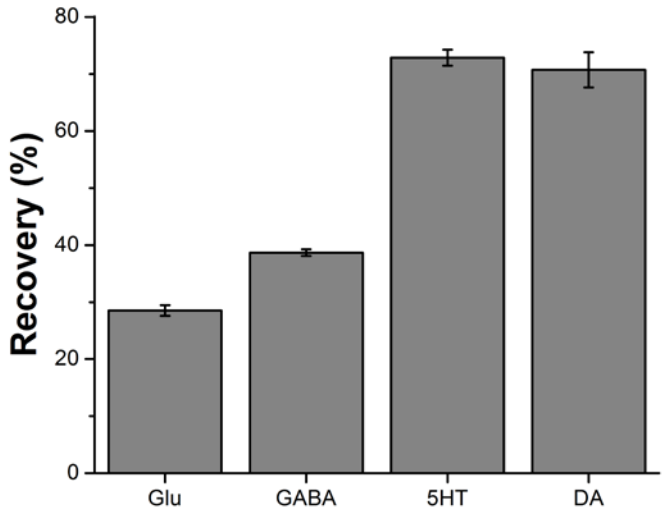

Figure 2-8 Recovery of four isotopically labeled metabolites spiked into plasma prior to solvent precipitation and derivatization. Percent recovery calculated as measured concentration after precipitation, relative to concentration spiked into serum. The average of three extraction replicates is shown. Error bars represent the standard error of the mean.

Table 2-6 Application of 70 compound method to analyze rat dialysate and human CSF. The average of 3 repeated injections with standard deviation is reported below. Values for analytes were reported only if they were above the limit of detection.

	Concentration (nM)							Concentration (nM)						
Analyte	Rat Dialysate			Human CSF				Analyte	Rat Dialysate			Human CSF		
ACh	12.2	±	0.1	1.19	±	0.04		Thr	691	±	7	65	±	2
Ch	1212	±	5	14	±	2		VMA						
CA	2170	±	90	300	±	30		Trp	141	±	4	20.9	±	0.2
His	930	±	10	91.4	±	0.8		MOPEG	4.3	±	0.3			
Ans								Kyo						
Carn	14.0	±	0.4					Cys	503	±	9			
HTau								KA						
Tau	1820	±	70	33	±	2		Spd	2.38	±	0.08	0.19	±	0.02
Arg	1380	±	70	211	±	6		PhEt	0.53	±	0.02			
Hist	0.76	±	0.08	0.20	±	0.03		TrpA						
Asn	40	±	1	6.6	±	0.3		NAS	0.23	±	0.02			
Ser	4100	±	250	570	±	40		5HIAA	390	±	6	2.4	±	0.2
Gln	37300	±	1300	4080	±	60		5HTOL	1.9	±	0.1			
HSer	2920	±	20	266	±	7		HCY	4.91	±	0.03			
Cit	390	±	10					3HAA						
ETA	6980	±	310	124	±	4		HCA	1050	±	30	4.7	±	0.3
Asp	108	±	7	15	±	2		HVA	1130	±	40	4.4	±	0.4
Agm								DOMA	0.47	±	0.02			
Glc	633000	±	85000	55400	±	840		Kyn	7.1	±	0.3			
Gly	690	±	10	52	±	5		Spm	2.9	±	0.1			
Glu	21	±	1	4.9	±	0.1		DOPEG	1.26	±	0.03			
BAla	5.8	±	0.9					5HTP						
Ala	5260	±	160	306	±	8		OA						
NAP	1.0	±	0.1	0.74	±	0.02		NM	0.30	±	0.01			
GABA	40.5	±	0.6	3.3	±	0.2		Tyr	350	±	20	76.6	±	0.3
Pro	1326	±	8	13.8	±	0.2		3HK						
Ado	112.8	±	0.6					Syn						
Val	1760	±	20	104	±	2		5HT	0.89	±	0.02			
Met	855	±	6	26.2	±	0.5		DOPAC	598	±	5	0.6	±	0.1
Orn	196	±	3	54.9	±	0.8		3MT	8.5	±	0.2			
GSH	74	±	2					LDOPA	4.00	±	0.04			
Lys	4030	±	170	249	±	7		TyrA	0.21	±	0.02			
Put	0.83	±	0.03	0.41	±	0.03		NE	1.00	±	0.08			
Leu	2200	±	140	102	±	4		E						
Phe	710	±	5	66.9	±	0.8		DA	29.4	±	0.8			

Table 2-7 Application of 70 compound method after protein precipitation for human serum. The average of 3 repeated injections with standard deviation is reported below. Values for analytes were reported only if they were above the limit of detection (LOD).

Analyte	LoD (nM)	Concentration (nM) Human Serum	Analyte	LoD (nM)	Concentration (nM) Human Serum
ACh	4	380 ± 10	Thr	30	62000 ± 5000
Ch	50	15200 ± 200	VMA	20	
CA	50		Trp	30	51000 ± 3000
His	30	37000 ± 1000	MOPEG	5	20 ± 5
Ans	3	160 ± 20	Kyo	5	31 ± 3
Carn	6	14 ± 3	Cys	30	1600 ± 100
HTau	500	160000 ± 10000	KA	40	220 ± 30
Tau	60	115000 ± 2000	Spd	2	41 ± 0.6
Arg	10	7100 ± 300	PhEt	1	
Hist	2	41 ± 2	TrpA	2	
Asn	70	20900 ± 800	NAS	2	5 ± 4
Ser	700	45000 ± 4000	5HIAA	5	67 ± 4
Gln	10	180000 ± 10000	5HTOL	10	16 ± 2
HSer	100	65000 ± 2000	HCY	30	
Cit	20	9400 ± 200	3HAA	20	76 ± 6
ETA	10	6300 ± 100	HCA	10	56 ± 7
Asp	200	2300 ± 200	HVA	20	57 ± 1
Agm	20		DOMA	6	
Glc	500	1050000 ± 90000	Kyn	40	2380 ± 50
Gly	200	102000 ± 4000	Spm	2	39 ± 3
Glu	30	21800 ± 700	DOPEG	2	
BAla	20	2300 ± 400	5HTP	30	
Ala	70	254000 ± 8000	OA	2	
NAP	7	24 ± 2	NM	2	
GABA	4	115 ± 4	Tyr	40	56000 ± 1000
Pro	30	24300 ± 3000	3HK	200	
Ado	3		Syn	4	
Val	40	160000 ± 10000	5HT	3	300 ± 40
Met	8	21800 ± 300	DOPAC	5	
Orn	200	27400 ± 300	3MT	4	
GSH	90		LDOPA	2	390 ± 20
Lys	40	37000 ± 1000	TyrA	8	
Put	0.4	13 ± 1	NE	3	3.2 ± 0.7
Leu	40	139000 ± 3000	E	4	
Phe	30	63000 ± 3000	DA	2	

Table 2-8 Application of 70 compound method with a protein precipitation step for fly bodies and heads. The average of 3 repeated injections with standard deviation is reported below. Values for analytes were reported only if they were above the limit of detection.

	Amount (pmol/fly)							Amount (pmol/fly)						
Analyte	Fly Bodies			Fly Heads			Analyte	Fly Bodies			Fly Heads			
ACh	2.64	±	0.08	0.212	±	0.011	Thr	18.4	±	1.8	0.98	±	0.04	
Ch	312	±	8.8	66.36	±	1.14	VMA							
CA							Trp	17.1	±	0.9	0.44	±	0.02	
His	2.7	±	0.1	0.27	±	0.04	MOPEG							
Ans							Kyo							
Carn							Cys							
HTau	21	±	6				KA	1.9	±	0.1	0.4	±	0.04	
Tau	278.5	±	4.1	88.81	±	3.19	Spd	0.03	±	0.002	0.01	±	0.0003	
Arg	0.45	±	0.01	0.06	±	0.004	PhEt	0.336	±	0.015	0.005	±	0.0004	
Hist	1.92	±	0.13	0.772	±	0.011	TrpA	1.85	±	0.09	0.024	±	0.002	
Asn	6.5	±	0.7	0.74	±	0.04	NAS	29.61	±	0.7	4.24	±	0.242	
Ser				0.8	±	0.4	5HIAA	0.47	±	0.07	0.025	±	0.001	
Gln	54.99	±	0.59	5.61	±	0.14	5HTOL							
HSer	4.5	±	1.1	0.4	±	0.01	HCY							
Cit							3HAA							
ETA	44.03	±	0.92	5.56	±	0.27	HCA	0.07	±	0.01				
Asp							HVA							
Agm							DOMA							
Glc	3170	±	295	1111.5	±	0.2	Kyn	8	±	0.7				
Gly	8	±	1	0.8	±	0.004	Spm							
Glu	1.1	±	0.2	0.21	±	0.03	DOPEG							
BAla	83.5	±	0.7	3.04	±	0.13	5HTP	184.1	±	3.6	1.83	±	0.04	
Ala	90.4	±	5.4	22.84	±	2.69	OA				0.003	±	0.0002	
NAP	0.16	±	0.01	0.009	±	0.0001	NM							
GABA	6.25	±	0.18	1.661	±	0.055	Tyr	8.4	±	0.2	0.35	±	0.007	
Pro	614.3	±	2.8	100.46	±	2.2	3HK	36	±	3	1.7	±	0.1	
Ado	31.1	±	0.12	2.599	±	0.038	Syn							
Val	22.3	±	0.3	2.17	±	0.1	5HT	81.66	±	10.34	5.98	±	0.666	
Met	16.17	±	0.58	1.186	±	0.025	DOPAC	0.09	±	0.003	0.013	±	0.001	
Orn							3MT							
GSH							LDOPA	1.5	±	0.13	0.541	±	0.026	
Lys	0.2	±	0.02				TyrA	11.89	±	0.64	0.062	±	0.001	
Put	0.08	±	0.001	0.0074	±	0.0003	NE							
Leu	53.6	±	1.9	3.84	±	0.04	E							
Phe	18.4	±	0.3	1.02	±	0.03	DA	0.22	±	0.01	0.005	±	0.0001	

Conclusions

These results demonstrate the utility of BzCl derivatization with HPLC-MS/MS for targeted neurochemical metabolomics. Improvements to the benzoylation of small neurochemicals resulted in a comprehensive, robust, and quantitative method to monitor 70 neurochemicals. This modified method improves sensitivity for compounds containing 1,2-diols and early eluting peaks such as acetylcholine, and was expanded to 4-fold more neurochemicals compared to prior studies. The method is suitable for multiple samples types, including CSF, serum, and tissue homogenate.

The results also indicate considerable potential for even wider use of BzCl as a MS labeling reagent. For example, the Michigan Regional Comprehensive Metabolomics Resource Core maintains a library of over 1,000 metabolites. Based on the reactivity of BzCl towards amines, phenols, thiols, and some alcohols, we estimate it could be used to label approximately 25% of these compounds. BzCl labeling is fast and simple to implement. Benzoylation improves sensitivity, retention, and quantification (via easily generated internal standards) with few drawbacks compared to direct detection of analytes.

CHAPTER 3: VENTRAL TEGMENTAL AREA NEUROTENSIN SIGNALING LINKS THE LATERAL HYPOTHALAMUS TO LOCOMOTOR ACTIVITY AND STRIATAL DOPAMINE EFFLUX IN MALE MICE

 Equal authorship was awarded to Patterson and Wong. Specific contributions from Wong to this work included development and optimization of a capillary liquid-chromatography mass spectrometry neurotensin peptide assay, and monoamine and amino acid analysis in mouse microdialysate.

Introduction

Dopamine (DA)-containing neurons of the ventral tegmental area (VTA) project widely in the forebrain, including to the nucleus accumbens (NAc); the release of DA within the NAc mediates motivation and is required for volitional activity[218]. Indeed, artificial activation of the VTA→NAc mesolimbic DA (MLDA) circuit underlies the motivating properties of natural rewards and drugs of abuse. Under normal conditions, a variety of physiologic and environmental parameters modulate NAc DA release to control motivation appropriately for conditions. Many physiologic parameters (including those related to fluid balance, energy stores, endocrine status, and infection) are initially sensed in the hypothalamus[219], which integrates these inputs and relays a composite signal to the MLDA and other effector systems.

The lateral hypothalamic area (LHA) represents the major link between the hypothalamus and the MLDA system. Indeed, animals will self-administer electrical or optogenetic stimulation of lateral hypothalamic neurons (intrahypothalamic self-

stimulation), consistent with the motivating properties of LHA output[220, 221]. Specific subsets of LHA neurons likely mediate distinct aspects of MLDA regulation. LHA neurons that contain the neuropeptide hypocretin (HCRT) (also known as orexin) project to the VTA and promote MLDA activity[222, 223]. Melanin-concentrating hormone-containing LHA neurons project to the NAc (among other places) and modulate motivated behaviors such as feeding[224].

The peptide neurotensin (NT) has been implicated in control of feeding and the MLDA system. A substantial percentage of VTA DA neurons express NT receptor 1 (NTR1), administration of NT in rodents activates VTA DA neurons and stimulates DA release in the NAc, and NT injection acutely decreases feeding and alters locomotor activity[225-229]. NT neurons are found throughout the brain, including the LHA. LHA NT neurons innervate and inhibit local LHA HCRT neurons, as well as projecting directly to the VTA[220, 230, 231]. Many LHA NT neurons express the leptin receptor (LepRb) and thus respond directly to leptin (an adipokine that signals the repletion of body energy stores); ablation of LepRb from LHA NT neurons prevents the inhibition of HCRT neurons by leptin and blunts MLDA function and locomotor activity[231]. Furthermore, many VTA DA neurons contain NTR1 and NT can augment the activity of VTA DA neurons (by enhancing the postsynaptic response to glutamate (Glu) on N-methyl-D-aspartate receptors)[227]. Similarly, intrahypothalamic self-stimulation for optogenetic activation of LHA neurons is blunted by NTR1 antagonists[220]. Thus, LHA NT neurons, by releasing NT into the VTA, could modulate MLDA function to link hypothalamic signals to NAc DA release. Here, we interrogate this putative circuit by pharmacogenetically activating LHA NT neurons to examine VTA and NAc neurotransmitter release, along with

resultant locomotor behavior.

Materials and Methods

Animals

Adult mice (8–12 wk of age) were used for all experiments. All animals were bred in our colony in the Unit for Laboratory Animal Medicine at the University of Michigan in accordance with the guidelines and approval of the University Committee on the Care and Use of Animals. Mice were housed in a temperature and humidity controlled room with 12-hour light, 12-hour dark cycles with access to food and water ad libitum. Adequate measures were taken to prevent animal pain and discomfort throughout the course of the experiments. In addition, all animal experiments were conducted within the guidelines of Animal Research Reporting in vivo Experiments. The Nt^{cre}, $Rpl22^{tm1.1Psam}$ (Rpl22-HA reporter), $Gt(ROSA)26^{Sortm14(CAG-tdTomato)Hze}$ (ROSA26-tdTomato), and *GAD1-GFP* mouse lines have been previously described[231-233]. The Nt^{cre} and $Rpl22^{tm1.1Psam}$ or $Gt(ROSA)26^{Sortm14(CAG-tdTomato)Hze}$ mice were intercrossed to generate compound heterozygous reporter mice (Nt^{cre}-HA and Nt^{cre}-tdTomato, respectively).

Stereotaxic injection and VTA cannulation

Nt^{cre} mice were anesthetized via isoflurane before the initiation of surgical procedures. Stereotaxic viral injections were made bilaterally into the LHA with a guide cannula and injector using the next coordinates: anterior-posterior −1.34, medial-lateral ±1.13, dorsal-ventral −5.2. Three hundred nL of adenovirus-associated virus (AAV)-hM3Dq-mCherry[110, 234] (prepared by the University of Iowa or University of North

Carolina Vector Core) was injected into the LHA using a 500-nL Hamilton syringe at the rate of 20 nL/min. Bilateral injections were performed in animals receiving AAV-hM3Dq to ensure adequate infection. After 5 minutes of time after injection, the injector and cannula were removed from the animal and the incision site was closed. Mice were allowed 1–2 weeks to recover before experimentation.

For experiments requiring intra-VTA injection of the water soluble NTR1 antagonist, SR142948A (Sigma), mice were implanted with an indwelling 26-guage stainless steel cannula with a removable dummy injector (Plastics One) aimed at the VTA using the next coordinates: AP −3.2, ML −0.5, DV −4.3. After 1 week of recovery, the dummy was removed and replaced with an injector with a 4.4-mm projection used to deliver 65 nL of SR142948A (5μM), 15 minutes before ip clozapine-N-oxide (CNO) administration.

Metabolic and behavioral profiling

*Nt^{cre};*LHA-hM3Dq-mCherry mice (n = 5) were analyzed *via* the Comprehensive Laboratory Monitoring System (Columbus Instruments), as previously described[231]. Briefly, mice were placed into the sealed chambers with ad libitum access to food and water. After 2 days of acclimation, animals were treated with vehicle for 2 days and then with CNO (0.3 mg/kg, IP) for 2 days; treatments were every 12 hours (6 am and 6 pm). Oxygen consumption (VO_2), carbon dioxide production (VCO_2), spontaneous motor activity, and Z-activity were monitored continuously during this time. Data shown are for the first 12 hours after each treatment.

Open-field activity was determined in separate cohorts of *Nt^{cre};*LHA-hM3Dq-

mCherry mice (n = 6–8). Mice were removed from their home cages during the light-cycle and acclimated for 2 hours in an open-field arena (ENV-017M; Med Associates, Inc.) in the absence of food and water. After acclimation, open-field activity was recorded every minute after 30 minutes of baseline, 30 minutes after saline injection, 30 minutes after antagonist injection (when applicable), and 90 minutes after CNO. For experiments involving dopamine receptor 1 (D1R) antagonism, mice were pretreated with the D1R antagonist, SCH23390 (0.1 mg/kg, ip, dissolved in PBS; Sigma), 30 minutes after vehicle administration and 30 minutes before CNO treatment.

Mouse locomotor behavior during microdialysis (n = 6) was monitored using Logitech webcams above a Raturn (Bioanalytical Systems, Inc.) as previously described[68, 235]. Webcams used a custom motion-monitoring program (Mark Dow) through image acquisition toolbox in Matlab 2009 (Mathworks, Natick) software. Threshold of motion detection software was selected to not detect small motions (such as breathing or whisker movement) but only large motions such as walking, running, and rearing. Data were collected every 1 min and then binned into longer intervals to correlate to facilitate comparisons with data from neurochemical assays.

Perfusion fixation and immunohistochemistry

After experimentation, all mice were perfused with fixative to verify viral, indwelling cannula, and/or microdialysis probe placement. Mice were only included in the results if mCherry expressing cell bodies were confined to the LHA, and histological analysis revealed correct cannula placement.

Animals received an overdose of sodium pentobarbital and were then perfused

transcardially with phosphate buffered saline (PBS; pH 7.4) followed by 10% formalin. The brain was removed and postfixed in 10% formalin for 2–4 hours and then dehydrated in 30% sucrose in PBS until the time of sectioning. Brains were cut on a freezing sliding microtome in 30-μm coronal sections on a sliding microtome, collected in 4 representative series, and stored at −20°C in cryoprotectant. Sections were thoroughly washed with PBS to remove the cryoprotectant before immunostaining.

To immunostain for the product of the *Fos* gene (cFos), free-floating brain sections were pretreated consecutively with the next reagents in PBS: 1% H_2O_2, 0.3% glycine, and 0.03% sodium dodecyl sulfate. Samples were then blocked in 3% normal donkey serum/3% Triton X-100 in PBS and then incubated with goat anti-cFos (1:1000; Santa Cruz Biotechnology, Inc.) overnight in the same buffer. Sections were washed in PBS, incubated in biotinylated donkey-antigoat (1:200; Jackson ImmunoResearch) for 2 hours, followed by avidin-biotin-complex labeling (Vectastain Elite kit; Vector Laboratories). Signals were developed with metal-enhanced diaminobenzidine (Thermo-Pierce) resulting in a brown precipitate.

For mCherry/tdTomato and hemaglutinin (HA) immunostaining, sections were blocked as described above and then incubated in rabbit anti-red fluorescent protein (dsRed) (1:1000; Clontech) or mouse anti-HA (1:1000; Covance) overnight, respectively. Brain sections were washed and then incubated with Alexa Fluor-conjugated secondary antibodies (1:200; Invitrogen). Sections were mounted onto gelatin-coated slides and coverslipped with ProLong Antifade mounting medium (Life Technologies).

Microscopy and image analysis

Microscopic images were obtained using an Olympus BX-51 microscope with a DP30BW camera (Olympus). Images from fluorescent labeling experiments were pseudocolored and merged using Adobe Photoshop.

Microdialysis, analysis of amino acid (AA) and neuropeptide concentrations.

Custom-made side-by-side microdialysis probes (1-mm dialyzing membrane) were inserted into NAc or VTA using the next coordinates: AP +1.30, ML ±1.20, DV −4.85; and AP −2.98, ML ±0.48, DV −5.17, respectively. For the monoamine and AA assay, probes were made using regenerated cellulose (Spectrum Laboratories) and inserted bilaterally in the NAc. For neuropeptide measurement in the VTA, probes were made using AN69 membrane (Hospal) and a single probe was inserted. For NT antagonist experiments, a dialysis probe was implanted in the NAc and a microinjection cannula (Plastics One) was implanted in the ipsilateral VTA. Probes and cannulae were secured with skull screws and acrylic dental cement. After surgery, mice were allowed to recover for 24 h with free access to food and water.

Experiments were performed 24 h after probe implantation. Microdialysis probes were flushed at a flow rate of 2 μL/min with artificial cerebrospinal fluid for 30 min using a Fusion 400 syringe pump (Chemyx). Perfusion flow rate was then reduced to 1 μL/min for monoamine and AA assay or 0.6 μL/min for the NT assay and allowed to flush for an additional 1.5 h before baseline collections.

Samples were collected every 5 min for monoamine and AA assay in the NAc and every 20 min for the monoamine and AA and NT assays in the VTA. The total volume of

dialysate for VTA NT was 12 μL, of which 3 μL were removed, and 1 μL acetonitrile was added for analysis by the monoamine and AA assay described below.

Monoamine and AA analysis

Samples were analyzed according to a slightly modified version of a recently described method[31]. To 5 μL samples, we added 2.5 μL of 100 mM sodium tetraborate, 2.5 μL of benzoyl chloride (2% in acetonitrile vol/vol), 2.5 μL of internal standard, and 2.5 μL d_4-acetylcholine internal standard before liquid chromatography-mass spectrometry (LC-MS) analysis. For VTA, 3-μL samples 1.5 μL of each reagent listed above were added before LC-MS analysis. Samples were analyzed using a Waters nanoAquity UPLC equipped with an Acquity HSS T3 C18 column (1 × 100 mm, 1.8 μm, 100-Å pore size) interfaced to an Agilent 6410 triple quadrupole mass spectrometer. Mobile phase A consisted of 10mM ammonium formate and 0.15% (vol/vol) formic acid in water. Mobile phase B was acetonitrile. The flow rate was 100 μL/min, and sample injection volume was 5 μL. The mobile phase gradient was: initial, 0% B; 0.01 min, 23% B; 2.51 min, 23% B; 3 min, 50% B; 5.2 min, 60% B; 6.46 min, 65%; 6.47 min, 100% B; 7 min, 100% B; 7.01 min, 0% B; and 8.0 min, 0% B. Peaks were processed using Agilent MassHunter Workstation Quantitative Analysis for QQQ version B.05.00.

Neurotensin detection with capillary LC-MS

NT was measured using a capillary LC-MS method similar to that previously described[67, 68]. Capillary columns and electrospray ionization emitter tips were made in-house[68]. Five-microliter samples were injected using a WPS-3000TPL autosampler,

desalted by rinsing the column with 0.1% formic acid in water at 3500 psi for 8 minutes using a 100DM high pressure syringe pump (Teledyne ISCO), and then separated by a gradient elution with an Agilent 1100 HPLC pump. For the gradient, mobile phase A was 0.1% formic acid in H_2O and mobile phase B was 0.1% formic acid in MeOH. The mobile phase gradient was as follows: initial, 10% B; 2 min, 100% B; 6 min, 100% B; 6.1 min, 10% B; and 8 min, 10% B. A Valco 6-port valve was used to switch between loading/desalting and elution. Assays were controlled automatically using Thermo-Fisher Xcalibur software.

The column was interfaced to a PV-550 nanospray electrospray ionization source (New Objective) coupled to a Thermo-Fischer LTQ XL linear ion trap mass spectrometer. The MS^2 pathway for NT (doubly charged) was mass-to-charge ratio (*m/z)* 558.7 → 579.0 *m/z* with an isolation width set at 3 *m/z*. Standard addition tests with NT showed that there was no significant effect of artificial cerebrospinal fluid matrix. In vitro recovery of NT was 14 ± 1%.

Statistics

Student's t test was used when only 2 groups were compared. One-way ANOVA with Bonferroni post hoc analysis was used when comparing 3 or more groups. Data were analyzed and graphs were generated using GraphPad Prism software. Differences were deemed significant if $P < .05$. Activity data are binned and presented as mean ± SEM. All in vivo microdialysis data are expressed as percent baseline ± SEM.

Results

Activation of LHA NT neurons promotes DA-dependent activity

LHA NT neurons respond to a variety of physiologic signals (including nutritional cues, dehydration, and inflammation), and are hypothesized to play a role in the modulation of motivated behaviors, including locomotor activity, in response to these signals[231, 236, 237]. To understand the function of LHA NT cells and the neural mechanisms by which they mediate their effects, we employed the stereotaxic injection of AAVs that mediate the cre-dependent expression of designer receptors exclusively activated by designer drugs (DREADDs) (expressed as DREADD-mCherry fusion proteins)[110, 234]. DREADDs are genetically engineered muscarinic receptor variants that are insensitive to endogenous ligands, but which are activated by the otherwise biologically inert CNO[110, 234]; CNO activates neurons containing the Gq-coupled hM3Dq DREADD variant. To confirm the cre-dependent expression of hM3Dq-mCherry in LHA NT neurons after viral injection, we performed unilateral injections of AAV-hM3Dq-mCherry into the LHA of Nt^{cre}-HA mice, which express an HA epitope-tagged ribosomal protein[233]. Immunostaining against HA and mCherry demonstrated the restriction of hMD3q-mCherry to LHA NT-HA neurons (Figure 3-1 A).

To examine the response to activation of LHA NT cells, we injected the activating AAV-hM3Dq-mCherry bilaterally into the LHA of Nt^{cre} animals (Figure 3-1 B) and, after at least 1 week of recovery, treated these Nt^{cre};LHA-hM3Dq-mCherry animals with vehicle or CNO (Figure 3-1 C and D). CNO treatment increased cFos-immunoreactivity (IR) in the LHA; this cFos-IR was mainly restricted to mCherry-IR neurons (Figure 3-1 C and D), consistent with the CNO-dependent activation of hM3Dq-mCherry-expressing

LHA NT cells. CNO also increased cFOS-IR in the NAc, consistent with the notion that LHA NT neurons modulate the MLDA system (Figure 3-1 E and F).

We also treated Nt^{cre};LHA-hM3Dq-mCherry animals with vehicle or CNO in a metabolic chamber to determine the potential effect of LHA NT cell activation on locomotor activity and VO_2 (Figure 3-2 A-G). Pharmacogenetic activation of LHA NT cells nearly doubled ambulatory activity, and increased Z-axis activity by 8-fold during the 3 hours after CNO. Activation of LHA NT cells also increased VO_2 and VCO_2, consistent with the increased locomotor activity exhibited by these animals. Thus, the activation of LHA NT cells promotes locomotor activity in vivo.

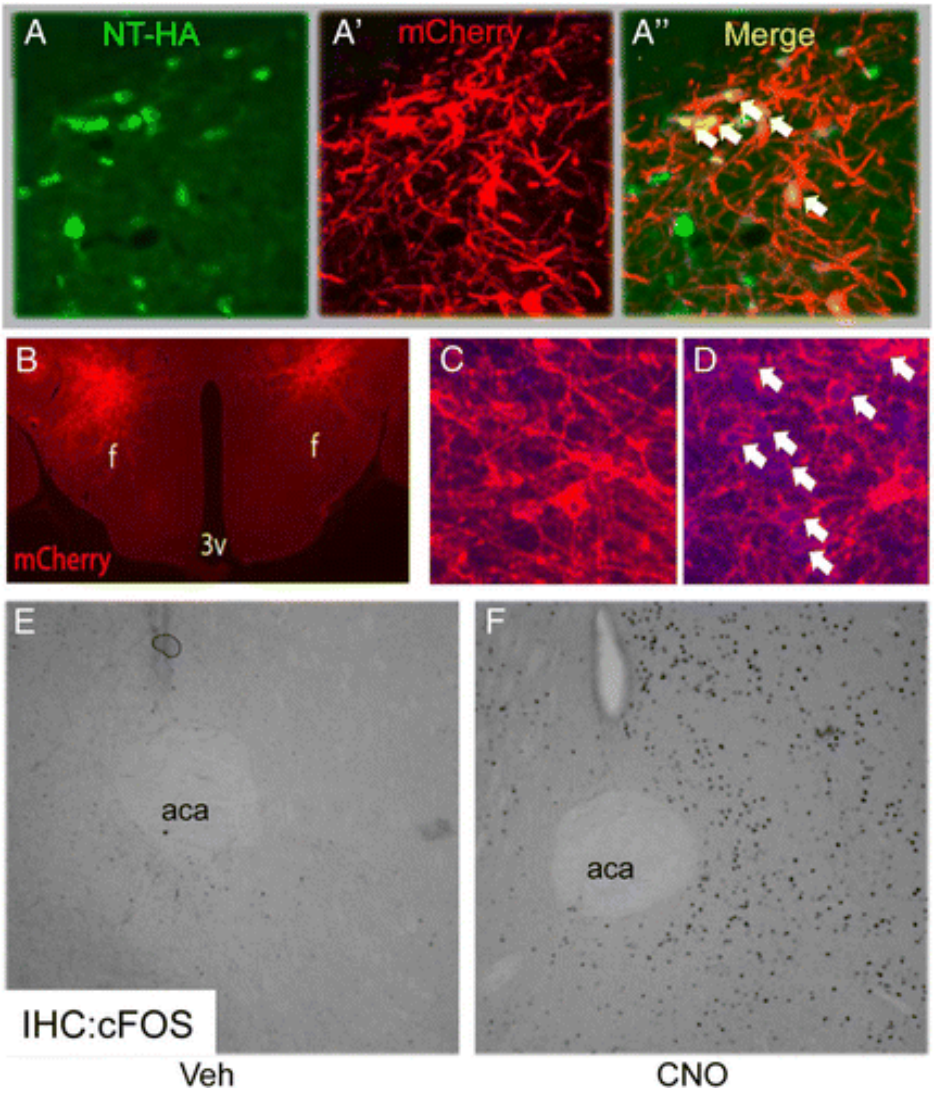

Figure 3-1 Activation of LHA NT neurons increases cFOS in LHA NT cells and in the NAc. Cre-inducible AAV-hM3Dq-mCherry was injected unilaterally into the LHA of male Nt^{cre} HA (A, A', and A") or bilaterally into the LHA of Nt^{cre} mice (B–F). A, A', and A", Representative image showing NT-HA-IR (A), mCherry-IR (A'), and merged channels (A") in the LHA. Arrows denote representative colocalized cells. B, Representative image of mCherry-IR in the hypothalamus after bilateral injection. C and D, Animals were injected with vehicle (Veh; ip) (C) or CNO (0.3 mg/kg, ip) (D) and perfused 2 hours later. Shown are representative images of mCherry-IR (red) and cFOS-IR (purple, pseudocolored). Arrows denote colocalized neurons. F, fornix; 3v, third cerebral ventricle. E and F, Representative images showing cFOS-IR (black) after Veh (E) or CNO (F) in the NAc. aca, anterior commissure.

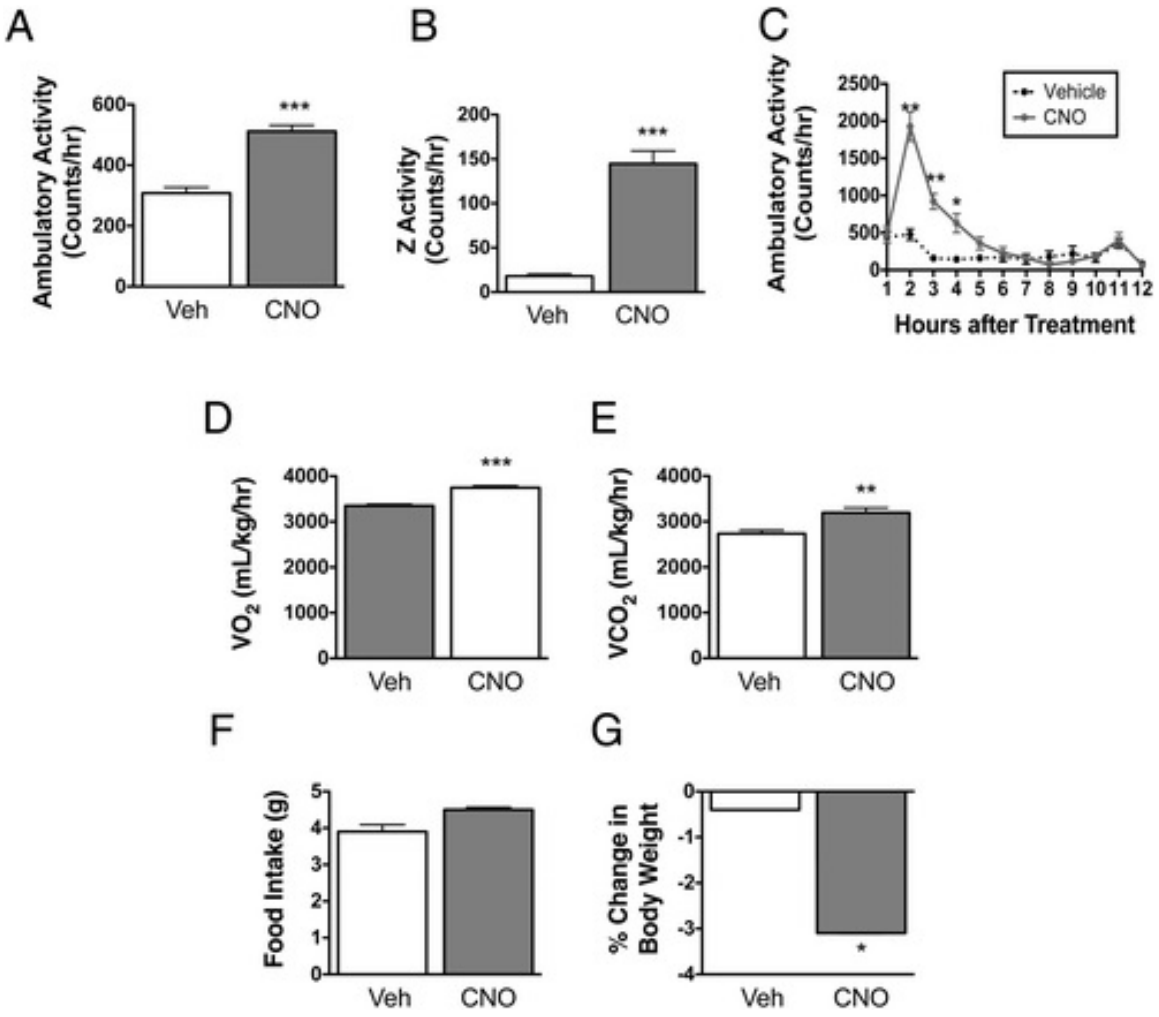

Figure 3-2 Activation of LHA NT neurons increases ambulatory activity and energy expenditure. Nt^{cre};LHA-hM3Dq-mCherry mice were acclimated to the Comprehensive Laboratory Monitoring System (CLAMS) for 2 days and treated with vehicle (Veh; ip) or CNO (0.3 mg/kg, ip) on separate days. Ambulatory activity (A and C), Z-activity (B), VO_2 (D) and VCO_2 (E) (both corrected for lean body mass), food intake (F), and change in body weight (G) are plotted for the subsequent 12 hours. All data are plotted at mean ± SEM, n = 8. Significance was determined by Student's t test. *, $P < .05$; **, $P < .01$; ***, $P \leq .001$.

We have previously shown that, outside of the LHA, synaptic terminals from LHA NT cells primarily target midbrain regions, including the VTA[231]. Because NT can enhance the activity of VTA DA cells[220, 238] and the release of VTA-derived DA into the striatum promotes locomotor activity[239], and we observed increased cFOS-IR in the NAc after activation of LHA NT cells, we examined the potential role for DA in the locomotor activity that accompanies the hM3Dq-mediated activation of LHA NT cells (Figure 3-3).

Systemic administration of the D1R antagonist, SCH23390, did not significantly reduce baseline locomotor activity of animals in activity chambers but blunted the hM3Dq-mediated increase in activity to baseline levels. Thus, the activation of LHA NT cells promotes DA-dependent locomotor activity, suggesting that activation of LHA NT neurons promotes DA release in the NAc.

To assess this possibility, we performed in vivo microdialysis to examine the release of DA and its metabolites in the NAc of mice after the pharmacogenetic activation of LHA NT neurons in Nt^{cre};LHA-hM3Dq-mCherry animals (Figure 3-4 and

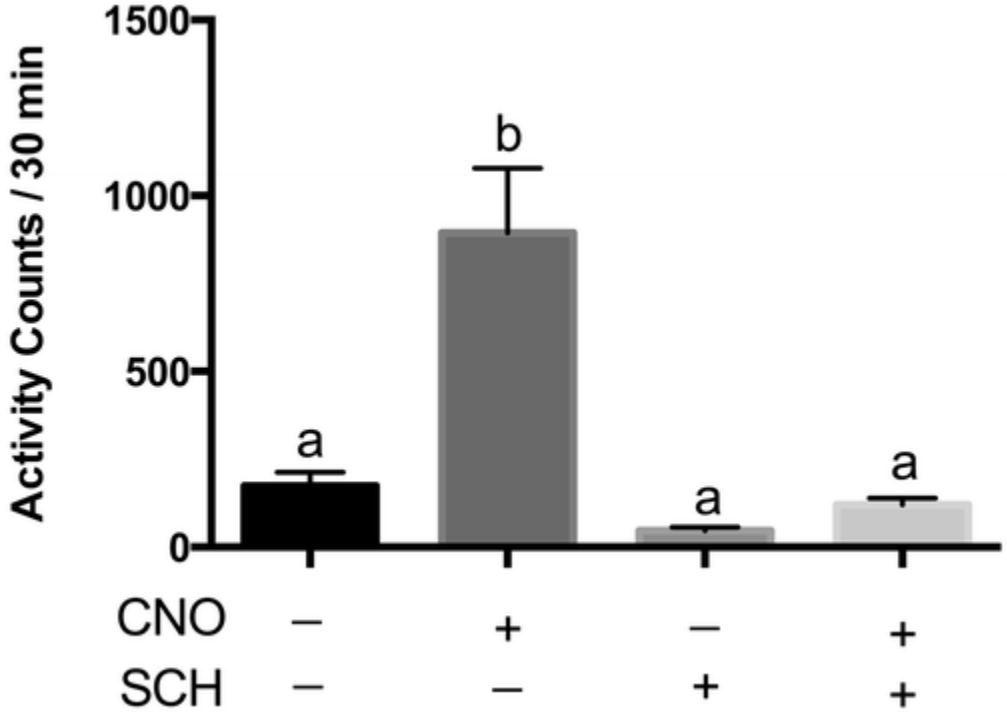

Figure 3-3 Blockade of ambulatory activity induced by hM3Dq-mediated activation of LHA NT neurons is blocked by peripheral administration of a D1R antagonist. $Nt^{cre;}$LHA-hM3Dq-mCherry mice were acclimated to an open field area for 2 hours during the light cycle, after which time, their activity was monitored for 30 minutes after vehicle or CNO (0.3 mg/kg, ip) administration. Additional animals were pretreated with an ip injection (0.1 mg/kg) of the D1R antagonist, SCH23390 (SCH), 30 minutes before CNO administration. Activity (counts per min) is binned for the 30 minutes after vehicle (+/− SCH) and averaged per 30 minutes for CNO treatment (+/− SCH). All data are plotted as mean ± SEM, n = 7–8. Significance was determined by repeated measures ANOVA followed by Bonferroni post hoc analysis. Different letters indicate significant differences ($P \leq .001$); all other comparisons $P > .05$.

Figure 3-5). Locomotor activity was acutely increased by the injection of vehicle, although activity returned to baseline before the injection of CNO, which promoted a larger and sustained increase in locomotor activity (Figure 3-4A, consistent with Figure 3-2 and Figure 3-3). Although neither the extracellular concentration of DA nor its metabolites (3,4-dihydroxyphenylacetic acid (DOPAC), 3-methoxytyrosine (3MT), and homovanillic acid (HVA)) were altered by the injection of vehicle, CNO doubled the extracellular concentration of DA, which (like locomotor activity) peaked 30 minutes after CNO injection and remained elevated for at least the next 90 minutes. CNO also significantly increased the extracellular concentrations of DOPAC, 3MT, and HVA; the peaks of 3MT and HVA were prolonged relative to DA and DOPAC, consistent with the requirement for the cellular uptake of DA or DOPAC for the production of 3MT and HVA by intracellular monoamine oxidase. The increase in these metabolites also supports the notion that the increased extracellular DA observed reflects enhanced release rather than decreased DA reuptake. Thus, the activation of LHA NT neurons promotes NAc DA efflux, consistent with the DA dependence of the enhanced locomotor activity exhibited by mice after the activation of LHA NT cells.

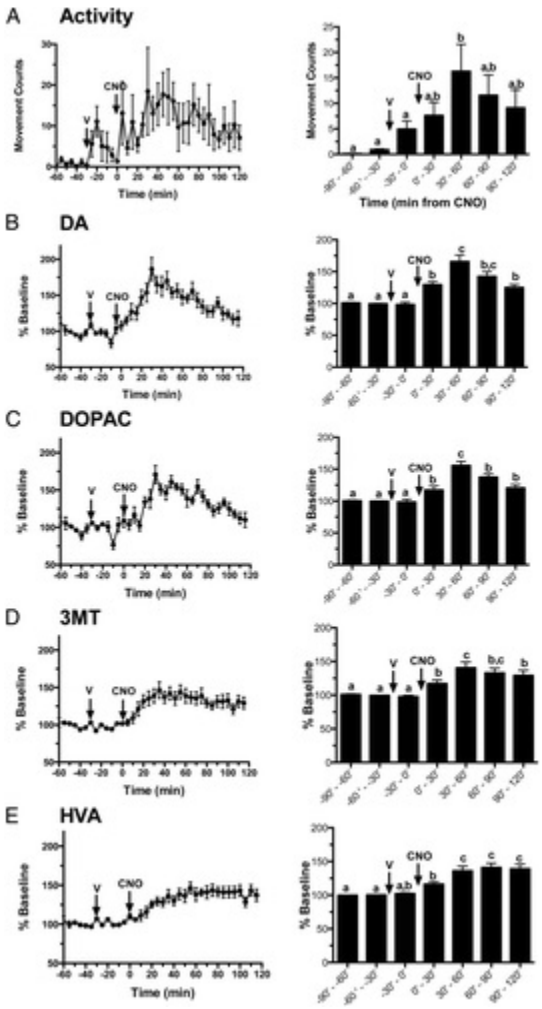

Figure 3-4 Extracellular DA and metabolites in NAc of Nt^{cre};LHA-hM3Dq-mCherry mice. Bilateral microdialysis probes were implanted into the NAc to monitor the effect of hM3Dq-mediated activation of LHA NT neurons. Vehicle was administered at t = −30 minutes, followed by CNO (0.3 mg/kg, ip, at t = 0 min) (arrows). Locomotor behavior from quantification of video (A) during microdialysis. Dialysate was assessed for (B) DA, (C) DOPAC, (D) 3MT, and (E) HVA. Locomotor behavior is shown as movement counts ± SEM. All in vivo microdialysis data are expressed as percent baseline ± SEM; n = 6–8. Left panels show data in 5-minute bins; right panels show 30-minute bins. Significance was determined by one-way ANOVA followed by Bonferroni post hoc analysis. Different letters indicate significant differences ($P \leq .05$).

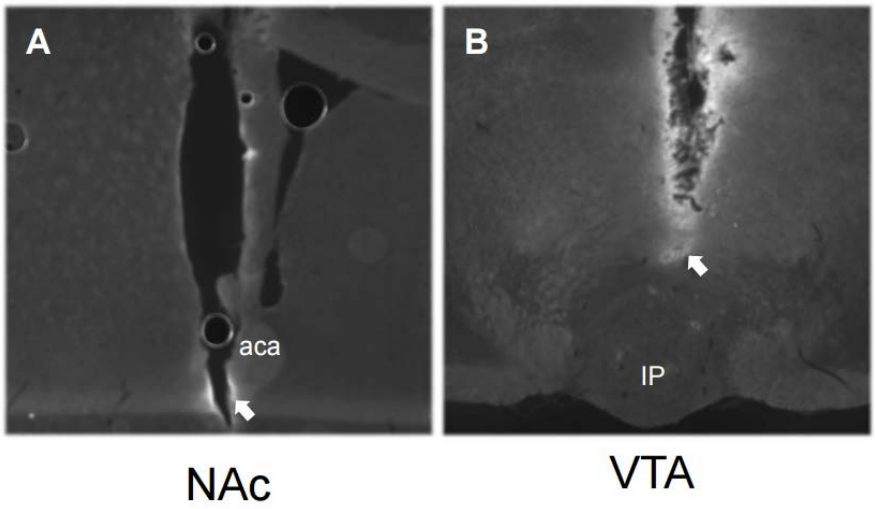

Figure 3-5 Microdialysis probe and indwelling cannula placement. A-B) Representative images of NAc microdialysis probe placement (A) and VTA cannula placement (B). Arrows indicate termination of probe (A) or acute injector tip (B). aca= anterior commissure , IP=interpeduncular nucleus.

Our finding that LHA NT cells project to the VTA, but not the NAc[231], suggests that neurotransmitters released by LHA NT neurons into the VTA act on DA neurons to promote the release of DA in the NAc. Because NT can postsynaptically increase N-methyl-D-aspartate-dependent Glu signaling in VTA DA neurons[220], we implanted microdialysis cannulae in the VTA of Nt^{cre};LHA-hM3Dq-mCherry animals and measured the extracellular concentration of NT (as well as GABA and Glu) in the VTA at baseline, after vehicle treatment, and after CNO administration (Figure 3-6). Although LHA NT neurons express Gad1 (a marker of GABA neurons) (Figure 3-6A), CNO did not detectably increase the extracellular concentrations of GABA or Glu in the VTA (Figure 3-6, B and C). In contrast, however, the extracellular concentration of NT increased by almost 2-fold during the 20 minutes after CNO treatment (Figure 3-6D), demonstrating that the activation of LHA NT neurons promotes NT efflux into the VTA. Importantly, VTA NT concentrations return to baseline within 20 minutes of stimulation, suggesting

that CNO-mediated activation of LHA NT cells promotes acute (rather than prolonged) VTA NT release.

To directly examine the possibility that LHA NT neurons may promote NAc DA efflux by acutely releasing NT into the VTA, we implanted VTA injection cannulae along with NAc microdialysis cannulae in Nt^{cre};LHA-hM3Dq-mCherry animals to examine extracellular DA in the NAc in the presence of VTA-applied SR14298A (an antagonist of NT1 receptors) (Figure 3-7 and Figure 3-5). Although the application of SR14298A into the VTA did not alter NAc DA concentrations in the absence of CNO treatment, it abrogated the ability of activated LHA NT cells to promote NAc DA efflux. Thus, the acute release of NT into the VTA by LHA NT neurons promotes prolonged NAc DA efflux.

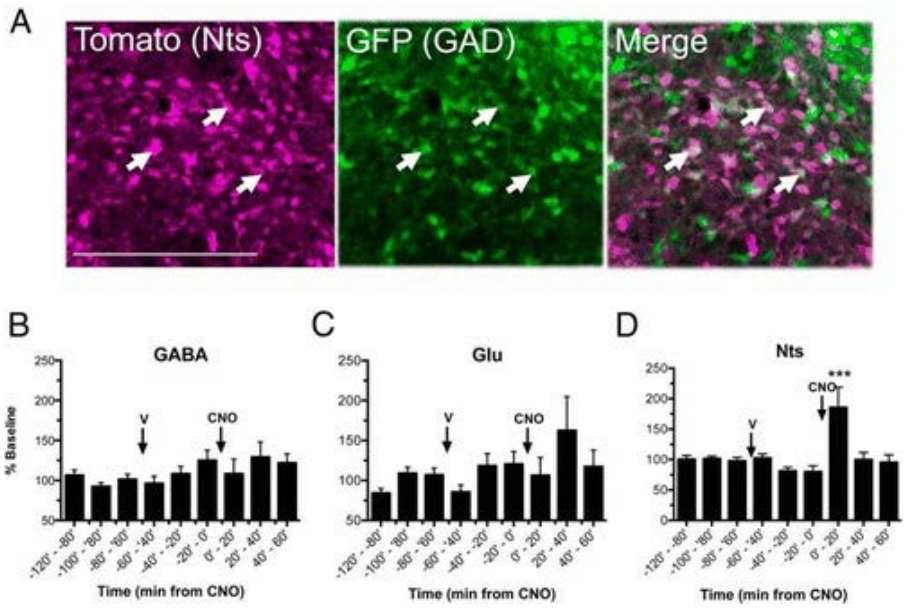

Figure 3-6 Neurotransmitter content and release by LHA NT neurons. Nt^{cre} mice were bred to the ROSA26-tdTomato and Gad1-GFP backgrounds to generate animals expressing tdTomato in in NT neurons and GFP in Gad1 cells. A, Representative images showing tdTomato-IR (NT; purple, left), GFP-IR (Gad1; green, middle) and merged (right) channels in the LHA of Ntcre tdTomato;GAD1-GFP mice. Arrowheads indicate examples of colocalization. B–D, Extracellular concentrations of (B) GABA, (C) Glu, and (D) NT in the VTA of Ntcre;LHA-hM3Dq-mCherry mice. Vehicle (t = −60 min) and CNO (0.3 mg/kg, ip; t = 0 min) were administered systemically. In vivo microdialysis data are expressed as percent baseline ± SEM; n = 6. Significance was determined by one-way ANOVA followed by Bonferroni post hoc analysis; ***, $P \leq .001$ vs other times.

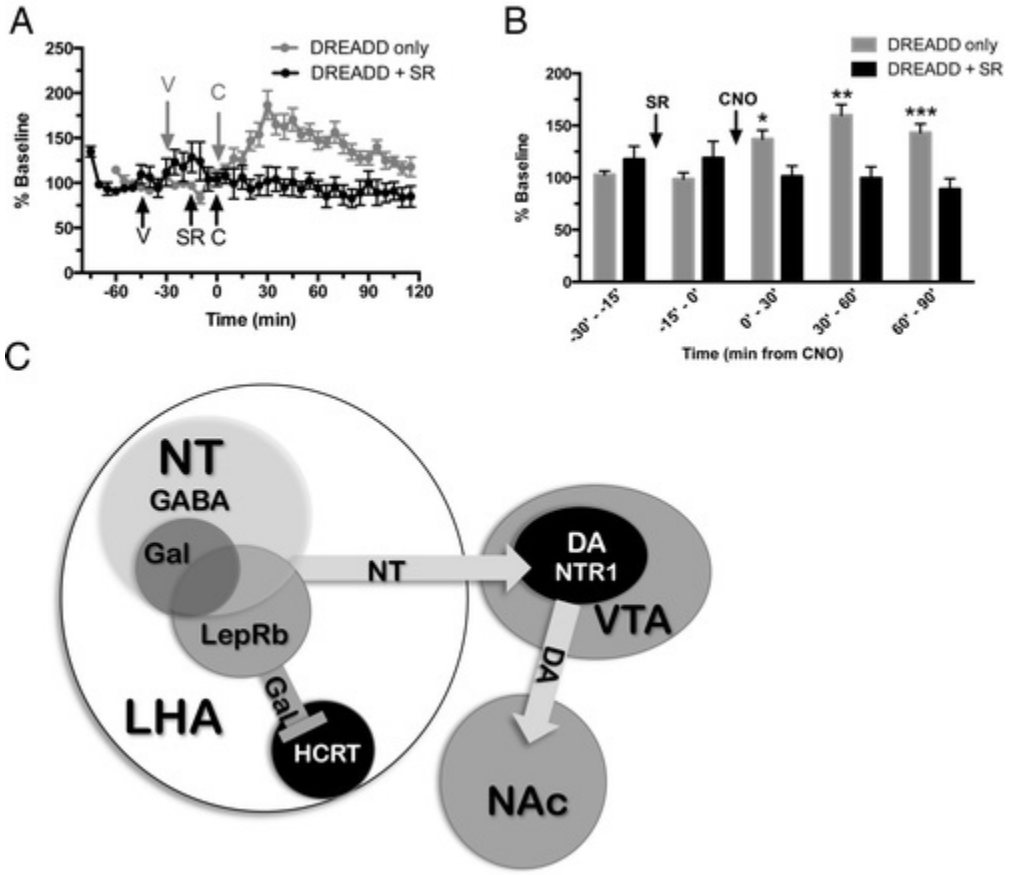

Figure 3-7 Effect of NT1R antagonism on LHA NT-DREADD-evoked NAc DA release. Unilateral microdialysis probes were implanted into the NAc with ipsilateral cannulation of the VTA. Vehicle, NtsR1-antagonist SR142948A (SR; dose via intra-VTA injection) and CNO (0.3 mg/kg, ip; t = 0 min) were administered at the indicated times. A, Extracellular DA concentrations in the NAc. B, Data from A plotted in 15- or 30-minute bins. Data are expressed as percent baseline ± SEM; n = 6. Significance was determined by one-way ANOVA followed by Bonferroni post hoc analysis. *, P < .1; **, P < .01; ***, P < .001. C, Model of the control of the MLDA system via LHA NT neurons. LHA NT neurons contain the neurotransmitter GABA. Some of these NT neurons express the LepRb and locally regulate HCRT neuronal function, via the neuropeptide Gal. A potentially separate population of LHA NT neurons may directly project to the VTA and release NT onto NTR1-expressing DA neurons to regulate the MLDA system through projections to the NAc. Note that although the figure is simplified for easier viewing, it is possible that interneurons could lie between LHA NT neurons and OX or DA neurons.

Discussion

Our present results reveal that LHA NT neurons stimulate NAc DA release to promote motivated behaviors such as ambulatory activity, thus revealing an important function for these cells. Additionally, we have mapped the circuits and mechanisms by which LHA NT neurons mediate this effect: LHA NT neurons project to the VTA, where they promote acute NT release; NT acts on NTR1 in the VTA to promote prolonged NAc DA release (Figure 3-7).

In addition to the use of genetic (e.g., Nt^{cre}, AAV-hM3Dq-mCherry) and pharmacologic techniques, this analysis required the fabrication and use of microdialysis probes small enough to permit the neuroanatomically precise sampling of extracellular fluid in the mouse NAc and VTA, as well as the development of techniques to quantitatively measure NT at physiologic concentrations in the resultant samples. To our knowledge, this represents the first report to measure changes in neuropeptide release in the intact mouse; this technique enabled us to directly assess the timing and amplitude of intra-VTA NT release induced by pharmacogenetic activation of LHA NT neurons. The requirement that we collect sufficient sample volume to permit NT detection by subsequent MS analysis dictates a prolonged (20 min) sampling time, thus limiting temporal resolution. Even so, it is clear that DREADD-mediated activation of LHA NT neurons promotes acute NT release and also that VTA NT concentrations return to baseline by 20 min after stimulation.

In contrast to the rapid rise and fall of VTA NT concentrations, the hM3Dq-promoted increase in NAc DA concentration (which requires VTA NT signaling) continues for at least 2 h, much longer than the increase in VTA NT. These findings

suggest that VTA NT promotes a durable increase in NAc DA release (and accompanying locomotor behavior) that continues long after VTA NT has returned to baseline and that the action of LHA NT cells mediates the long-term rather than acute modulation of the MLDA system. Consistent with this long-term activation, Kempadoo et al[220] showed that NTR1 antagonism blocks the increase postsynaptic NDMA response of VTA DA neurons to the optogenetic activation of LHA→VTA fibers. That LHA NT neurons should mediate lasting effects on MLDA function makes teleological sense, because many LHA NT cells respond directly to leptin[231], which reflects long-term energy stores and mediates largely chronic (rather than acute) effects on neural systems[240].

Although we have recently demonstrated that the hM3Dq-mediated activation of LHA NT neurons also inhibits LHA HCRT neurons[230], the mechanism for this effect is distinct from that by which LHA NT neurons promote NAc DA efflux. Not only do the neural connections by which these responses occur differ (intra-LHA vs LHA→VTA projections) but also NT (which is required for increased NAc DA efflux) is not responsible for controlling the activity of HCRT cells. Rather, the inhibitory neuropeptide, galanin (Gal), which is found in some LHA NT neurons, inhibits the firing of HCRT cells[230]. Thus, LHA NT neurons mediate their effects on HCRT cells and the MLDA via distinct neurotransmitters. We do not know whether these distinct mechanisms of LHA NT neuron action reflect different patterns of neurotransmitter release by these cells in the LHA and VTA, or merely the innate responsiveness of HCRT and VTA neurons to the different neuropeptides.

Interestingly, although LHA NT neurons display markers of gamma amino

butyric acid (GABA) production and release (*Gad1* and *Slc32a1*), we did not detect VTA GABA release upon activation of these neurons. Although it is possible that the long collection times for VTA microdialysis samples (which are required for NT detection) could fail to detect a transient increase in VTA GABA after the activation of LHA NT cells, this technique readily detects prolonged release of DA and its metabolites downstream in the NAc. We were also unable to detect a role for GABA in the acute inhibition of HCRT neurons by LHA NT cells[230]. Thus although LHA NT neurons are genetically GABAergic, GABA release by these cells may play less important roles than their neuropeptide transmitters.

Because LHA NT neurons respond to a variety of physiologic signals (such as leptin, dehydration, and inflammation), this LHA NT→VTA NTR1→NAc DA circuit that we have mapped may link these stimuli to the long-term modulation of VTA DA neurons, NAc DA efflux, and thus locomotor activity and other DA-dependent behaviors. Indeed, disruption of LepRb in LHA NT cells diminishes locomotor activity and measures of MLDA function[231], suggesting that leptin action on LHA NT cells may control MLDA function by modulating NT release in the VTA. Additional work will be required to understand the contribution of NT signaling to the control of MLDA function by the various stimuli that modulate the activity of LHA NT neurons.

CHAPTER 4: SIMULTANEOUS *IN VIVO* MICRODIALYSIS AND LOCAL OPTOGENETIC STIMULATION TO MEASURE OPIOID PEPTIDE RELEASE IN DYNORPHIN CONTAINING CELLS IN MOUSE NUCLEUS ACCUMBENS SHELL

Introduction

The mesocorticolimbic pathway, a major component of the brain's reward circuit, is comprised of neuronal projections from the ventral tegmental area, medial prefrontal cortex, basolateral amygdala, and hippocampus to the nucleus accumbens (NAc)[241, 242]. Disruption of the mesocorticolimbic pathway is implicated in diseases including mood disorders and addiction. Studies have linked both positive and negative reinforcement behavior responses to discrete sub nuclei in the NAc[243-245]. To fully understand what drives these opposing behaviors, it is important to monitor neurochemical changes that correlate with behavioral output.

Opioid neuropeptides are key neuromodulators in the regulation of mood disorders. There are four G protein-coupled receptors that bind endogenous opioids: kappa, mu, delta, and opioid receptor like-1 (also referred to as nociceptin or orphaninFQ receptors)[90, 246, 247]. Kappa opioid receptors (KOR) are expressed on GABAergic medium spiny neurons in the NAc and are the receptors for the endogenous peptide dynorphin (Dyn)[248-250]. Mu and delta opioid receptors are also present on GABAergic medium spiny

neurons in the striatum, with a high affinity for endogenous enkephalins (ENK), leu-enkephalin (LE) and met-enkephalin (ME)[251].

Opioids in the brain are derived from three prohormones, proopiomelaocortin, prodynorphin, and proenkephalin. The precursor peptide prodynorphin is cleaved into Dyn and three copies of LE[88, 249]. Proenkephalin is cleaved into one LE, four ME, and two extended-ME peptides[88]. These biosynthetic pathways that generate bioactive peptides are important for opioid-related neuromodulation, and are not fully understood in studies using current analytical techniques. Methods to selectively modulate opioid containing neurons combined with muliplex analytical techniques will allow a broader understanding of these processes.

Endogenous opioid activity modulates a wide variety of behaviors. For example, KOR agonists induce place aversions, depression-like behavior, and dysphoria in both human and animal models[252-254]. Dyn-containing axon terminals and cell bodies are located in the NAc[243, 255], and regulate monoamine cells *via* presynaptic KOR. However, the mechanisms underlying endogenous Dyn regulation of KOR-mediated negative affective behaviors are unclear[243, 256, 257].

Current technologies utilizing genetics and optics (optogenetics), allow selective activation or inhibition of specific subsets of neurons with photostimulation[258]. Previous work demonstrated that photostimulation of distinct subpopulations of ventral NAcSh (NAc shell) DYN-expressing cells results in aversive behavioral responses such as conditioned place aversion and a reduction in operant self-stimulation[243]. In contrast, photostimulating dorsal NAc Dyn-expressing cells caused positive reinforced behaviors. All of these behaviors were blocked by selective KOR antagonist administration[243]. To

determine if these behaviors correlate with release of Dyn, we selectively activated discrete Dyn-expressing cell in the NAcSh using optogenetic photostimulation and monitored endogenous opioid peptides (Dyn fragment A_{1-8} (DYN), LE, and ME) and small molecule release into the extracellular space to determine if actual release of DYN occurred. We developed a capillary liquid chromatography-mass spectrometry (LC-MS) method, incorporating an isotopically labeled internal standard to monitor opioid peptides DYN (fragment dynorphin A_{1-8}), LE, and ME, and developed a custom in-house optogenetic-microdialysis (opto-dialysis) probe to simultaneously photostimulate and sample neurochemical release locally within the stimulated region. We applied this method and sampling technique to investigate regional differences between the ventral NAcSh (vNAcSh) and dorsal NAcSh (dNAcSh).

Methods

Chemicals

Dynorphin A_{1-8} (abbreviated DYN) and LE were purchased from American Peptide (Sunnyvale, CA); ME was purchased from Sigma Aldrich (St. Louis, MO). Isotopically labeled leucine ($^{13}C_6{}^{15}N_1$-leucine) was used to create an isotopically labeled dynorphin A_{1-8} internal standard (DYN*) through the University of Michigan's protein synthesis core. Water, methanol, and acetonitrile for mobile phases are Burdick & Jackson HPLC grade purchased from VWR (Radnor, PA). All other chemicals were purchased from Sigma Aldrich (St. Louis, MO) unless otherwise noted. Artificial cerebrospinal fluid (aCSF) consisted of 145 mM NaCl, 2.67 mM KCl, 1.4 mM $CaCl_2$, 1.01 mM $MgSO_4$, 1.55 mM Na_2HPO_4, and 0.45 mM $Na_2H_2PO_4$ adjusted to pH 7.4 with

NaOH. Ringer solution consisted of 148 mM NaCl, 2.7 mM KCl, 2.4mM $CaCl_2$, and 0.85 mM $MgCl_2$ adjusted pH to 7.4 with NaOH. In experiments that used high K^+ ringer solution NaCl was adjusted to 48 mM and KCl was adjusted to 100 mM, all other chemicals remained the same.

Animals

Adult male C57BL/6 mice (Envigo, 5 – 6 weeks of age) were used for initial experiments to determine perfusion media conditions and effects of probe design. For optogenetic studies, adult male preprodynorphin-IRES-cre (*dyn-Cre*) mice were provided by the Michael Bruchas lab at the Washington University in St. Louis, MO[243]. Mice were unilaterally injected with 300 nL of AAV5-DIO-ChR2-eYFP (Washington University in St. Louis, Hope Center Viral Vector Core, viral titer 2×10^{13} vg/mL) into either the dNAcSh or vNAcSh and were allowed to recover from surgery at Washington University in St. Louis 1 week prior to shipment. Mice were then acclimated for 2-3 weeks at the University of Michigan before microdialysis probe implantation.

In vivo microdialysis

Mice were group housed in temperature and humidity controlled rooms with 12 h light/dark cycles with access to food and water *ad libitum.* The University of Michigan Unit for Laboratory Animal Medicine approved animal procedures and they were in accordance with the National Institute of Health Guidelines for the Care and Use of Laboratory Animals. All experiments were conducted within the guidelines of Animal Research Reporting *in vivo* Experiments. Surgical procedures for inserting probes were

similar to previous described[259]. Briefly, mice were anesthetized in an induction chamber with 5% isoflurane prior to surgical procedures and placed in a Model 963 stereotaxic frame (David Kopf Instruments, Tujunga, CA, USA) equipped with a mouse ear and bite bar. Mice were maintained under anesthesia with 1-2% isoflurane during cannulation procedures. A custom-made 1 mm polyacrylonitrile membrane (Hospal AN69) concentric probe, with or without fiber optics (provided by the Michael Bruchas lab from Washington University in St. Louis), was inserted into either the dNAcSh (stereotaxic coordinates from bregma: +1.3 anterior-posterior [AP], ±0.5 medial-lateral [ML], -4.5 mm dorsal-ventral [DV]) or vNAcSh (stereotaxic coordinates from bregma: +1.3 [AP], ±0.5 [ML], -5.0 mm [DV]). Light power from a 473-nm laser was measured at the membrane to ensure satisfactory light power (defined as ≥ 5 mW at a distance of 1 mm from the end of fiber optic) before implantation of microdialysis probes integrated with fiber optic (opto-dialysis probe). Implanted probes were secured using two bone screws and dental cement. Mice were allowed to recover 24 h with free access to food and water prior to baseline collection for microdialysis studies.

For microdialysis studies, the fiber optic was connected to the laser via a tether running through a Ratturn (Bioanalytical Systems, Inc.) along with microdialysis perfusion lines. Microdialysis probes were flushed for 1 h using a Fusion 400 syringe pump (Chemyx, Stafford, TX USA) at a flow rate of 2 μL/min. The flow rate was lowered to 0.8 μL/min and flushed for an additional 1 h prior to fraction collection. Microdialysis fractions were collected every 15 min, resulting in a 12 μL sample. Two μL of sample was removed for benzoyl chloride (BzCl) derivatization to monitor small

molecules, and the remaining 10 μL was spiked with 1.1 μL of 100 pM isotopically labeled DYN* (10 pM final concentration) and was used for peptide analysis.

When experiments were completed, mice were euthanized and perfused with paraformaldehyde. Brains were extracted to confirm probe placement and virus expression by histology. Mice with verified virus expression and correct probe placement were included in the data set.

Optogenetic stimulation

On the day of the experiment, mice were connected to a laser *via* a tether alongside the microdialysis perfusion lines. An Arduino was programmed and connected to the 473-nm laser to provide stimulation frequency of 10 Hz, 10-ms pulse width. The laser was manually operated and turned on and off during a single 15 min fraction after 4 baseline collections. Six additional fractions were collected after the photostimulation, followed by two fractions with high 100 mM K^+ ringer solution. High K^+ ringer solution, which elicits exocytosis in neurons, was perfused following photostimulation to confirm functionality of local neuronal activity.

Peptide assays with capillary LC-MS

An assay was developed to monitor opioid peptides (DYN, LE, and ME) using capillary LC-MS[67, 73, 259, 260]. Capillary columns and electrospray ionization emitter tips were prepared in-house[73, 259, 260]. Capillary columns were prepared using a 10 cm length of 50/360 μm (inner diameter/outer diameter) fused silica capillary packed with 5 μm

Altima^{TM} C18 particles to a bed length of 3.5 cm. The column was connected to a fused silica ESI emitter tip using a Teflon connector.

Five μL samples were injected, onto the capillary column as described in the materials and methods section in Chapter 3. An Agilent 1100 HPLC pump (Santa Clara, CA) to deliver the elution gradient containing water with 0.1% FA for mobile phase A and mobile phase B was MeOH with 0.1% FA delivered as initial 0% B; 1 min, 30 %B; 4 min, 50% B; 4.1 min 100% B; 7 min, 100% B; 7.1 min, 0%B; and 10 min, 0% B.

The capillary column was interfaced to a linear ion trap (LTQ XL, Thermo Scientific), operating in positive mode. The MS^2 pathway for opioid peptides DYN, LE, and ME were detected using *m/z* values of 491 → 435, 556 → 397, and 574 → 397 respectively. Isotopically labeled DYN* (+7 mass shift, isotopically labeled $^{13}C_6{}^{15}N_1$-leucine) internal standard was detected using *m/z* values of 495 → 438. *In vitro* recovery of a 1 mm probe for DYN, LE, and ME were 12 ± 2%, 13 ± 3%, and 13 ± 2%.

Fresh DYN, LE, and ME standards, spiked with DYN* for the opioid assay were prepared daily. Standards were analyzed with capillary LC-MS at 0.01, 0.05, 0.1, 1, 10, 20, 50, and 100 pM concentrations in triplicate to determine linearity, reproducibility, and limits of detection[209]. Opioid analytes were normalized to DYN*. Limits of detection for DYN, LE, and ME were 0.2 ± 0.04, 0.5 ± 0.3, and 0.6 ± 0.4 pM in 5 μL determined each day of experimentation.

Mice that had average basal levels above the limits of detection and had appropriate probe placement and virus expression were used for the study. In total, 37 mice were run for the optogenetic experiments: 21 dNAcSh and 16 vNAcSh. From these 37 mice, 10 were excluded due to inadequate virus expression or probe placement: 6

dNAcSh and 4 vNAcSh. The remaining mice were then excluded if their average basal concentration was below the limit of detection for each analyte, determined the day of the experiment with triplicate calibration curves. For DYN, of the 27 remaining mice, 7 were excluded due to basal levels below the limit of detection: 4 from the dNAcSh shell study and 3 from the vNAcSh study. For LE 4 mice were excluded, and for ME 2 mice were removed.

Small molecule analysis using benzoyl chloride (BzCl) LC-MS

For small molecule analysis, dialysate samples were derivatized with BzCl and analyzed by LC-MS[31, 128]. This BzCl assay targeted choline (Ch), acetylcholine (ACh), histamine, taurine, glutamine, serine, aspartate, glycine, glutamate, glucose, 4-aminobutyric acid (GABA), adenosine, phenylalanine, serotonin and metabolite 5-hydroxyindoleacetic acid, norepinephrine and metabolite normetanephrine, tyrosine, and dopamine and metabolites 3,4-dihydroxyphenylacetic acid, 3-methoxytyramine, and homovanillic acid. Two µL dialysate were aliquoted from the peptide samples and were derivatized with 1.5 µL sodium carbonate, 100 mM; 1.5 µL BzCl, 2% (*v/v*) BzCl in acetonitrile; 1.5 µL isotopically labeled internal standard mixture diluted in 50% (*v/v*) acetonitrile containing 1% (*v/v*) sulfuric acid, and spiked with deuterated ACh and Ch (C/D/N isotopes, Pointe-Claire, Canada). Derivatized samples were analyzed using Thermo Fisher Accela UHPLC system interfaced to a Thermo Fisher TSQ Quantum Ultra triple quadrupole mass spectrometer fitted with a HESI II ESI probe, operating in multiple reaction monitoring. Five µL samples were injected onto a Phenomenex core-shell biphenyl Kinetex HPLC column (2.1 mm x 100 mm). Mobile phase A was 10 mM

ammonium formate with 0.15% formic acid, and mobile phase B was acetonitrile. The mobile phase was delivered an elution gradient at 450 µL/min as follows: initial, 0% B; 0.01 min, 19% B; 1 min, 26% B; 1.5 min, 75% B; 2.5 min, 100% B; 3 min, 100% B; 3.1 min, 5% B; and 3.5 min, 5% B. Thermo Xcalibur QuanBrowser (Thermo Fisher Scientific) was used to automatically process and integrate peaks. Each peak was visually inspected to ensure proper integration.

Statistical analyses

Statistics were performed in Graphpad Prism 7.0a (for Student's t-test and two-way ANOVA) or IBM SPSS Statistics software. The University of Michigan Center for Statistical Consultation and Research (CSCAR, consultant Yumeng Li) helped design a linear mixed model analysis appropriate for the optogenetic-dialysis study. The linear mixed model analysis was chosen to account for variations within and between mice and to account for missing data points within individual animals following sample loss or mechanical failure of the instrument. The linear mixed model was used to determine differences in basal conditions, effect of photostimulation relative to basal conditions, and prolonged effects after photostimulation relative to basal conditions. Linear mixed models were used to compare between genotypes within each region sampled, and between regions within *dyn-Cre* + and *dyn-Cre* – genotypes. In all cases, significance was defined as $p \leq 0.05$.

Results and Discussion

Detection of opioid peptides

We established a method to measure the opioid peptides DYN, LE, and ME using an isotopically labeled DYN* as an internal standard for quantitative analysis. High concentration injections of DYN* did not result in cross talk with endogenous DYN (Figure 4-1) demonstrating that the addition of DYN* does not contribute to endogenous DYN signal. DYN, LE, and ME standards were prepared in ringer solution, spiked with DYN*, and detected within 5 min after loading and desalting steps as shown by the capillary LC-MS reconstructed ion chromatographic trace (Figure 4-2). Standard addition tests with opioid peptides indicated no significant effect of dialysate matrix for any targeted analyte (Figure 4-3).

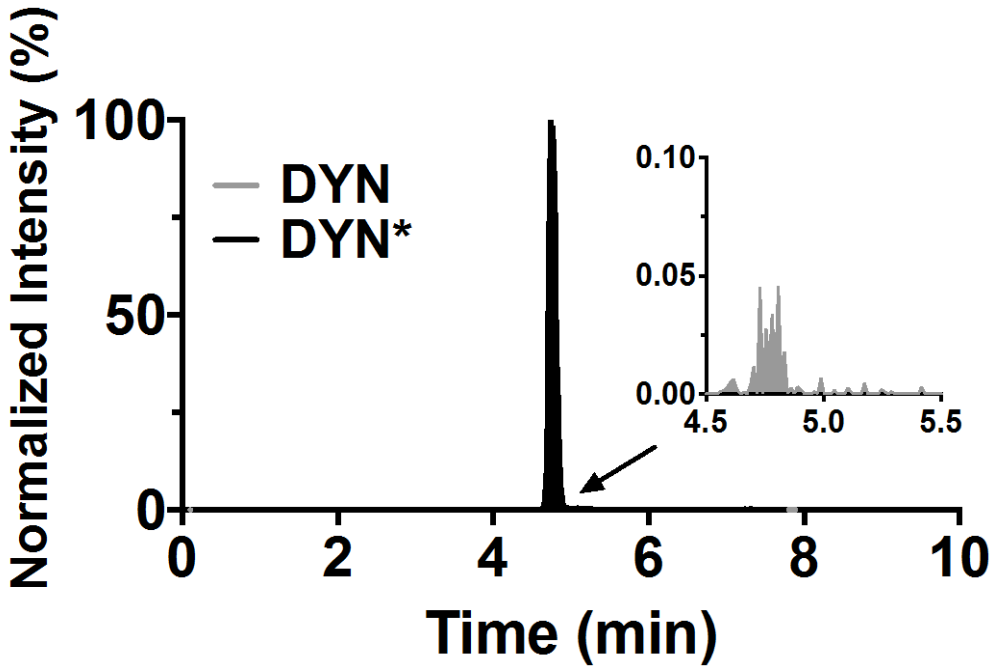

Figure 4-1 High concentration injections of DYN* did not show significant traces of endogenous DYN. A 500 pM sample of DYN* was injected while monitoring both the endogenous DYN (491 → 435 *m/z*) and isotopically labeled DYN* (495 → 438 *m/z*) mass-to-charge transitions.

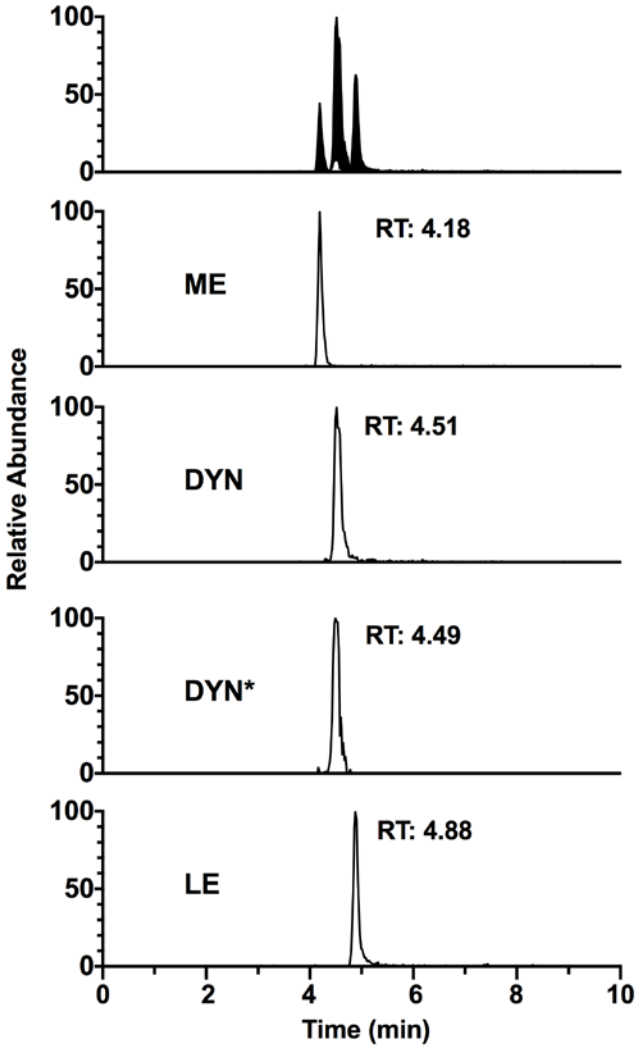

Figure 4-2 LC-MS chromatograms of 100 pM standards. Total ion chromatogram (top) and reconstructed ion chromatograms ME, DYN, isotopically labeled DYN*, and LE (lower), in order of retention time. Standards were made in ringer solution.

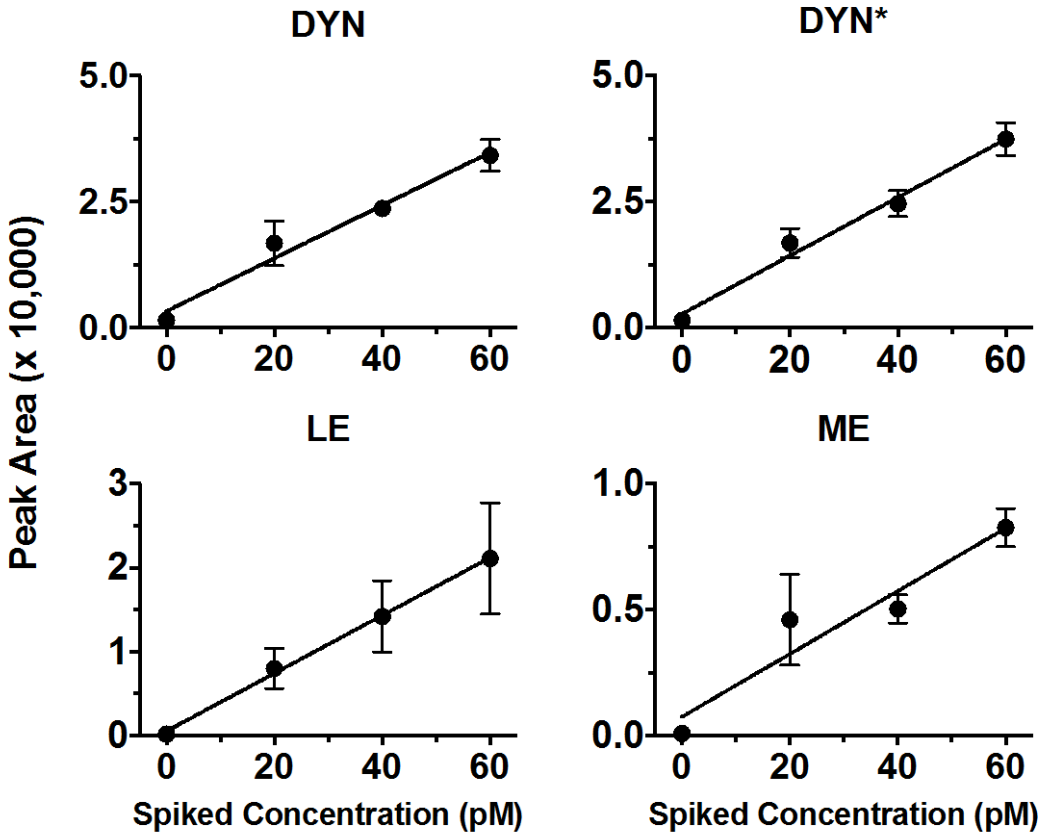

Figure 4-3 Bulk dialysate was collected and spiked with known amounts of standard. A linear response shows no effect of ionization suppression from the matrix. Four replicates per sample; data shown as average ± SD.

We previously applied a variation of this method for the detection of neurotensin, orexins, oxytocin, and vasopressin[73, 259, 260]. The addition of the DYN* isotope to our assay improves quantification by improving relative standard deviation (RSD) for repeated injections of standards (Figure 4-4). The internal standard accounts for variability during the LC injection and ionization into the mass spectrometer. If the internal standard is consistently added to each sample, it can be used in a ratio of analyte/internal standard to account for variability during analysis. We custom synthesized an isotopically labeled DYN* with a mass shift of +7 with a +3.5 *m/z* shift, because we detect the +2 charge state. DYN* is fully resolved by our linear ion trap and is not present in the dialysate (Figure 4-1). Ratios of DYN, LE, and ME to a consistent

DYN* were used for calibrations and analysis of standards for quantitative analysis for experiments. An ideal assay would include isotopically labeled internal standards for each analyte of interest. However, the addition of analytes to detect in the ion trap reduces points per peak and custom labeled isotopes are cost prohibitive. Because of the structural similarity between ME/LE and DYN, we included DYN* as our only internal standard. This method was therefore suitable to apply towards studying basal and evoked neuropeptide concentrations.

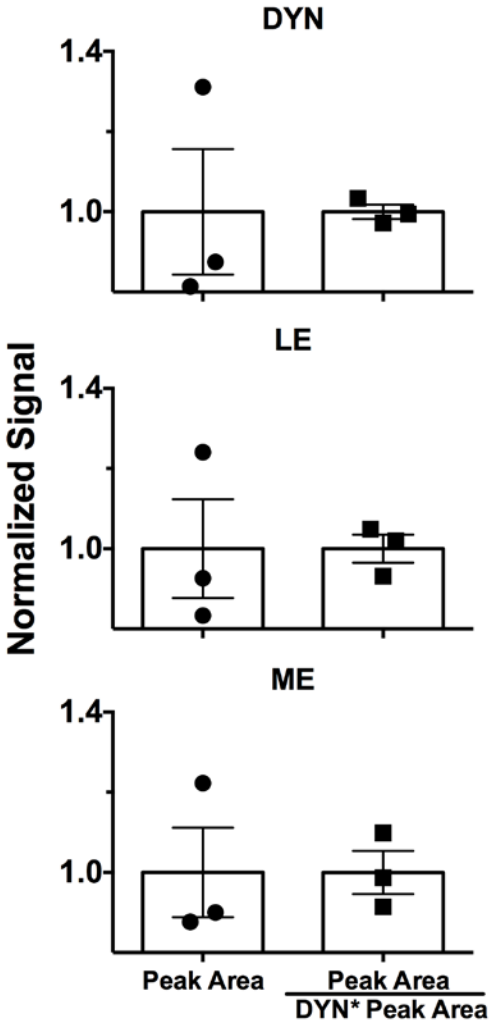

Figure 4-4 Addition of isotopically labeled DYN* results in better quantification. Peak area (left) and peak area ratios of DYN, LE, and ME, to isotopically labeled DYN* (right) are shown with triplicate standard injections. Signals were normalized to their respective averages. RSD for DYN, LE, and ME was 27, 21, and 19%, respectively, when only using peak area (left). RSD was reduced to 3, 6, and 9% when a ratio of analyte to internal standard, DYN*, peak area was used (right). Data shown as average ± SD.

Effect of Ca^{2+} in perfusion media

To validate the developed capillary LC-MS method for detecting dynamic changes *in vivo*, we monitored basal DYN, LE and ME, and locally K^+ stimulated release in the NAcSh. Pilot studies were performed using aCSF perfusion through the microdialysis probe to monitor basal conditions, followed by 30 min of 75 mM K^+ aCSF for local depolarization studies. Infusion of media with elevated K^+ through the microdialysis probe causes a steep concentration gradient across the membrane that allows the diffusion of K^+ into the extracellular space. This influx of K^+ ions disrupts the equilibrium of ions outside and inside the cell, which causes the neuron's resting membrane potential to depolarize, resulting in vesicular exocytosis. Local depolarization of neurons with K^+ is normally a reliable way to confirm that neurons are viable and responsive to stimuli. However, pilot studies using standard aCSF conditions with 75 mM K^+ aCSF resulted in measurable positive changes from basal DYN measurements in only half of the animals (7 of 14 pilot mice; Figure 4-5), whereas LE and ME were consistently stimulated to >1000% baseline in mice, indicating the K^+ stimulation did result in exocytosis as expected.

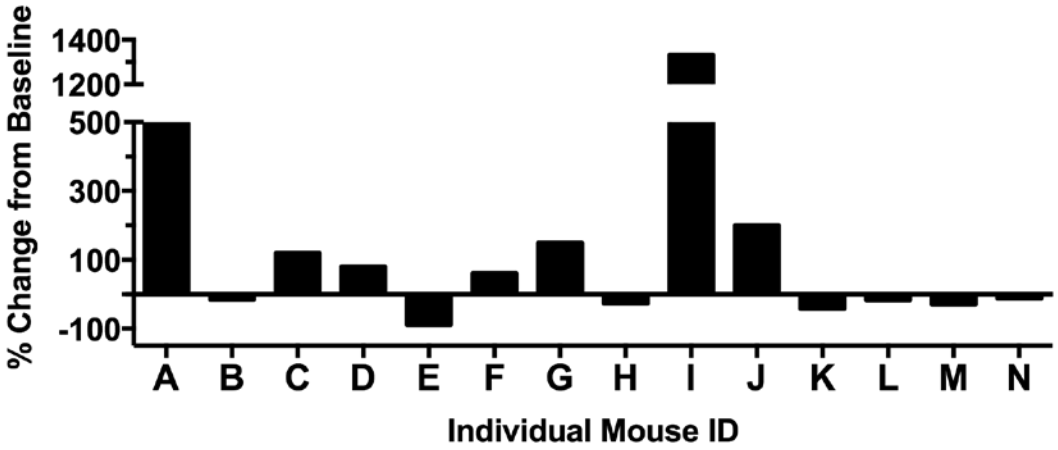

Figure 4-5 Effect of 75 mM K^+ aCSF on DYN from local depolarization of the NAcSh in individual mice A – N, normalized to their average baseline. Of the 14 mice tested, only 7 mice demonstrated increased dynorphin following K^+ stimulation.

A previous study showed that dynorphin B, another fragment from the precursor prodynorphin, was released in a Ca^{2+} dependent manner, and could be stimulated with 100 mM K^+ ringer solution[26]. You ZB *et al.* tested media with 1.2 mM Ca^{2+} or without Ca^{2+} followed by 100 mM K^+ stimulation in the rat striatum and substantia nigra, and found that the effect of K^+ local depolarization was Ca^{2+} dependent. We repeated this experiment using media with either 1.2 mM or 2.5 mM Ca^{2+} followed by a 100 mM K^+ local stimulation in the NAcSh of mice while monitoring DYN, LE, and ME (Figure 4-6). We demonstrated that mice infused with 2.5 mM Ca^{2+} followed by a 100 mM K^+ local stimulation resulted in reliable release of opioid peptides.

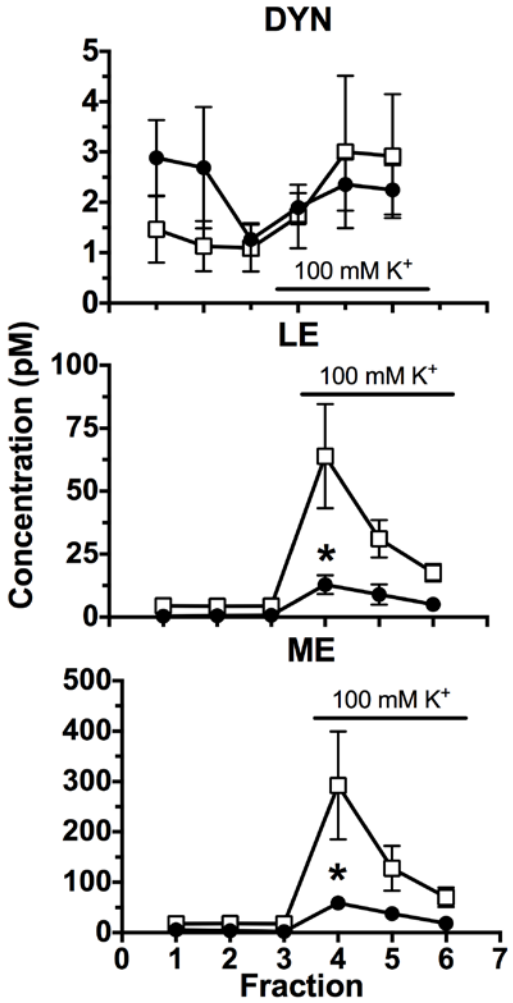

Figure 4-6 Effect of Ca^{2+} concentration in perfusion media followed by 100 mM K^+ stimulation. Filled circles represent 1.2 mM Ca^{2+}, and open squared indicate 2.5 mM Ca^{2+} ringer solution. Three baseline fractions were collected, followed by local depolarization of mouse NAcSh. Data shown as average ± SEM, n = 4 for each group of mice. Significance was determined by two-way ANOVA followed by Bonferroni post hoc analysis. * indicates $P \leq 0.05$.

Increased Ca^{2+} in the perfusion media resulted in stable DYN baseline, and elevated LE ($t(6) = 1.20$, $p < 0.05$), and ME ($t(6) = 3.43$, $p < 0.05$) baseline (Figure 4-7A). While the basal LE and ME levels were increased, there was no difference in the effect of 100 mM K^+ stimulation when normalized to its baseline (Figure 4-7B). Based on these results we decided to run all subsequent experiments using 2.5 mM Ca^{2+} ringer solution as the perfusion media.

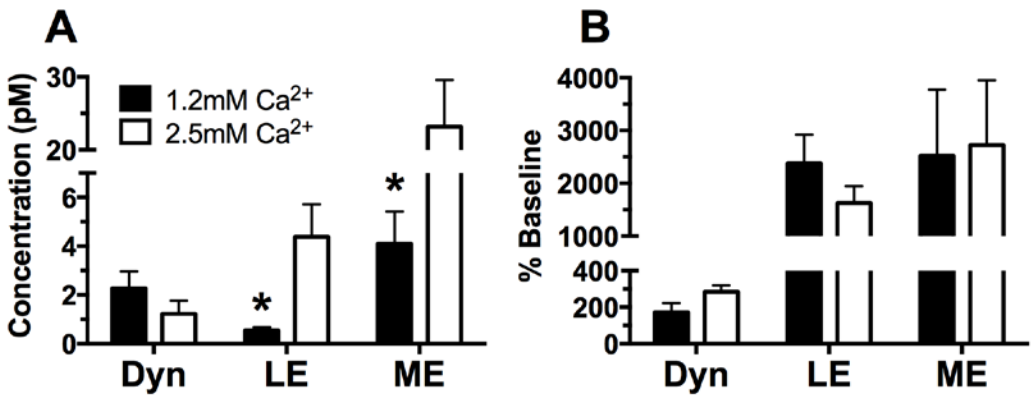

Figure 4-7 Effect of basal Ca^{2+} concentration in perfusion media (A) and 100 mM K^{+} evoked release normalized to each animal's average baseline (B). Elevated Ca^{2+} results in elevated LE and ME, and has no effect on DYN (A). When normalized to its baseline, there is no significant difference between 1.2 or 2.5 mM Ca^{2+} perfusion media. Data shown as average ± SEM, n = 4 for each group of mice. Significance was determined by Student's t-test. * indicates $P \leq 0.05$.

While stimulated responses were consistently observed for all opioid peptides in both conditions, DYN appeared to be delayed relative to LE and ME. This delay could be due to delayed neuronal release or slow peptide collection due to peptide adsorption anywhere from the probe membrane to vial storage. We tested adsorption *in vitro* and found that probes responded to changes in peptide stocks as expected (Figure 4-8).

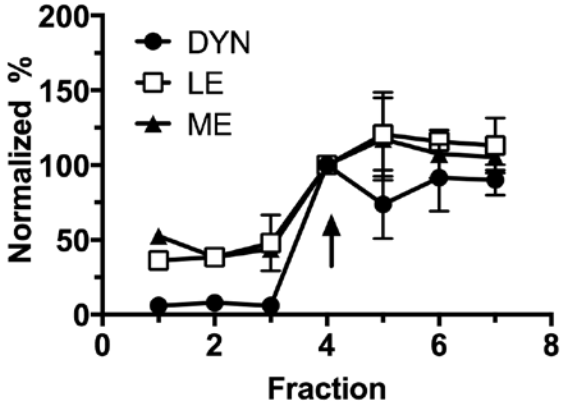

Figure 4-8 Trace of an *in vitro* step change from low to high stock concentrations showing peptides response. Probes were equilibrated in a 100 pM of DYN, LE, and ME stock, before 3 fractions were collected. Probes were quickly moved to a stock containing 1 nM Dyn and 400 pM LE and ME, and 4 additional fractions were collected to determine if there was a delay in response to the concentration change. The arrow indicates the first fraction in which the peptide was expected to change. Data was normalized to fraction 4, the fraction expected to reflect elevated concentration stock change. Data shown as average ± SD, n = 2 or 4 probes.

We previously reported that polyethylenimine (PEI) surface modification increases recovery of positively charged peptides by neutralizing the negatively charged AN69 membrane[75]. We hypothesized that PEI modification would increase DYN recovery, whereas neutral LE and ME would be unaffected. We attempted to increase relative recovery of DYN by performing a surface modification of the AN69 PAN probe membrane and fused silica collection lines with the polycation PEI. While DYN has a positive net charge of 2.0 at pH 7.0, we found that PEI modification of AN69 probes did not result in significant improvements in DYN, LE, or ME (Table 4-1).

Table 4-1 *In vitro* recovery for opioid peptides with or without PEI-modification to AN69 membrane and fused silica collection lines. Net charge was estimated using equation $Z = \sum_i N_i \frac{10^{pKa_i}}{10^{pH}+10^{pKa_i}} - \sum_j N_j \frac{10^{pKa_j}}{10^{pH}+10^{pKa_j}}$, where N represents number of reside/termini and *i* and *j* represent basic or acidic residue/termini, respectively. Data expressed as average ± SD, n = 2 probes per group.

Peptide	MW	Net Charge	Recovery (%) Untreated AN69 probe	Recovery (%) PEI-AN69 probe
DYN	981	2	9.4 ± 0.8	9.7 ± 0.7
LE	556	0	9.5 ± 1	9.6 ± 3
ME	574	0	11.8 ± 1	11.6 ± 3

Optogenetic-dialysis probe design

We developed a customizable microdialysis probe with an integrated fiber optic to locally sample near the site of optogenetic photostimulation in the brain. Traditional dialysis probes incorporate an inlet and outlet tubing ensheathed in a semi-permeable membrane enclosed with epoxy, and further ensheathed in a stiff cannula for rigidity and robustness. Our initial design encased both an inlet-outlet dialysis assembly and fiber optic probe protruding 1-2 mm beyond a protective cannula (Figure 4-9 A and B). When the probe was fully assembled, the smallest stainless steel cannula that could be used resulted in 812 μm outer diameter. Pilot studies with this probe resulted in poor or

undetectable levels of opioid peptides even with high K^+ stimulation, likely due to severe tissue damage. We re-designed the probe, removing the outer cannula and used the natural rigid property of the fiber optic to support the dialysis inlet-outlet assembly. Removing the outer cannula decreased the diameter of the probe approximately 1.5-fold to 480 μm outer diameter (Figure 4-9 A and C). *In vivo* tests showed that the probe was rigid enough to be stereotactically inserted into the brain, and that high K^+ reliably resulted in an increase of all opioid peptides using the modified shaft-less design. This "opto-dialysis" probe was used in all experiments (Figure 4-10).

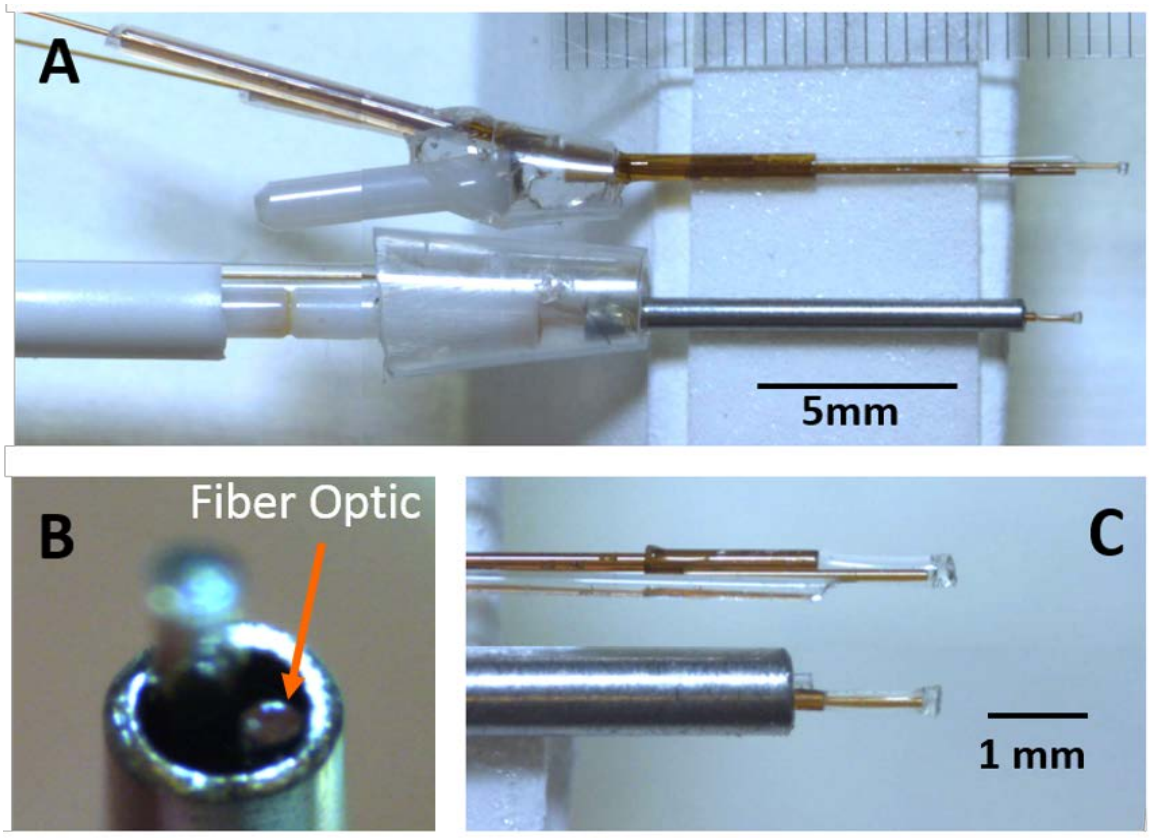

Figure 4-9 Two iterations of the optogenetic-dialysis probe incorporating microdialysis membrane assembly and fiber optic. The first generation of the optogenetic-dialysis probe used a stainless steel cannula encasing the inlet-outlet-membrane assembly and the fiber optic (bottom A, B). A top view of the first generation probe shows the fiber optic (orange arrow) next to the microdialysis membrane and encased in the stainless steel cannula (B). By removing the outer cannula support for the second generation, we reduced the diameter of the probe from 812 to 480 μm while maintaining enough support to be implanted in the brain (top A, C).

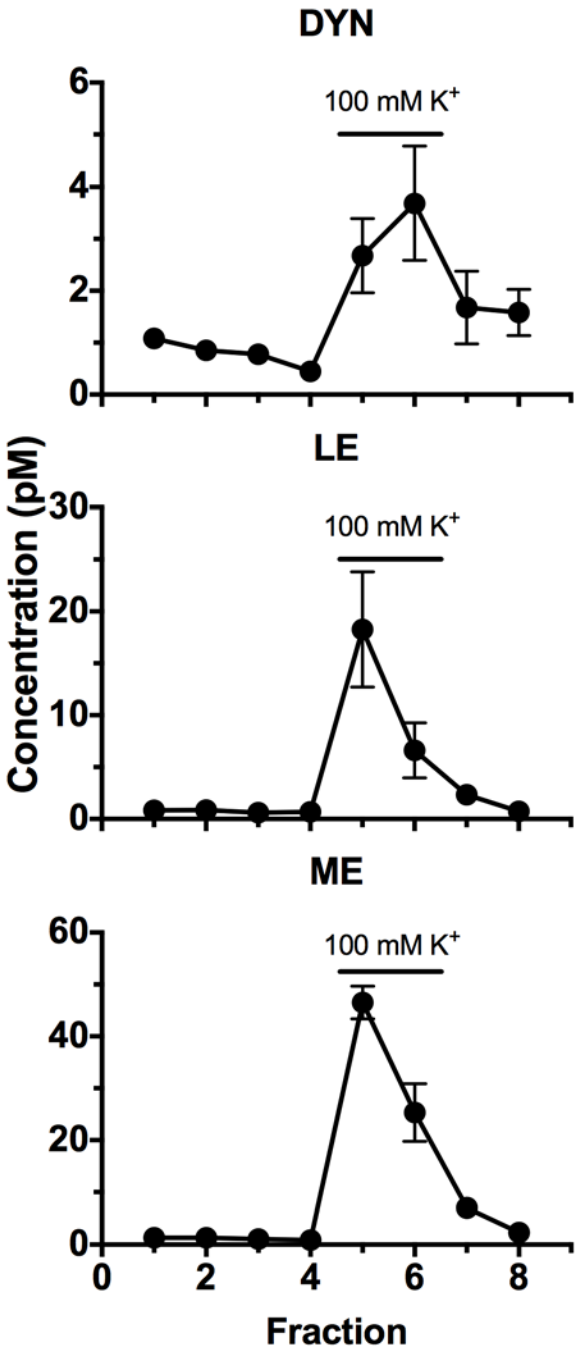

Figure 4-10 Optogenetic probe design *in vivo* tests show reliable K^+ depolarization stimulation. Data shown as average ± SEM, n = 2 mice

Photostimulation of DYN-containing cells elicits opioid peptide release

A previous study showed that photostimulation of DYN-expressing cells in distinct NAcSh sub-regions resulted in contrasting behavior responses. Photostimulation of vNAcSh DYN-expressing neurons produced a robust aversive behavioral response, whereas photostimulation of dNAcSh engaged positive reinforced behaviors, which were blocked by local administration of a KOR antagonist[243].

A proof of concept ELISA tissue slice experiment showed that photostimulation of channelrhodopsin (ChR2)-expressing DYN neurons in the NAcSh significantly increased Dyn-A release relative to non-ChR2 neurons in controls[243]. While this important *ex vivo* study showed that photostimulation can elicit Dyn-A release, the entire NAcSh region was stimulated without differentiating behaviorally relevant dorsal and ventral NAcSh sub-regions, and neuronal circuitry was not intact, which precludes any secondary effects of output nuclei. While ELISA assays provide valuable information and have low limits of detection, they are subject to cross-reactivity and non-specific signals, and require large sample volumes to probe a single analyte. Discrete region-specific measurement of a wide neurochemical panel in the intact brain during photostimulation will better elucidate the mechanisms driving opposing behaviors in the dNAcSh and vNAcSh. To this end, we applied our capillary LC-MS method and optogenetic-dialysis probes to locally photostimulate and sample from ChR2-expressing neurons in the dNAcSh and vNAcSh.

For optogenetic-dialysis experiments, fractions were collected on ice at 15 min intervals with a flow rate of 0.8 μL/min flow rate, generating 12 μL volumes. Three baseline fractions were collected prior to a 15 min photostimulation at 10 Hz (10 ms

pulse width). Six additional fractions were collected after the photostimulation to determine if there was a delayed or prolonged effect, followed by 2 fractions of 100 mM high K^+ stimulation to confirm that neurons were still viable and sensitive to stimuli. Mice were included in the study if 100 mM K^+ stimulation resulted in a positive increase in analytes at the end of the experiment and if correct probe placement and viral expression were confirmed. For each analyte, data from each mouse were included if the average basal concentration was at or above the limit of detection determined the day of the experiment (see Methods for further details).

To determine if there was a difference in basal concentrations between genotypes (*Cre* + and *Cre* -) and between regions (dorsal and ventral), average basal concentration for each mouse was averaged together within their respective groups (Figure 4-11). When basal levels were compared between genotypes within specific regions, concentrations of DYN were elevated in vNAcSh ($t(10) = 4.675$, $p < 0.01$), LE ($t(10) = 2.271$, $p < 0.05$), and ME ($t(10) = 2.454$, $p < 0.05$) in *dyn-Cre* - mice. There were no significant differences for peptides in the dNAcSh. When basal levels were compared between regions, there was elevated DYN ($t(12) = 2.4$, $p < 0.05$) and ME ($t(12) = 2.183$, $p < 0.05$) in dNAcSh *dyn-Cre* + mice compared to vNAcSh *dyn-Cre* + mice, and elevated LE ($t(9) = 2.416$, $p < 0.05$) in vNAcSh *dyn-Cre* - mice compared to dNAcSh *dyn-Cre* - (Figure 4-11). These changes in basal conditions show an effect of genotype for all opioid peptides in vNAcSh. When comparing between regions, we observed elevated DYN and ME, and similar LE in dNAcSh, associated with the previously reported positive place preference behavior. This elevated DYN is unexpected, as DYN is associated with negative emotional states[252-254].

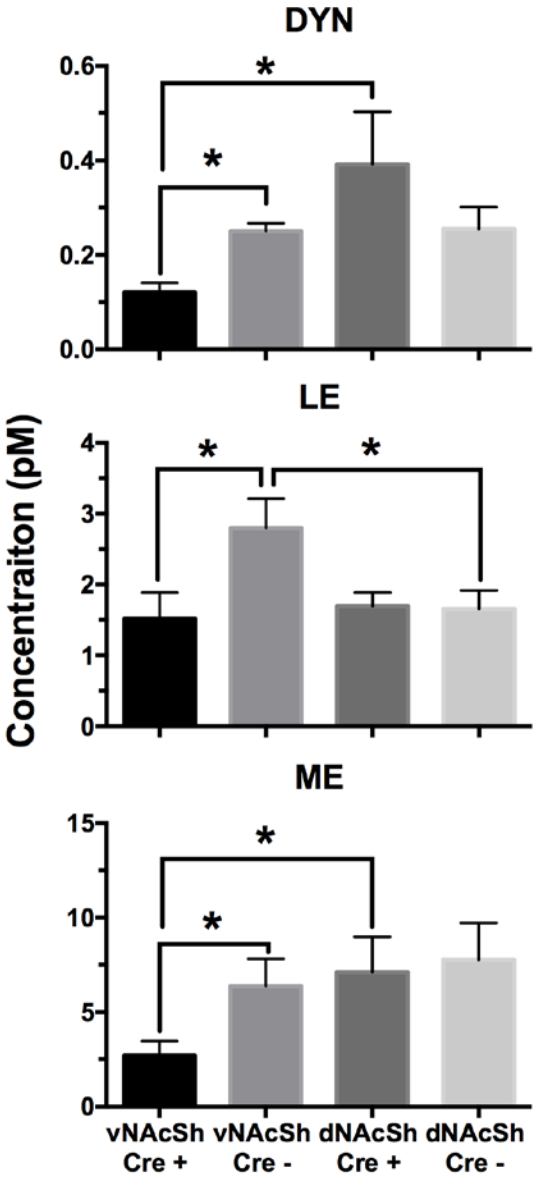

Figure 4-11 Average basal opioid peptide concentrations for each group of mice tested. Data shown as average ± SEM for each group of mice, n = 5 – 7 mice per group. Significance was determined by unpaired Student's t-test. * indicates $P \leq 0.05$.

While the average basal levels are informative of the resting state of neurons, observing dynamic changes in response to photostimulation of DYN-containing neurons in the vNAcSh and dNAcSh revealed intriguing opioid peptide results. Three basal fractions were collected prior to a 10 Hz (10 ms pulse width) photostimulation in all groups. An additional 6 fractions were collected after the laser photostimulation was

terminated (Figure 4-12). A significant increase of photostimulated DYN in *dyn-Cre* + mice was observed in both the vNAcSh (interaction effect; $t = 3.941$, $p < 0.001$) and dNAcSh (interaction effect; $t = 3.012$, $p = 0.003$), compared with *dyn-cre* - mice. There was also a significant difference between the *dyn-Cre* + and *dyn-Cre* - mice in the six post-stimulated fractions in the vNAcSh (interaction effect; $t = 2.499$, $p = 0.014$). As DYN is associated with negative emotional states, it is interesting that the increase of DYN in the *dyn-Cre* + vNAcSh, associated with the aversive behavior phenotype. For *dyn-cre* + mice, DYN in the vNAcSh is elevated relative to dNAcSh stimulated release (interaction effect; $t = 2.749$, $p = 0.007$) and post collection (interaction effect; $t = 2.806$, $p = 0.006$). The DYN increase and prolonged elevation relative to basal fractions was only observed in the aversive behavior phenotype mice, stimulated in the vNAcSh. Increased ME was associated with photostimulation in *dyn-Cre* + mice (interaction effect; $t = 2.824$, $p = 0.006$). This is somewhat surprising, as the photostimulation should only directly activate DYN-containing neurons that express ChR2, and DYN-containing neurons do not co-localize with pre-enkephalin (the precursor to ME)[261]. However, with 15 min fractions, it is possible that this increase in ME is a downstream response to DYN release or there is a differential cleavage of DYN forming the LE peptide.

The BzCl derivatization LC-MS method monitored 22 small molecules, however only GABA, Glu, and DA results are discussed in these results (Figure 4-12). Small molecule analysis revealed that GABA was increased ($t = 2.363$, $p = 0.020$) and had a prolonged response ($t = 4.744$, $p < 0.0001$) following vNAcSh photostimulation. This increase was greater in *dyn-Cre* + mice than *dyn-Cre* - mice. GABA in the dNAcSh did not have an effect from the stimulation, but there was a significance in overall between

dyn-*Cre* + mice and *dyn-Cre* – mice ($t = 2.910$, $p = 0.004$). Stimulation of Glu in both vNAcSh and dNAcSh were not significant. The increased and prolonged change in vNAcSh GABA is not surprising as vNAcSh DYN had significant and prolonged effect of stimulation, as DYN-containing neurons are GABAergic.

Photostimulation of dNAcSh DYN-containing neurons gives rise to a preference behavior phenotype. This corresponds to an increase in LE (interaction effect; $t = 5.384$, $p < 0.0001$) in *dyn-Cre* + mice stimulated in the dNAcSh. The magnitude of this stimulation-mediated LE effect is greater in the dNAcSh compared to the vNAcSh (interaction effect; $t = -2.552$, $p = 0.12$). Photostimulation also resulted in an immediate DA increase (interaction effect; $t = 5.007$, $p < 0.0001$) and a prolonged elevation (interaction effect; $t = 2.081$, $p = 0.039$). This surge in LE and DA specifically in the dNAcSh is interesting as ENK and DA increases in the striatum are associated with reward[74, 262] and stimulation elicits a positive preference behavior.

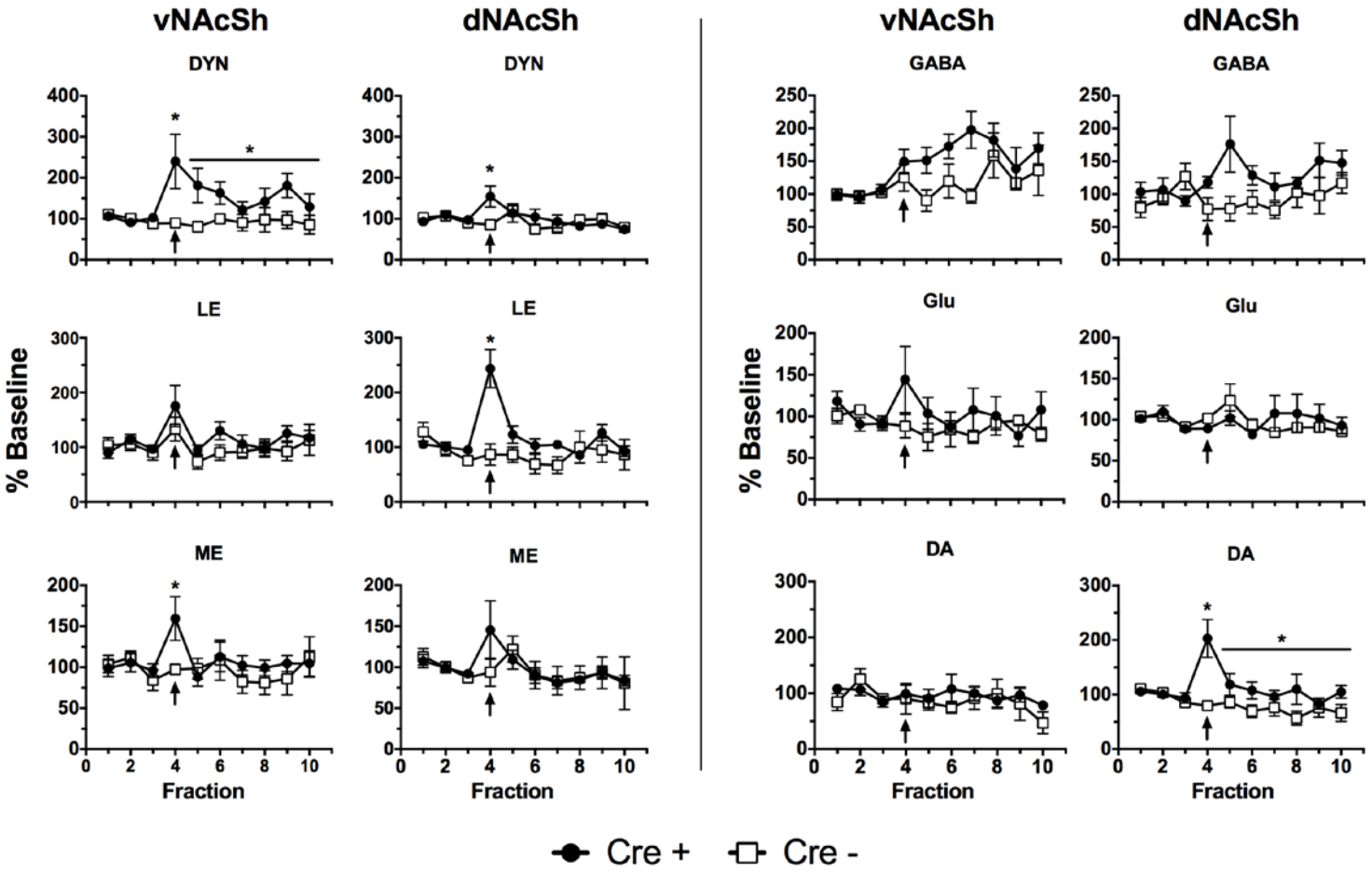

Figure 4-12 Extracellular opioid peptides and small molecules in vNAcSh and dNAcSh in *dyn-Cre* mice. Custom-made integrated optogenetic-dialysis probes were implanted into sub-regions of the NAcSh to measure the effect of photostimulation (indicated by arrow), and potential delayed or prolonged effects. Data normalized to average basal concentration and shown as average ± SEM for each group of mice, n = 5 – 7 mice per group. Significance was determined using a linear mixed model analysis. * indicates $P \leq 0.05$.

Conclusions

We developed and applied an integrated optogenetic-microdialysis probe and a capillary LC-MS assay to sample and detect photostimulated release of the opioid peptides DYN, LE, and ME, and small molecules in two discrete sub-regions within the NAcSh in *dyn-Cre* mice. While a preliminary *ex vivo* ELISA assay showed Dyn-A release, it did not distinguish between discrete sub-regions and precluded detection of changes in other analytes such as LE, ME and monoamines. This report builds on the previous findings and provides sub-region-specific data for a large panel of analytes. We show that basal levels differ between regions, and that photostimulation elicits distinct changes in dorsal and ventral sub-regions of the NAcSh. Specifically, the vNAcSh associated with aversion behavior and resulted in an immediate increase and prolonged effect for DYN and GABA, whereas in dNAcSh associated with positive reinforcement and saw a robust increase in LE and DA.

This study provided valuable information on neurochemical dynamics of specific opioid peptide fragments in sub-regions of the NAcSh. It is likely that monitoring other opioid fragments would give a better and more complete understanding of the dynamics associated with opposing behaviors. Monitoring release at downstream projection sites would further elucidate the role of endogenous opioids in negative and positive affective behaviors.

This study demonstrates the ability to measure locally stimulated release of opioid peptides and small molecules using a multiplex technique. This approach provides a comprehensive understanding of the complex and unique local dynamic changes occurring with photostimulation.

CHAPTER 5: IN VIVO QUANTIFICATION OF STRIATAL OPIOID PEPTIDES FOLLOWING 6-HYDROXYDOPAMINE LESIONS

Introduction

Parkinson's disease (PD) is a progressive neurodegenerative disorder characterized by the loss of nigrostriatal dopamine (DA) neurons. The cardinal motor features of PD are slowness of movement (bradykinesia), tremor, rigidity, and postural instabilities. Loss of striatal DA severely impacts signaling throughout the basal ganglia – a group of subcortical structures essential for executing normal movements. The striatum is the largest structure and primary input of the basal ganglia, where (among other inputs), cortical glutamate and midbrain DA converge to impact downstream nuclei. DA acts on D1-like (D1R) and D2-like receptors (D2R) on striatal GABAergic medium spiny neurons (MSNs), which represent 95% of the total neurons in the striatum[263]. In addition to GABA, striatal MSNs contain and release neuropeptides. Approximately half of MSNs express D1R and contain mRNA for substance P and prodynorphin[261, 264]. These neurons project to the substantia nigra pars reticulata (SNr) and globus pallidus internus (GPi), and comprise the "direct pathway" of the basal ganglia[265-267]. The other subtype of MSNs express D2R and contain proenkephalin mRNA[261, 264]. These neurons project to the globus pallidus external segment (GPe) and make up the first portion of the "indirect pathway" of the basal ganglia[265-267] (Figure 5-1).

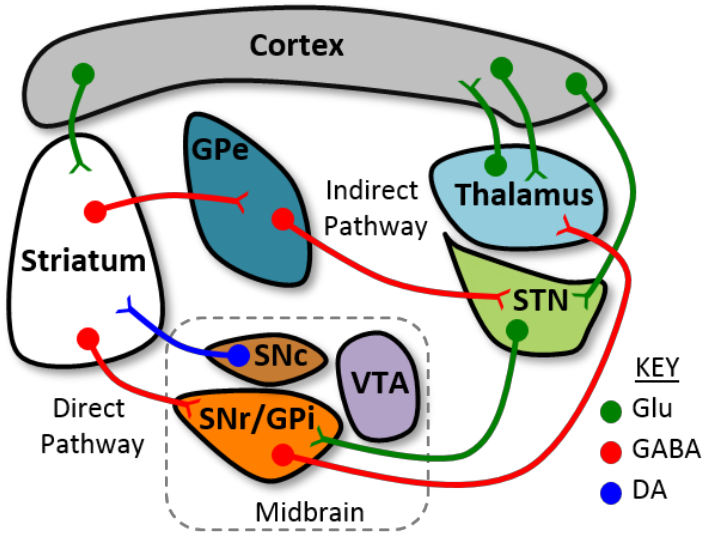

Figure 5-1 Simplified basal ganglia diagram showing excitatory (glutamatergic), inhibitory (GABAergic), and dopaminergic neuron pathways that are involved in coordinated movement. The indirect pathway is comprised of striatal GABAergic neurons that express D2 receptors and project to the globus pallidus external segment (GPe). Direct pathway GABAergic neurons originating in the striatum contain D1 receptors and project to the substantia nigra pars reticulata (SNr) and globus pallidus internus (GPi). Striatum-projecting dopaminergic neurons from the substantia nigra pars compacta (SNc) are lost in Parkinson's disease, possibly leading to imbalances in the output of direct and indirect pathway projection neurons. Other structures shown are the subthalamic nucleus (STN), which is part of the indirect pathway, and the ventral tegmental area (VTA), a major component of the mesolimbic circuit.

Opioid peptide processing and effects in Parkinson's disease

Both prodynorphin and proenkephalin are inactive pro-hormone precursors that require protease processing to produce biologically functional peptides[85, 86]. Protease-mediated propeptide processing into functional neuropeptides likely occurs during axonal transport of the propeptides in dense core vesicles[268]. Prodynorphin products include neo-endorphin, dynorphin A (produces dynorphin A_{1-8}; abbreviated DYN throughout the text), dynorphin B, and bridge peptide domain sequences[86]. Proenkephalin contains four copies of met-enkephalin (ME), two extended copies of ME, and one copy of leu-enkephalin (LE)[87, 88]. Although prodynorphin contains five LE sequences, prodynorphin products (i.e. dynorphin A and dynorphin B) rarely co-localize with LE due to the lack of cleavage of the dibasic Arg-Arg sequence[85, 86, 89]; therefore, it is generally believed that

prodynorphin is not a source of LE. Proenkephalin is the primary source of LE, even though it only contains one copy of the LE sequence[86]. These peptide precursors (proenkephalin and prodynorphin) are present in the brain, and processing produces many potential peptides, including opioid and non-opioid fragments. The extent of pro-hormone processing depends on the available endoproteases in a given cell type and brain region. Disruption of opioid peptide metabolism has been implicated in depression, anxiety, addiction, and diseases such as PD[90-93]. One study of dynorphin A_{1-17} metabolism in the unilateral 6-hydroxydopamine (6OHDA) lesion rat model of PD suggested disrupted enzymatic degradation between hemispheres[91].

The four opioid receptors, kappa, mu, delta, and opioid receptor like 1 (also called ORL1, nociceptin, or orphaninFQ receptors) have high affinities for dynorphin, β-endorphin and endomorphin, enkephalins, and nociceptin, respectively (Table 5-1).

Table 5-1 Endogenous opioid peptides and their receptors.

Precursor	Endogenous peptide	Affinity for opioid receptors
Pro-opiomelanocortin	β-endorphin	δ, μ δ >> μ
Pro-enkephalin	Met-enkephalin Leu-enkephalin	μ, δ μ = δ
Pro-dynorphin	Dynorphin A Dynorphin B Neoendorphin	κ, μ, δ κ >> μ and δ
Pro-nociceptin	Nociceptin	ORL1

DA signaling affects the expression of opioid peptide mRNA within MSNs. Chronic DA agonist administration decreases enkephalin (ENK) mRNA[269] and increases

dynorphin expression in rodents[270]. Conversely, DA antagonists or striatal DA lesions decrease prodynorphin mRNA and increase proenkephalin mRNA[271, 272]. Similar patterns are also observed in monkeys following MPTP-induced DA depletion[273, 274] and in human PD patients[275].

DA modulates mRNA expression of striatal opioid neuropeptide precursors, but it is not clear how this relates to extracellular neuropeptide concentrations (i.e., tonic levels) and release dynamics. mRNA expression studies provide insight into neuronal content, but do not necessarily reflect the specific fragments or the levels of proteins and peptides generated or released. It is unknown how the influence of DA on peptide expression relates to neurotransmitters such as 4-aminobutyric acid (GABA), glutamate and other signaling molecules within the striatum. DA exerts significant neuromodulatory influence on multiple transmitter systems and overall striatal activity, and its loss contributes to abnormal movements in PD. It is therefore important to understand the interaction between these neurotransmitters and neuropeptides in order to develop novel therapies counteracting abnormal pathological neurochemical processes.

The interplay between DA and opioids, and their selective expression in striatal neurons, has given rise to research targeting opioid systems as PD therapeutics. For example, delta opioid receptor (whose endogenous ligands are ENK) agonists enhance locomotor activity in rat and non-human primate models of PD[276-278]. Likewise, delta opioid receptor knockout mice display attenuated motor responses to psychostimulants[279]. Therefore, activating delta opioid receptors can rescue some of the motor deficits induced by DA depletion. A wide variety of opioid modulating drugs have been evaluated for L-DOPA induced dyskinesias (LIDs, involuntary movements) alleviation[280-284]. Selective

mu receptor antagonists[285, 286], and kappa agonists[287] reduce LIDs in primates. Limited human clinical trials using kappa agonists[288], and non-selective opioid antagonists[283, 289] show potential promise.

Although measurement of neuropeptide mRNA precursors with tissue content experiments provides insight into single time points, monitoring extracellular neuropeptides *in vivo* provides information on their temporal dynamics and specific peptide products. Microdialysis is a versatile sampling tool that allows for repeated collection of extracellular neurochemicals, but many challenges arise when applying microdialysis for neuropeptide collection. Neuropeptide concentrations are typically in the low pM range in the extracellular space. This low concentration, coupled with low peptide recovery in microdialysis requires an analytical method that is sensitive and selective. We applied direct monitoring of endogenous peptides and small molecules using microdialysis and capillary liquid chromatography-mass spectrometry (LC-MS) to gain additional insight into actions of DA on striatal opioid peptide neurochemistry.

We first established a sensitive method to detect basal ME, LE, and dynorphin fragment $A_{1\text{-}8}$ (DYN) opioid neuropeptide concentrations. We then used the 6OHDA hemilesion model of PD to unilaterally ablate nigrostriatal DA neurons and probed neurochemical concentration differences between lesioned and unlesioned hemispheres. We also investigated how evoked changes (i.e., K^+ stimulations) were differentially affected between the hemispheres. Our findings suggest a bidirectional dysregulation of direct and indirect pathway opioid neuropeptides in the striatum following loss of DA input. Furthermore, our results show enhanced inhibitory tone and loss of energy metabolism in the DA depleted striatum.

Methods

Chemicals

DYN and LE were purchased from American Peptide (Sunnyvale, CA), and ME was purchased from Sigma Aldrich (St. Louis, MO). Isotopically labeled DYN (DYN* $^{13}C_6$ $^{15}N_1$-mass shift +7 Da) was contracted through the University of Michigan's protein synthesis core. Water, methanol, and acetonitrile for mobile phases are Burdick & Jackson HPLC grade purchased from VWR (Radnor, PA). All other chemicals were purchased from Sigma Aldrich (St. Louis, MO) unless otherwise noted. Ringer solution consisted of 148 mM NaCl, 2.7 mM KCl, 2.5 mM $CaCl_2$, and 0.85 mM $MgCl_2$ adjusted pH to 7.4 with NaOH.

Animals

Adult male Sprague-Dawley rats (Envigo, Indianapolis, IN) weighing between 150-175 g were used for all 6OHDA lesion experiments. Rats were housed with access to food and water *ad libitum* in a temperature and humidity controlled room with 12 h light/dark cycles. For surgeries, animals were anesthetized using 1-4% isoflurane with 400 mL/min oxygen. Following the procedure, animals were given the antibiotic Gentamycin (2.5 mg/mL, i.p.) in a saline solution, to prevent dehydration and infection. All animals were treated as approved by the Unit for Laboratory Animal Medicine at the University of Michigan, the National Institute of Health Guidelines for the Care and Use of Laboratory Animals. All precautions were taken to prevent animal discomfort through the course of the experiments. In addition, all animal experiments were conducted within the guidelines of Animal Research Reporting *in vivo* Experiments.

Unilateral lesion with 6OHDA

Unilateral nigrostriatal lesions used 8 μg of 6OHDA (Sigma Aldrich, St. Louis, MO) dissolved in 4 μL of saline containing 0.02% ascorbic acid[260, 290]. Dissolved 6OHDA was injected into the medial forebrain bundle using stereotaxic coordinates from bregma, AP -4.0 mm, ML ±1.3 mm, and DV -7.6 mm from top of skull. A 30G guide needle was connected to a 50 μL syringe with a 50 cm length of fused silica capillary (200/360 μm inner diameter/outer diameter). 6OHDA was infused at a rate of 1 μl/min over a 4 min period. After infusion, the injection needle was left in place for an additional 1 min before retracting from the brain. Betadine solution (Purdue Products, Stamford, CT) was used to clean the surgical site and a steel wound clip was used to close the incision. Following surgery, rats were housed individually in a temperature and humidity controlled room with 12 h light/dark cycles with food and water available *ad libitum*. Two weeks after the lesion, animals were tested with amphetamine (5 mg/kg i.p.) to determine the number of ipsilateral turns. This test has previously shown that animals which exhibit > 7 ipsilateral turns/1 min had > 95% loss of DA[291]. Animals that turned > 7 ipsilateral turns/1 min were enrolled in the study.

Microdialysis

For all studies, 6OHDA lesioned rats that passed the amphetamine rotation test were included. Custom-made concentric microdialysis probes (3mm dialyzing membrane) were implanted bilaterally into the 6OHDA lesioned and non-lesioned dorsolateral striatum. Rats were anesthetized with 1-4% isoflurane and placed into a stereotaxic frame (David Kopf, Tujunga, CA). A burr hole was placed above the striatum

using the AP +0.5 mm and ML ±3.4 mm coordinates from bregma, and microdialysis probes were lowered -7.0 mm from top of skull. Probes were made using AN69 membrane (Hospal, Bologna, Italy) and were secured with skull screws and acrylic dental cement. Following surgery, rats were allowed to recover for 24 h with free access to food and water.

Experiments were performed 24 h after probe implantation. Microdialysis probes were flushed with ringer solution for 1 h at a flow rate of 2 μL/min using a Fusion 400 syringe pump (Chemyx, Stafford, TX). Flow rate was reduced to 0.8 μL/min and allowed to flush for an additional 1 h prior to baseline collections.

Dialysate samples were treated in a similar manner as described in the methods section of Chapter 4. Briefly, 12 μL dialysate were collected, and 2 μL were removed for the monoamine and amino acid assay and 1.1 μL DYN* was added for peptide assay. Peptide assay samples were immediately injected on the capillary LC-MS system following collection. The 2 μL dialysate aliquoted for the monoamine and amino acid assay were derivatized using a modified method, and described in Chapter 4, before LC-MS analysis[31, 128].

For high K^+ ringer solution perfusion, the perfusion media was modified to contain 100 mM KCl and 48 mM NaCl. $CaCl_2$ and $MgCl_2$ concentrations were not changed.

At the completion of the experiment, animals were euthanized and brains were extracted and stored in 4% paraformaldehyde at 4 °C. Probe placement was confirmed with histology. Animals were included in the data set if both probes were flowing and had confirmed probe placements.

Peptide assays with capillary LC-MS

The capillary LC-MS assay described in the methods section of Chapter 4 was applied to monitor opioid peptides (DYN, LE, and ME) with internal standard DYN*[67, 68, 70, 73]. The MS^2 pathway for opioid peptides DYN, LE, and ME were detected using *m/z* values of 491.5 → 435, 556 → 397, and 574 → 397 respectively. Isotopically labeled DYN* internal standard was detected using m/z values of 495 → 438. Animals that had average basal levels above the limits of detection were used for the study.

Small molecule neurochemical analysis using QQQ MS

Dialysate samples were derivatized with benzoyl chloride (BzCl) and analyzed by LC-MS as described in the methods section of Chapter 4[31, 128].

Statistical analyses

All statistical analyses were performed in Prism 7 (GraphPad, La Jolla, CA). Two-way ANOVA with Bonferroni post hoc analysis, and paired Student's *t* test were used. In all instances, differences were deemed significant if $P < 0.05$. Data presented as mean ± SEM unless otherwise noted. Animals were included in the data set if both 6OHDA lesion and non-lesion probes in the dorsolateral striatum were confirmed through histology.

Results and Discussion

Effects of 6OHDA on basal striatal concentrations of opioid neuropeptides

Basal striatal DYN and ENK concentrations were compared between 6OHDA-lesioned and intact hemispheres (Figure 5-2). Striatal DA lesions resulted in opposing

regulation of DYN and ENK (Figure 5-3). DYN concentrations were reduced 25% relative to the intact hemisphere, while LE and ME were both increased in the lesioned striatum 80% and 133% respectively (paired two-tailed t-tests: DYN $t_6 = 2.7$, $p = 0.04$; LE $t_6 = 3.7$, $p = 0.01$; ME $t_6 = 3.6$, $p = 0.02$). These data demonstrate that an opposing dysregulation of striatal opioid peptides occurs in the absence of DA. This result is consistent with opioid peptide mRNA expression studies[261, 270], and is the first demonstration of *extracellular* opioid peptide levels following DA lesions. Although the mechanisms underlying these changes are not fully understood, our results suggest that a lack of tonic DA receptor stimulation results in enhanced proenkephalin synthesis and decreased prodynorphin synthesis. These changes could be a direct effect of DA on synthesis, or a longer-term compensatory mechanism as the 6OHDA rats have chronic DA depletion. Because DA inhibits the indirect pathway, it is plausible that increased ENK release and subsequent activation of delta and mu opioid receptors (which are inhibitory G-protein coupled receptors) could autoregulate MSNs to potentiate cellular inhibition in the absence of DA. Striatal MSNs are rich in opioid receptors[261, 292, 293] and delta opioid agonists have antiparkinsonian effects in rat[260, 276-278, 294-297] and non-human primate models[277]. Similarly, decreased striatal DYN following DA loss could reflect a kappa opioid receptor-mediated disinhibition of the direct pathway. Further studies should examine the potential antiparkinsonian effects of kappa opioid receptor antagonists to more clearly establish the mechanism of down regulated DYN and its effects in the direct and indirect pathways.

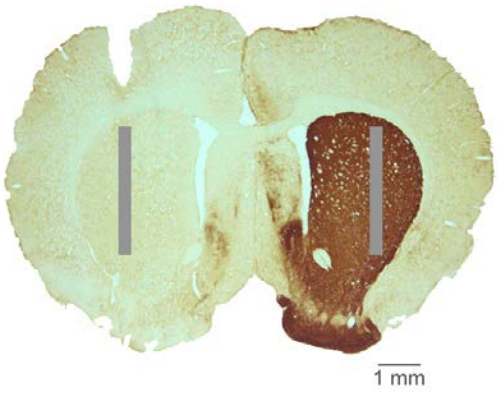

Figure 5-2 Bilateral probe placement in unilateral 6OHDA lesioned striatum. Tyrosine hydroxylase immunohistochemistry of unilateral 6OHDA lesioned rat coronal brain sections shows the lack of striatal DA terminals (left, light) and presence of DA terminals (right, brown). Representative probe placements indicated by gray boxes.

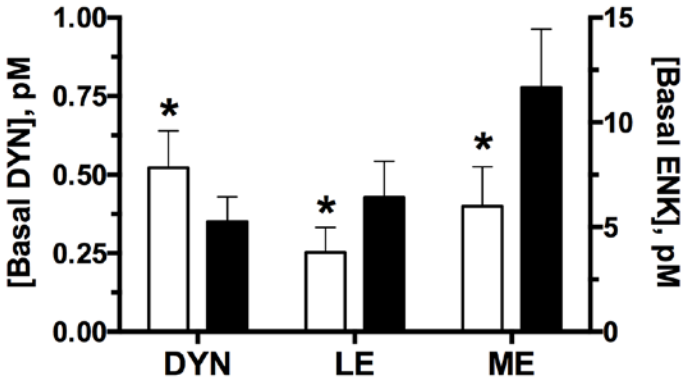

Figure 5-3 Effect of lesion on basal peptide concentrations. Comparison of lesion (black bars) vs. unlesioned (open bars) side demonstrates decreased DYN and increased LE and ME release in lesioned striatum. Paired two-tailed Student's *t* test statistics were performed to compare basal levels. All data expressed as percent non-lesion ± SEM. *p-value < 0.05, n = 7 rats.

Effects of 6OHDA on basal small molecule concentrations

The 6OHDA hemisphere had basal extracellular levels of 1, 0.4, 30, 55, 260, and 80 nM for DA, 3MT, DOPAC, HVA, Glc, and GABA respectively, while the intact hemisphere showed 14, 7, 2000, 3000, 220, and 50 nM (not corrected for probe recovery). As expected following 6OHDA lesions, we detected an 83% reduction in DA ($t_6 = 15$, $p < 0.0001$) and major reductions in DA metabolites (Figure 5-4) relative to the contralateral intact hemisphere. Specifically we found an 85% decrease in 3MT ($t_6 = 47$, $p < 0.0001$), 94% decrease in DOPAC ($t_6 = 47$, $p < 0.0001$) and 90% decrease in HVA ($t_6 = 130$, $p < 0.0001$) in the lesioned hemisphere compared to the intact hemisphere (Fig. 6). The 6OHDA-lesioned hemisphere showed significantly elevated glucose (40%, $t_6 = 2.6$, $p = 0.04$) and GABA (222%, $t_6 = 2.7$, $p = 0.03$) compared to the intact hemisphere. Trends for increased 5HT, DOPA and NM in the depleted hemisphere were also present, but not significant. These results complement previous studies showing adaptive changes in gene expression of DYN, ENK, and the GABA biosynthesis enzyme GAD67[298, 299].

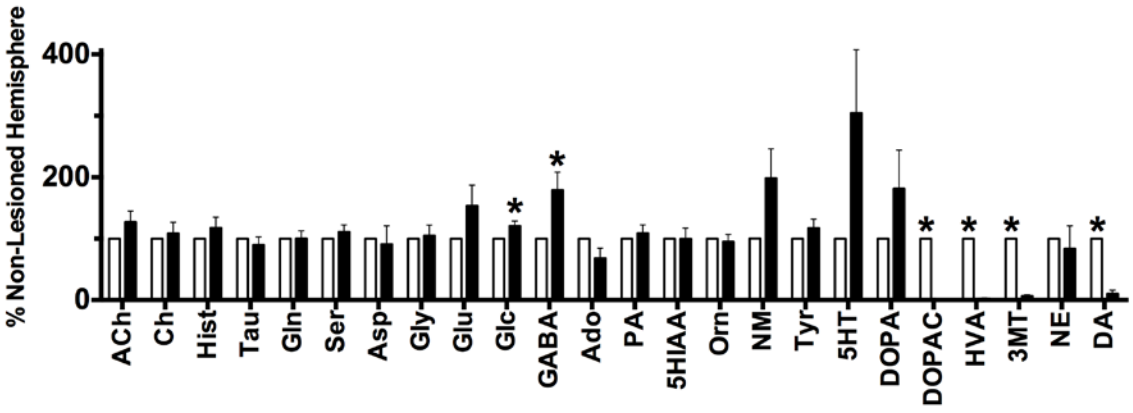

Figure 5-4 Effect of 6OHDA lesion on small molecule concentrations. Small molecule assay normalized to intact non-lesion hemisphere (open bars) show complete depletion of DA and metabolites in 6OHDA lesion hemisphere (black bars). Glc and GABA are up regulated in 6OHDA lesion hemisphere. Paired two-tailed Student's *t* test statistics were performed to compare basal levels. All data expressed as percent non-lesion ± SEM. *p-value < 0.05, n = 7 rats.

Concentrations of the inhibitory transmitter GABA and ENKs were higher in the lesioned hemisphere compared to the non-lesioned control side. These are likely related because opioids and GABA are co-expressed in both direct and indirect pathway MSNs[94]. Therefore, DA loss results in processes consistent with inhibition of striatal output. Our findings do not address the effects of these neurochemical changes in downstream brain regions because we only sampled from the striatum and not from the GPe or the SNr/GPi output nuclei.

The finding that 6OHDA lesions elevate extracellular glucose was unanticipated and demonstrates the power of our comprehensive approach to neurochemical measurements. The glucose increase may reflect underutilized energy reserves due to greater neuronal inhibition in this hemisphere. Imaging studies show glucose hypometabolism in PD brains relative to healthy individuals[205, 300-303]. Many of these studies were performed in humans with various stages of PD compared to healthy individuals. Our results are unique, demonstrating alterations within individual animals. We show elevated extracellular striatal glucose in the DA-depleted striatum as compared to the intact hemisphere, suggesting reduced glucose metabolism.

PD has also been linked to glucose intolerance and diabetes[304-307]. It is estimated that 50-80% of patients with PD have abnormal glucose tolerance[307]. Several studies have attempted to link the likelihood of developing PD with the onset of diabetes with mixed results[308-310].

K+ stimulated release of striatal opioid peptides

To test the amount of opioid peptides readily releasable in neurons, we perfused a 100 mM K+ ringer solution through the probes to induce depolarization. We perfused K+ for 30 min to investigate the effects of lesion on initial stimulated peptide release, allowed 1 h recovery, and then perfused K+ for another 30 min to examine peptide repackaging (Figure 5-5). The first K+ perfusion resulted in higher peptide release than the second perfusion, indicating no priming effects (contrary to previously reported potentiation with other neuropeptides, including oxytocin and vasopressin)[311, 312]. DYN, LE, and ME increased by 380%, 3100% and 3900% respectively in the lesioned hemisphere following the first K+ stimulation. There were no significant differences in opioid peptide release between the lesioned and unlesioned hemispheres (two-way ANOVA).

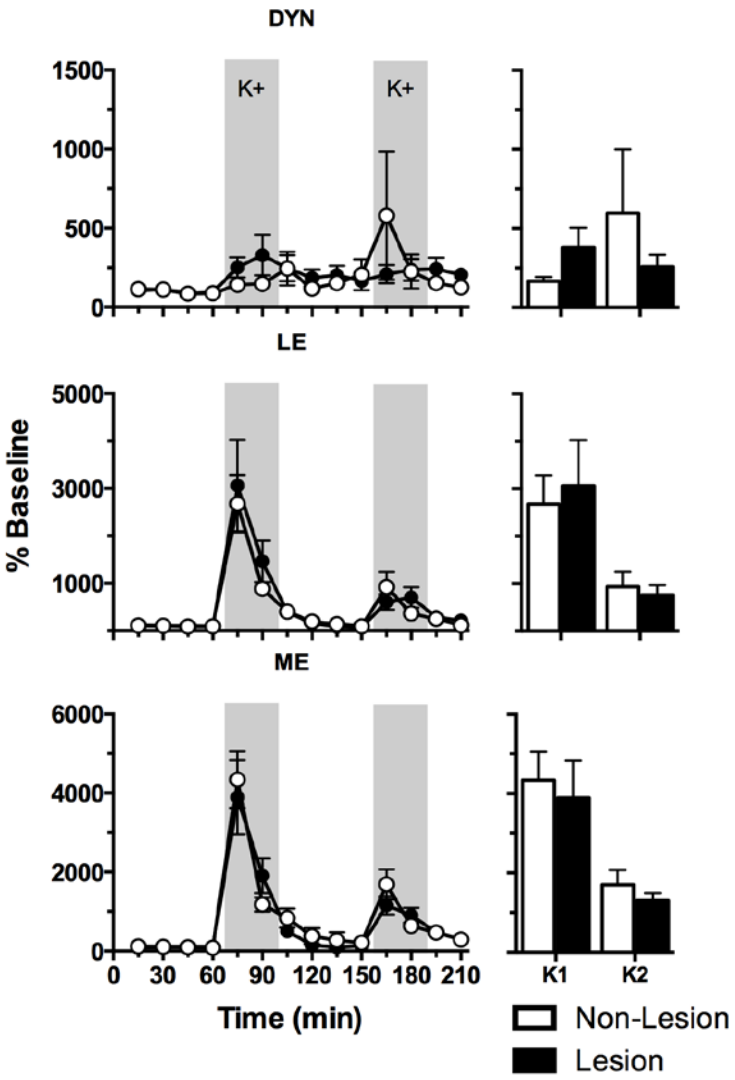

Figure 5-5 Effect of multiple K+ stimulations on striatal peptide release. Unilaterally lesioned rats received two 30-minute K+ stimulations (left, gray boxes). No differences in K+ stimulated peptide release were observed between lesioned (black circles) and non-lesioned (open circles) sides (two-way ANOVA). Highest concentration achieved during first and second K+ stimulation for each probe is shown (right) for each peptide. Paired two-tailed Student's t test statistics were performed to compare lesion and non-lesion sides and showed no significance for all peptides. All data expressed as average concentration ± SEM. n = 7 rats

Intact and DA depleted striata released the same amount of peptide following the initial K+ induced depolarization; 0.8 ± 0.2 and 1 ± 0.2 pM DYN, 120 ± 50 and 140 ± 30 pM LE, and 280 ± 140 and 360 ± 50 ME, respectively. Evoked release was reduced in both hemispheres following the second K+ stimulation (Figure 5-5). This suggests that

there is no absolute difference in intracellular stores of the targeted peptides and that the observed extracellular differences reside in basal release probability. This is consistent with the conclusion that DA tonically modulates striatal MSNs[269-272]. However, previous studies showed increased proenkephalin mRNA expression and reduced prodynorphin expression in DA lesioned animals[298, 299]. While these mRNA findings suggest altered intracellular neuropeptide stores, no differences were observed with K+ stimulation. It is important to note that we only monitored one fragment of dynorphin. Previous studies show changes to opioid peptide mRNA expression in PD models, so it is possible that other dynorphin fragments are affected. It is possible that DA lesions elevate ME and LE and reduce DYN at resting conditions, but that strong stimuli (e.g., high K+ perfusion) cause recruitment of additional intracellular peptides *via* increased packaging or production. These results also demonstrate that priming does not occur in striatal ME, LE, and DYN systems, as it does with other neuropeptides such as hypothalamic OT and vasopressin[313]. Understanding fundamental neurochemical differences will be imperative for the development and understanding of future opioid-based drugs to treat PD.

Conclusions

Applying advanced *in vivo* microdialysis sampling and LC-MS measurements, we showed that 6OHDA lesions alter extracellular opioid neuropeptide concentrations in the striatum. Loss of DA increased ENK and reduced DYN release. These data align with and corroborate two decades of mRNA expression studies suggesting that DA signaling regulates striatal neuropeptide dynamics. We also found parallel small molecule changes (GABA, and glucose), confirming that dopaminergic influence over striatal networks is multifaceted and may affect both neuronal activity and energy metabolism. We

investigated one fragment of dynorphin (DYN; dynorphin A_{1-8}), but it is possible that metabolism *via* enzymatic cleavage of the prohormone precursors of dynorphin and enkephalin could be altered, and were not investigated in this study. Previous results show differences in the biotransformation of exogenous dynorphin A $_{1-17}$ in 6OHDA rats[91], but did not address the exogenous *in vivo* fragments in the extracellular space. The present data demonstrate key features of neuropeptide release dynamics under basal and stimulated conditions and are important for understanding how DA loss in PD affects striatal circuits.

These findings relate abnormal opioid peptide signaling with striatal dysregulation following DA depletion. These studies further our understanding of the complex physiological processes underlying basal ganglia function and dysfunction, and may lead to alternative therapeutic targets and treatments for PD beyond the standard DA replacement therapy.

CHAPTER 6: A POTENTIAL OXYTOCIN TREATMENT FOR L-DOPA INDUCED DISKINESIAS

Introduction

Parkinson's disease (PD) is a progressive neurodegenerative disorder characterized by the loss of nigrostriatal dopamine (DA) neurons. The cardinal motor features of PD are slowness of movement (bradykinesia), tremor, rigidity, and postural instabilities. Current therapies aim to relieve PD symptoms, but do not slow disease progression, and often cause significant side effects. The primary treatment for PD is DA replacement therapy. For example, administration of the DA precursor L-DOPA supplies the brain with exogenous DA to compensate for DA depletion. L-DOPA treatment controls many PD motor symptoms, but remains ineffective for psychiatric, gastrointestinal and olfactory impairments[314, 315]. Chronic DA replacement therapy causes L-DOPA induced dyskinesias (LIDs) within 10 years of treatment in the majority of PD patients[316-318]. LIDs are associated with the severity of dopamine loss, dysregulation of dopamine neurons, abnormal neuronal firing patterns, aberrant basal ganglia-thalamo-cortical signaling, and excessive DA D1-like receptor (D1R) activation (for comprehensive review see Bastide et al., 2015)[319, 320]. Selective DA D2-like receptor (D2R) agonists, such as ropinirole, produce fewer dyskinesias than L-DOPA, suggesting that alternative treatments to shift toward D2R activation could be important alternative

therapies. However, D2R agonists are less effective at improving PD symptoms compared to L-DOPA[321].

Oxytocin in the striatum

Endogenous neuropeptide oxytocin (OT) receptors are expressed in brain regions that regulate movement, including the striatum, subthalamic nucleus, globus pallidus, and substantia nigra[322]. OT is a 9 amino acid polypeptide with wide ranging actions throughout the nervous system and periphery and is commonly studied for its role in maternity, affiliative behaviors and pair bonding[81]. The significance of OT in dopamine-mediated movement and PD is unclear, but PD patients have lower brain OT levels post mortem[323]. Rodent studies have shown that systemic OT treatment modulates DA-stimulated stereotypies and hyperactivity induced by cocaine or amphetamine[324]. This suggests that OT may counter abnormal movements associated with increased brain DA levels. D2R and OT receptors (OTR) can form heteromers within the striatum, which are expressed on "indirect pathway" medium spiny neurons projecting to the globus pallidus[325]. Therefore, OT may modulate DA-mediated activity in the indirect pathway. OT-based treatments have not been studied for the potential to decrease chronic L-DOPA induced AIMs, but showed promise in a pilot study (Michael J Fox Foundation, Dyskinesia Challenge 2013). It was hypothesized that exogenous OT administration would activate the indirect pathway to balance the dysregulated striatal output pathways during L-DOPA treatment.

To test this hypothesis and further examine striatal OT, a method was developed to monitor striatal OT levels, and to quantitatively assess abnormal involuntary

movements (AIMs) in 6-hydroxydopamine (6OHDA) lesioned, L-DOPA treated dyskinetic rats. Systemic OT was administered to 6OHDA rats that were chronically treated with L-DOPA (to induce dyskinesias), revealing an inverse correlation between OT dose and AIMs elicited by L-DOPA treatments. These findings demonstrate that OT may be a promising therapy to be used in conjunction with current L-DOPA regimens.

Methods

Chemicals

OT, and isotopically labeled OT (OT* $^{13}C_2{}^{15}N_1$-mass shift +3 Da) were purchased from American Peptide (Sunnyvale, CA). Water, methanol, and acetonitrile for mobile phases are Burdick & Jackson HPLC grade purchased from VWR (Radnor, PA). All other chemicals were purchased from Sigma Aldrich (St. Louis, MO) unless otherwise noted. Ringer solution consisted of 148 mM NaCl, 2.7 mM KCl, 2.5 mM $CaCl_2$, and 0.85 mM $MgCl_2$ adjusted pH to 7.4 with NaOH.

Animals

Adult male Sprague-Dawley rats (Envigo, Indianapolis, IN) weighing between 150-175 g were used for all 6OHDA lesion experiments as described in Chapter 5. All animals were treated as approved by the Unit for Laboratory Animal Medicine at the University of Michigan, the National Institute of Health Guidelines for the Care and Use of Laboratory Animals. In addition, all animal experiments were conducted within the guidelines of Animal Research Reporting *in vivo* Experiments.

Unilateral lesion with 6OHDA

Unilateral nigrostriatal lesions used 8 μg of 6OHDA (Sigma Aldrich, St. Louis, MO) dissolved in 4 μL of saline containing 0.02% ascorbic acid, and the protocols for surgery and selection criteria were described in the methods section of Chapter 5.

L-DOPA treatment and AIMs rating

Two weeks after amphetamine testing, unilaterally lesioned rats received 21 d of L-DOPA treatment (levodopa 6 mg/kg + benserazide 15 mg/kg, s.c., once daily) to induce AIMs. Following 3 weeks of treatment, animals were assessed for dyskinetic behaviors according to a modified method developed by Cenci and colleagues[326, 327]. Dyskinetic movements were classified based on four subtypes: (i) locomotor AIMs (ii) axial AIMs, i.e. twisted posture or choreiform twisting of the neck and upper body contralateral to the lesion; (iii) forelimb AIMs, i.e. jerky or dystonic movements in contralateral forelimbs and/or purposeless grabbing movement of the contralateral paw; (iv) orolingual AIMs, i.e. orofacial muscle twitching, empty masticatory movements and tongue protrusion. Each AIM subtype was rated on a severity scale from 0 to 4 (0 = not observed; 1 = occasional; 2 = frequent; 3 = continuous but interrupted by sensory distraction; 4 = continuous, severe and not interrupted by sensory distraction, i.e. tapping on the animal's cage) at each monitored period. AIM scores were counted as the sum of all 4 subtypes for each period and were plotted across each individual time point. Maximum AIM score for each time point was 16. All rats enrolled in these studies had developed moderate-severe AIMs (severity grade ≥ 2 on each of the first 3 AIM subtypes) within the 3 weeks of chronic treatment prior to experiments. Approximately 20% of rats did not meet these criteria and were excluded from the study. AIM scoring was performed 8 times during the L-DOPA treatment period (8 measurements every 20 min for 2 h). During the experiments, students performing the AIM scoring were blinded to the dose the rat was given.

Microdialysis

Rats were enrolled in the L-DOPA study if they were lesioned, passed the amphetamine rotation tests described in the methods section of Chapter 5, and were stably dyskinetic after chronic L-DOPA treatment.

Custom-made concentric microdialysis probes (3 mm dialyzing membrane) were implanted bilaterally into the 6OHDA lesioned and non-lesioned dorsolateral striatum as described in Chapter 5. Microdialysis probes were flushed with ringer solution for 1 h at a flow rate of 2 μL/min using a Fusion 400 syringe pump (Chemyx, Stafford, TX). Flow rate was reduced to 0.9 μL/min and allowed to flush for an additional 1 h prior to baseline collections. Samples were collected every 15 min. Samples were immediately injected on the capillary LC-MS system following collection (45 min baseline and 2 h post treatment).

For high K^+ ringer solution perfusion, the perfusion media was modified to contain 100 mM KCl and 48 mM NaCl. $CaCl_2$ and $MgCl_2$ concentrations were not changed.

At the completion of the experiment, animals were euthanized and brains were extracted and stored in 4% paraformaldehyde at 4 °C. Probe placement was confirmed with histology. Animals were included in the data set if both probes were flowing and had confirmed probe placements.

Oxytocin assays with capillary LC-MS

OT was detected using the capillary LC-MS described in the materials and methods section of Chapter 3[67, 68, 70, 73]. An Agilent 1100 HPLC pump (Santa Clara, CA)

was used to deliver the elution gradient containing water with 0.1% FA for mobile phase A and mobile phase B as MeOH with 0.1% FA delivered as initial 0% B; 1 min, 30 %B; 4 min, 50% B; 4.1 min 100% B; 7 min, 100% B; 7.1 min, 0%B; and 10 min, 0% B.

The capillary column was interfaced to a linear ion trap (LTQ XL, Thermo Scientific). The MS^2 pathway for endogenous OT and isotopically labeled OT were 1007 → 723 and 1010 → 993 *m/z*, respectively. *In vitro* recovery of a 2.5 mm probe for OT was 32 ± 9%.

OT standards were prepared daily. Calibration curves were run in triplicate to determine linearity, reproducibility, and limits of detection. The limit of detection for OT was 11 pM, respectively, in 5 μL. Animals that had average basal levels above the limits of detection were used for the study.

Statistical analyses

All statistical analyses were performed in Prism 7 (GraphPad, La Jolla, CA). Two-way ANOVA with Bonferroni post hoc analysis, and paired Student's *t* test were used. In all instances, differences were deemed significant if $P < 0.05$. Data presented as mean ± SEM unless otherwise noted. Only rats that had correct probe placements were included in the data set.

Results and Discussion

Systemic OT as a potential treatment of L-DOPA induced dyskinesia

To determine if OT mitigates AIMs, we performed a dose-response behavioral and microdialysis experiment targeting the dorsolateral striatum of 6OHDA lesioned rats that developed stable dyskinetic behavior (AIM score > 6) with 3 weeks of chronic L-

DOPA. Following three baseline microdialysis collections, rats received a final injection of L-DOPA (levodopa 6 mg/kg + benserazide 15 mg/kg, s.c.) to induce dyskinesia and an acute injection of saline or OT (0.01, 0.1, 1.0, and 10.0 mg/kg, i.p.). AIM scores were assessed at the beginning of each fraction (by a student blinded to treatment conditions) and OT levels were monitored (Figure 6-1).

As expected, higher OT doses produced higher OT concentrations in the dorsolateral striatum (Figure 6-1A). Specifically, 1.0 mg/kg was higher than saline ($F(2,20) = 4.731$, $p = 0.02$) at fraction 5 ($p < 0.001$), fraction 6 ($p < 0.001$), fraction 7 ($p < 0.01$), and 10.0 mg/kg is higher than saline ($F(2,20) = 6.637$, $p = 0.006$), at fraction 4 ($p < 0.001$) and fraction 5 ($p < 0.01$). While there was no significant interaction at 0.1 mg/kg ($F(2,20) = 0.8614$, $p = 0.4$), the post hoc analysis showed that fraction 5 ($p < 0.01$) was higher than saline. A dose response curve was generated from this data by summing the measured OT from fractions 4 – 11 for each rat, and plotting against the logarithmic dose (Figure 6-1B). The dose response curve demonstrates increasing dose effects from 0.01 to 10.0 mg/kg, but does not plateau. Higher doses were not used, in order to reduce the number of animals required and the associated costs of the experiment, and because higher doses are not relevant in humans. OT is administered to humans at sub-μg/kg doses (*via* intravenous[328] and intranasal administration[329, 330]) for labor induction and for social cognition treatment in autism and schizophrenia. The OT doses used in this study are significantly higher because i.p. administration results in partial degradation of OT prior to reaching the brain.

LIDs were reduced in animals co-treated with OT. AIMs were recorded after the rat received saline or OT treatment with L-DOPA, but not prior to the treatment, as the

rats were in a baseline resting state. All doses tested were significantly different from control saline treatment (Figure 6-2A). Post hoc analysis is summarized in Figure 6-2C. A dose response curve for the sum of AIM score from fractions 4 – 11 (i.e. post drug treatment) for each animal, plotted against the logarithmic dose (Figure 6-1B). Analysis of the best fit shows the bottom and top thresholds are 27 and 67, respectively, and the half maximal effective concentration (EC_{50}) is 0.01 mg/kg (Figure 6-2B).

These results show that an acute administration of OT with L-DOPA treatment decreases AIMs in LIDs. One possible mechanism underlying the beneficial effects of OT on AIMs is altered indirect pathway signaling. Indeed, OTR form heteromers with D2R in the indirect pathway[325], and may facilitate D2R-mediated signaling[325]. Systemic OT may therefore potentiate DA-mediated inhibition of striatopallidal GABA release compared to L-DOPA alone. Accordingly, OT may shift the balance of striatal output to favor indirect pathway signaling. Additional measurements of small molecule transmitter release in downstream basal ganglia nuclei are needed to test this hypothesis. It is possible that the effect of systemic OT on motor output may be due to OTR activation in other brain regions outside of the striatum. To confirm a striatal origin, local striatal OT administration would need to reduce AIMs, or local application of an OT receptor antagonist could be used to block OT. It is also possible that OT alters the bioavailability or pharmacodynamics of L-DOPA. Striatal microdialysate measurement of L-DOPA following OT administration would help rule out this possibility.

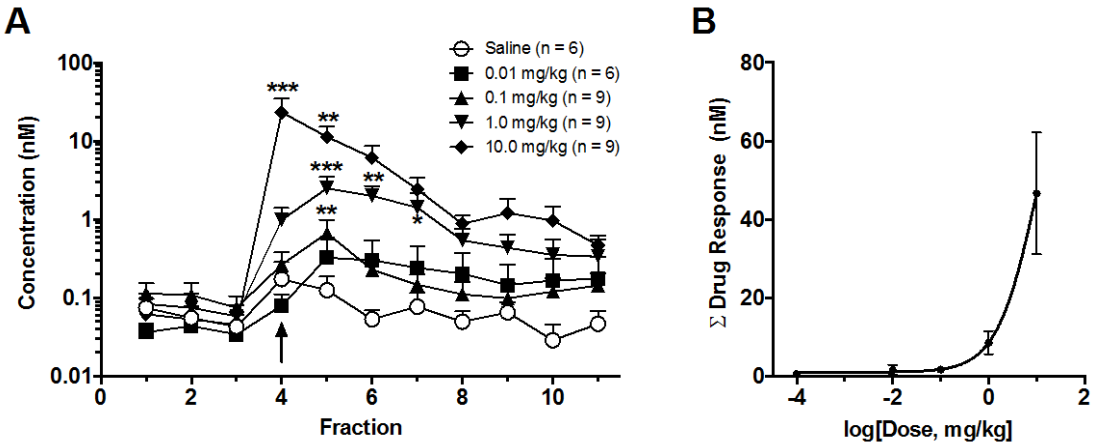

Figure 6-1 Effect of acute systemic OT dose on measured OT in the dorsal lateral striatum (A) and transformation into dose response curve (B). Rats were given a single dose of OT after three baseline measurements. The arrow indicates the first fraction that OT is expected to be present in the dialysate (A). A dose response curve was generated by the sum of OT measured in fractions 4 -11, plotted against the dose (B). While this study only tested to a maximum of 10.0 mg/kg, higher doses would be required to achieve a plateau on the dose response that was cost prohibitive and would be higher than relevant doses. A multiple comparison two-way ANOVAs with Bonferroni post hoc were run on each data set comparing each dose to the saline. Data shown as average ± SEM.* $p < 0.05$, ** $p < 0.01$, and *** $p < 0.001$.

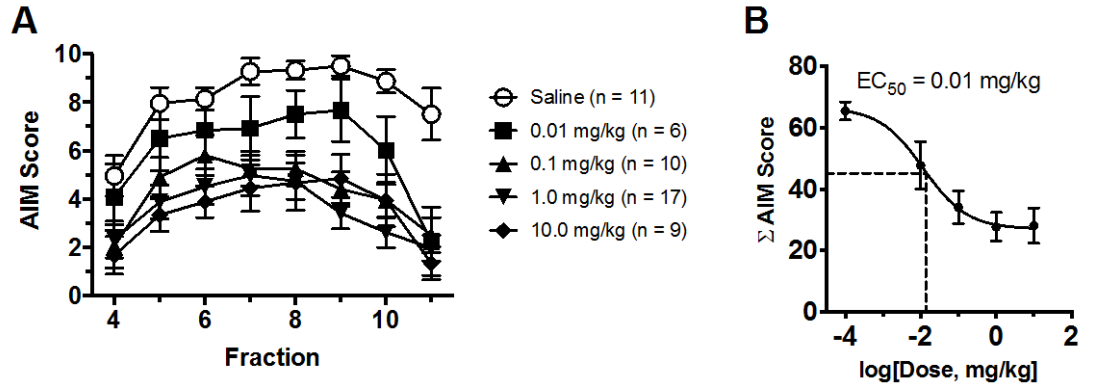

C

	Fraction (Compared to Saline)							
Dose	4	5	6	7	8	9	10	11
0.01 mg/kg	n.s.	n.s.	n.s.	n.s.	n.s.	n.s.	n.s.	***
0.1 mg/kg	*	*	n.s.	***	***	***	***	***
1.0 mg/kg	*	***	**	***	***	***	***	***
10.0 mg/kg	*	***	**	***	***	***	***	***

Figure 6-2 Effect of AIM score on dose. AIM score was measured from fractions 4 – 11 because rats were in a resting state during baseline conditions. Rats were given a single dose of OT after three baseline measurements, and AIM score was accessed at each time point by a student blinded to treatment conditions (A). A dose response curve was generated by the sum of AIMs measured in fractions 4 -11, plotted against the dose (B) Two-way ANOVAs were run on each data set comparing each dose to the saline summarized in a table (C). Data shown as average ± SEM.* $p < 0.05$, ** $p < 0.01$, and *** $p < 0.001$.

Isotopically labeled OT crosses the blood brain barrier

To confirm that our OT measurements in the dorsolateral striatum reflected OT injection and were not due to a secondary central response to L-DOPA or OT treatment, we injected isotopically labeled OT* (1.0 mg/kg, i.p.) and monitored both the isotopically labeled *m/*z transition (1010 > 993 *m/z*) and the endogenous OT transition (1007 > 723 *m/z*) (Figure 6-3A). After treatment, increases in OT* ($F(1, 11) = 7.596$, $p = 0.01$) were significantly different than endogenous OT, demonstrating that striatal OT measurements primarily reflect injected OT, and not secondary downstream release. No differences in concentration were observed following equivalent injections of either isotopically labeled OT* or endogenous OT (Figure 6-3B), demonstrating that the isotopically labeled compound exhibits similar kinetics and is not processed differently in rats.

Our results show that isotopically labeled OT* is measurable in the rat brain, but do not address how systemic OT* reaches the microdialysis probe, which is controversial. The brain is protected by a selectively permeable barrier (the blood brain barrier; BBB) separating circulating blood from brain extracellular fluid. Mechanical insertion of a microdialysis probe compromises the integrity of the BBB, raising the possibility that our OT* and OT measurements reflected OT that 'leaked' into the brain, rather that OT that crossed the BBB. A recent microdialysis and radioimmunoassay study suggest that systemically administered i.p. OT reaches the mouse amygdala and hippocampus[331]. The authors also state, that even if the BBB was leaking, the calculated maximum contribution of OT in the brain due to the leak would be minimal[331]. Other studies suggest OT crosses the BBB by showing increases in OT cerebrospinal fluid following intranasal OT administration[331-335].

Another study used blood oxygenation level dependent imaging to monitor brain activity in areas with OT receptors[333]. Subjects received either i.p. or intracerebroventricular (ICV, which circumvents the BBB) injection of OT and activation profiles were observed. The study hypothesized that activation profiles would be similar if both routes of administration allowed equivalent access of OT in the brain. Different profiles were observed between the i.p. and ICV injections groups, suggesting that i.p. OT does not cross the BBB at the same efficiency as ICV injection[333]. However, NAc shell activity was significantly increased 20 min post i.p., corresponding with our 15 min collection fractions.

Several reports demonstrate biphasic BBB permeability changes, with increased permeability directly following microdialysis probe insertion, restored BBB integrity from 8 – 48 h, and a second permeability increase after 24 – 48 h[153, 336-345]. Our microdialysis experiments were performed 18 – 24 h after probe insertion to minimize alterations in BBB permeability. To confirm BBB integrity during this period, systemic injections of BBB-impermeable compounds 18 – 24 h after probe insertion should be performed. A pilot study from our lab administered systemic injections of dopamine (which does not cross the BBB), and did not alter measured dopamine concentrations in the dorsolateral striatum (data not shown). This pilot study suggests that the BBB is intact during this period following microdialysis probe implantation (pilot data from Omar Mabrouk, manuscript in preparation), but more rigorous tests should be performed with OT.

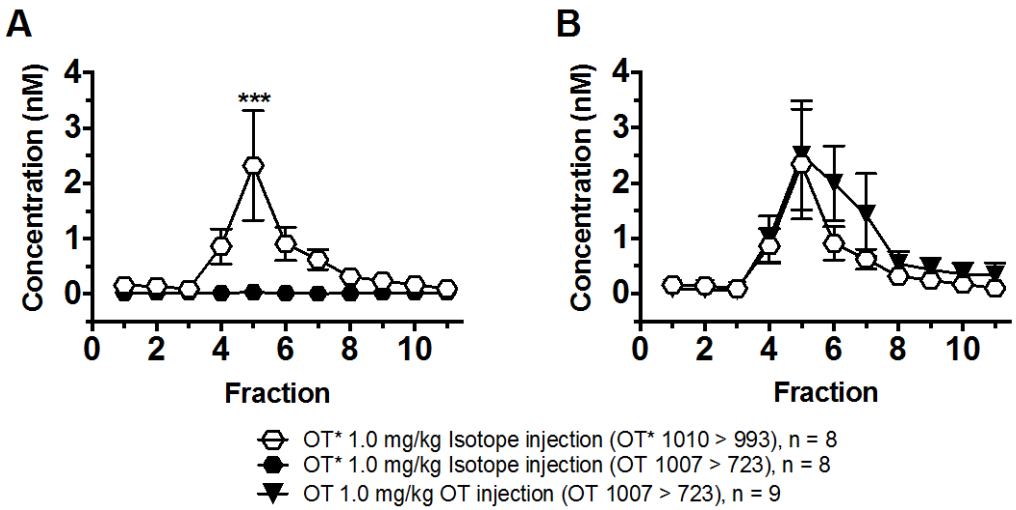

Figure 6-3 Systemic injection of isotopically labeled OT* measured in the dorsal lateral striatum. Systemic injection of OT* results in an increase of isotopically labeled OT* at the probe, but not change endogenous OT (A). Similar doses of OT* and OT are overlaid (B). Two-way ANOVA statistics with Bonferroni post hoc, data shown as average ± SEM. *** $p < 0.001$.

Conclusions

Applying advanced *in vivo* microdialysis sampling and LC-MS measurements, we showed that OT administration reduces dyskinesia associated with chronic L-DOPA treatment. Our studies demonstrate the first direct evidence that systemically administered OT produces antidyskinetic effects in an established rat model of PD. We showed that systemic OT could potentially be used in conjunction with traditional L-DOPA treatment to reduce the dyskinetic symptoms associated with chronic L-DOPA exposure. This preliminary study shows promising results, but significant further preclinical testing must be performed to confirm the validity of this approach and to determine safety, efficacy, route and frequency of administration, and appropriate dosing in humans before it can be translated into patient treatment. OT may therefore alleviate the symptoms associated with chronic L-DOPA treatment, and prolong the ability to use DA replacement therapy to treat PD symptoms without causing disabling side effects.

CHAPTER 7: FUTURE DIRECTIONS

This thesis describes the development and application of liquid chromatography-mass spectrometry (LC-MS) techniques to interrogate small molecule and neuropeptide dynamics *in vivo*. A simple and robust derivatization method was optimized and expanded to label 70 small molecule neurochemicals in various biological media with improved analysis by LC-MS. This improved method is widely applicable and has the potential to be customized and optimized to monitor compounds with primary and secondary amines, as well as phenols, in various media. Capillary LC-MS methods to monitor neurotensin, oxytocin, and opioid neuropeptides in microliter volumes of dialysate were also developed. This goal was achieved by optimizing capillary LC-MS conditions for low limits of detection, improving recovery of neuropeptides across the dialysis membrane with surface modifications, and reducing adsorption of peptides to surfaces from storage to detection with simple organic addition.

Microdialysis sampling and LC-MS techniques were also used in pharmacogenetic (designer receptors exclusively activated by designer drugs; DREADDs) and optogenetic experiments to study small molecules and neuropeptides, leading to the discovery and confirmation of previously unrecognized neuronal circuits. DREADDs experiments revealed a population of neurons implicated in the control of feeding (lateral hypothalamic area neurons containing the peptide neurotensin) and

demonstrated that activity of these neurons modulates mesolimbic dopamine release in the nucleus accumbens (NAc). This modulation of dopamine release promotes motivated behaviors and locomotor activity[70]. We monitored ventral tegmental area neurotensin release and prolonged elevated dopamine in the NAc using complementary LC-MS techniques[70]. In a separate study, we used optogenetics to stimulate dynorphin-containing neurons in two discrete regions in the NAc shell, which produced opposing behaviors. Results obtained using our LC-MS method demonstrated that both basal levels of opioid peptides and stimulated release were different between NAc shell sub-regions, showing that sub-regional neurochemical profiles can drive opposing behaviors.

These complementary LC-MS techniques provide a more comprehensive understanding of neurochemical mechanisms in multiple brain circuits. These methods can be further expanded to monitor other neurochemicals of interest, and could be applied to a multitude of future relevant studies. Future improvements in temporal and spatial resolution, and improved analytical methods for analyte detection will advance our understanding of brain circuitry.

Understanding the composition of neuropeptide fragments in vivo

Neuropeptides are involved in various homeostatic processes and serve as transmitters in the central nervous system. Given their complex biosynthetic and metabolic pathways, understanding the enzymatic processing of precursor neuropeptides and metabolites by monitoring their intra- and extracellular composition would give researchers valuable insight into normal physiological functions and abnormalities in disease. It is important to study neuropeptides, but *in vivo* research is limited due to low

picomolar concentrations in the brain and inadequate detection techniques. Most commercially available immunoassay techniques offer low limits of detection, but only target one analyte, require large sample volumes, are time consuming, and can be non-specific due to cross-reactivity. Commonly used immunoassays, such as radioimmunoassays and enzyme linked immunosorbent assays, detect analytes based on the molecular recognition and binding of antigens to antibodies. Cross-reactivity of interfering compounds with similar binding affinity to the antibody generates signal, reducing the sensitivity and accuracy of the assay, and leading to over-estimation of the analyte. To improve sensitivity and accuracy (by reducing cross-reactivity interferences), two-site immunoradiometric assays utilize two analyte specific antibodies and have been used to study brain natriuretic peptide[346, 347], alpha-1-foetoprotein[348], and parathyroid hormone-related peptide[349].

Some of the limitations of traditional immunoassays are being overcome by efforts in miniaturization and multiplexing. Advancements in immunoassays include bead-based techniques, nanoparticles, and microarrays (Refer to Woolley and Hayes 2013, and Roper and Guillo 2009 for a comprehensive review)[350, 351]. One type of microarray, the micromosaic immunoassay, immobilizes a series of antibodies or antigens on a solid surface with a second set of channels perpendicular to the patterned lines[352]. Sample is flowed over the pattern, allowing for multiple screens to be run in parallel[351, 352]. These micromosaic immunoassays have been used to detect C-reactive protein, myoglobin, and troponin I[353, 354], but require long incubation times and should be improved by coupling with signal amplification. Even with advancement in immunoassay

development, many of the same challenges are present and often require multiple optimized assays for a comprehensive analysis.

An advantage of the capillary LC-MS setup is pre-concentration of microliters of peptide to nanoliters, with nano-ESI prior to MS^n detection. The work in this thesis employed targeted assays that rely on known mass-to-charge (*m/z)* transition pathways to unique identify a known peptide. However, targeted approaches preclude the detection of other fragments of possible interest. Additionally, low sample throughput due to instrument limitations, and varying sensitivity among peptides is problematic for *in vivo* studies, which may generate many samples. The benefits that arise from multiplexing capabilities of MS^n detection, and high selectivity and sensitivity of known analytes (resulting from characteristic retention times and unique *m/z* transitions of the peptides of interest), outweigh these setbacks.

As discussed in Chapter 5, the opioid peptides dynorphin and enkephalins are dysregulated in Parkinson's disease and represent potential therapeutic targets. Dynorphin peptides are produced by endoproteolytic processing of the precursor polypeptide prodynorphin, which results in multiple endogenous fragments other than the specific endogenous dynorphin fragment focused on in this thesis[85]. Previous dynorphin peptide metabolite studies were primarily performed in tissue extracts[85, 92, 93, 355] and *in vivo* investigations into dynorphin peptides and metabolites have been limited by technical challenges. Several studies infused opioid neuropeptide dynorphin $A_{1\text{-}17}$ into striatum-targeted microdialysis probes in rats and detected the resulting fragments secondary to enzymatic cleavage in the dialysate[91, 356]. When applied to unilateral 6-hydroxydopamine (6OHDA) lesioned rats, the biotransformation of a single dynorphin

fragment A_{1-17} into various fragments was altered relative to the intact DA hemisphere[91]. These *in vivo* studies did not address endogenous fragments prior to peptide infusion and did not monitor other fragments from prodynorphin, such as dynorphin B_{1-13}, big dynorphin$_{1-32}$, or their metabolites.

A fundamental study to detect and monitor multiple extracellular endogenous peptide fragments *in vivo* can be performed using our capillary LC-MS and microdialysis techniques. Preliminary work to develop a method to monitor 12 commercially available dynorphin fragments with capillary LC-MS shows promise for at least 8 fragments, but has yet to be tested *in vivo* (Table 7-1). Further capillary LC-MS optimization, improvements in recovery with microdialysis, and reduction in peptide loss due to adsorption would contribute to a more sensitive and selective analytical assay.

With further development and validation focused on improving sensitivity, collection, and detection, this method could be used to examine differences between 6OHDA lesioned and non-lesioned hemispheres, monitor the differential release of fragments from photostimulation in multiple brain regions, study the effects of kappa-agonist and antagonist administration on dynorphin metabolism, and to confirm neuronal tetrodotoxin sensitivity. Other fundamental dynorphin studies should examine mechanisms underlying delayed dynorphin A_{1-8} release with high potassium stimulation, and determine if this effect is specific to a single fragment or more broadly affects the precursor, or enzymatic processing. It is possible that the dynorphin in released vesicles following stimulation is not fully cleaved,

Table 7-1 Summary of dynorphin fragments with limits of detection (LOD) and calibration curve slope. Five µL injections of standards prepared in aqueous ringer solution or standards prepared in aqueous ringer solution with optimal acetonitrile (ACN) were run in triplicate to determine LOD and slope. Direct infusion of peptides below the horizontal dashed line yield unique *m/z* transitions, but were not successfully detected using capillary LC-MS^n at concentrations ≤ 1 nM. *LOD* was calculated using equations: $LOB = mean_{blank} + 1.645(Stdev_{blank})$, and $LOD = LOB + 1.645(Stdev_{low\ concentration\ sample})$, where *LOB* represents the limit of the blank, and *Stdev* represents the standard deviation[209].

Net charge was calculated using equation $z = \sum_i N_i \frac{10^{pKai}}{10^{pH}+10^{pKai}} - \sum_j N_j \frac{10^{pH}}{10^{pH}+10^{pKaj}}$, where *N* represents number of residue/termini and *i* and *j* represent basic or acid residue/termini, respectively[357].

Dynorphin Fragment	MW	Net charge	MS1	MS2	Optimal ACN %	LOD (pM) with 0% ACN	LOD (pM) with optimal ACN %	Slope (pM^{-1}) with 0% ACN	Slope (pM^{-1}) with optimal ACN%
A 1-6	712	1	357	492	5	1.2	0.8	82	111
A 1-7	868	2	435	426	5	37	11	40	63
A 1-8	981	2	491	435	5	2.8	2.8	265	601
A 1-9	1137	3	380	488	5	19	7.8	126	205
A 1-10	1234	3	412.5	528	15	21	15	38	206
A 9 -17	1184	2	396	520	5	12	4.7	22	51
B 1-9	1142	2	382	491	15	3	1.4	67	212
B 1-13	1571	3	524.5	726.5	15	46	102	5.5	94
A 1-17	2147.5	4	538	529.4					
A 2-17	1983	4	497	488.5					
A 1-13	1604	5	402	475					
Big 1-32	3985	9	570.5	645					

Improvement to benzoyl chloride derivatization workflow (Advancements in small molecule detection in the brain)

The benzoyl chloride (BzCl) derivation method described in Chapter 2 has many advantages but is limited by the slow, repetitive pipetting of multiple reagents. The technical challenges associated with collecting and derivatizing a large number of samples underscores the need to automate the derivatization procedure. For example, one collaborative microdialysis study used BzCl derivatization to monitor 20 neurotransmitters of interest with 1 min temporal resolution and aimed to correlate neurotransmitter dynamics simultaneously from two discrete brain regions during an adaptive choice behavior assay (*Pettibone JR 2016, in preparation*). A single experiment produced 200 samples (100 from each brain region), each requiring three manually pipetted reagents into each vial. Over the course of 25 experiments, over 5,000 samples were derivatized and analyzed with LC-MS.

Automating the BzCl reaction would save time offline, reduce human error by minimizing sample handling (thereby improving reproducibility), and could potentially enable online derivatization to achieve real time analysis. Reagent addition could be automated using a sample prep autosampler programmed to pick up and disperse μL volumes of the reagents into programmed vial locations immediately after collection. Another alternative is to use a microfluidic device, made of either glass or polydimethylsiloxane (PDMS), in which the reagents are added sequentially with mixing channels between each addition. While commercial reagent tees are available, a single chip customized to integrate all reagent additions, would simplify the overall setup and reduce dead volumes that increase sampling rise times (Figure 7-1). This chip could be

used as a standalone set-up incorporated into the dialysis lines, and fractions could be collected offline in vials before being injected onto a column with an autosampler.

With integrated reagent addition, the temporal resolution would be limited to the lowest sample volume accurately handled by instrumentation (*i.e.*, if 1 μL sample volumes could be reproducibly injected onto a column and levels were detectable, a minimum of 1 μL derivatized sample would be collected). If the collection time and separation-analysis time could be matched along with reasonable scan rates, online LC-MS analysis could be achieved. An eight-port valve could be incorporated into the flow path in order to switch between sample loading and injection onto the LC column to prevent sample loss (Figure 7-1B). A similar experiment was conducted in which non-derivatized endogenous serotonin was measured with 1 min temporal resolution using microdialysis coupled to capillary UHPLC with electrochemical detection[358]. By using MS instead of electrochemical detection, the number of analytes that can be detected increases significantly. While MS can detect neurotransmitters directly without a dedicated separation step[35], LC separation would reduce interferences that ultimately reduce the number of ions reaching the detector.

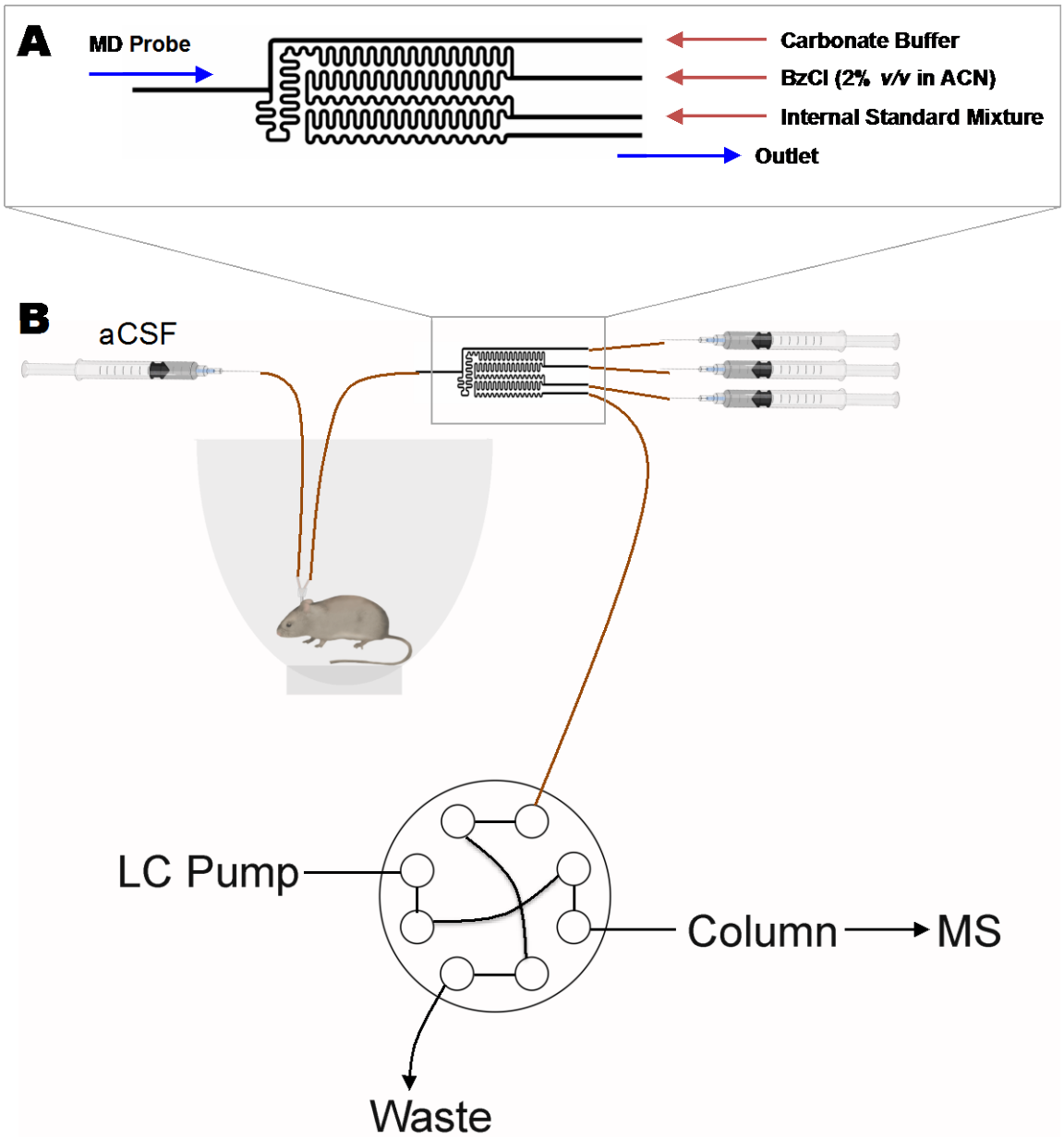

Figure 7-1 Potential microfluidic chip design to integrate microdialysis sampling with online benzoyl chloride derivatization. Microdialysate would flow through the chip (A) and three reagents would be added and mixed in the serpentine channels, between additions. The mixture could be collected offline into individual vials or integrated into an online set up for real-time analysis (B). An eight-port valve would switch between loading and elution of the dialysate. Artist Becca Weisz created images of the syringes, mouse, and probe.

Improvements in spatial resolution of microdialysis

Advancements in LC-MS detection of a variety of neurochemicals at low levels have allowed for the development of new miniaturized microdialysis sampling probes.

One advantage of making probes in house is the potential to create probes that integrate microstimulators with the ability to sample near the site of stimulation. For example, probes combined with platinum wire electrodes can be used to study local neurochemical dynamics during deep brain stimulation (DBS). Sample collection within the site of activation is critical for understanding local mechanisms of action, which may contribute to the beneficial effects of DBS for symptomatic treatment of Parkinson's disease, dystonia, tremor, and depression. Custom probes may also be integrated with fiber optics for concurrent microdialysis with optogenetic stimulation or inhibition of specific neuronal classes, as described in Chapter 4.

Conventional microdialysis probes have limited spatial resolution in the brain because they are 1-4 mm in length with 200-500 μm diameters. Improvements in microdialysis spatial resolution would allow the investigation of extracellular concentration gradients within small brain structures, which are currently not possible with conventional probes. Electrochemical detection methods have shown catecholamine differences across ~150 μm distances in the nucleus accumbens shell[359]. Push-pull probes sample from discrete areas (~ 4 nL sampled volume) and have shown chemical differences between midbrain regions less than 200 μm apart (i.e., red nucleus vs. ventral tegmental area)[360]. Further miniaturization of sampling probes[361, 362] through microfabrication is a promising approach that will improve spatial resolution and minimize tissue damage[363-367].

Microfabrication in silicon by bulk micromachining and lithography has been used to produce push-pull sampling probes 85 μm wide by 70 μm thick by 11 mm long[362]. These microfabricated push-pull sampling probes were successfully used to

sample basal concentrations from the striatum of anesthetized rats. Push-pull probes allow the sampling of small and large molecular weight neurochemicals and proteins, but are prone to clogging due to the lack of membrane. Furthermore, push-pull methods require vacuum pumps to draw samples, further complicating the sampling setup. A miniaturized sampling probe with an incorporated membrane would circumvent these issues, but fabrication is challenging. A polysilicon semipermeable membrane was fabricated in a miniaturized microdialysis probe and was expected to exclude large molecular weight compounds[367]. However, these probes were never tested for neurochemical sampling *in vitro* or *in vivo*. Our lab developed microfabricated dialysis probes with embedded nanoporous anodic aluminum oxide membranes and used them to sample an anesthetized rat striatum *in vivo*[361] (Figure 7-2). As compared to the small conventional probe, the microfabricated probes have 75% less surface area and 83% less sampling area, indicating a 6-fold improved spatial resolution and less tissue disruption.

While the merits of miniaturized sampling probes are appealing, employing these probes *in vivo* presents many challenges. For example, low flow rates are needed to mitigate pressure (due to the structural strength of the membrane), resulting in either small sample volumes (nL) or reduced temporal resolution for larger volume collections. Small sample volumes (nL) are cumbersome to manipulate manually and challenge the sensitivity of current analytical technologies. Currently, temporal resolution is sacrificed to produce μL sample volumes for LC-MS analysis. For example, 20 min were required to collect 2 μL of dialysate for analysis[361, 362]. The use of segmented flow for droplets with direct-MS detection could be used to preserve temporal resolution[35]. Segmented flow could be achieved by incorporating a third channel into the microfabricated probe to

create droplets close to the sampling area. Droplets could also be generated after probe outlet by using a commercially available reagent tee, or microfabricating a tee to reduce volume requirements. If segmented flow is achieved, it may be possible directly detect neurotransmitters with MS.

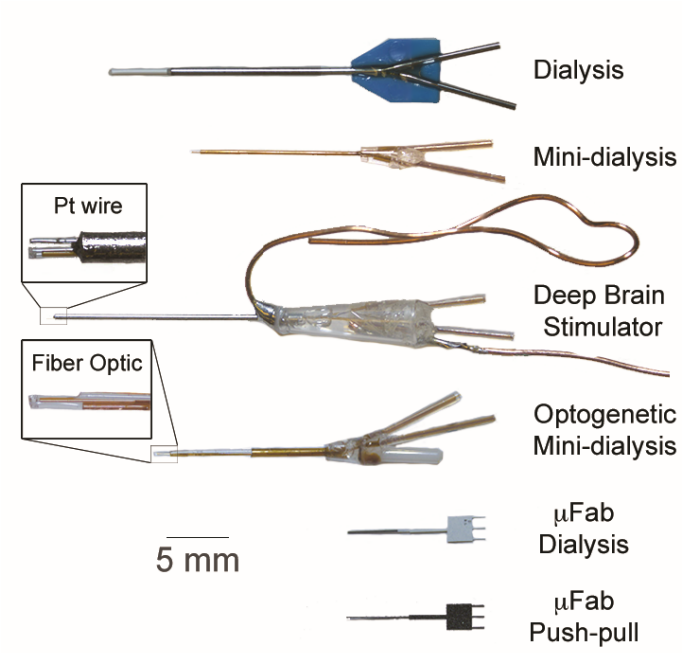

Figure 7-2 Comparison of different dialysis probes. The top probe is a conventional microdialysis probe that is commercially available. The mini-dialysis probe is fabricated in-house for routine use in rodents. The 'deep brain stimulator' integrates a platinum wire electrode, which can be used to deliver electrical pulses in brain tissue. The 'optogenetic mini-dialysis' probe integrates a fiber optic probe along side the dialysis membrane allowing for sampling of locally stimulated tissue. No sheath is required for the optogenetic mini-dialysis probe as it can withstand insertion into the brain as is. 'μFab dialysis' and 'μFab push-pull' are silicon-based probes fabricated by lithography and bulk micromachining techniques. The 'μFab dialysis' probe directly integrates a 4 mm long nanoporous anodic aluminum oxide membrane at the tip. The 'μFab push-pull' consists of two 20 m square orifices at the tip.

Conclusions

Studying the complexity and intricacy of neuronal circuitry requires analytical techniques with high sensitivity and selectivity. This thesis work developed methods to monitor a wide range of small molecule neurochemicals and low picomolar levels of neuropeptides. We applied these methods to study previously unconfirmed neuronal circuits and to examine neurochemical alterations in Parkinson's disease models.

Advances in LC-MS technologies will allow for the improved application of microdialysis. These advancements will allow sampling and detection within discrete sub-regions of the brain with the potential for online analysis. These techniques will provide the precise measurements needed for modern neurobiological experiments to examine brain circuits and neurochemical changes in normal behavior and disease. Further refinement of these techniques will enable fundamental neurochemical studies and will expand the scope of neuroscientific analyses.

APPENDIX A: Preparation of Benzoyl Chloride Standards and Internal Standards

Note: This is an example preparation of standards and $^{13}C_6$-benzoyl chloride (BzCl) labeled internal standards (IS) that can be used for calibrations and reagents. The concentrations can be adjusted to meet the needs of ones' experimental parameters.

Main Stock (Refer to)

1. Make all 'Stock' solutions (mM concentration) using HPLC-grade water.
2. Add all 'Volume of Stock' to a 2 mL plastic vial **EXCEPT ACh + Ch**[*].
3. Add HPLC-water to bring the final volume to 2000 µL (*Main Stock*).
4. Check that all analytes in the *Main Stock* are present with your LC-MS method by derivatizing with standard BzCl (2% *v/v*):
    a. Make derivatizing solutions:
        i. Carbonate buffer (100 mM); 12.4mg : 1000 µL HPLC-water
        ii. BzCl (2% *v/v*); 12 µL BzCl : 588 µL acetonitrile
        iii. 'Pseudo IS'; 248 µL water : 247 µL acetonitrile : 5 µL sulfuric acid

[*] ACh and Ch are not added to the *Main Stock* because the *Main Stock* is used to generate $^{13}C_6$-BzCl labeled IS. ACh and Ch are not labeled since they do not have the correct functional groups for derivatization. Since the IS mixture is a reagent that is added to samples, unlabeled ACh and Ch would generate high background signals during analysis since they would not have an isotope shift relative to endogenous ACh and Ch *m/z*.

b. Prepare top calibration sample

    i. Dilute '*Main Stock*' 100-fold; 99 µL HPLC-water : 1 µL '*Main Stock*'

    ii. Dilute this solution 5-fold further in aCSF/media; 40 µL aCSF : 10 µL

c. Derivatize top calibration sample by sequentially adding 25 µL of each reagent to 50 µL of sample (i.e. 25 µL carbonate buffer : 25 µL BzCl (2% *v/v*) : 25 µL 'Pseudo IS'). Vortex between each reagent addition.

d. Run derivatized standard on LC-MS and make sure all expected peaks are present in the chromatogram (except ACh + Ch, since they are not present in '*Main Stock*').

e. If all analytes are present, proceed to making $^{13}C_6$-BzCl IS mixture and calibration standard mixture. If not, remake or adjust levels accordingly by remaking the '*Main Stock*' (Steps 1-3) until satisfactory.

Table A-1 Preparation of *Main Stock*

Analyte	Stock (mM)	Volume of Stock (μL)	Final Concentration in *Main Stock* (μM)
ACh	25	---	---
Ch	1000	---	---
Gly	20	100	1000
GABA	20	10	100
Ser	20	250	2500
Hist	20	5	50
Tau	40	100	2000
Asp	20	20	200
Glu	20	100	1000
Ado	5	40	100
5HT	20	1	10
NE	20	1	10
DA	20	1	10
HVA	20	25	250
5HIAA	10	20	100
NM	20	1	10
3MT	20	1	10
DOPAC	20	100	1000
Gln	100	100	5000
L-DOPA	20	1	10
E	20	1	10
GSH	100	2	100
Tyr	2	250	250
Phe	20	100	1000
5HTP	20	10	100
Glc	100	500	25000
	Analyte Volume	1739 μL	
	HPLC-Water	261 μL	
	Total Volume	2000 μL	

$^{13}C_6$-BzCl labeled internal standard mixture (No ACh or Ch)

1. Prepare $^{13}C_6$-BzCl (2% *v/v)* in acetonitrile (6 µL $^{13}C_6$-BzCl : 294 µL acetonitrile).
2. Dilute 250 µL *Main Stock* with 250 µL HPLC-water.
3. Derivatize 500 µL sample by sequentially adding 250 µL carbonate buffer, 250 µL $^{13}C_6$-BzCl (2% *v/v*), and 1 µL formic acid. Vortex between each reagent addition. If precipitate does not dissolve with vortexing, small volumes (1 µL increments) of additional formic acid can be added with vigorous vortexing until solution is clear.
4. Aliquot 20 µL in individual vials and store in -80°C freezer. Use a frozen aliquot each day and discard after single use.

Internal standards for ACh and Ch, d_4-ACh and d_4-Ch respectively, are added separately since they do not label with BzCl.

d_4-ACh and d_4-Ch stock

1. Prepare 1 mM stocks of d_4-ACh and d_4-Ch in HPLC-water.
2. Dilute both stocks into a single vial to a final concentration of 12.5 µM d_4-ACh and 500 µM d_4-Ch (390 µL HPLC-water : 10 µL d_4-ACh : 400 µL d_4-Ch).
3. Aliquot 10 µL in individual vials and store in -80°C freezer. Use a frozen aliquot each day and discard after 2-3 freeze-thaw cycles.

Calibration standard mixture (with ACh and Ch)

1. Make a vial of '*Concentrated Standard*'
    a. Take 998 µL of *Main Stock*, and add 1 µL ACh (25 mM) and 1 µL Ch (1 M).
2. Dilute the '*Concentrated Standard*' 100-fold in aCSF; 990 µL aCSF : 10 µL *Concentrated Standard*.
3. Aliquot 20 µL in individual vials and store in -80°C freezer. Use a frozen aliquot each day and discard after single use.

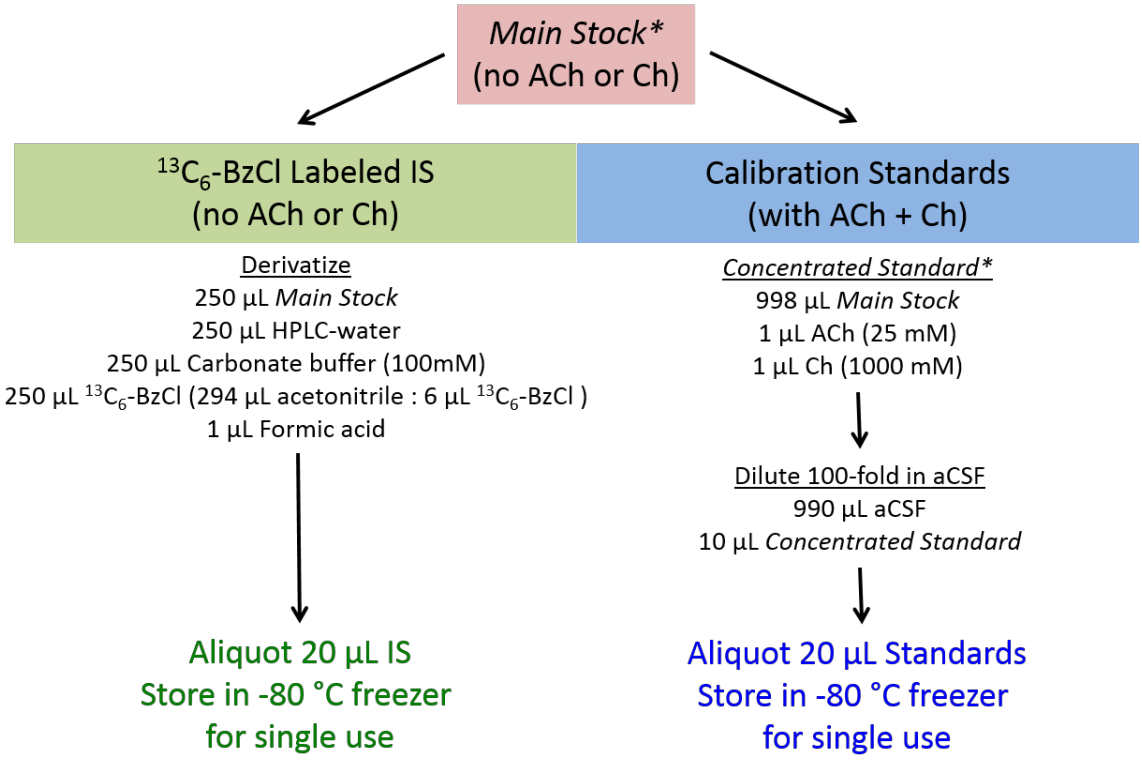

Figure A-1 Overview of *$^{13}C_6$-BzCl IS* and *Calibration Standard* procedure.

Example calibration curve procedure in aCSF (Refer to Figure A-2 *and* Table A-2*)*

Calibration standards are designated L1 (lowest concentration) – L6 (highest concentration) in the XCalibur QuanBrowser software. For consistency with this scheme, all six points of the standards will be referred to L1 – L6, followed by Table A-2 with correlated concentrations (based on the *Main Stock* prepared from).

1. Take a single aliquot of frozen '*Calibration Standard'* and thaw to room temperature.
2. Prepare samples L6 – L1 prior to derivatization
    a. Dilute thawed *Calibration Standard* 5-fold in aCSF to yield highest calibration point L6
    b. Dilute L6 2-fold into aCSF to yield L5
    c. Dilute L5 2-fold into aCSF to yield L4, and 10-fold to yield L3
    d. Dilute L4 10-fold into aCSF to yield L2
    e. Dilute L3 10-fold into aCSF to yield L1

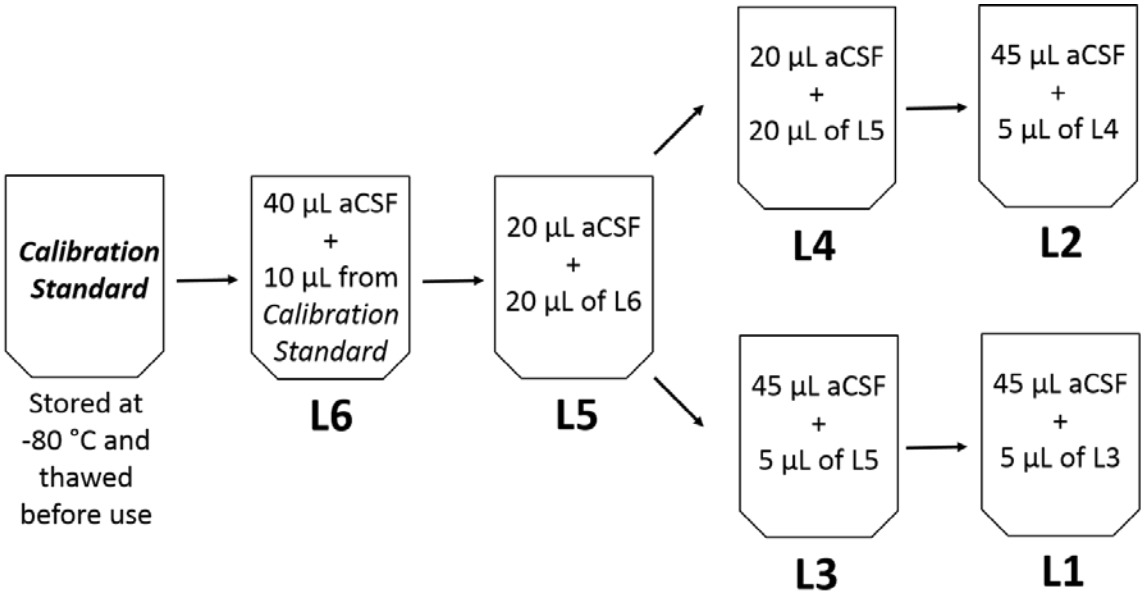

Figure A-2 Calibration curve standard preparation.

3. Aliquot a volume of standard representative to the experimental conditions and derivatize using prepared reagents in a 2 : 1 : 1 : ratio, vortexing between each reagent addition (i.e. if the samples generated in the experiment are 3 μL, then aliquot 3 μL and derivatize with 1.5 μL of each reagent).
    a. Reagents
        i. Carbonate buffer (100 mM); 12.4 mg : 1000 μL HPLC-water
        ii. BzCl (2% *v/v*); 12 μL BzCl : 588 μL acetonitrile
        iii. IS mixture; 245 μL HPLC-water : 245 μL acetonitrile : 5 μL sulfuric acid : 5 μL $^{13}C_6$-BzCl labeled IS mixture : 1 μL d_4 Stock

Table A-2 Final concentration in each calibration standard, vials L6 – L1.

	Concentration (nM)					
Analyte	L6	L5	L4	L3	L2	L1
ACh	50	25	12.5	2.5	1.25	0.25
Ch	2000	1000	500	100	50	10
3MT	20	10	5	1	0.5	0.1
5HIAA	200	100	50	10	5	1
5HT	20	10	5	1	0.5	0.1
5HTP	200	100	50	10	5	1
Ado	200	100	50	10	5	1
Asp	400	200	100	20	10	2
DA	20	10	5	1	0.5	0.1
DOPAC	2000	1000	500	100	50	10
E	20	10	5	1	0.5	0.1
GABA	200	100	50	10	5	1
Glc	50000	25000	12500	2500	1250	250
Gln	10000	5000	2500	500	250	50
Glu	2000	1000	500	100	50	10
Gly	2000	1000	500	100	50	10
GSH	200	100	50	10	5	1
Hist	100	50	25	5	2.5	0.5
HVA	500	250	125	25	12.5	2.5
LDOPA	20	10	5	1	0.5	0.1
NE	20	10	5	1	0.5	0.1
NM	20	10	5	1	0.5	0.1
PA	2000	1000	500	100	50	10
Ser	5000	2500	1250	250	125	25
Tau	4000	2000	1000	200	100	20
Tyr	500	250	125	25	12.5	2.5

APPENDIX B: Microdialysis Probe Fabrication

A. Side-by-side microdialysis probe fabrication

Materials

- Inlet = 40/100 (i.d./o.d.) fused silica capillary (5 cm)
- Outlet = 75/150 fused silica capillary (6 cm)
- Shaft = 250/360 fused silica capillary (11 mm)*
    - Covered with 30G thin wall Teflon tubing (5 mm)
- Inlet cover = 150/360 fused silica capillary (8 mm)
    - Covered with 30G thin wall Teflon tubing (7mm)
- Outlet cover = 180/360 fused silica capillary (10 mm)
    - Covered with 30G thin wall Teflon tubing (9 mm)
- Microdialysis semi-permeable membrane
- Glue:
    - Thin cyanoacrylate glue
    - Five minute epoxy

*Can be adjusted to appropriate length required for surgical needs

Instructions

1. Place the inlet and outlet capillaries side-by-side and slide the outlet capillary down equal to the length of the desired active area (i.e. if you want to make a 1 mm probe, offset the outlet 1mm below the inlet).
2. Using a needle, apply thin liquid glue to adhere capillaries together.
    a. Only apply the least amount of glue needed
3. Carefully slide a piece of microdialysis membrane over both the inlet and outlet, avoiding pinching and kinking of membrane. Cut excess membrane off.
    a. Cutting the membrane at a 45° angle can help if it is problematic to slide over both capillaries
4. Mix a small amount of 5-minute epoxy, and let slightly harden to a consistency that is able to hold stiff peaks. Once the correct consistency is achieved, use a clean hypodermic needle and carefully fill the end of the membrane to create a complete glue plug (~100 – 150 μm thickness).
    a. If you use the epoxy too early you will get a large glue plug. If you use the epoxy too late, it will be too stiff and not fill the tip of the membrane completely, leaving you with a hole for perfusion media to leak out of.
    b. Be careful not to get epoxy on the exterior of the membrane.
    c. Let the glue plug dry for 2-3 h before proceeding.
5. Once the glue plug is dry, gently tap/move the membrane down the capillary until the inlet is ~100 μm away from the glue plug.

6. Mix a small amount of 5-minute epoxy and carefully apply a small amount around the entire backside of the membrane. You should see the glue fill the back. Let dry overnight.
    a. If you apply too much, the glue can wick up the membrane and clog the outlet. If you are careful you can create an even seal around the entire membrane.
    b. If you do not let the epoxy completely dry before proceeding to the next step, I have found that when wet epoxy comes in contact with the thin cyanoacrylate glue, the epoxy never fully dries and can be easily removed with minimal effort (i.e. fluid from perfusion media).

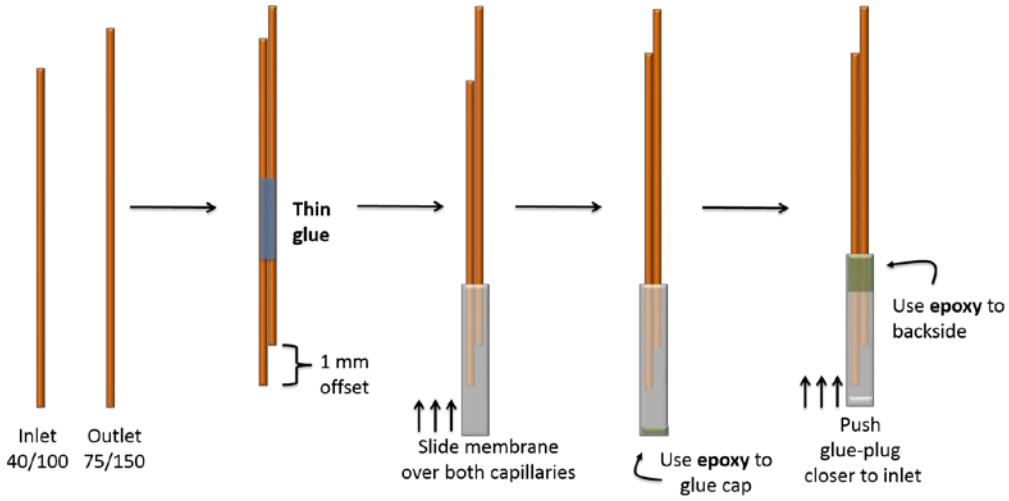

Figure B-1 Side-by-side microdialysis probe, steps 1 – 6.

7. Take 30G thin walled Teflon tubing and slide over the joint side of the 250/360 capillary shaft until the top 5 mm is covered.
    a. Use a sharp razor blade and gently score the Teflon closest to the joint. This scoring will help glue to hold Teflon in place.

8. Carefully slide the 250/360 capillary shaft over the membrane, and adjust the until the desired membrane active area (distance between the glue plug and shaft, where molecules can diffuse).
9. Use a pipette and apply a drop of thin cyanoacrylate to the back of the shaft.
10. Take 30G thin walled Teflon tubing and slide over the inlet and outlet cover capillaries until all but ~ 1mm of capillary is covered.
    a. Use a sharp razor blade and gently score the Teflon closest to the exposed capillary. This scoring will help glue to hold Teflon in place.

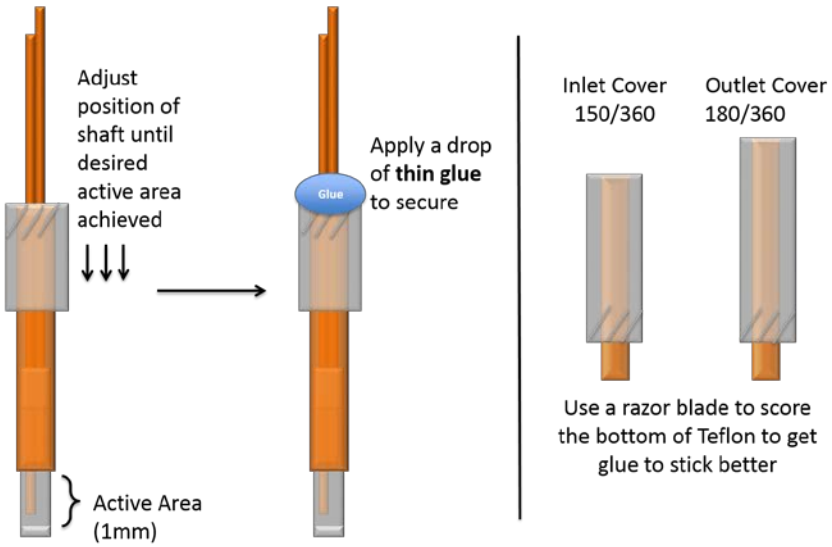

Figure B-2 Side-by-side microdialysis probe, steps 7 – 10.

11. Slide the inlet and outlet covers over the respective inlet and outlet, forming a Y-junction with the shaft.
12. Apply thin cyanoacrylate glue using a needle to the Y-joint to secure the inlet and outlet covers.
13. Use a plastic pipette tip, and cut a small piece off the pipette tip to use as a junction cover.

14. Mix a small amount of 5-minute epoxy and quickly apply a liberal amount around the entire joint.
15. Carefully slide the small pipette tip over the membrane and up to the joint with epoxy.
    a. It's helpful to bring the epoxy up the inlet and outlet to better reinforce the probe.
16. Let dry overnight.
17. Cut excess inlet and outlet capillaries as close to the inlet and outlet covers right before use.

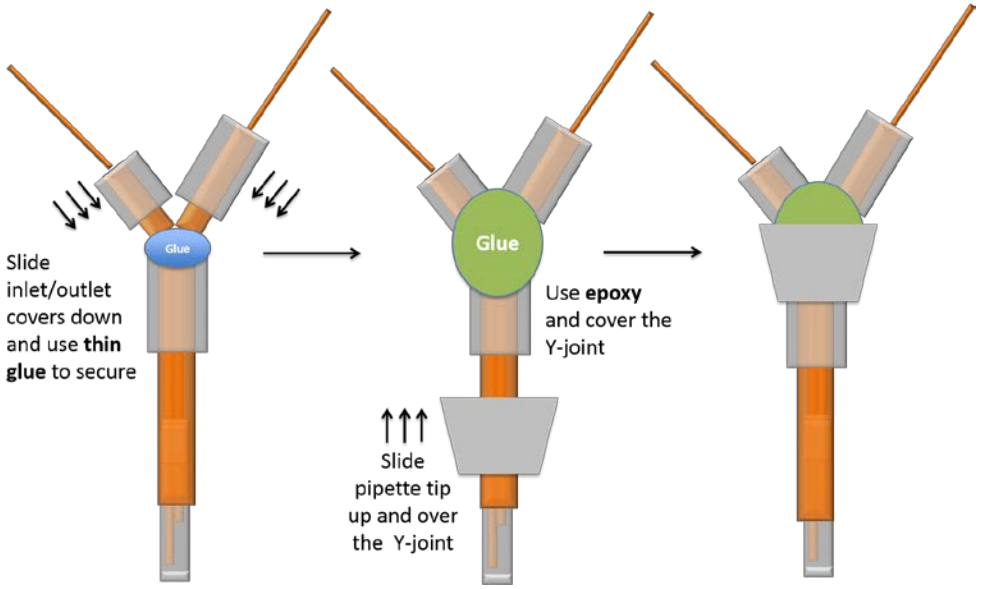

Figure B-3 Side-by-side microdialysis probe, steps 11 – 15.

B. Concentric microdialysis probe fabrication

Materials

- Inlet = 40/100 (i.d./o.d.) fused silica capillary (5 cm)
- Outlet = 75/150 fused silica capillary (4 cm)
- Shaft = 24G stainless steel tubing (11 mm)*
- Inlet cover = 150/360 fused silica capillary (8 mm)
    - Covered with 30G thin wall Teflon tubing (7mm)
- Outlet cover = 180/360 fused silica capillary (10 mm)
    - Covered with 30G thin wall Teflon tubing (9 mm)
- Microdialysis semi-permeable membrane
- Glues:
    - Thin cyanoacrylate glue
    - Gel superglue
    - Five minute epoxy
    - Glue accelerator

*Can be adjusted to appropriate length required for surgical needs

Instructions

1. Take 30G thin walled Teflon tubing and slide over the inlet and outlet cover capillaries until all but ~ 1mm of capillary is covered.
    a. Use a sharp razor blade and gently score the Teflon closest to the exposed capillary. This scoring will help glue to hold Teflon in place.

2. Slide the inlet and outlet covers over the respective inlet and outlet and secure with thin cyanoacrylate (applied to the joint side/exposed capillary side of inlet/outlet cover)
3. Trim the outlet capillary so that it is approximately half the length of the shaft when measured from joint to tip (i.e. if shaft is 11 mm, cut so the outlet is approximately 5.5 mm).

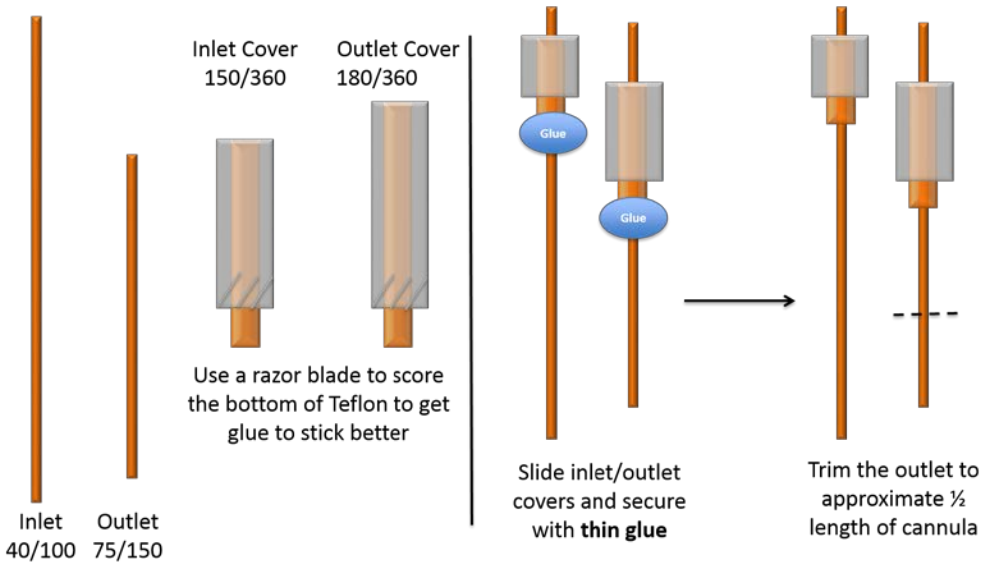

Figure B-4 Concentric microdialysis probe, steps 1 – 3.

4. Take the inlet and the trimmed outlet and slide into the cannula until the inlet and outlet covers form a Y-joint.
5. Use gel glue and liberally apply around the Y-joint to secure the inlet and outlets.
    a. I twist the cannula at the joint to ensure that the glue is fully around the joint.
    b. If you use the thin cyanoacrylate it will wick up the cannula and clog the probe.

6. Once the joint is secured, use a pipette to apply the glue accelerator around the joint. Let dry for a few minutes.

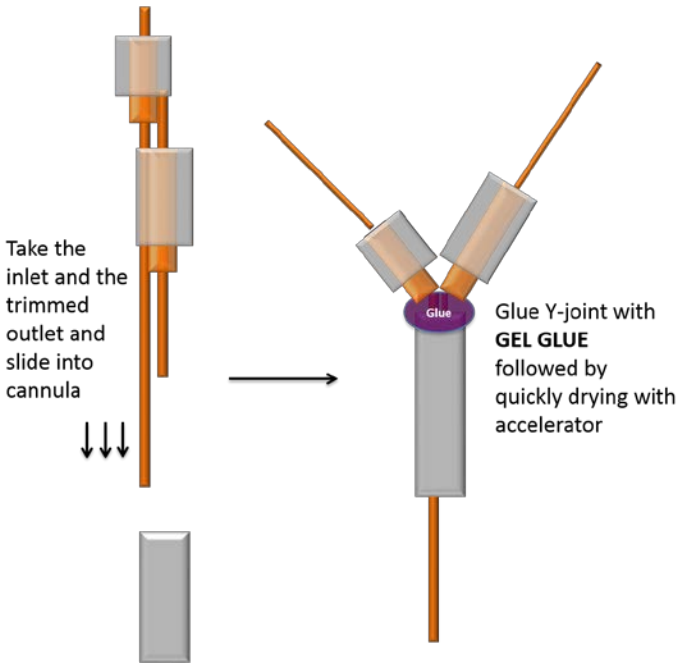

Figure B-5 Concentric microdialysis probe, steps 4 – 6.

7. Use a plastic pipette tip, and cut a small piece off the pipette tip to use as a junction cover.
8. Mix a small amount of 5-minute epoxy and quickly apply a liberal amount around the entire joint.
9. Carefully slide the small pipette tip up to the joint and secure with epoxy.
    a. It's helpful to bring the epoxy up the inlet and outlet to better reinforce the probe.
10. Let dry overnight.
11. Cut the excess inlet to ~100 µm less than desired area length (i.e. if you want a 1 mm probe, cut the inlet so ~0.9 mm is exposed).
12. Slide microdialysis membrane into the cannula over the protruding inlet.

a. I like to make sure the membrane goes in at least > 2 mm into the shaft so glue does not clog the membrane.

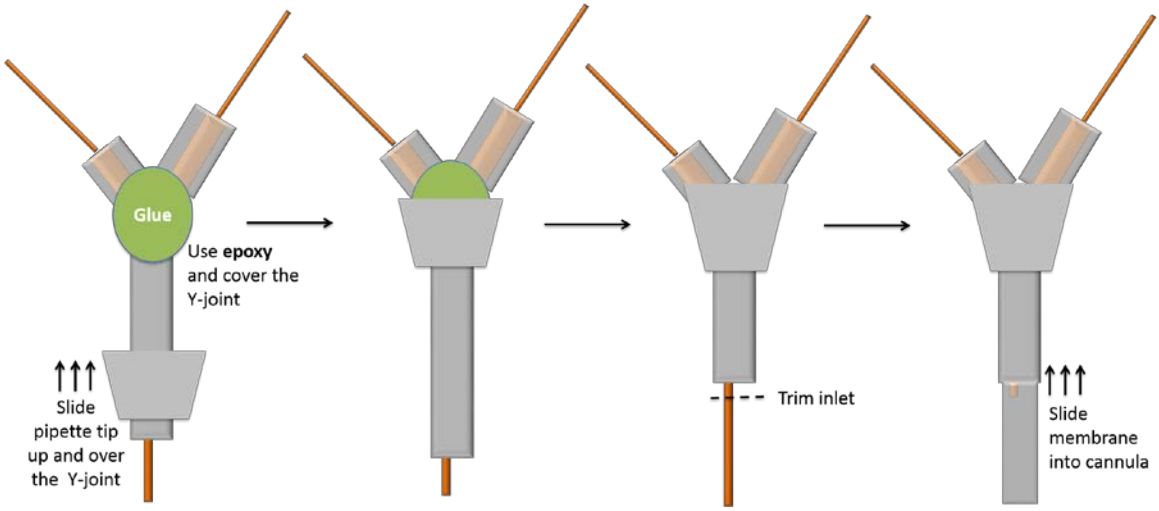

Figure B-6 Concentric microdialysis probe, steps 7 – 12.

13. Mix a small amount of 5-minute epoxy and carefully apply a small amount around the entire backside of the membrane while the epoxy is fluid.
    a. If you apply too much, the glue can wick up the membrane and clog the probe. If you are careful you can create an even seal around the entire membrane. Be careful not to get too much glue onto the actual membrane.
14. Wait until the 5-minute epoxy is at a consistency that is able to hold stiff peaks. Once the correct consistency is achieved, use a clean hypodermic needle and carefully fill the end of the membrane to create a complete glue plug (~ 100 – 150 µm thickness).
    a. If you use the epoxy too early you will get a large glue plug. If you use the epoxy too late, it will be too stiff and not fill the tip of the membrane completely, leaving you with a hole for perfusion media to leak out of.

b. Be careful not to get epoxy on the exterior of the membrane.

15. Use a clean hypodermic needle to gently position the membrane so that the glue plug is ~ 100 µm away from the inlet.

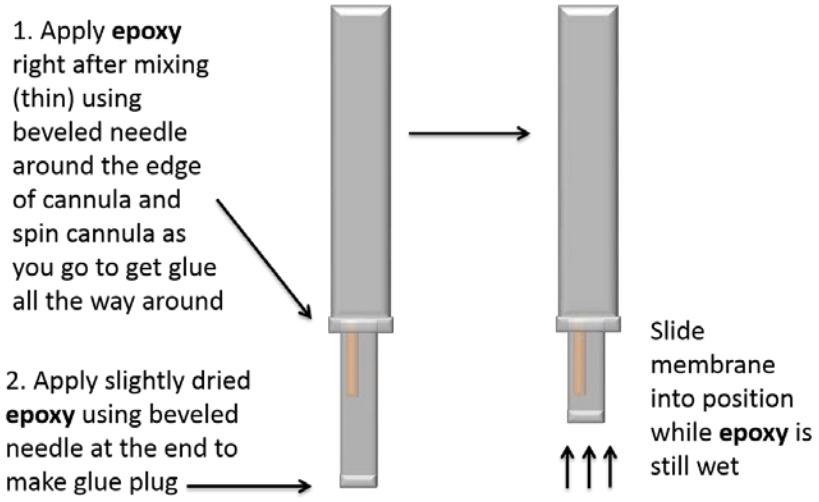

Figure B-7 Concentric microdialysis probe, steps 13 – 15.

16. Let dry overnight.

17. Cut excess inlet and outlet capillaries as close to the inlet and outlet covers right before use.

C. Optogenetic-dialysis probe fabrication

Materials

- Inlet = 40/100 (i.d./o.d.) fused silica capillary (5 cm)
- Outlet = 75/150 fused silica capillary (6 cm)
- Holder = 450/670 fused silica capillary (5 mm)
- Inlet cover = 150/360 fused silica capillary (8 mm)
    - Covered with 30G thin wall Teflon tubing (7mm)
- Outlet cover = 180/360 fused silica capillary (10 mm)
    - Covered with 30G thin wall Teflon tubing (9 mm)
- Microdialysis semi-permeable membrane
- Fiber optic fiber (14 mm) with attached ferrule*
- Glue:
    - Thin cyanoacrylate glue
    - Gel superglue
    - Five minute epoxy
    - Glue accelerator

*Can be adjusted to appropriate length required for surgical needs

Instructions

1. Place the inlet and outlet capillaries side-by-side and slide the outlet capillary down equal to the length of the desired active area (i.e. if you want to make a 1 mm probe, offset the outlet 1mm below the inlet).
2. Using a needle, apply thin liquid glue to adhere capillaries together.

    a. Only apply the least amount of glue needed
3. Carefully slide a piece of microdialysis membrane over both the inlet and outlet, avoiding pinching and kinking of membrane. Cut excess membrane off.
    a. Cutting the membrane at a 45° angle can help if it is problematic to slide over both capillaries
4. Mix a small amount of 5-minute epoxy, and let slightly harden to a consistency that is able to hold stiff peaks. Once the correct consistency is achieved, use a clean hypodermic needle and carefully fill the end of the membrane to create a complete glue plug.
    a. If you use the epoxy too early you will get a large glue plug. If you use the epoxy too late, it will be too stiff and not fill the tip of the membrane completely, leaving you with a hole for perfusion media to leak out of.
    b. Be careful not to get epoxy on the exterior of the membrane.
    c. Let the glue plug dry for 2-3 h before proceeding.
5. Once the glue plug is dry, gently tap/move the membrane down the capillary until the inlet is ~100 μm away from the glue plug.
6. Mix a small amount of 5-minute epoxy and carefully apply a small amount around the entire backside of the membrane. You should see the glue fill the back. Let dry overnight.

a. If you apply too much, the glue can wick up the membrane and clog the outlet. If you are careful you can create an even seal around the entire membrane

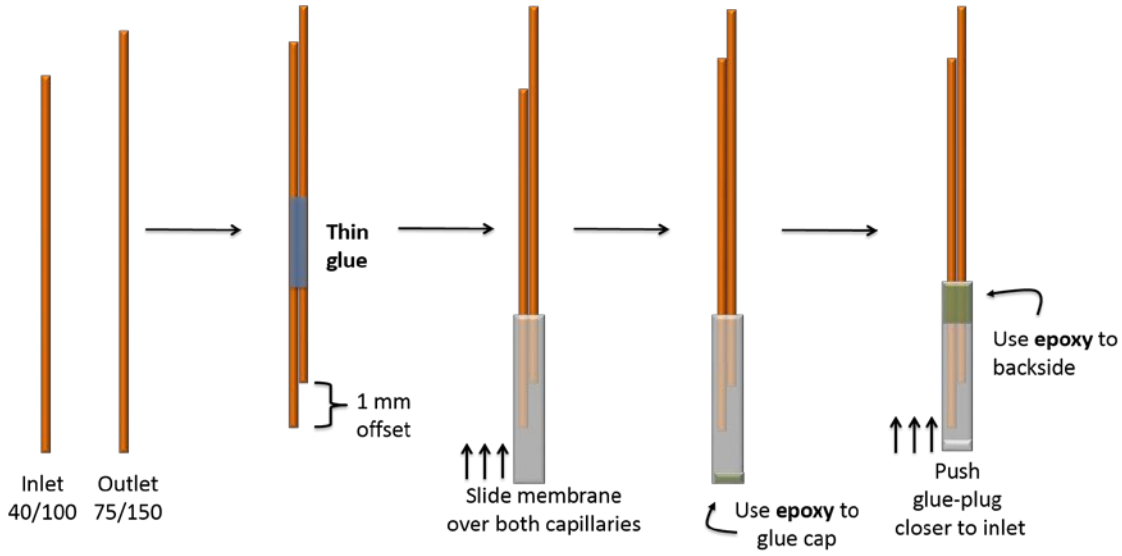

Figure B-8 Opto-dialysis probe, steps 1 – 6.

7. Slide the 450/670 capillary holder over the back side of the inlet/outlet assembly, followed by sliding the fiber optic into the backside of the capillary holder.
    a. The fiber optic is rigid cannot handle much angled force.
8. Position the fiber optic so the tip is next to the outlet, keeping the capillary holder is as close as possible to the ferrule.
9. Carefully apply the thin cyanoacrylate glue to the secure the capillary holder to the inlet/outlet assembly and fiber optic together.
    a. Careful to not apply so much glue that it results in wicking onto the membrane.
10. Take 30G thin walled Teflon tubing and slide over the inlet and outlet cover capillaries until all but ~ 1mm of capillary is covered.

a. Use a sharp razor blade and gently score the Teflon closest to the exposed capillary. This scoring will help glue to hold Teflon in place.

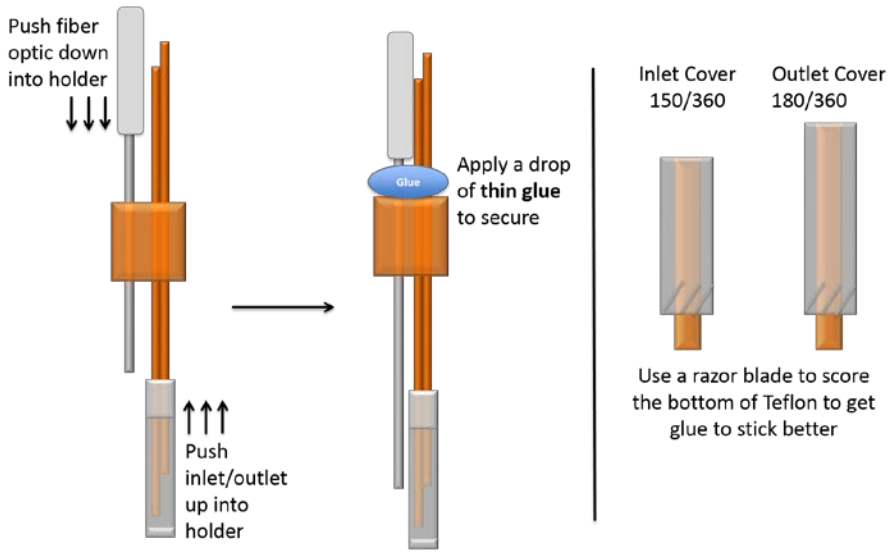

Figure B-9 Opto-dialysis probe, steps 7 – 10.

11. Slide the inlet and outlet covers over the respective inlet and outlet and secure with thin cyanoacrylate (applied to the joint side/exposed capillary side of inlet/outlet cover)
12. Use a large plastic pipette tip, and cut a small piece off the pipette tip to use as a junction cover.
13. Use gel glue and apply around the entire joint.
14. Carefully slide the pipette tip over the membrane/fiber optic and up to the joint with glue.
15. Apply some glue accelerator to the joint.
    a. I find it helpful to let the joint dry, for a few minutes and reinforce with 5-minute epoxy around the inlet/outlet covers and fiber optic.

16. Cut excess inlet and outlet capillaries as close to the inlet and outlet covers right before use.

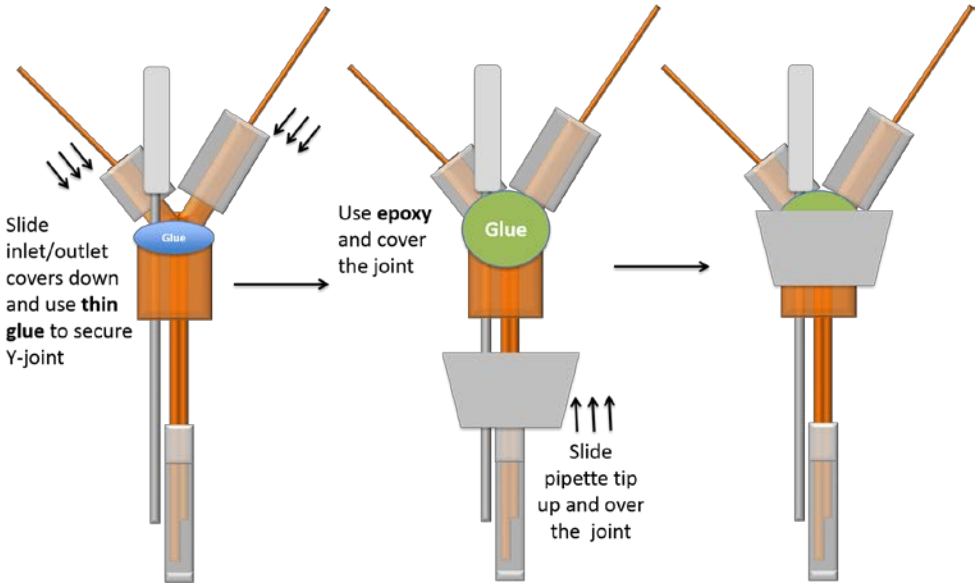

Figure B-10 Opto-dialysis probe, steps 11 – 15.

REFERENCES

1. Magnoni, S.; Mac Donald, C. L.; Esparza, T. J.; Conte, V.; Sorrell, J.; Macri, M.; Bertani, G.; Biffi, R.; Costa, A.; Sammons, B.; Snyder, A. Z.; Shimony, J. S.; Triulzi, F.; Stocchetti, N.; Brody, D. L., Quantitative assessments of traumatic axonal injury in human brain: concordance of microdialysis and advanced MRI. *Brain : a journal of neurology* **2015,** *138* (Pt 8), 2263-77.

2. Perry, M.; Li, Q.; Kennedy, R. T., Review of recent advances in analytical techniques for the determination of neurotransmitters. *Analytica Chimica Acta* **2009,** *653* (1), 1-22.

3. Zetterström, T.; Sharp, T.; Marsden, C. A.; Ungerstedt, U., In vivo measurement of dopamine and its metabolites by intracerebral dialysis: changes after d-amphetamine. *Journal of Neurochemistry* **1983,** *41* (6), 1769-1773.

4. Huang, T.; Yang, L.; Gitzen, J.; Kissinger, P. T.; Vreeke, M.; Heller, A., Detection of basal acetylcholine in rat brain microdialysate. *Journal of chromatography. B, Biomedical applications* **1995,** *670* (2), 323-7.

5. Tsai, T. H., Separation methods used in the determination of choline and acetylcholine. *Journal of chromatography. B, Biomedical sciences and applications* **2000,** *747* (1-2), 111-22.

6. Guerrieri, A.; Palmisano, F., An acetylcholinesterase/choline oxidase-based amperometric biosensor as a liquid chromatography detector for acetylcholine and choline determination in brain tissue homogenates. *Anal Chem* **2001,** *73* (13), 2875-2882.

7. Potter, P. E.; Meek, J. L.; Neff, N. H., Acetylcholine and choline in neuronal tissue measured by HPLC with electrochemical detection. *Journal of Neurochemistry* **1983,** *41* (1), 188-194.

8. Zapata, A.; Chefer, V. I.; Shippenberg, T. S.; Denoroy, L., Detection and quantification of neurotransmitters in dialysates. *Current protocols in neuroscience / editorial board, Jacqueline N. Crawley ... [et al.]* **2009,** *Chapter 7*, Unit 7 4 1-30.

9. Dorresteijn, R. C.; Berwald, L. G.; Zomer, G.; de Gooijer, C. D.; Wieten, G.; Beuvery, E. C., Determination of amino acids using o-phthalaldehyde-2-mercaptoethanol derivatization effect of reaction conditions. *Journal of Chromatography A* **1996,** *724* (1–2), 159-167.

10. Hanczkó, R.; Molnár-Perl, I., Derivatization, stability and chromatographic behavior ofo-phthaldialdehyde amino acid and amine derivatives:o-Phthaldialdehyde/ 2-mercaptoethanol reagent. *Chromatographia* **2003,** *57* (1), S103-S113.

11. Bert, L.; Robert, F.; Denoroy, L.; Stoppini, L.; Renaud, B., Enhanced temporal resolution for the microdialysis monitoring of catecholamines and excitatory amino acids using capillary electrophoresis with laser-induced fluorescence detection. Analytical developments and in vitro validations. *Journal of chromatography. A* **1996,** *755* (1), 99-111.

12. Kaul, S.; Faiman, M. D.; Lunte, C. E., Determination of GABA, glutamate and carbamathione in brain microdialysis samples by capillary electrophoresis with fluorescence detection. *ELECTROPHORESIS* **2011,** *32* (2), 284-291.

13. Robert, F.; Bert, L.; Lambas-Senas, L.; Denoroy, L.; Renaud, B., In vivo monitoring of extracellular noradrenaline and glutamate from rat brain cortex with 2-min microdialysis sampling using capillary electrophoresis with laser-induced fluorescence detection. *J Neurosci Methods* **1996,** *70* (2), 153-62.

14. Li, H.; Wang, H.; Chen, J. H.; Wang, L. H.; Zhang, H. S.; Fan, Y., Determination of amino acid neurotransmitters in cerebral cortex of rats administered with baicalin prior to cerebral ischemia by capillary electrophoresis-laser-induced fluorescence detection. *Journal of chromatography. B, Analytical technologies in the biomedical and life sciences* **2003,** *788* (1), 93-101.

15. Li, Y. M.; Qu, Y.; Vandenbussche, E.; Arckens, L.; Vandesande, F., Analysis of extracellular gamma-aminobutyric acid, glutamate and aspartate in cat visual cortex by in vivo microdialysis and capillary electrophoresis-laser induced fluorescence detection. *J Neurosci Methods* **2001,** *105* (2), 211-5.

16. Szökő, É.; Tábi, T., Analysis of biological samples by capillary electrophoresis with laser induced fluorescence detection. *J Pharm Biomed Anal* **2010,** *53* (5), 1180-1192.

17. Roth, M., Fluorescence reaction for amino acids. *Anal Chem* **1971,** *43* (7), 880-882.

18. Allison, L. A.; Mayer, G. S.; Shoup, R. E., o-Phthalaldehyde derivatives of amines for high-speed liquid chromatography/electrochemistry. *Anal Chem* **1984,** *56* (7), 1089-96.

19. Joseph, M. H.; Davies, P., Electrochemical activity of o-phthalaldehyde-mercaptoethanol derivatives of amino acids. Application to high-performance liquid chromatographic determination of amino acids in plasma and other biological materials. *Journal of chromatography* **1983,** *277,* 125-36.

20. Boyd, B. W.; Witowski, S. R.; Kennedy, R. T., Trace-level amino acid analysis by capillary liquid chromatography and application to in vivo microdialysis sampling with 10-s temporal resolution. *Anal Chem* **2000,** *72* (4), 865-71.

21. McKenzie, J. A. M.; Watson, C. J.; Rostand, R. D.; German, I.; Witowski, S. R.; Kennedy, R. T., Automated capillary liquid chromatography for simultaneous determination of neuroactive amines and amino acids. *Journal of Chromatography A* **2002,** *962* (1–2), 105-115.

22. Bowser, M. T.; Kennedy, R. T., In vivo monitoring of amine neurotransmitters using microdialysis with on-line capillary electrophoresis. *ELECTROPHORESIS* **2001,** *22* (17), 3668-76.

23. Lada, M. W.; Vickroy, T. W.; Kennedy, R. T., High temporal resolution monitoring of glutamate and aspartate in vivo using microdialysis on-line with capillary electrophoresis with laser-induced fluorescence detection. *Anal Chem* **1997,** *69* (22), 4560-5.

24. Zhou, S. Y.; Zuo, H.; Stobaugh, J. F.; Lunte, C. E.; Lunte, S. M., Continuous in vivo monitoring of amino acid neurotransmitters by microdialysis sampling with on-line derivatization and capillary electrophoresis separation. *Anal Chem* **1995,** *67* (3), 594-9.

25. Chen, H. L.; Zhang, X. J.; Qi, S. D.; Xu, H. X.; Sung, J. J.; Bian, Z. X., Simultaneous determination of glutamate and aspartate in rat periaqueductal gray matter microdialysates by capillary electrophoresis with laser-induced fluorescence. *Journal of chromatography. B, Analytical technologies in the biomedical and life sciences* **2009,** *877* (27), 3248-52.

26. You, Z. B.; Nylander, I.; Herrera-Marschitz, M.; O'Connor, W. T.; Goiny, M.; Terenius, L., The striatonigral dynorphin pathway of the rat studied with In vivo microdialysis—I. Effects of K+-depolarization, lesions and peptidase inhibition. *Neuroscience* **1994,** *63* (2), 415-425.

27. Herrera-Marschitz, M.; You, Z. B.; Goiny, M.; Meana, J. J.; Silveira, R.; Godukhin, O. V.; Chen, Y.; Espinoza, S.; Pettersson, E.; Loidl, C. F.; Lubec, G.; Andersson, K.; Nylander, I.; Terenius, L.; Ungerstedt, U., On the origin of extracellular glutamate levels monitored in the basal ganglia of the rat by in vivo microdialysis. *Journal of neurochemistry* **1996,** *66* (4), 1726-35.

28. Buck, K.; Voehringer, P.; Ferger, B., Rapid analysis of GABA and glutamate in microdialysis samples using high performance liquid chromatography and tandem mass

spectrometry. *J Neurosci Methods* **2009,** *182* (1), 78-84.

29. González, R. R.; Fernández, R. F.; Vidal, J. L. M.; Frenich, A. G.; Pérez, M. L. G., Development and validation of an ultra-high performance liquid chromatography–tandem mass-spectrometry (UHPLC–MS/MS) method for the simultaneous determination of neurotransmitters in rat brain samples. *J Neurosci Methods* **2011,** *198* (2), 187-194.

30. Ji, C.; Li, W.; Ren, X.-d.; El-Kattan, A. F.; Kozak, R.; Fountain, S.; Lepsy, C., Diethylation labeling combined with UPLC/MS/MS for simultaneous determination of a panel of monoamine neurotransmitters in rat prefrontal cortex microdialysates. *Anal Chem* **2008,** *80* (23), 9195-9203.

31. Song, P.; Mabrouk, O. S.; Hershey, N. D.; Kennedy, R. T., In vivo neurochemical monitoring using benzoyl chloride derivatization and liquid chromatography – mass spectrometry. *Analytical chemistry* **2012,** *84* (1), 412-419.

32. Zhang, L.-H.; Cai, H.-L.; Jiang, P.; Li, H.-D.; Cao, L.-J.; Dang, R.-L.; Zhu, W.-Y.; Deng, Y., Simultaneous determination of multiple neurotransmitters and their metabolites in rat brain homogenates and microdialysates by LC-MS/MS. *Analytical Methods* **2015,** *7* (9), 3929-3938.

33. Zhang, X.; Rauch, A.; Lee, H.; Xiao, H.; Rainer, G.; Logothetis, N. K., Capillary hydrophilic interaction chromatography/mass spectrometry for simultaneous determination of multiple neurotransmitters in primate cerebral cortex. *Rapid Communications in Mass Spectrometry* **2007,** *21* (22), 3621-3628.

34. Zheng, X.; Kang, A.; Dai, C.; Liang, Y.; Xie, T.; Xie, L.; Peng, Y.; Wang, G.; Hao, H., Quantitative analysis of neurochemical panel in rat brain and plasma by liquid chromatography–tandem mass spectrometry. *Anal Chem* **2012,** *84* (22), 10044-10051.

35. Song, P.; Hershey, N. D.; Mabrouk, O. S.; Slaney, T. R.; Kennedy, R. T., Mass spectrometry "sensor" for in vivo acetylcholine monitoring. *Anal Chem* **2012,** *84* (11), 4659-4664.

36. Annesley, T. M., Ion suppression in mass spectrometry. *Clinical Chemistry* **2003,** *49* (7), 1041-1044.

37. Uutela, P.; Ketola, R. A.; Piepponen, P.; Kostiainen, R., Comparison of different amino acid derivatives and analysis of rat brain microdialysates by liquid chromatography tandem mass spectrometry. *Analytica Chimica Acta* **2009,** *633* (2), 223-231.

38. Heaton, J.; Gray, N.; Cowan, D. A.; Plumb, R. S.; Legido-Quigley, C.; Smith, N. W., Comparison of reversed-phase and hydrophilic interaction liquid chromatography for

the separation of ephedrines. *Journal of Chromatography A* **2012,** *1228* (0), 329-337.

39. Alpert, A. J., Hydrophilic-interaction chromatography for the separation of peptides, nucleic acids and other polar compounds. *Journal of chromatography* **1990,** *499*, 177-96.

40. Buszewski, B.; Noga, S., Hydrophilic interaction liquid chromatography (HILIC)--a powerful separation technique. *Anal Bioanal Chem* **2012,** *402* (1), 231-47.

41. Zhang, X.; Rauch, A.; Xiao, H.; Rainer, G.; Logothetis, N. K., Mass spectrometry-based neurochemical analysis: perspectives for primate research. *Expert review of proteomics* **2008,** *5* (5), 641-52.

42. Chirita, R.-I.; West, C.; Finaru, A.-L.; Elfakir, C., Approach to hydrophilic interaction chromatography column selection: Application to neurotransmitters analysis. *Journal of Chromatography A* **2010,** *1217* (18), 3091-3104.

43. Danaceau, J. P.; Chambers, E. E.; Fountain, K. J., Hydrophilic interaction chromatography (HILIC) for LC–MS/MS analysis of monoamine neurotransmitters. *Bioanalysis* **2012,** *4* (7), 783-794.

44. Tufi, S.; Lamoree, M.; de Boer, J.; Leonards, P., Simultaneous analysis of multiple neurotransmitters by hydrophilic interaction liquid chromatography coupled to tandem mass spectrometry. *Journal of Chromatography A* **2015,** *1395* (0), 79-87.

45. Bhandare, P.; Madhavan, P.; Rao, B.; Someswar rao, N., Determination of amino acid without derivatization by using HPLC - HILIC column. *J. Chem. Pharm. Res.* **2010,** *2* (2), 372-380.

46. Guo, K.; Ji, C.; Li, L., Stable-isotope dimethylation labeling combined with LC−ESI MS for quantification of amine-containing metabolites in biological samples. *Anal Chem* **2007,** *79* (22), 8631-8638.

47. Song, Y.; Quan, Z.; Evans, J. L.; Byrd, E. A.; Liu, Y.-M., Enhancing capillary liquid chromatography/tandem mass spectrometry of biogenic amines by pre-column derivatization with 7-fluoro-4-nitrobenzoxadiazole. *Rapid Communications in Mass Spectrometry* **2004,** *18* (9), 989-994.

48. Song, Y.; Shenwu, M.; Dhossche, D. M.; Liu, Y.-M., A capillary liquid chromatographic/tandem mass spectrometric method for the quantification of γ-aminobutyric acid in human plasma and cerebrospinal fluid. *Journal of Chromatography B* **2005,** *814* (2), 295-302.

49. Greco, S.; Danysz, W.; Zivkovic, A.; Gross, R.; Stark, H., Microdialysate analysis of monoamine neurotransmitters—A versatile and sensitive LC–MS/MS method. *Analytica Chimica Acta* **2013,** *771*, 65-72.

50. Inagaki, S.; Tano, Y.; Yamakata, Y.; Higashi, T.; Min, J. Z.; Toyo'oka, T., Highly sensitive and positively charged precolumn derivatization reagent for amines and amino acids in liquid chromatography/electrospray ionization tandem mass spectrometry. *Rapid Communications in Mass Spectrometry* **2010,** *24* (9), 1358-1364.

51. Zhang, M.; Fang, C.; Smagin, G., Derivatization for the simultaneous LC/MS quantification of multiple neurotransmitters in extracellular fluid from rat brain microdialysis. *J Pharm Biomed Anal* **2014,** *100*, 357-64.

52. Guo, K.; Li, L., High-performance isotope labeling for profiling carboxylic acid-containing metabolites in biofluids by mass spectrometry. *Anal Chem* **2010,** *82* (21), 8789-8793.

53. Cai, H. L.; Zhu, R. H.; Li, H. D., Determination of dansylated monoamine and amino acid neurotransmitters and their metabolites in human plasma by liquid chromatography-electrospray ionization tandem mass spectrometry. *Analytical biochemistry* **2010,** *396* (1), 103-11.

54. Guo, K.; Li, L., Differential 12C-/13C-isotope dansylation labeling and fast liquid chromatography/mass spectrometry for absolute and relative quantification of the metabolome. *Anal Chem* **2009,** *81* (10), 3919-32.

55. Vander Weele, C. M.; Porter-Stransky, K. A.; Mabrouk, O. S.; Lovic, V.; Singer, B. F.; Kennedy, R. T.; Aragona, B. J., Rapid dopamine transmission within the nucleus accumbens: dramatic difference between morphine and oxycodone delivery. *The European journal of neuroscience* **2014,** *40* (7), 3041-54.

56. Wotjak, C. T.; Landgraf, R.; Engelmann, M., Listening to neuropeptides by microdialysis: Echoes and new sounds? *Pharmacology Biochemistry and Behavior* **2008,** *90* (2), 125-134.

57. Gruber, S. H.; Nomikos, G. G.; Mathe, A. A., d-Amphetamine-induced increase in neurotensin and neuropeptide Y outflow in the ventral striatum is mediated via stimulation of dopamine D1 and D2/3 receptors. *Journal of neuroscience research* **2002,** *69* (1), 133-9.

58. Marinelli, P. W.; Lam, M.; Bai, L.; Quirion, R.; Gianoulakis, C., A microdialysis profile of dynorphin A(1-8) release in the rat nucleus accumbens following alcohol administration. *Alcoholism, clinical and experimental research* **2006,** *30* (6), 982-90.

59. Rocha, L. L.; Evans, C. J.; Maidment, N. T., Amygdala kindling modifies extracellular opioid peptide content in rat hippocampus measured by microdialysis. *Journal of neurochemistry* **1997,** *68* (2), 616-24.

60. Taylor, B. K.; Fu, W.; Kuphal, K. E.; Stiller, C. O.; Winter, M. K.; Chen, W.; Corder, G. F.; Urban, J. H.; McCarson, K. E.; Marvizon, J. C., Inflammation enhances Y1 receptor signaling, neuropeptide Y-mediated inhibition of hyperalgesia, and substance P release from primary afferent neurons. *Neuroscience* **2014,** *256* (0), 178-194.

61. Andren, P. E.; Caprioli, R. M., Determination of extracellular release of neurotensin in discrete rat brain regions utilizing in vivo microdialysis/electrospray mass spectrometry. *Brain research* **1999,** *845* (2), 123-9.

62. Behrens, H. L.; Chen, R.; Li, L., Combining microdialysis, nanoLC-MS, and MALDI-TOF/TOF to detect neuropeptides secreted in the crab, cancer borealis. *Anal Chem* **2008,** *80* (18), 6949-6958.

63. Emmett, M. R.; Caprioli, R. M., Micro-electrospray mass spectrometry: ultra-high-sensitivity analysis of peptides and proteins. *Journal of the American Society for Mass Spectrometry* **1994,** *5* (7), 605-13.

64. Fu, Q.; Li, L., De novo sequencing of neuropeptides using reductive isotopic methylation and investigation of ESI QTOF MS/MS fragmentation pattern of neuropeptides with N-terminal dimethylation. *Anal Chem* **2005,** *77* (23), 7783-7795.

65. Haskins, W. E.; Wang, Z.; Watson, C. J.; Rostand, R. R.; Witowski, S. R.; Powell, D. H.; Kennedy, R. T., Capillary LC-MS2 at the attomole level for monitoring and discovering endogenous peptides in microdialysis samples collected in vivo. *Anal Chem* **2001,** *73* (21), 5005-14.

66. Lanckmans, K.; Stragier, B.; Sarre, S.; Smolders, I.; Michotte, Y., Nano-LC-MS/MS for the monitoring of angiotensin IV in rat brain microdialysates: limitations and possibilities. *Journal of separation science* **2007,** *30* (14), 2217-24.

67. Li, Q.; Zubieta, J. K.; Kennedy, R. T., Practical aspects of in vivo detection of neuropeptides by microdialysis coupled off-line to capillary LC with multistage MS. *Anal Chem* **2009,** *81* (6), 2242-50.

68. Mabrouk, O. S.; Kennedy, R. T., Simultaneous oxytocin and arg-vasopressin measurements in microdialysates using capillary liquid chromatography-mass spectrometry. *J Neurosci Methods* **2012,** *209* (1), 127-33.

69. Maes, K.; Bechade, G.; Van Schoors, J.; Van Wanseele, Y.; Van Liefferinge, J.; Michotte, Y.; Harden, S. N.; Chambers, E. E.; Claereboudt, J.; Smolders, I.; Van Eeckhaut, A., An ultrasensitive nano UHPLC-ESI-MS/MS method for the quantification of three neuromedin-like peptides in microdialysates. *Bioanalysis* **2015,** *7* (5), 605-19.

70. Patterson, C. M.; Wong, J. M.; Leinninger, G. M.; Allison, M. B.; Mabrouk, O. S.; Kasper, C. L.; Gonzalez, I. E.; Mackenzie, A.; Jones, J. C.; Kennedy, R. T.; Myers, M. G., Jr., Ventral tegmental area neurotensin signaling links the lateral hypothalamus to

locomotor activity and striatal dopamine efflux in male mice. *Endocrinology* **2015,** *156* (5), 1692-700.

71. Van Eeckhaut, A.; Maes, K.; Aourz, N.; Smolders, I.; Michotte, Y., The absolute quantification of endogenous levels of brain neuropeptides in vivo using LC-MS/MS. *Bioanalysis* **2011,** *3* (11), 1271-85.

72. van Midwoud, P. M.; Rieux, L.; Bischoff, R.; Verpoorte, E.; Niederlander, H. A., Improvement of recovery and repeatability in liquid chromatography-mass spectrometry analysis of peptides. *Journal of proteome research* **2007,** *6* (2), 781-91.

73. Zhou, Y.; Mabrouk, O. S.; Kennedy, R. T., Rapid preconcentration for liquid chromatography-mass spectrometry assay of trace level neuropeptides. *Journal of the American Society for Mass Spectrometry* **2013,** *24* (11), 1700-9.

74. DiFeliceantonio, A. G.; Mabrouk, O. S.; Kennedy, R. T.; Berridge, K. C., Enkephalin surges in dorsal neostriatum as a signal to eat. *Current Biology* **2012,** *22* (20), 1918-1924.

75. Zhou, Y.; Wong, J.-M. T.; Mabrouk, O. S.; Kennedy, R. T., Reducing adsorption to improve recovery and in vivo detection of neuropeptides by microdialysis with LC-MS. *Analytical chemistry* **2015,** *87* (19), 9802-9809.

76. Fricker, L. D., Neuropeptide-processing enzymes: applications for drug discovery. *The AAPS journal* **2005,** *7* (2), E449-E455.

77. Fugère, M.; Day, R., Cutting back on pro-protein convertases: the latest approaches to pharmacological inhibition. *Trends in Pharmacological Sciences* **2005,** *26* (6), 294-301.

78. Tegge, A. N.; Southey, B. R.; Sweedler, J. V.; Rodriguez-Zas, S. L., Comparative analysis of neuropeptide cleavage sites in human, mouse, rat, and cattle. *Mammalian Genome* **2008,** *19* (2), 106-120.

79. Sossin, W. S.; Fisher, J. M.; Scheller, R. H., Cellular and molecular biology of neuropeptide processing and packaging. **1989**.

80. Kitabgi, P., Neurotensin and neuromedin N are differentially processed from a common precursor by prohormone convertases in tissues and cell lines. *Results and problems in cell differentiation* **2010,** *50*, 85-96.

81. Ross, H. E.; Young, L. J., Oxytocin and the neural mechanisms regulating social cognition and affiliative behavior. *Frontiers in neuroendocrinology* **2009,** *30* (4), 534-47.

82. Koneru, A.; Satyanarayana, S.; Rizwan, S., Endogenous opioids: their physiological role and receptors. *Global J Pharmacol* **2009,** *3* (3), 149-153.

83. Okuda-Ashitaka, E.; Ito, S., Nocistatin: a novel neuropeptide encoded by the gene for the nociceptin/orphanin FQ precursor. *Peptides* **2000,** *21* (7), 1101-9.

84. Mollereau, C.; Simons, M. J.; Soularue, P.; Liners, F.; Vassart, G.; Meunier, J. C.; Parmentier, M., Structure, tissue distribution, and chromosomal localization of the prepronociceptin gene. *Proceedings of the National Academy of Sciences of the United States of America* **1996,** *93* (16), 8666-70.

85. Day, R.; Lazure, C.; Basak, A.; Boudreault, A.; Limperis, P.; Dong, W.; Lindberg, I., Prodynorphin processing by proprotein convertase 2. Cleavage at single basic residues and enhanced processing in the presence of carboxypeptidase activity. *The Journal of biological chemistry* **1998,** *273* (2), 829-36.

86. Day, R.; Trujillo, K.; Akil, H., Prodynorphin biosynthesis and posttranslational processing. In *Opioids*, Springer: 1993; pp 449-470.

87. Comb, M.; Seeburg, P. H.; Adelman, J.; Eiden, L.; Herbert, E., Primary structure of the human Met- and Leu-enkephalin precursor and its mRNA. *Nature* **1982,** *295* (5851), 663-6.

88. Zamir, N.; Palkovits, M.; Weber, E.; Mezey, E.; Brownstein, M. J., A dynorphinergic pathway of Leu-enkephalin production in rat substantia nigra. *Nature* **1984,** *307* (5952), 643-5.

89. Khachaturian, H.; Sherman, T. G.; Lloyd, R. V.; Civelli, O.; Douglass, J.; Herbert, E.; Akil, H.; Watson, S. J., Pro-dynorphin is endogenous to the anterior pituitary and is co-localized with LH and FSH in the gonadotrophs. *Endocrinology* **1986,** *119* (3), 1409-11.

90. Al-Hasani, R.; Bruchas, M. R., Molecular mechanisms of opioid receptor-dependent signaling and behavior. *Anesthesiology* **2011,** *115* (6), 1363-81.

91. Klintenberg, R.; Andren, P. E., Altered extracellular striatal in vivo biotransformation of the opioid neuropeptide dynorphin A(1-17) in the unilateral 6-OHDA rat model of Parkinson's disease. *Journal of mass spectrometry : JMS* **2005,** *40* (2), 261-70.

92. Ljungdahl, A.; Hanrieder, J.; Falth, M.; Bergquist, J.; Andersson, M., Imaging mass spectrometry reveals elevated nigral levels of dynorphin neuropeptides in L-DOPA-induced dyskinesia in rat model of Parkinson's disease. *PloS one* **2011,** *6* (9), e25653.

93. Zamir, N.; Skofitsch, G.; Bannon, M. J.; Helke, C. J.; Kopin, I. J.; Jacobowitz, D. M., Primate model of Parkinson's disease: alterations in multiple opioid systems in the basal ganglia. *Brain research* **1984,** *322* (2), 356-60.

94. Mabrouk, O. S.; Li, Q.; Song, P.; Kennedy, R. T., Microdialysis and mass spectrometric monitoring of dopamine and enkephalins in the globus pallidus reveal reciprocal interactions that regulate movement. *Journal of neurochemistry* **2011,** *118* (1), 24-33.

95. Bernay, B.; Gaillard, M. C.; Guryca, V.; Emadali, A.; Kuhn, L.; Bertrand, A.; Detraz, I.; Carcenac, C.; Savasta, M.; Brouillet, E.; Garin, J.; Elalouf, J. M., Discovering new bioactive neuropeptides in the striatum secretome using in vivo microdialysis and versatile proteomics. *Molecular & cellular proteomics : MCP* **2009,** *8* (5), 946-58.

96. Baseski, H. M.; Watson, C. J.; Cellar, N. A.; Shackman, J. G.; Kennedy, R. T., Capillary liquid chromatography with MS3 for the determination of enkephalins in microdialysis samples from the striatum of anesthetized and freely-moving rats. *Journal of mass spectrometry : JMS* **2005,** *40* (2), 146-53.

97. Hou, X.; Xie, F.; Sweedler, J. V., Relative quantitation of neuropeptides over a thousand-fold concentration range. *Journal of the American Society for Mass Spectrometry* **2012,** *23* (12), 2083-93.

98. Schmerberg, C. M.; Li, L., Mass spectrometric detection of neuropeptides using affinity-enhanced microdialysis with antibody-coated magnetic nanoparticles. *Anal Chem* **2013,** *85* (2), 915-22.

99. Husson, S. J.; Clynen, E.; Baggerman, G.; De Loof, A.; Schoofs, L., Discovering neuropeptides in Caenorhabditis elegans by two dimensional liquid chromatography and mass spectrometry. *Biochemical and biophysical research communications* **2005,** *335* (1), 76-86.

100. Jensen, S. M.; Hansen, H. S.; Johansen, T.; Malmlöf, K., In vivo and in vitro microdialysis sampling of free fatty acids. *J Pharm Biomed Anal* **2007,** *43* (5), 1751-1756.

101. Takeda, S.; Sato, N.; Ikimura, K.; Nishino, H.; Rakugi, H.; Morishita, R., Novel microdialysis method to assess neuropeptides and large molecules in free-moving mouse. *Neuroscience* **2011,** *186*, 110-9.

102. Herbaugh, A. W.; Stenken, J. A., Antibody-enhanced microdialysis collection of CCL2 from rat brain. *J Neurosci Methods* **2011,** *202* (2), 124-7.

103. Pettersson, A.; Amirkhani, A.; Arvidsson, B.; Markides, K.; Bergquist, J., A feasibility study of solid supported enhanced microdialysis. *Anal Chem* **2004,** *76* (6), 1678-82.

104. Pettersson, A.; Markides, K.; Bergquist, J., Enhanced microdialysis of neuropeptides. *Acta biochimica Polonica* **2001,** *48* (4), 1117-20.

105. Silva, A. I.; de Matos, A. N.; Brons, I. G.; Mateus, M., An overview on the development of a bio-artificial pancreas as a treatment of insulin-dependent diabetes mellitus. *Medicinal research reviews* **2006,** *26* (2), 181-222.

106. Maes, K.; Van Liefferinge, J.; Viaene, J.; Van Schoors, J.; Van Wanseele, Y.; Béchade, G.; Chambers, E. E.; Morren, H.; Michotte, Y.; Vander Heyden, Y.; Claereboudt, J.; Smolders, I.; Van Eeckhaut, A., Improved sensitivity of the nano ultra-high performance liquid chromatography-tandem mass spectrometric analysis of low-concentrated neuropeptides by reducing aspecific adsorption and optimizing the injection solvent. *Journal of Chromatography A* **2014,** *1360* (0), 217-228.

107. Grohganz, H.; Rischer, M.; Brandl, M., Adsorption of the decapeptide Cetrorelix depends both on the composition of dissolution medium and the type of solid surface. *European Journal of Pharmaceutical Sciences* **2004,** *21* (2–3), 191-196.

108. Hyenstrand, P.; Metcalf, J. S.; Beattie, K. A.; Codd, G. A., Losses of the cyanobacterial toxin microcystin-LR from aqueous solution by adsorption during laboratory manipulations. *Toxicon : official journal of the International Society on Toxinology* **2001,** *39* (4), 589-94.

109. Rada, P. V.; Páez, X.; Hernández, L. F.; Avena, N. M.; Hoebel, B. G., Chapter 4.3 Microdialysis in the study of behavior reinforcement and inhibition. In *Handbook of Behavioral Neuroscience*, Ben, H. C. W.; Thomas, I. F. H. C., Eds. Elsevier: 2006; Vol. Volume 16, pp 351-375.

110. Armbruster, B. N.; Li, X.; Pausch, M. H.; Herlitze, S.; Roth, B. L., Evolving the lock to fit the key to create a family of G protein-coupled receptors potently activated by an inert ligand. *Proceedings of the National Academy of Sciences of the United States of America* **2007,** *104* (12), 5163-8.

111. Deisseroth, K., Optogenetics. *Nat Meth* **2011,** *8* (1), 26-29.

112. Nair, S. G.; Strand, N. S.; Neumaier, J. F., DREADDing the lateral habenula: a review of methodological approaches for studying lateral habenula function. *Brain research* **2013,** *1511*, 93-101.

113. Freeze, B. S.; Kravitz, A. V.; Hammack, N.; Berke, J. D.; Kreitzer, A. C., Control of basal ganglia output by direct and indirect pathway projection neurons. *The Journal of neuroscience : the official journal of the Society for Neuroscience* **2013,** *33* (47), 18531-9.

114. Ahmari, S. E.; Spellman, T.; Douglass, N. L.; Kheirbek, M. A.; Simpson, H. B.; Deisseroth, K.; Gordon, J. A.; Hen, R., Repeated cortico-striatal stimulation generates persistent OCD-like behavior. *Science (New York, N.Y.)* **2013,** *340* (6137), 1234-9.

115. Chen, B. T.; Yau, H. J.; Hatch, C.; Kusumoto-Yoshida, I.; Cho, S. L.; Hopf, F. W.; Bonci, A., Rescuing cocaine-induced prefrontal cortex hypoactivity prevents compulsive cocaine seeking. *Nature* **2013,** *496* (7445), 359-62.

116. Urban, D. J.; Roth, B. L., DREADDs (designer receptors exclusively activated by designer drugs): chemogenetic tools with therapeutic utility. *Annual review of pharmacology and toxicology* **2015,** *55*, 399-417.

117. Bock, R.; Shin, J. H.; Kaplan, A. R.; Dobi, A.; Markey, E.; Kramer, P. F.; Gremel, C. M.; Christensen, C. H.; Adrover, M. F.; Alvarez, V. A., Strengthening the accumbal indirect pathway promotes resilience to compulsive cocaine use. *Nature neuroscience* **2013,** *16* (5), 632-638.

118. Sasaki, K.; Suzuki, M.; Mieda, M.; Tsujino, N.; Roth, B.; Sakurai, T., Pharmacogenetic modulation of orexin neurons alters sleep/wakefulness states in mice. *PloS one* **2011,** *6* (5), e20360.

119. Anikeeva, P.; Andalman, A. S.; Witten, I.; Warden, M.; Goshen, I.; Grosenick, L.; Gunaydin, L. A.; Frank, L. M.; Deisseroth, K., Optetrode: a multichannel readout for optogenetic control in freely moving mice. *Nat Neurosci* **2012,** *15* (1), 163-70.

120. Michaelides, M.; Anderson, S. A.; Ananth, M.; Smirnov, D.; Thanos, P. K.; Neumaier, J. F.; Wang, G. J.; Volkow, N. D.; Hurd, Y. L., Whole-brain circuit dissection in free-moving animals reveals cell-specific mesocorticolimbic networks. *The Journal of clinical investigation* **2013,** *123* (12), 5342-50.

121. Royer, S.; Zemelman, B. V.; Barbic, M.; Losonczy, A.; Buzsaki, G.; Magee, J. C., Multi-array silicon probes with integrated optical fibers: light-assisted perturbation and recording of local neural circuits in the behaving animal. *The European journal of neuroscience* **2010,** *31* (12), 2279-91.

122. Taylor, H.; Schmiedt, J. T.; Carcak, N.; Onat, F.; Di Giovanni, G.; Lambert, R.; Leresche, N.; Crunelli, V.; David, F., Investigating local and long-range neuronal network dynamics by simultaneous optogenetics, reverse microdialysis and silicon probe recordings in vivo. *J Neurosci Methods* **2014,** *235*, 83-91.

123. Parrot, S.; Denoroy, L.; Renaud, B.; Benetollo, C., Why optogenetics needs in vivo neurochemistry. *ACS chemical neuroscience* **2015**.

124. Quiroz, C.; Orru, M.; Rea, W.; Ciudad-Roberts, A.; Yepes, G.; Britt, J. P.; Ferre, S., Local control of extracellular dopamine levels in the medial nucleus accumbens by a glutamatergic projection from the infralimbic cortex. *The Journal of neuroscience : the official journal of the Society for Neuroscience* **2016,** *36* (3), 851-9.

125. Bass, C. E.; Grinevich, V. P.; Gioia, D.; Day-Brown, J. D.; Bonin, K. D.; Stuber, G. D.; Weiner, J. L.; Budygin, E. A., Optogenetic stimulation of VTA dopamine neurons

reveals that tonic but not phasic patterns of dopamine transmission reduce ethanol self-administration. *Frontiers in Behavioral Neuroscience* **2013,** *7*, 173.

126. Carter, M. E.; Yizhar, O.; Chikahisa, S.; Nguyen, H.; Adamantidis, A.; Nishino, S.; Deisseroth, K.; de Lecea, L., Tuning arousal with optogenetic modulation of locus coeruleus neurons. *Nat Neurosci* **2010,** *13* (12), 1526-1533.

127. Miyazaki, Kayoko W.; Miyazaki, K.; Tanaka, Kenji F.; Yamanaka, A.; Takahashi, A.; Tabuchi, S.; Doya, K., Optogenetic activation of dorsal raphe serotonin neurons enhances patience for future rewards. *Current Biology* **2014,** *24* (17), 2033-2040.

128. Wong, J. M.; Malec, P. A.; Mabrouk, O. S.; Ro, J.; Dus, M.; Kennedy, R. T., Benzoyl chloride derivatization with liquid chromatography-mass spectrometry for targeted metabolomics of neurochemicals in biological samples. *Journal of chromatography. A* **2016,** *1446*, 78-90.

129. Knee, J. M.; Rzezniczak, T. Z.; Barsch, A.; Guo, K. Z.; Merritt, T. J. S., A novel ion pairing LC/MS metabolomics protocol for study of a variety of biologically relevant polar metabolites. *Journal of Chromatography B* **2013,** *936*, 63-73.

130. Michopoulos, F.; Whalley, N.; Theodoridis, G.; Wilson, I. D.; Dunkley, T. P. J.; Critchlow, S. E., Targeted profiling of polar intracellular metabolites using ion-pair-high performance liquid chromatography and -ultra high performance liquid chromatography coupled to tandem mass spectrometry: Applications to serum, urine and tissue extracts. *Journal of Chromatography A* **2014,** *1349*, 60-68.

131. Virgiliou, C.; Sampsonidis, I.; Gika, H. G.; Raikos, N.; Theodoridis, G. A., Development and validation of a HILIC-MS/MS multitargeted method for metabolomics applications. *ELECTROPHORESIS* **2015,** *36* (18), 2215-2225.

132. Wei, R.; Li, G.; Seymour, A. B., High-throughput and multiplexed LC/MS/MRM method for targeted metabolomics. *Analytical chemistry* **2010,** *82* (13), 5527-5533.

133. Yan, Z.; Yan, R., Increase the accessibility and scale of targeted metabolomics: Construction of a human urinary metabolome-wide multiple reaction monitoring library using directly-coupled reversed-phase and hydrophilic interaction chromatography. *Analytica Chimica Acta* **2015,** *894*, 65-75.

134. Yuan, M.; Breitkopf, S. B.; Yang, X.; Asara, J. M., A positive/negative ion-switching, targeted mass spectrometry-based metabolomics platform for bodily fluids, cells, and fresh and fixed tissue. *Nature protocols* **2012,** *7* (5), 872-81.

135. Dettmer, K.; Aronov, P. A.; Hammock, B. D., Mass spectrometry-based metabolomics. *Mass spectrometry reviews* **2007,** *26* (1), 51-78.

136. Gummer, J.; Banazis, M.; Maker, G.; Solomon, P.; Oliver, R.; Trengove, R., Use of mass spectrometry for metabolite profiling and metabolomics. *Australian Biochemist* **2009,** *40* (3), 5-8.

137. Cox, J. M.; Butler, J. P.; Lutzke, B. S.; Jones, B. A.; Buckholz, J. E.; Biondolillo, R.; Talbot, J. A.; Chernet, E.; Svensson, K. A.; Ackermann, B. L., A validated LC-MS/MS method for neurotransmitter metabolite analysis in human cerebrospinal fluid using benzoyl chloride derivatization. *Bioanalysis* **2015,** *7* (19), 2461-75.

138. Aflaki, F.; Ghoulipour, V.; Saemian, N.; Salahinejad, M., A simple method for benzoyl chloride derivatization of biogenic amines for high performance liquid chromatography. *Analytical Methods* **2014,** *6* (5), 1482-1487.

139. Özdestan, Ö.; Üren, A., A method for benzoyl chloride derivatization of biogenic amines for high performance liquid chromatography. *Talanta* **2009,** *78* (4–5), 1321-1326.

140. Asan, A.; Isildak, I., Determination of major phenolic compounds in water by reversed-phase liquid chromatography after pre-column derivatization with benzoyl chloride. *Journal of Chromatography A* **2003,** *988* (1), 145-149.

141. Gao, S.; Wilson, D. M.; Edinboro, L. E.; McGuire, G. M.; Williams, S. G.; Thomas Karnes, H., Improvement of sensitivity for the determination of propylene glycol in rat plasma and lung tissue using HPLC/tandem MS and derivatization with benzoyl chloride. *Journal of liquid chromatography & related technologies* **2003,** *26* (20), 3413-3431.

142. Dai, W.; Huang, Q.; Yin, P.; Li, J.; Zhou, J.; Kong, H.; Zhao, C.; Lu, X.; Xu, G., Comprehensive and highly sensitive urinary steroid hormone profiling method based on stable isotope-labeling liquid chromatography–mass spectrometry. *Analytical chemistry* **2012,** *84* (23), 10245-10251.

143. Chirita-Tampu, R.-I.; Fougere, L.; West, C., Advantages of HILIC mobile phases for LC–ESI–MS–MS analysis of neurotransmitters. *LCGC Europe* **2013,** *26* (3).

144. Starke, K.; Hedler, L.; Steppeler, A., Metabolism of endogenous and exogenous noradrenaline in guinea-pig atria. *Naunyn Schmiedebergs Arch Pharmacol* **1981,** *317* (3), 193-8.

145. Furukawa, N.; Arai, N.; Goshima, Y.; Miyamae, T.; Ohshima, E.; Suzuki, F.; Fujita, K.; Misu, Y., Endogenously released DOPA is a causal factor for glutamate release and resultant delayed neuronal cell death by transient ischemia in rat striata. *Journal of neurochemistry* **2001,** *76* (3), 815-24.

146. Elsworth, J. D.; Roth, R. H.; Redmond, D. E., Jr., Relative importance of 3-methoxy-4-hydroxyphenylglycol and 3,4-dihydroxyphenylglycol as norepinephrine metabolites in rat, monkey, and humans. *Journal of neurochemistry* **1983,** *41* (3), 786-93.

147. Cannazza, G.; Baraldi, M.; Braghiroli, D.; Tait, A.; Parenti, C., High-performance liquid chromatographic method for the quantification of anthranilic and 3-hydroxyanthranilic acid in rat brain dialysate. *J Pharm Biomed Anal* **2003,** *32* (2), 287-93.

148. Notarangelo, F. M.; Wu, H. Q.; Macherone, A.; Graham, D. R.; Schwarcz, R., Gas chromatography/tandem mass spectrometry detection of extracellular kynurenine and related metabolites in normal and lesioned rat brain. *Analytical biochemistry* **2012,** *421* (2), 573-81.

149. Fuller, R. W.; Snoddy, H. D.; Marshall, W. S., Lowering of rat brain 3-methoxy-4-hydroxyphenylethylene glycol sulphate (MOPEG sulphate) concentration by 2,6-dichlorobenzylidene aminoguanidine. *The Journal of pharmacy and pharmacology* **1977,** *29* (6), 375-6.

150. Hashiguti, H.; Nakahara, D.; Maruyama, W.; Naoi, M.; Ikeda, T., Simultaneous determination of in vivo hydroxylation of tyrosine and tryptophan in rat striatum by microdialysis-HPLC: relationship between dopamine and serotonin biosynthesis. *Journal of neural transmission. General section* **1993,** *93* (3), 213-23.

151. Beck, O.; Borg, S.; Jonsson, G.; Lundman, A.; Valverius, P., Measurement of 5-hydroxytryptophol and 5-hydroxyindoleacetic acid in human and rat brain and plasma. *Journal of neural transmission* **1984,** *59* (1), 57-67.

152. Piletz, J. E.; Aricioglu, F.; Cheng, J. T.; Fairbanks, C. A.; Gilad, V. H.; Haenisch, B.; Halaris, A.; Hong, S.; Lee, J. E.; Li, J.; Liu, P.; Molderings, G. J.; Rodrigues, A. L.; Satriano, J.; Seong, G. J.; Wilcox, G.; Wu, N.; Gilad, G. M., Agmatine: clinical applications after 100 years in translation. *Drug discovery today* **2013,** *18* (17-18), 880-93.

153. Benveniste, H.; Drejer, J.; Schousboe, A.; Diemer, N. H., Elevation of the extracellular concentrations of glutamate and aspartate in rat hippocampus during transient cerebral ischemia monitored by intracerebral microdialysis. *Journal of neurochemistry* **1984,** *43* (5), 1369-74.

154. Funatsu, S.; Kondoh, T.; Kawase, T.; Ikeda, H.; Nagasawa, M.; Denbow, D. M.; Furuse, M., Long-term consumption of dried bonito dashi (a traditional Japanese fish stock) reduces anxiety and modifies central amino acid levels in rats. *Nutritional neuroscience* **2015,** *18* (6), 256-64.

155. Heinzen, E. L.; Pollack, G. M., Pharmacokinetics and pharmacodynamics of L-arginine in rats: a model of stimulated neuronal nitric oxide synthesis. *Brain research* **2003,** *989* (1), 67-75.

156. Qureshi, A. I.; Ali, Z.; Suri, M. F.; Shuaib, A.; Baker, G.; Todd, K.; Guterman, L. R.; Hopkins, L. N., Extracellular glutamate and other amino acids in experimental

intracerebral hemorrhage: an in vivo microdialysis study. *Critical care medicine* **2003,** *31* (5), 1482-9.

157. Anderzhanova, E.; Rayevsky, K. S.; Saransaari, P.; Riitamaa, E.; Oja, S. S., Effects of sydnocarb and D-amphetamine on the extracellular levels of amino acids in the rat caudate-putamen. *European journal of pharmacology* **2001,** *428* (1), 87-95.

158. Dross, K.; Kewitz, H., Concentration and origin of choline in the rat brain. *Naunyn Schmiedebergs Arch Pharmacol* **1972,** *274* (1), 91-106.

159. Saulskaya, N. B.; Fofonova, N. V.; Sudorgina, P. V., Activation of the NO-ergic system of the nucleus accumbens on presentation of contextual danger signals. *Neuroscience and behavioral physiology* **2010,** *40* (8), 907-12.

160. Ida, S.; Kuriyama, K., Simultaneous determination of cysteine sulfinic acid and cysteic acid in rat brain by high-performance liquid chromatography. *Analytical biochemistry* **1983,** *130* (1), 95-101.

161. Lada, M. W.; Kennedy, R. T., In vivo monitoring of glutathione and cysteine in rat caudate nucleus using microdialysis on-line with capillary zone electrophoresis-laser induced fluorescence detection. *J Neurosci Methods* **1997,** *72* (2), 153-9.

162. Mu, C.; Zhang, Q.; Wu, D.; Zhang, Y.; Zhang, Q., Simultaneous quantification of catecholamines in rat brain by high-performance liquid chromatography with on-line gold nanoparticle-catalyzed luminol chemiluminescence detection. *Biomedical Chromatography* **2015,** *29* (1), 148-155.

163. Hagberg, H.; Lehmann, A.; Sandberg, M.; Nystrom, B.; Jacobson, I.; Hamberger, A., Ischemia-induced shift of inhibitory and excitatory amino acids from intra- to extracellular compartments. *Journal of cerebral blood flow and metabolism : official journal of the International Society of Cerebral Blood Flow and Metabolism* **1985,** *5* (3), 413-9.

164. Silver, I. A.; Erecinska, M., Extracellular glucose concentration in mammalian brain: continuous monitoring of changes during increased neuronal activity and upon limitation in oxygen supply in normo-, hypo-, and hyperglycemic animals. *The Journal of neuroscience : the official journal of the Society for Neuroscience* **1994,** *14* (8), 5068-76.

165. Weinreich, D.; Weinreich, C. A., Endogenous levels of histidine in histamine-containing neurons and other identified nerve cells of Aplysia californica. *Comparative biochemistry and physiology. C: Comparative pharmacology* **1977,** *56* (1), 1-4.

166. Do, K. Q.; Mattenberger, M.; Streit, P.; Cuenod, M., In vitro release of endogenous excitatory sulfur-containing amino acids from various rat brain regions. *Journal of neurochemistry* **1986,** *46* (3), 779-86.

167. Ueland, P. M.; Helland, S.; Broch, O. J.; Schanche, J. S., Homocysteine in tissues of the mouse and rat. *The Journal of biological chemistry* **1984,** *259* (4), 2360-4.

168. Donabedian, H., Quorum sensing and its relevance to infectious diseases. *Journal of Infection* **2003,** *46* (4), 207-214.

169. Fontana, M.; Pecci, L.; Duprè, S.; Cavallini, D., Antioxidant Properties of Sulfinates: Protective Effect of Hypotaurine on Peroxynitrite-Dependent Damage. *Neurochemical Research* **2004,** *29* (1), 111-116.

170. Speciale, C.; Wu, H. Q.; Gramsbergen, J. B.; Turski, W. A.; Ungerstedt, U.; Schwarcz, R., Determination of extracellular kynurenic acid in the striatum of unanesthetized rats: effect of aminooxyacetic acid. *Neuroscience letters* **1990,** *116* (1-2), 198-203.

171. Kai, M.; Nakashima, A.; Ohkura, Y., High-performance liquid chromatographic separation of kyotorphin, a basic Tyr-Arg dipeptide, in rat brain tissue and quantification using fluorimetric detection. *Journal of chromatography. B, Biomedical sciences and applications* **1997,** *688* (2), 205-12.

172. Richards, D. A.; Silva, M. A.; Murphy, N.; Wigmore, S. J.; Mirza, D. F., Extracellular amino acid levels in the human liver during transplantation: a microdialysis study from donor to recipient. *Amino acids* **2007,** *33* (3), 429-37.

173. Fernandez, A. I.; Cantabrana, B.; Sanchez, M.; Hidalgo, A., Extracellular and intracellular effects of polyamines on smooth muscle contractions. *Life sciences* **1995,** *57* (9), 855-61.

174. Sakurai, E.; Monura, A.; Yamakami, J.; Hikichi, N., In-vivo microdialysis measurement of 5-hydroxytryptamine and its metabolites, 5-hydroxyindoleacetic acid and N-acetyl 5-hydroxytryptamine, in rat blood: effects of histamine-receptor antagonists. *The Journal of pharmacy and pharmacology* **1996,** *48* (9), 911-3.

175. Roeder, T., Octopamine in invertebrates. *Prog Neurobiol* **1999,** *59* (5), 533-61.

176. Berry, M. D., Mammalian central nervous system trace amines. Pharmacologic amphetamines, physiologic neuromodulators. *Journal of Neurochemistry* **2004,** *90* (2), 257-271.

177. Abhilash, M.; Alex, M.; Mathews, V. V.; Nair, R. H., Chronic effect of aspartame on ionic homeostasis and monoamine neurotransmitters in the rat brain. *International journal of toxicology* **2014**, 1091581814537087.

178. Vivo, M.; Camon, L.; de Vera, N.; Martinez, E., Extracellular putrescine content after acute excitotoxic brain damage in the rat. *Neuroscience letters* **2002,** *330* (1), 74-8.

179. D'Andrea, G.; Terrazzino, S.; Fortin, D.; Cocco, P.; Balbi, T.; Leon, A., Elusive amines and primary headaches: historical background and prospectives. *Neurological sciences : official journal of the Italian Neurological Society and of the Italian Society of Clinical Neurophysiology* **2003,** *24 Suppl 2*, S65-7.

180. Goldstein, D. S.; Eisenhofer, G.; Kopin, I. J., Sources and significance of plasma levels of catechols and their metabolites in humans. *The Journal of pharmacology and experimental therapeutics* **2003,** *305* (3), 800-11.

181. Wardlaw, S. L.; Burant, C. F.; Klein, S.; Meece, K.; White, A.; Kasten, T.; Lucey, B. P.; Bateman, R. J., Continuous 24-hour leptin, proopiomelanocortin, and amino acid measurements in human cerebrospinal fluid: correlations with plasma leptin, soluble leptin receptor, and amino acid levels. *The Journal of clinical endocrinology and metabolism* **2014,** *99* (7), 2540-8.

182. Jiang, L.; He, L.; Fountoulakis, M., Comparison of protein precipitation methods for sample preparation prior to proteomic analysis. *Journal of Chromatography A* **2004,** *1023* (2), 317-320.

183. Park, S.; Alfa, R. W.; Topper, S. M.; Kim, G. E. S.; Kockel, L.; Kim, S. K., A genetic strategy to measure circulating drosophila insulin reveals genes regulating insulin production and secretion. *PLoS Genet* **2014,** *10* (8), e1004555.

184. Novotny, M.; Alasandro, M.; Konishi, M., Microcolumn liquid chromatography of benzoyl derivatives of steroid metabolites. *Anal Chem* **1983,** *55* (14), 2375-7.

185. Redmond, J. W.; Tseng, A., High-pressure liquid chromatographic determination of putrescine, cadaverine, spermidine and spermine. *Journal of Chromatography A* **1979,** *170* (2), 479-481.

186. Higa, S.; Suzuki, T.; Hayashi, A.; Tsuge, I.; Yamamura, Y., Isolation of catecholamines in biological fluids by boric acid gel. *Analytical biochemistry* **1977,** *77* (1), 18-24.

187. Wuts, P. G.; Greene, T. W., *Greene's protective groups in organic synthesis*. John Wiley & Sons: 2006.

188. Scheline, R. R., A rapid synthesis of 3-o-methylgallic acid. *Acta Chemica Scandinavica* **1966,** *20* (4).

189. Hillemann, H., Beiträge zur kenntnis des phenazins, I. mitteil.: Über die einwirkung von dimethylsulfat auf phenazin. 1-methoxy-phenazin und 1-oxy-phenazin. *Berichte der deutschen chemischen Gesellschaft (A and B Series)* **1938,** *71* (1), 34-41.

190. El-Kholy, S.; Stephano, F.; Li, Y.; Bhandari, A.; Fink, C.; Roeder, T., Expression analysis of octopamine and tyramine receptors in Drosophila. *Cell Tissue Res* **2015,** *361* (3), 669-684.

191. Evans, P.; Maqueira, B., Insect octopamine receptors: a new classification scheme based on studies of cloned Drosophila G-protein coupled receptors. *Invert Neurosci* **2005,** *5* (3-4), 111-118.

192. Livingstone, M. S.; Tempel, B. L., Genetic dissection of monoamine neurotransmitter synthesis in Drosophila. *Nature* **1983,** *303* (5912), 67-70.

193. Monastirioti, M.; Linn, C. E., Jr.; White, K., Characterization of drosophila tyramine beta-hydroxylase gene and isolation of mutant flies lacking octopamine. *The Journal of neuroscience : the official journal of the Society for Neuroscience* **1996,** *16* (12), 3900-11.

194. Zucchi, R.; Chiellini, G.; Scanlan, T. S.; Grandy, D. K., Trace amine-associated receptors and their ligands. *British Journal of Pharmacology* **2006,** *149* (8), 967-978.

195. Evans, P. H.; Michael Fox, P., Enzymatic N-acetylation of indolealkylamines by brain homogenates of the honeybee, Apis mellifera. *Journal of Insect Physiology* **1975,** *21* (2), 343-353.

196. Finocchiaro, L.; Callebert, J.; Launay, J. M.; Jallon, J. M., Melatonin biosynthesis in Drosophila: Its nature and Its effects. *Journal of Neurochemistry* **1988,** *50* (2), 382-387.

197. Paxon, T. L.; Powell, P. R.; Lee, H.-G.; Han, K.-A.; Ewing, A. G., Microcolumn separation of amine metabolites in the fruit fly. *Analytical chemistry* **2005,** *77* (16), 5349-5355.

198. Savitz, J.; Drevets, W. C.; Smith, C. M.; Victor, T. A.; Wurfel, B. E.; Bellgowan, P. S. F.; Bodurka, J.; Teague, T. K.; Dantzer, R., Putative neuroprotective and neurotoxic kynurenine pathway metabolites are associated with hippocampal and amygdalar volumes in subjects with major depressive disorder. *Neuropsychopharmacology* **2015,** *40* (2), 463-471.

199. Pegg, A. E.; Casero, R. A., Jr., Current status of the polyamine research field. *Methods in molecular biology (Clifton, N.J.)* **2011,** *720*, 3-35.

200. Lewandowski, N. M.; Ju, S.; Verbitsky, M.; Ross, B.; Geddie, M. L.; Rockenstein, E.; Adame, A.; Muhammad, A.; Vonsattel, J. P.; Ringe, D.; Cote, L.; Lindquist, S.; Masliah, E.; Petsko, G. A.; Marder, K.; Clark, L. N.; Small, S. A., Polyamine pathway contributes to the pathogenesis of Parkinson disease. *Proceedings of the National Academy of Sciences of the United States of America* **2010,** *107* (39), 16970-16975.

201. Morrison, L. D.; Kish, S. J., Brain polyamine levels are altered in Alzheimer's disease. *Neuroscience letters* **1995,** *197* (1), 5-8.

202. Aldini, G.; Orioli, M.; Carini, M.; Maffei Facino, R., Profiling histidine-containing dipeptides in rat tissues by liquid chromatography/electrospray ionization tandem mass spectrometry. *Journal of mass spectrometry* **2004,** *39* (12), 1417-1428.

203. Boldyrev, A. A.; Aldini, G.; Derave, W., Physiology and pathophysiology of carnosine. *Physiological reviews* **2013,** *93* (4), 1803-45.

204. Gawryluk, J. W.; Wang, J. F.; Andreazza, A. C.; Shao, L.; Young, L. T., Decreased levels of glutathione, the major brain antioxidant, in post-mortem prefrontal cortex from patients with psychiatric disorders. *The international journal of neuropsychopharmacology / official scientific journal of the Collegium Internationale Neuropsychopharmacologicum (CINP)* **2011,** *14* (1), 123-30.

205. Edison, P.; Ahmed, I.; Fan, Z.; Hinz, R.; Gelosa, G.; Ray Chaudhuri, K.; Walker, Z.; Turkheimer, F. E.; Brooks, D. J., Microglia, amyloid, and glucose metabolism in Parkinson's disease with and without dementia. *Neuropsychopharmacology* **2013,** *38* (6), 938-949.

206. Mosconi, L.; Pupi, A.; De Leon, M. J., Brain glucose hypometabolism and oxidative stress in preclinical Alzheimer's disease. *Annals of the New York Academy of Sciences* **2008,** *1147*, 180-195.

207. Peppard, R. F.; Martin, W. R.; Clark, C. M.; Carr, G. D.; McGeer, P. L.; Calne, D. B., Cortical glucose metabolism in Parkinson's and Alzheimer's disease. *Journal of neuroscience research* **1990,** *27* (4), 561-8.

208. Vander Borght, T.; Minoshima, S.; Giordani, B.; Foster, N. L.; Frey, K. A.; Berent, S.; Albin, R. L.; Koeppe, R. A.; Kuhl, D. E., Cerebral metabolic differences in Parkinson's and Alzheimer's diseases matched for dementia severity. *Journal of nuclear medicine : official publication, Society of Nuclear Medicine* **1997,** *38* (5), 797-802.

209. Armbruster, D. A.; Pry, T., Limit of blank, limit of detection and limit of quantitation. *The Clinical Biochemist Reviews* **2008,** *29* (Suppl 1), S49-S52.

210. Santos, S. M.; Garcia-Nimo, L.; Sa Santos, S.; Tavares, I.; Cocho, J. A.; Castanho, M. A., Neuropeptide kyotorphin (tyrosyl-arginine) has decreased levels in the cerebro-spinal fluid of Alzheimer's disease patients: potential diagnostic and pharmacological implications. *Frontiers in aging neuroscience* **2013,** *5*, 68.

211. Ueda, H.; Shiomi, H.; Takagi, H., Regional distribution of a novel analgesic dipeptide kyotorphin (Tyr-Arg) in the rat brain and spinal cord. *Brain research* **1980,** *198* (2), 460-4.

212. Ribeiro, M. M.; Pinto, A. R.; Domingues, M. M.; Serrano, I.; Heras, M.; Bardaji, E. R.; Tavares, I.; Castanho, M. A., Chemical conjugation of the neuropeptide kyotorphin and ibuprofen enhances brain targeting and analgesia. *Molecular pharmaceutics* **2011,** *8* (5), 1929-40.

213. Sigrist, S. J.; Andlauer, T. F. M., Fighting the famine with an amine: synaptic strategies for smart search. *Nat Neurosci* **2011,** *14* (2), 124-126.

214. Yang, Z.; Yu, Y.; Zhang, V.; Tian, Y.; Qi, W.; Wang, L., Octopamine mediates starvation-induced hyperactivity in adult Drosophila. *Proceedings of the National Academy of Sciences* **2015,** *112* (16), 5219-5224.

215. Canelas, A. B.; ten Pierick, A.; Ras, C.; Seifar, R. M.; van Dam, J. C.; van Gulik, W. M.; Heijnen, J. J., Quantitative evaluation of intracellular metabolite extraction techniques for yeast metabolomics. *Analytical chemistry* **2009,** *81* (17), 7379-7389.

216. Dietmair, S.; Timmins, N. E.; Gray, P. P.; Nielsen, L. K.; Krömer, J. O., Towards quantitative metabolomics of mammalian cells: development of a metabolite extraction protocol. *Analytical biochemistry* **2010,** *404* (2), 155-164.

217. Mushtaq, M. Y.; Choi, Y. H.; Verpoorte, R.; Wilson, E. G., Extraction for metabolomics: access to the metabolome. *Phytochemical Analysis* **2014,** *25* (4), 291-306.

218. Hyman, S. E.; Malenka, R. C.; Nestler, E. J., Neural mechanisms of addiction: the role of reward-related learning and memory. *Annual review of neuroscience* **2006,** *29*, 565-98.

219. Berthoud, H.-R., Interactions between the “cognitive” and “metabolic” brain in the control of food intake. *Physiology & Behavior* **2007,** *91* (5), 486-498.

220. Kempadoo, K. A.; Tourino, C.; Cho, S. L.; Magnani, F.; Leinninger, G. M.; Stuber, G. D.; Zhang, F.; Myers, M. G.; Deisseroth, K.; de Lecea, L.; Bonci, A., Hypothalamic neurotensin projections promote reward by enhancing glutamate transmission in the VTA. *The Journal of neuroscience : the official journal of the Society for Neuroscience* **2013,** *33* (18), 7618-26.

221. Shizgal, P.; Fulton, S.; Woodside, B., Brain reward circuitry and the regulation of energy balance. *International journal of obesity and related metabolic disorders : journal of the International Association for the Study of Obesity* **2001,** *25 Suppl 5*, S17-21.

222. Boutrel, B.; Cannella, N.; de Lecea, L., The role of hypocretin in driving arousal and goal-oriented behaviors. *Brain research* **2010,** *1314*, 103-11.

223. Sakurai, T.; Amemiya, A.; Ishii, M.; Matsuzaki, I.; Chemelli, R. M.; Tanaka, H.; Williams, S. C.; Richardson, J. A.; Kozlowski, G. P.; Wilson, S.; Arch, J. R.; Buckingham, R. E.; Haynes, A. C.; Carr, S. A.; Annan, R. S.; McNulty, D. E.; Liu, W. S.;

Terrett, J. A.; Elshourbagy, N. A.; Bergsma, D. J.; Yanagisawa, M., Orexins and orexin receptors: a family of hypothalamic neuropeptides and G protein-coupled receptors that regulate feeding behavior. *Cell* **1998,** *92* (4), 573-85.

224. Georgescu, D.; Sears, R. M.; Hommel, J. D.; Barrot, M.; Bolanos, C. A.; Marsh, D. J.; Bednarek, M. A.; Bibb, J. A.; Maratos-Flier, E.; Nestler, E. J.; DiLeone, R. J., The hypothalamic neuropeptide melanin-concentrating hormone acts in the nucleus accumbens to modulate feeding behavior and forced-swim performance. *The Journal of neuroscience : the official journal of the Society for Neuroscience* **2005,** *25* (11), 2933-40.

225. Leonetti, M.; Brun, P.; Sotty, F.; Steinberg, R.; Soubrié, P.; Bert, L.; Renaud, B.; Suaud-Chagny, M.-F., The neurotensin receptor antagonist SR 142948A blocks the efflux of dopamine evoked in nucleus accumbens by neurotensin ejection into the ventral tegmental area. *Naunyn-Schmiedeberg's Archives of Pharmacology 365* (6), 427-433.

226. Luttinger, D.; King, R. A.; Sheppard, D.; Strupp, J.; Nemeroff, C. B.; Prange, A. J., Jr., The effect of neurotensin on food consumption in the rat. *European journal of pharmacology* **1982,** *81* (3), 499-503.

227. Opland, D.; Sutton, A.; Woodworth, H.; Brown, J.; Bugescu, R.; Garcia, A.; Christensen, L.; Rhodes, C.; Myers, M., Jr.; Leinninger, G., Loss of neurotensin receptor-1 disrupts the control of the mesolimbic dopamine system by leptin and promotes hedonic feeding and obesity. *Molecular metabolism* **2013,** *2* (4), 423-34.

228. Panayi, F.; Colussi-Mas, J.; Lambas-Senas, L.; Renaud, B.; Scarna, H.; Berod, A., Endogenous neurotensin in the ventral tegmental area contributes to amphetamine behavioral sensitization. *Neuropsychopharmacology* **2004,** *30* (5), 871-879.

229. Sahu, A.; Carraway, R. E.; Wang, Y.-P., Evidence that neurotensin mediates the central effect of leptin on food intake in rat. *Brain research* **2001,** *888* (2), 343-347.

230. Goforth, P. B.; Leinninger, G. M.; Patterson, C. M.; Satin, L. S.; Myers, M. G., Jr., Leptin acts via lateral hypothalamic area neurotensin neurons to inhibit orexin neurons by multiple GABA-independent mechanisms. *The Journal of neuroscience : the official journal of the Society for Neuroscience* **2014,** *34* (34), 11405-15.

231. Leinninger, G. M.; Opland, D. M.; Jo, Y. H.; Faouzi, M.; Christensen, L.; Cappellucci, L. A.; Rhodes, C. J.; Gnegy, M. E.; Becker, J. B.; Pothos, E. N.; Seasholtz, A. F.; Thompson, R. C.; Myers, M. G., Jr., Leptin action via neurotensin neurons controls orexin, the mesolimbic dopamine system and energy balance. *Cell metabolism* **2011,** *14* (3), 313-23.

232. Abe, H.; Yanagawa, Y.; Kanbara, K.; Maemura, K.; Hayasaki, H.; Azuma, H.; Obata, K.; Katsuoka, Y.; Yabumoto, M.; Watanabe, M., Epithelial localization of green

fluorescent protein-positive cells in epididymis of the GAD67-GFP knock-in mouse. *Journal of andrology* **2005,** *26* (5), 568-77.

233. Sanz, E.; Yang, L.; Su, T.; Morris, D. R.; McKnight, G. S.; Amieux, P. S., Cell-type-specific isolation of ribosome-associated mRNA from complex tissues. *Proceedings of the National Academy of Sciences* **2009,** *106* (33), 13939-13944.

234. Krashes, M. J.; Koda, S.; Ye, C.; Rogan, S. C.; Adams, A. C.; Cusher, D. S.; Maratos-Flier, E.; Roth, B. L.; Lowell, B. B., Rapid, reversible activation of AgRP neurons drives feeding behavior in mice. *The Journal of clinical investigation 121* (4), 1424-1428.

235. Mabrouk, O. S.; Semaan, D. Z.; Mikelman, S.; Gnegy, M. E.; Kennedy, R. T., Amphetamine stimulates movement through thalamocortical glutamate release. *Journal of neurochemistry* **2014,** *128* (1), 152-61.

236. Grossberg, A. J.; Zhu, X.; Leinninger, G. M.; Levasseur, P. R.; Braun, T. P.; Myers, M. G., Jr.; Marks, D. L., Inflammation-induced lethargy is mediated by suppression of orexin neuron activity. *The Journal of neuroscience : the official journal of the Society for Neuroscience* **2011,** *31* (31), 11376-86.

237. Watts, A. G.; Boyle, C. N., The functional architecture of dehydration-anorexia. *Physiol Behav* **2010,** *100* (5), 472-7.

238. Stowe, Z. N.; Nemeroff, C. B., The electrophysiological actions of neurotensin in the central nervous system. *Life sciences* **1991,** *49* (14), 987-1002.

239. Nestler, E. J., Is there a common molecular pathway for addiction? *Nat Neurosci* **2005,** *8* (11), 1445-9.

240. Myers, M. G.; Olson, D. P., Central nervous system control of metabolism. *Nature* **2012,** *491* (7424), 357-363.

241. Britt, Jonathan P.; Benaliouad, F.; McDevitt, Ross A.; Stuber, Garret D.; Wise, Roy A.; Bonci, A., Synaptic and behavioral profile of multiple glutamatergic inputs to the nucleus accumbens. *Neuron* **2012,** *76* (4), 790-803.

242. Russo, S. J.; Nestler, E. J., The brain reward circuitry in mood disorders. *Nat Rev Neurosci* **2013,** *14* (9), 609-625.

243. Al-Hasani, R.; McCall, Jordan G.; Shin, G.; Gomez, Adrian M.; Schmitz, Gavin P.; Bernardi, Julio M.; Pyo, C.-O.; Park, Sung I.; Marcinkiewcz, Catherine M.; Crowley, Nicole A.; Krashes, Michael J.; Lowell, Bradford B.; Kash, Thomas L.; Rogers, John A.; Bruchas, Michael R., Distinct subpopulations of nucleus accumbens dynorphin neurons drive aversion and reward. *Neuron* **2015,** *87* (5), 1063-1077.

244. Castro, D. C.; Berridge, K. C., Opioid hedonic hotspot in nucleus accumbens shell: mu, delta, and kappa maps for enhancement of sweetness "liking" and "wanting". *The Journal of neuroscience : the official journal of the Society for Neuroscience* **2014,** *34* (12), 4239-50.

245. Hamid, A. A.; Pettibone, J. R.; Mabrouk, O. S.; Hetrick, V. L.; Schmidt, R.; Vander Weele, C. M.; Kennedy, R. T.; Aragona, B. J.; Berke, J. D., Mesolimbic dopamine signals the value of work. *Nat Neurosci* **2016,** *19* (1), 117-26.

246. Bunzow, J. R.; Saez, C.; Mortrud, M.; Bouvier, C.; Williams, J. T.; Low, M.; Grandy, D. K., Molecular cloning and tissue distribution of a putative member of the rat opioid receptor gene family that is not a μ, δ or κ opioid receptor type. *FEBS letters* **1994,** *347* (2-3), 284-288.

247. Henderson, G.; McKnight, A. T., The orphan opioid receptor and its endogenous ligand—nociceptin/orphanin FQ. *Trends in pharmacological sciences* **1997,** *18* (4), 293-300.

248. Besson, M. J.; Graybiel, A. M.; Quinn, B., Co-expression of neuropeptides in the cat's striatum: an immunohistochemical study of substance P, dynorphin B and enkephalin. *Neuroscience* **1990,** *39* (1), 33-58.

249. Chavkin, C.; James, I. F.; Goldstein, A., Dynorphin is a specific endogenous ligand of the kappa opioid receptor. *Science (New York, N.Y.)* **1982,** *215* (4531), 413-5.

250. Gerfen, C. R.; Young, W. S., 3rd, Distribution of striatonigral and striatopallidal peptidergic neurons in both patch and matrix compartments: an in situ hybridization histochemistry and fluorescent retrograde tracing study. *Brain research* **1988,** *460* (1), 161-7.

251. Shippenberg, T. S.; LeFevour, A.; Chefer, V. I., Targeting endogenous mu- and delta-opioid receptor systems for the treatment of drug addiction. *CNS & neurological disorders drug targets* **2008,** *7* (5), 442-53.

252. Mucha, R. F.; Millan, M. J.; Herz, A., Aversive properties of naloxone in non-dependent (naive) rats may involve blockade of central beta-endorphin. *Psychopharmacology* **1985,** *86* (3), 281-5.

253. Pfeiffer, A.; Brantl, V.; Herz, A.; Emrich, H. M., Psychotomimesis mediated by kappa opiate receptors. *Science (New York, N.Y.)* **1986,** *233* (4765), 774-6.

254. Shippenberg, T. S.; Zapata, A.; Chefer, V. I., Dynorphin and the pathophysiology of drug addiction. *Pharmacology & therapeutics* **2007,** *116* (2), 306-21.

255. Van Bockstaele, E. J.; Gracy, K. N.; Pickel, V. M., Dynorphin-immunoreactive neurons in the rat nucleus accumbens: ultrastructure and synaptic input from terminals containing substance P and/or dynorphin. *J Comp Neurol* **1995,** *351* (1), 117-33.

256. Bruchas, M. R.; Land, B. B.; Chavkin, C., The dynorphin/kappa opioid system as a modulator of stress-induced and pro-addictive behaviors. *Brain research* **2010,** *1314*, 44-55.

257. Bruchas, M. R.; Schindler, A. G.; Shankar, H.; Messinger, D. I.; Miyatake, M.; Land, B. B.; Lemos, J. C.; Hagan, C. E.; Neumaier, J. F.; Quintana, A.; Palmiter, R. D.; Chavkin, C., Selective p38alpha MAPK deletion in serotonergic neurons produces stress resilience in models of depression and addiction. *Neuron* **2011,** *71* (3), 498-511.

258. Deisseroth, K., Optogenetics. *Nature methods* **2011,** *8* (1), 26-29.

259. Patterson, C. M.; Wong, J.-M. T.; Leinninger, G. M.; Allison, M. B.; Mabrouk, O. S.; Kasper, C. L.; Gonzalez, I. E.; Mackenzie, A.; Jones, J. C.; Kennedy, R. T., Ventral tegmental area neurotensin signaling links the lateral hypothalamus to locomotor activity and striatal dopamine efflux in male mice. *Endocrinology* **2015**.

260. Mabrouk, O. S.; Marti, M.; Salvadori, S.; Morari, M., The novel delta opioid receptor agonist UFP-512 dually modulates motor activity in hemiparkinsonian rats via control of the nigro-thalamic pathway. *Neuroscience* **2009,** *164* (2), 360-369.

261. Curran, E. J.; Watson, S. J. J., Dopamine receptor mRNA expression patterns by opioid peptide cells in the nucleus accumbens of the rat: a double in situ hybridization study. *The Journal of Comparative Neurology* **1995,** *361* (1), 57-76.

262. Di Chiara, G.; Imperato, A., Drugs abused by humans preferentially increase synaptic dopamine concentrations in the mesolimbic system of freely moving rats. *Proceedings of the National Academy of Sciences of the United States of America* **1988,** *85* (14), 5274-8.

263. Chang, H. T.; Kitai, S. T., Projection neurons of the nucleus accumbens: an intracellular labeling study. *Brain research* **1985,** *347* (1), 112-116.

264. Egan, M. F.; Hurd, Y.; Hyde, T. M.; Weinberger, D. R.; Wyatt, R. J.; Kleinman, J. E., Alterations in mRNA levels of D2 receptors and neuropeptides in striatonigral and striatopallidal neurons of rats with neuroleptic-induced dyskinesias. *Synapse* **1994,** *18* (3), 178-189.

265. Albin, R. L.; Young, A. B.; Penney, J. B., The functional anatomy of basal ganglia disorders. *Trends in Neurosciences* **1989,** *12* (10), 366-375.

266. DeLong, M. R., Primate models of movement disorders of basal ganglia origin. *Trends in neurosciences* **1990,** *13* (7), 281-5.

267. Surmeier, D. J.; Ding, J.; Day, M.; Wang, Z.; Shen, W., D1 and D2 dopamine-receptor modulation of striatal glutamatergic signaling in striatal medium spiny neurons. *Trends in Neurosciences* **2007,** *30* (5), 228-235.

268. Hanrieder, J.; Ljungdahl, A.; Falth, M.; Mammo, S. E.; Bergquist, J.; Andersson, M., L-DOPA-induced dyskinesia is associated with regional increase of striatal dynorphin peptides as elucidated by imaging mass spectrometry. *Molecular & cellular proteomics : MCP* **2011,** *10* (10), M111 009308.

269. Jolkkonen, J.; Granata, R.; Jenner, P.; Marsden, C. D., Acute and subchronic effects of dopamine agonists on neuropeptide gene expression in the rat striatum. *Neuropeptides* **1995,** *29* (2), 109-14.

270. Gerfen, C. R.; McGinty, J. F.; Young, W. S., 3rd, Dopamine differentially regulates dynorphin, substance P, and enkephalin expression in striatal neurons: in situ hybridization histochemical analysis. *The Journal of neuroscience : the official journal of the Society for Neuroscience* **1991,** *11* (4), 1016-31.

271. Le Moine, C.; Normand, E.; Guitteny, A. F.; Fouque, B.; Teoule, R.; Bloch, B., Dopamine receptor gene expression by enkephalin neurons in rat forebrain. *Proceedings of the National Academy of Sciences of the United States of America* **1990,** *87* (1), 230-4.

272. Steiner, H.; Gerfen, C. R., Enkephalin regulates acute D2 dopamine receptor antagonist-induced immediate-early gene expression in striatal neurons. *Neuroscience* **1999,** *88* (3), 795-810.

273. Augood, S. J.; Emson, P. C.; Mitchell, I. J.; Boyce, S.; Clarke, C. E.; Crossman, A. R., Cellular localisation of enkephalin gene expression in MPTP-treated cynomolgus monkeys. *Brain research. Molecular brain research* **1989,** *6* (1), 85-92.

274. Schneider, J. S.; Decamp, E.; Wade, T., Striatal preproenkephalin gene expression is upregulated in acute but not chronic parkinsonian monkeys: implications for the contribution of the indirect striatopallidal circuit to parkinsonian symptomatology. *The Journal of neuroscience : the official journal of the Society for Neuroscience* **1999,** *19* (15), 6643-9.

275. Nisbet, A. P.; Foster, O. J.; Kingsbury, A.; Eve, D. J.; Daniel, S. E.; Marsden, C. D.; Lees, A. J., Preproenkephalin and preprotachykinin messenger RNA expression in normal human basal ganglia and in Parkinson's disease. *Neuroscience* **1995,** *66* (2), 361-76.

276. Hill, M. P.; Hille, C. J.; Brotchie, J. M., Delta-opioid receptor agonists as a therapeutic approach in Parkinson's disease. *Drug news & perspectives* **2000,** *13* (5), 261-8.

277. Hille, C. J.; Fox, S. H.; Maneuf, Y. P.; Crossman, A. R.; Brotchie, J. M., Antiparkinsonian action of a δ opioid agonist in rodent and primate models of Parkinson's Disease. *Experimental Neurology* **2001,** *172* (1), 189-198.

278. Mabrouk, O. S.; Volta, M.; Marti, M.; Morari, M., Stimulation of delta opioid receptors located in substantia nigra reticulata but not globus pallidus or striatum restores motor activity in 6-hydroxydopamine lesioned rats: new insights into the role of delta receptors in parkinsonism. *Journal of neurochemistry* **2008,** *107* (6), 1647-1659.

279. Chefer, V. I.; Kieffer, B. L.; Shippenberg, T. S., Contrasting effects of mu opioid receptor and delta opioid receptor deletion upon the behavioral and neurochemical effects of cocaine. *Neuroscience* **2004,** *127* (2), 497-503.

280. Fox, S.; Silverdale, M.; Kellett, M.; Davies, R.; Steiger, M.; Fletcher, N.; Crossman, A.; Brotchie, J., Non-subtype-selective opioid receptor antagonism in treatment of levodopa-induced motor complications in Parkinson's disease. *Movement Disorders* **2004,** *19* (5), 554-560.

281. Klintenberg, R.; Svenningsson, P.; Gunne, L.; Andren, P. E., Naloxone reduces levodopa-induced dyskinesias and apomorphine-induced rotations in primate models of parkinsonism. *Journal of neural transmission (Vienna, Austria : 1996)* **2002,** *109* (10), 1295-307.

282. Potts, L. F.; Park, E. S.; Woo, J.-M.; Dyavar Shetty, B. L.; Singh, A.; Braithwaite, S. P.; Voronkov, M.; Papa, S. M.; Mouradian, M. M., Dual κ-agonist/μ-antagonist opioid receptor modulation reduces levodopa-induced dyskinesia and corrects dysregulated striatal changes in the nonhuman primate model of Parkinson disease. *Annals of neurology* **2015,** *77* (6), 930-941.

283. Rascol, O.; Fabre, N.; Blin, O.; Poulik, J.; Sabatini, U.; Senard, J.-M.; Ané, M.; Montastruc, J.-L.; Rascol, A., Naltrexone, an opiate antagonist, fails to modify motor symptoms in patients with Parkinson's disease. *Movement Disorders* **1994,** *9* (4), 437-440.

284. Samadi, P.; Grégoire, L.; Bédard, P. J., Opioid antagonists increase the dyskinetic response to dopaminergic agents in parkinsonian monkeys: interaction between dopamine and opioid systems. *Neuropharmacology* **2003,** *45* (7), 954-963.

285. Henry, B.; Fox, S. H.; Crossman, A. R.; Brotchie, J. M., μ- and δ-Opioid receptor antagonists reduce levodopa-induced dyskinesia in the MPTP-lesioned primate model of Parkinson's Disease. *Experimental Neurology* **2001,** *171* (1), 139-146.

286. Koprich, J. B.; Fox, S. H.; Johnston, T. H.; Goodman, A.; Le Bourdonnec, B.; Dolle, R. E.; DeHaven, R. N.; DeHaven-Hudkins, D. L.; Little, P. J.; Brotchie, J. M., The selective mu-opioid receptor antagonist adl5510 reduces levodopa-induced dyskinesia

without affecting antiparkinsonian action in mptp-lesioned macaque model of Parkinson's disease. *Movement Disorders* **2011,** *26* (7), 1225-1233.

287. Cox, H.; Togasaki, D. M.; Chen, L.; Langston, J. W.; Di Monte, D. A.; Quik, M., The selective kappa-opioid receptor agonist U50,488 reduces L-dopa-induced dyskinesias but worsens parkinsonism in MPTP-treated primates. *Exp Neurol* **2007,** *205* (1), 101-7.

288. Giuffra, M.; Mouradian, M. M.; Davis, T. L.; Ownby, J.; Chase, T. N., Dynorphin agonist therapy of Parkinson's disease. *Clinical neuropharmacology* **1993,** *16* (5), 444-7.

289. Manson, A. J.; Katzenschlager, R.; Hobart, J.; Lees, A. J., High dose naltrexone for dyskinesias induced by levodopa. *Journal of Neurology, Neurosurgery & Psychiatry* **2001,** *70* (4), 554-556.

290. Marti, M.; Trapella, C.; Viaro, R.; Morari, M., The nociceptin/orphanin FQ receptor antagonist J-113397 and L-DOPA additively attenuate experimental parkinsonism through overinhibition of the nigrothalamic pathway. *The Journal of neuroscience : the official journal of the Society for Neuroscience* **2007,** *27* (6), 1297-307.

291. Marti, M.; Mela, F.; Bianchi, C.; Beani, L.; Morari, M., Striatal dopamine-NMDA receptor interactions in the modulation of glutamate release in the substantia nigra pars reticulata in vivo: opposite role for D1 and D2 receptors. *Journal of neurochemistry* **2002,** *83* (3), 635-44.

292. Akil, H.; Watson, S. J.; Young, E.; Lewis, M. E.; Khachaturian, H.; Walker, J. M., Endogenous opioids: biology and function. *Annual review of neuroscience* **1984,** *7* (1), 223-255.

293. Mansour, A.; Fox, C. A.; Burke, S.; Meng, F.; Thompson, R. C.; Akil, H.; Watson, S. J., Mu, delta, and kappa opioid receptor mRNA expression in the rat CNS: an in situ hybridization study. **1994**.

294. Hudzik, T. J.; Howell, A.; Payza, K.; Cross, A. J., Antiparkinson potential of δ-opioid receptor agonists. *European journal of pharmacology* **2000,** *396* (2–3), 101-107.

295. Mabrouk, O. S.; Viaro, R.; Volta, M.; Ledonne, A.; Mercuri, N.; Morari, M., Stimulation of delta opioid receptor and blockade of nociceptin/orphanin FQ receptor synergistically attenuate parkinsonism. *The Journal of neuroscience : the official journal of the Society for Neuroscience* **2014,** *34* (39), 12953-62.

296. Maneuf, Y. P.; Mitchell, I. J.; Crossman, A. R.; Brotchie, J. M., On the role of enkephalin cotransmission in the GABAergic striatal efferents to the globus pallidus. *Experimental Neurology* **1994,** *125* (1), 65-71.

297. Pinna, A.; Di Chiara, G., Dopamine-dependent behavioural stimulation by non-peptide delta opioids BW 373U86 and SNC 80: 3. Facilitation of D1 and D2 responses in unilaterally 6-hydroxydopamine-lesioned rats. *Behavioural pharmacology* **1998,** *9* (1), 15-21.

298. Carta, A.; Fenu, S.; Morelli, M., Alterations in GAD67, dynorphin and enkephalin mRNA in striatal output neurons following priming in the 6-OHDA model of Parkinson's disease. *Neurological Sciences* **2001,** *22* (1), 59-60.

299. Ziolkowska, B.; Horn, G.; Kupsch, A.; Hollt, V., The expression of proenkephalin and prodynorphin genes and the induction of c-fos gene by dopaminergic drugs are not altered in the straitum of MPTP-treated mice. *Journal of neural transmission. Parkinson's disease and dementia section* **1995,** *9* (2-3), 151-64.

300. Borghammer, P.; Hansen, S. B.; Eggers, C.; Chakravarty, M.; Vang, K.; Aanerud, J.; Hilker, R.; Heiss, W. D.; Rodell, A.; Munk, O. L.; Keator, D.; Gjedde, A., Glucose metabolism in small subcortical structures in Parkinson's disease. *Acta neurologica Scandinavica* **2012,** *125* (5), 303-10.

301. Kuhl, D. E.; Metter, E. J.; Riege, W. H., Patterns of local cerebral glucose utilization determined in Parkinson's disease by the [18F]fluorodeoxyglucose method. *Annals of neurology* **1984,** *15* (5), 419-24.

302. Kuhl, D. E.; Metter, E. J.; Riege, W. H.; Markham, C. H., Patterns of cerebral glucose utilization in Parkinson's disease and Huntington's disease. *Annals of neurology* **1984,** *15 Suppl*, S119-25.

303. Peppard, R. F.; Martin, W. R.; Carr, G. D.; Grochowski, E.; Schulzer, M.; Guttman, M.; McGeer, P. L.; Phillips, A. G.; Tsui, J. K.; Calne, D. B., Cerebral glucose metabolism in Parkinson's disease with and without dementia. *Archives of neurology* **1992,** *49* (12), 1262-8.

304. Boyd, A. E., 3rd; Lebovitz, H. E.; Feldman, J. M., Endocrine function and glucose metabolism in patients with Parkinson's disease and their alternation by L-Dopa. *The Journal of clinical endocrinology and metabolism* **1971,** *33* (5), 829-37.

305. Lipman, I. J.; Boykin, M. E.; Flora, R. E., Glucose intolerance in Parkinson's disease. *Journal of chronic diseases* **1974,** *27* (11-12), 573-9.

306. Pressley, J. C.; Louis, E. D.; Tang, M. X.; Cote, L.; Cohen, P. D.; Glied, S.; Mayeux, R., The impact of comorbid disease and injuries on resource use and expenditures in parkinsonism. *Neurology* **2003,** *60* (1), 87-93.

307. Sandyk, R., The relationship between diabetes mellitus and Parkinson's disease. *International Journal of Neuroscience* **1993,** *69* (1-4), 125-130.

308. Becker, C.; Brobert, G. P.; Johansson, S.; Jick, S. S.; Meier, C. R., Diabetes in patients with idiopathic Parkinson's disease. *Diabetes care* **2008,** *31* (9), 1808-12.

309. Powers, K. M.; Smith-Weller, T.; Franklin, G. M.; Longstreth, W. T., Jr.; Swanson, P. D.; Checkoway, H., Diabetes, smoking, and other medical conditions in relation to Parkinson's disease risk. *Parkinsonism & related disorders* **2006,** *12* (3), 185-9.

310. Scigliano, G.; Ronchetti, G.; Girotti, F., Autonomic nervous system and risk factors for vascular disease. Effects of autonomic unbalance in schizophrenia and Parkinson's disease. *Neurological Sciences* **2008,** *29* (1), 15-21.

311. Ludwig, M.; Bull, P. M.; Tobin, V. A.; Sabatier, N.; Landgraf, R.; Dayanithi, G.; Leng, G., Regulation of activity-dependent dendritic vasopressin release from rat supraoptic neurones. *The Journal of Physiology* **2005,** *564* (Pt 2), 515-522.

312. Ludwig, M.; Sabatier, N.; Bull, P. M.; Landgraf, R.; Dayanithi, G.; Leng, G., Intracellular calcium stores regulate activity-dependent neuropeptide release from dendrites. *Nature* **2002,** *418* (6893), 85-9.

313. Ludwig, M.; Leng, G., Dendritic peptide release and peptide-dependent behaviours. *Nat Rev Neurosci* **2006,** *7* (2), 126-136.

314. Brooks, D. J., Optimizing levodopa therapy for Parkinson's disease with levodopa/carbidopa/entacapone: implications from a clinical and patient perspective. *Neuropsychiatric disease and treatment* **2008,** *4* (1), 39-47.

315. Thanvi, B.; Lo, N.; Robinson, T., Levodopa-induced dyskinesia in Parkinson's disease: clinical features, pathogenesis, prevention and treatment. *Postgraduate medical journal* **2007,** *83* (980), 384-8.

316. Ahlskog, J. E.; Muenter, M. D., Frequency of levodopa-related dyskinesias and motor fluctuations as estimated from the cumulative literature. *Movement disorders : official journal of the Movement Disorder Society* **2001,** *16* (3), 448-58.

317. Fabbrini, G.; Brotchie, J. M.; Grandas, F.; Nomoto, M.; Goetz, C. G., Levodopa-induced dyskinesias. *Movement disorders : official journal of the Movement Disorder Society* **2007,** *22* (10), 1379-89; quiz 1523.

318. Hauser, R. A.; Rascol, O.; Korczyn, A. D.; Jon Stoessl, A.; Watts, R. L.; Poewe, W.; De Deyn, P. P.; Lang, A. E., Ten-year follow-up of Parkinson's disease patients randomized to initial therapy with ropinirole or levodopa. *Movement disorders : official journal of the Movement Disorder Society* **2007,** *22* (16), 2409-17.

319. Aubert, I.; Guigoni, C.; Hakansson, K.; Li, Q.; Dovero, S.; Barthe, N.; Bioulac, B. H.; Gross, C. E.; Fisone, G.; Bloch, B.; Bezard, E., Increased D1 dopamine receptor signaling in levodopa-induced dyskinesia. *Annals of neurology* **2005,** *57* (1), 17-26.

320. Bastide, M. F.; Meissner, W. G.; Picconi, B.; Fasano, S.; Fernagut, P. O.; Feyder, M.; Francardo, V.; Alcacer, C.; Ding, Y.; Brambilla, R.; Fisone, G.; Jon Stoessl, A.; Bourdenx, M.; Engeln, M.; Navailles, S.; De Deurwaerdere, P.; Ko, W. K.; Simola, N.; Morelli, M.; Groc, L.; Rodriguez, M. C.; Gurevich, E. V.; Quik, M.; Morari, M.; Mellone, M.; Gardoni, F.; Tronci, E.; Guehl, D.; Tison, F.; Crossman, A. R.; Kang, U. J.; Steece-Collier, K.; Fox, S.; Carta, M.; Angela Cenci, M.; Bezard, E., Pathophysiology of L-dopa-induced motor and non-motor complications in Parkinson's disease. *Prog Neurobiol* **2015,** *132*, 96-168.

321. Rascol, O.; Brooks, D. J.; Korczyn, A. D.; De Deyn, P. P.; Clarke, C. E.; Lang, A. E., A five-year study of the incidence of dyskinesia in patients with early Parkinson's disease who were treated with ropinirole or levodopa. *The New England journal of medicine* **2000,** *342* (20), 1484-91.

322. Vaccari, C.; Lolait, S. J.; Ostrowski, N. L., Comparative distribution of vasopressin V1b and oxytocin receptor messenger ribonucleic acids in brain. *Endocrinology* **1998,** *139* (12), 5015-33.

323. Purba, J. S.; Hofman, M. A.; Swaab, D. F., Decreased number of oxytocin-immunoreactive neurons in the paraventricular nucleus of the hypothalamus in Parkinson's disease. *Neurology* **1994,** *44* (1), 84-9.

324. Young, K. A.; Liu, Y.; Gobrogge, K. L.; Wang, H.; Wang, Z., Oxytocin reverses amphetamine-induced deficits in social bonding: evidence for an interaction with nucleus accumbens dopamine. *The Journal of neuroscience : the official journal of the Society for Neuroscience* **2014,** *34* (25), 8499-506.

325. Romero-Fernandez, W.; Borroto-Escuela, D. O.; Agnati, L. F.; Fuxe, K., Evidence for the existence of dopamine D2-oxytocin receptor heteromers in the ventral and dorsal striatum with facilitatory receptor-receptor interactions. *Molecular psychiatry* **2013,** *18* (8), 849-50.

326. Cenci, M. A.; Lee, C. S.; Bjorklund, A., L-DOPA-induced dyskinesia in the rat is associated with striatal overexpression of prodynorphin- and glutamic acid decarboxylase mRNA. *The European journal of neuroscience* **1998,** *10* (8), 2694-706.

327. Cenci, M. A.; Whishaw, I. Q.; Schallert, T., Animal models of neurological deficits: how relevant is the rat? *Nat Rev Neurosci* **2002,** *3* (7), 574-9.

328. Budden, A.; Chen, L. J.; Henry, A., High-dose versus low-dose oxytocin infusion regimens for induction of labour at term. *The Cochrane database of systematic reviews* **2014,** (10), CD009701.

329. Guastella, A. J.; Ward, P. B.; Hickie, I. B.; Shahrestani, S.; Hodge, M. A.; Scott, E. M.; Langdon, R., A single dose of oxytocin nasal spray improves higher-order social cognition in schizophrenia. *Schizophrenia research* **2015,** *168* (3), 628-33.

330. Yatawara, C. J.; Einfeld, S. L.; Hickie, I. B.; Davenport, T. A.; Guastella, A. J., The effect of oxytocin nasal spray on social interaction deficits observed in young children with autism: a randomized clinical crossover trial. *Molecular psychiatry* **2015**.

331. Neumann, I. D.; Maloumby, R.; Beiderbeck, D. I.; Lukas, M.; Landgraf, R., Increased brain and plasma oxytocin after nasal and peripheral administration in rats and mice. *Psychoneuroendocrinology* **2013,** *38* (10), 1985-93.

332. Chang, S. W.; Barter, J. W.; Ebitz, R. B.; Watson, K. K.; Platt, M. L., Inhaled oxytocin amplifies both vicarious reinforcement and self reinforcement in rhesus macaques (Macaca mulatta). *Proceedings of the National Academy of Sciences of the United States of America* **2012,** *109* (3), 959-64.

333. Ferris, C. F.; Yee, J. R.; Kenkel, W. M.; Dumais, K. M.; Moore, K.; Veenema, A. H.; Kulkarni, P.; Perkybile, A. M.; Carter, C. S., Distinct BOLD activation profiles following central and peripheral oxytocin administration in awake rats. *Frontiers in behavioral neuroscience* **2015,** *9*.

334. Modi, M. E.; Connor-Stroud, F.; Landgraf, R.; Young, L. J.; Parr, L. A., Aerosolized oxytocin increases cerebrospinal fluid oxytocin in rhesus macaques. *Psychoneuroendocrinology 45*, 49-57.

335. Striepens, N.; Kendrick, K. M.; Hanking, V.; Landgraf, R.; Wüllner, U.; Maier, W.; Hurlemann, R., Elevated cerebrospinal fluid and blood concentrations of oxytocin following its intranasal administration in humans. *Scientific Reports* **2013,** *3*, 3440.

336. Allen, D. D.; Crooks, P. A.; Yokel, R. A., 4-Trimethylammonium antipyrine: a quaternary ammonium nonradionuclide marker for blood-brain barrier integrity during in vivo microdialysis. *Journal of pharmacological and toxicological methods* **1992,** *28* (3), 129-35.

337. Benveniste, H.; Huttemeier, P. C., Microdialysis--theory and application. *Prog Neurobiol* **1990,** *35* (3), 195-215.

338. Caljon, G.; Caveliers, V.; Lahoutte, T.; Stijlemans, B.; Ghassabeh, G. H.; Van Den Abbeele, J.; Smolders, I.; De Baetselier, P.; Michotte, Y.; Muyldermans, S.; Magez, S.; Clinckers, R., Using microdialysis to analyse the passage of monovalent nanobodies through the blood-brain barrier. *Br J Pharmacol* **2012,** *165* (7), 2341-53.

339. Clapp-Lilly, K. L.; Roberts, R. C.; Duffy, L. K.; Irons, K. P.; Hu, Y.; Drew, K. L., An ultrastructural analysis of tissue surrounding a microdialysis probe. *J Neurosci Methods* **1999,** *90* (2), 129-42.

340. de Lange, E. C.; Danhof, M.; de Boer, A. G.; Breimer, D. D., Methodological considerations of intracerebral microdialysis in pharmacokinetic studies on drug transport across the blood-brain barrier. *Brain research. Brain research reviews* **1997,** *25* (1), 27-49.

341. Groothuis, D. R.; Ward, S.; Schlageter, K. E.; Itskovich, A. C.; Schwerin, S. C.; Allen, C. V.; Dills, C.; Levy, R. M., Changes in blood-brain barrier permeability associated with insertion of brain cannulas and microdialysis probes. *Brain research* **1998,** *803* (1-2), 218-30.

342. Major, O.; Shdanova, T.; Duffek, L.; Nagy, Z., Continuous monitoring of blood-brain barrier opening to Cr51-EDTA by microdialysis following probe injury. *Acta neurochirurgica. Supplementum* **1990,** *51*, 46-8.

343. Morgan, M. E.; Singhal, D.; Anderson, B. D., Quantitative assessment of blood-brain barrier damage during microdialysis. *The Journal of pharmacology and experimental therapeutics* **1996,** *277* (2), 1167-76.

344. Sumbria, R. K.; Klein, J.; Bickel, U., Acute depression of energy metabolism after microdialysis probe implantation is distinct from ischemia-induced changes in mouse brain. *Neurochem Res* **2011,** *36* (1), 109-16.

345. Westergren, I.; Nystrom, B.; Hamberger, A.; Johansson, B. B., Intracerebral dialysis and the blood-brain barrier. *Journal of neurochemistry* **1995,** *64* (1), 229-34.

346. Del Ry, S.; Clerico, A.; Giannessi, D.; Andreassi, M. G.; Caprioli, R.; Iascone, M. R.; Ferrazzi, P.; Biagini, A., Measurement of brain natriuretic peptide in plasma samples and cardiac tissue extracts by means of an immunoradiometric assay method. *Scandinavian journal of clinical and laboratory investigation* **2000,** *60* (2), 81-90.

347. Maalouf, R.; Bailey, S., A review on B-type natriuretic peptide monitoring: assays and biosensors. *Heart failure reviews* **2016**.

348. Stevenson, J. D.; Chapman, R. S.; Perry, B.; Logue, F. C., Evaluation and clinical application of a two-site immunoradiometric assay for alpha-1-foetoprotein using readily available reagents. *Annals of clinical biochemistry* **1987,** *24 (Pt 4)*, 411-8.

349. Kamp, K.; Feelders, R. A.; van Adrichem, R. C.; de Rijke, Y. B.; van Nederveen, F. H.; Kwekkeboom, D. J.; de Herder, W. W., Parathyroid hormone-related peptide (PTHrP) secretion by gastroenteropancreatic neuroendocrine tumors (GEP-NETs): clinical features, diagnosis, management, and follow-up. *The Journal of clinical endocrinology and metabolism* **2014,** *99* (9), 3060-9.

350. Roper, M. G.; Guillo, C., New technologies in affinity assays to explore biological communication. *Anal Bioanal Chem* **2009,** *393* (2), 459-65.

351. Woolley, C. F.; Hayes, M. A., Recent developments in emerging microimmunoassays. *Bioanalysis* **2013,** *5* (2), 245-64.

352. Bernard, A.; Michel, B.; Delamarche, E., Micromosaic immunoassays. *Anal Chem* **2001,** *73* (1), 8-12.

353. Murphy, B. M.; He, X.; Dandy, D.; Henry, C. S., Competitive immunoassays for simultaneous detection of metabolites and proteins using micromosaic patterning. *Anal Chem* **2008,** *80* (2), 444-50.

354. Wolf, M.; Juncker, D.; Michel, B.; Hunziker, P.; Delamarche, E., Simultaneous detection of C-reactive protein and other cardiac markers in human plasma using micromosaic immunoassays and self-regulating microfluidic networks. *Biosensors & bioelectronics* **2004,** *19* (10), 1193-202.

355. Trujillo, K. A.; Day, R.; Akil, H., Regulation of striatonigral prodynorphin peptides by dopaminergic agents. *Brain research* **1990,** *518* (1-2), 244-56.

356. Reed, B.; Zhang, Y.; Chait, B. T.; Kreek, M. J., Dynorphin A(1-17) biotransformation in striatum of freely moving rats using microdialysis and matrix-assisted laser desorption/ionization mass spectrometry. *Journal of neurochemistry* **2003,** *86* (4), 815-23.

357. Moore, D. S., Amino acid and peptide net charges: A simple calculational procedure. *Biochemical Education* **1985,** *13* (1), 10-11.

358. Zhang, J.; Jaquins-Gerstl, A.; Nesbitt, K. M.; Rutan, S. C.; Michael, A. C.; Weber, S. G., In vivo monitoring of serotonin in the striatum of freely moving rats with one minute temporal resolution by online microdialysis-capillary high-performance liquid chromatography at elevated temperature and pressure. *Anal Chem* **2013,** *85* (20), 9889-97.

359. Park, J.; Aragona, B. J.; Kile, B. M.; Carelli, R. M.; Wightman, R. M., In vivo voltammetric monitoring of catecholamine release in subterritories of the nucleus accumbens shell. *Neuroscience* **2010,** *169* (1), 132-42.

360. Slaney, T. R.; Mabrouk, O. S.; Porter-Stransky, K. A.; Aragona, B. J.; Kennedy, R. T., Chemical gradients within brain extracellular space measured using low flow push-pull perfusion sampling in vivo. *ACS chemical neuroscience* **2013,** *4* (2), 321-9.

361. Lee, W. H.; Ngernsutivorakul, T.; Mabrouk, O. S.; Wong, J.-M. T.; Dugan, C. E.; Pappas, S. S.; Yoon, H. J.; Kennedy, R. T., Microfabrication and in vivo performance of a microdialysis probe with embedded membrane. *Analytical chemistry* **2016,** *88* (2), 1230-1237.

362. Lee, W. H.; Slaney, T. R.; Hower, R. W.; Kennedy, R. T., Microfabricated sampling probes for in vivo monitoring of neurotransmitters. *Analytical chemistry* **2013,** *85* (8), 3828-3831.

363. Cepeda, D. E.; Hains, L.; Li, D.; Bull, J.; Lentz, S. I.; Kennedy, R. T., Experimental evaluation and computational modeling of tissue damage from low-flow push-pull perfusion sampling in vivo. *J Neurosci Methods* **2015,** *242*, 97-105.

364. Chen, J.; Wise, K. D.; Hetke, J. F.; Bledsoe, S. C., Jr., A multichannel neural probe for selective chemical delivery at the cellular level. *IEEE transactions on bio-medical engineering* **1997,** *44* (8), 760-9.

365. Lin, L.; Pisano, A. P., Silicon-procssed microneedles. *Journal of Microelectromechanical Systems* **1999,** *8* (1), 78-84.

366. McAllister, D. V.; Allen, M. G.; Prausnitz, M. R., Microfabricated microneedles for gene and drug delivery. *Annual review of biomedical engineering* **2000,** *2*, 289-313.

367. Zahn, J. D.; Trebotich, D.; Liepmann, D., Microdialysis microneedles for continuous medical monitoring. *Biomedical microdevices* **2005,** *7* (1), 59-69.